

**PHYSICOCHEMICAL PROPERTY IMPROVEMENT OF A FEW
ACTIVE PHARMACEUTICAL INGREDIENTS BY SOLID FORM
SCREENING**

**A Thesis
Submitted for the degree of
Doctor of Philosophy in Chemistry**

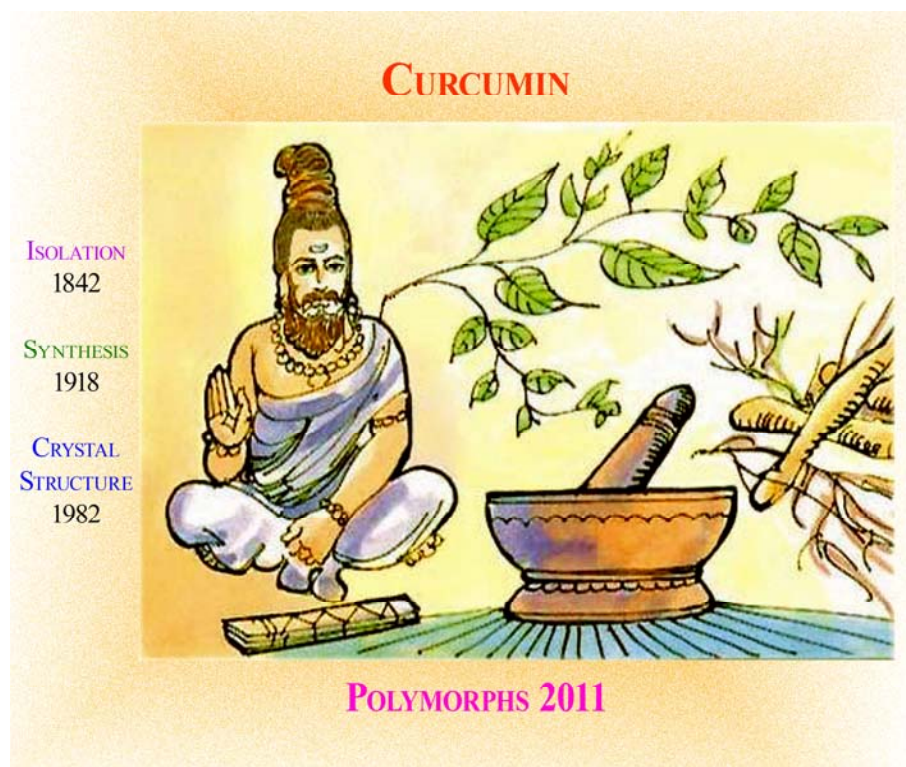
By

PALASH SANPHUI



**School of Chemistry
University of Hyderabad
Hyderabad 500 046
India**

April 2012



Curcumin, biologically active ingredient extracted from turmeric (Curcuma Longa) exhibit diverse pharmacological activities: antioxidant, anti-inflammatory, anti-HIV to anti-cancer activities. Curcumin was first isolated in 1842 By Vogel and then structure was determined by Milobedzka in 1910. It was synthesized by Lampe in 1918. First crystal structure of curcumin was determined by X-ray diffraction in 1982. In 2011 two new polymorphs and one amorphous phase was discovered by Sanphui et. al. Chem. Commun 2011, 47, 5013-5015.

DEDICATION

This Thesis is

Dedicated to my beloved Parents and Teachers



CERTIFICATE

This is to certify that the thesis entitled **“Physicochemical Property Improvement of a Few Active Pharmaceutical Ingredients by Solid Form Screening”** submitted by **Palash Sanphui** bearing Reg. No. CH07PH14 in partial fulfilment of the requirements for the award of Doctor of Philosophy in Chemistry is a bonafide work carried out by him under my supervision and guidance.

The thesis has not been submitted previously in part or in full to this or any other University or Institution for the award of any degree or diploma.

Dean
School of Chemistry

Prof. Ashwini Nangia
Thesis Supervisor

DECLARATION

I **Palash Sanphui** hereby declare that this thesis entitled “**Physicochemical Property Improvement of a few Active Pharmaceutical Ingredients by Solid Form Screening**” submitted by me under the guidance and supervision of **Prof. Ashwini Nangia** is a bonafide research work. I also declare that it has not been submitted previously in part or in full to this University or any other University or Institution for the award of any degree or diploma.

Name: **Palash sanphui**

Date:

April 2012

Hyderabad

Signature of the Student

Regd. No. 07CHPH14

ACKNOWLEDGEMENT

It is my immense pleasure to express my sincere gratitude to my Ph. D. supervisor **Prof. Ashwini Nangia**, for his constant cooperation, encouragement, kind guidance and for introducing me to this interesting research field. It has been great pleasure and fortune to work with him. I am also indebted to him for the work freedom he has given me during my Ph D tenure.

I would like to thank the Prof. M. V. Rajasekharan, Dean, School of Chemistry, and former Deans, for their constant inspiration and allowing me to avail the available facilities.

I am extremely thankful individually to all the faculty members of the School of Chemistry, Mr. Nageshwar Rao of Central Instrument Laboratory (CIL) and non teaching staff for their various help and cooperation on various occasions.

I wish to record my thanks to UGC for fellowship support. I also would like to thanks the DST and INSA programme for funding my visit to Madrid, Spain to attend IUCR **2011** conference.

I am deeply indebted to all my teachers starting from my elementary school to M. Sc., especially Dilip Sir, Asit sir, Prof. Niloy Gayen, Prof. Kalaynmoy Ganguli, Prof. R. P. Sarkar, Prof. Jayanta Kumar Ray, Prof. Amit Pathak, Prof. K. Biradha and Prof. Amit Basak for their wonderful teaching and education throughout my academics.

I would like to acknowledge my lab seniors Dr. Saikat Roy, Mr. Sreekanth Chandran, Dr. N. Jagadeesh Babu and Dr. Bipul Sarma, Dr. Ranjit Thakuria and Dr. Nabakamal Nath for their help and encouragement at various stages of my Ph. D. My sincere thanks to my labmates Surya, Rajesh, Kalyan, Maddileti, Sudalai, Geetha, Suresh, Kanishka, Sumanth, Uday, Sreenu, Kishore Swarupa and Narshima for maintaining a friendly and cooperative atmosphere in the lab.

Words are not enough to express my appreciation, gratitude and earnest feelings to my friend Tamal, Debudyuti and Snigdha for giving me their constant support and

encouragement throughout my Ph.D carrier. My pleasant association with some close friends in UOH such as Dinesh, Satyajit, Sudhanshu, Ritwik, Sandip, Anup, Santanu, Nayan, Raja, Naren, Mehaboob, Manajit, Rudra, Sugata is unforgettable. I would like to acknowledge few of my beloved seniors in UOH, Dr. Moloy, Dr. Rahul, Dr. Tejender, Dr. Prashanta, Dr. Tanmoy, Dr. Sushanta, Dr. Tapta Kanchan, Dr. Ravi, Dr. Rajesh, Dr. Pradip, Dr. Abhijit, Dr. Utpal, Dr. Suparna, Dr. Anindita, Dr. Raji, Dr. Bhaswati, Dr. Rumpa. I would also like to thank few of my friends in School of Chemistry Santosh, Sanghamitra, Soumya, Gupta, Hariprasad, Bala, Tirupati, Anji, Bhuban, Venu, Sajna, Ramsuresh, Sutanuka, Shaktidevi, Tridib, Sanjib, Ganesh, Krishna, Biju, Tulika, Nagarjuna, Swami, Arindam, Sandeep, Malkappa, Mousumi, Shuvra, Ganesh, Prabeen, Anand, Kishore, Prabhu Chaitanya, D. K., Ramu, Vikram, Srinivas, G. D. P, Rambabu, Poulami, Monima, Sridevi, Bharat, Kishore, Supratim, Pramiti, Chandu, Sudheer and Rajagopal. I would like to thank my M. Sc and B. Sc seniors and friends Ashutoshta, Lalitda, Madhushridi, Ram, Suman, Subrata, Supriyo, Palash, Arup, Joydeb, Nitai, Arnab, Shubhankar, Saunak, Aritro, Tulika, Papia, Sraboni, Joyati, Krishanu, Poulami, Joyeeta and Debasree

I thank my Brother in laws Sadhanda, Joydebda, Sandhyadi, Momotadi, Chhayadi, Mayadi and nice Swagata, Keya, Shreya, Shanti, Sathi and Akash for their support and encouragement.

The blessings and best wishes of my parents keep me active throughout my life. They made me what I am and I owe everything to them. Dedicating this thesis to them is a minor recognition for their invaluable support and encouragement.

Palash Sanphui

SYNOPSIS

This thesis entitled **“Physicochemical Property Improvement of a Few Active Pharmaceutical Ingredients by Solid Form Screening”** consists of eight chapters.

CHAPTER ONE

Introduction

Solid-state chemistry deals with the synthesis, structure, and properties of solid phase materials. It is well established that the physical properties of a solid depend not only on the molecule, but also on the ways in which the constituent molecules interact in the bulk phase through non-covalent interactions, notably hydrogen bonds. An understanding of the factors that determine crystal packing arrangement and the role of physicochemical properties is a challenging topic. Pharmaceutical chemists generally prefer to deliver crystalline forms (as tablets and capsules) of the active drug, mainly due to their inherent stability and high purity. These crystalline forms can be polymorphs, solvates/hydrates, salts and cocrystals. Again amorphous phases with short range order are sometimes useful because of their higher solubility than crystalline forms. The importance of new solid forms originates from the fact that they can exhibit a range of diverse biopharmaceutical properties e.g. solubility, stability, bioavailability, hygroscopicity, tableting, etc. Selection of the most suitable forms in terms of superior physicochemical properties is mostly favored for formulation purpose. This exercise requires inputs about crystallization, pharmacology and formulation.

The ability of a compound to exist in more than one crystalline modification is known as polymorphism, a phenomenon of tremendous importance in pharmaceutical development and materials science as one can tune the physical and chemical properties of substances. It is therefore important to know the best crystalline modification of active pharmaceutical ingredients (APIs) to enable a stable and soluble drug formulation. The screening of an API for all possible crystalline forms, by subjecting it to various crystallization conditions is of utmost importance. Even though metastable forms exhibit better solubility due to their higher free energy, they are not useful for drug formulation unless stabilized by polymers, excipients, additives etc.

Cocrystal is a multi-component assembly of two or more solids, generally in a definite stoichiometric ratio (at ambient conditions) interacting through non-covalent interactions; usually hydrogen bonds. At present, cocrystals of APIs are receiving increased attention from the scientific communities in academic, industry, and regulatory agencies, and several studies have discussed promising results concerning the improvement of biopharmaceutical properties. Moreover, such new solid phases of drugs may overcome problems in formulation and manufacturing. More than 50% APIs are formulated as salt form because of their high aqueous solubility. But for toxicological reasons only about 12 and so acidic or basic counterions are explored in a typical API salt screen. The availability of a large pool of molecules classified under the GRAS list as approved by the FDA increases the diversity of the compounds that can be rationally selected to form pharmaceutical cocrystals. Cocrystals are particularly relevant for APIs lacking ionizable functional groups to improve solubility and dissolution rate. They are preferable over salts because ionic species are more prone to be hygroscopic. Other important applications of cocrystals are isolating stereoisomer from racemic mixture, modifying the crystal structure for better tableting properties and inhibiting phase transformation between polymorphs.

CHAPTER TWO

Phase Transformation in Conformational Polymorphs of NSAID Nimesulide

Nimesulide is a nonsteroidal anti-inflammatory drug (NSAID) and a COX-2 inhibitor. The native crystal structure of Nimesulide (or form I) has been characterized by X-ray powder diffraction lines whereas full 3D coordinates are known for a second polymorph (form II). A detailed structural characterization and phase stability of nimesulide polymorphs was carried out. Rod like crystals of Form I (space group $Pca2_1$, number of symmetry-independent molecules, $Z' = 2$, A and B) were crystallized from EtOH concomitantly with Form II ($C2/c$, $Z' = 1$). These conformational polymorphs have different torsion angles at the phenoxy and sulfonamide groups. The crystal structures are stabilized by N-H \cdots O hydrogen bonds and C-H \cdots O, C-H $\cdots\pi$ interactions. The packing diagram for the two polymorphs shows a tape sequence of N-H \cdots O $_2$ N hydrogen bond as XYYX in form I and XYXY in form II, viewed along the b-axis (Figure 1).

Phase transition from the metastable form (II) to the stable modification (I) was studied using DSC, HSM, solid-state grinding, solvent-drop grinding, and slurry crystallization. The phase transition was monitored by IR, Raman and ss-NMR spectroscopy, and XRPD and single crystal X-ray diffraction. The stable polymorph I was obtained in excess during solution crystallization, grinding and slurry methods. Intrinsic dissolution and equilibrium solubility experiments show that the metastable form II dissolves much faster than the stable form I in pH 7 buffer.

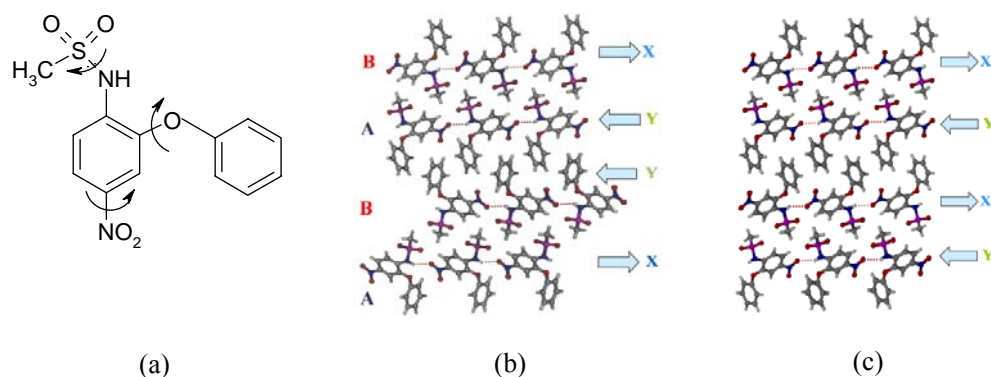


Figure 1 Flexible torsions in (a) Nimesulide and packing differences between (b) form I and (c) form II.

CHAPTER THREE

New Polymorphs of Curcumin and their Faster Dissolution

Curcumin, a hydrophobic phenol, is the principal curcuminoid in the popular Indian dietary spice turmeric. It is derived from the rhizome of the herb *Curcuma longa*. Curcumin is known for its wide-ranging pharmacological activity such as an antioxidant, antimalarial, anti-carcinogenic, anti-HIV agent, etc. Curcumin is safe even at high dose of 12 g/day in animal and human experiments. Despite its efficacy and safety, curcumin is not approved as a therapeutic agent because of poor absorption and bioavailability, and rapid metabolism and systematic elimination. The crystal structure of stable form 1 ($P2_1/n$, $Z'=1$) of curcumin is reported. During attempted cocrystallization experiments of curcumin, two new polymorphs, form 2 ($Pca2_1$, $Z'=2$) and form 3 ($Pbca$, $Z'=1$) were obtained in the presence of 4-hydroxypyridine and chrysin respectively. A new

amorphous phase was obtained from melt crystallization. Three crystalline polymorphs and one amorphous phase of curcumin are displayed in the Figure 2. Form 2 dissolved 3.1 times faster than commercial form 1 in 40% EtOH-water medium.



Figure 2 Three crystalline polymorphs and one amorphous phase of Curcumin

CHAPTER FOUR

Fast Dissolving Curcumin Cocrystals

Curcumin is the principal curcuminoid of the popular Indian spice turmeric. Despite the diverse pharmacological activities of this bioactive phenol, its application as a drug is severely limited by poor aqueous solubility. We report novel cocrystals of curcumin (**1**) with resorcinol and pyrogallol obtained by liquid-assisted grinding. Curcumin–resorcinol (**1a**) (1:1) and curcumin–pyrogallol (**1b**) (1:1) were characterized by X-ray diffraction, thermal analysis, FT-IR, FT-Raman, and ss-NMR spectroscopy. The 1:1 cocrystal stoichiometry is sustained by O–H \cdots O hydrogen bonds between the phenolic OH groups of the coformers to the carbonyl group of curcumin. The melting point of the cocrystals is in between that of curcumin and the coformer and the lower melting cocrystal **1b** is more soluble than higher melting **1a**. The dissolution rates of

curcumin-resorcinol (**1a**) and curcumin-pyrogallol (**1b**) in 40% EtOH–water are ~5 and ~12 times faster than that for curcumin (Figure 3).

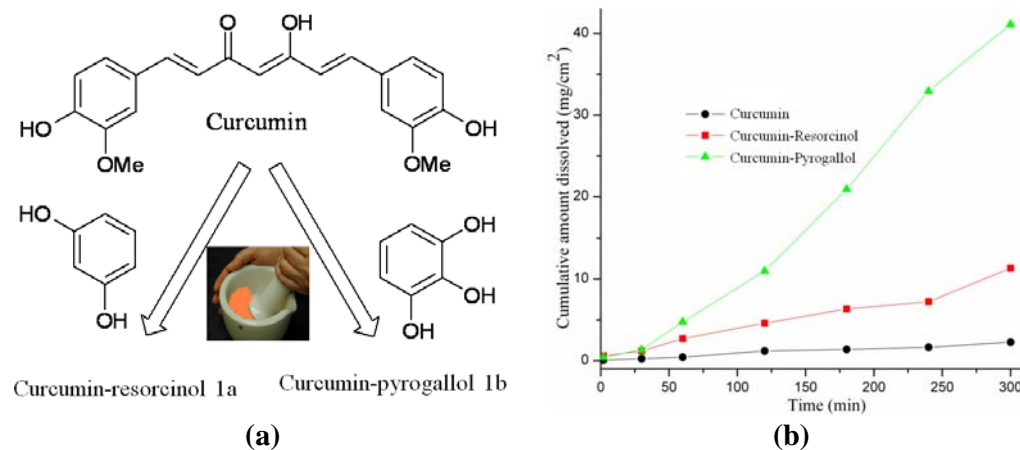


Figure 3 (a) Two novel cocrystals of curcumin with resorcinol and pyrogallol. (b) IDR experiments of cocrystals 1a and 1b compared to stable Form 1 indicates higher solubility compared to native Curcumin.

CHAPTER FIVE

Crystal Engineering of Stable Temozolomide Cocrystals

The antitumor prodrug Temozolomide (TMZ) decomposes in $\text{pH} \geq 7$ aqueous medium but is relatively stable in acidic conditions. Pure TMZ obtained as a white powder turns pink and then of brown color which is indicative of chemical degradation. Pharmaceutical cocrystals of TMZ were engineered with safe coformers (generally recognized as safe, GRAS chemicals) such as oxalic acid, succinic acid, salicylic acid, anthranilic acid, D,L-malic acid, D,L-tartaric acid, etc. to stabilize the drug as a cocrystal (Figure 4). All cocrystals were characterized by FT-IR, FT-Raman, powder X-ray diffraction (PXRD), and single crystal X-ray diffraction. Temozolomide cocrystals with organic acids in the pK_a range 2–6 were found to be more stable than the reference drug in physiological conditions. The half-life ($T_{1/2}$) of TMZ–oxalic and TMZ–salicylic acid is two times longer than TMZ (3.5 and 3.6 h vs. 1.7 h), and TMZ–succinic acid, TMZ–tartaric acid and TMZ–malic also exhibited longer half life (2.3, 2.5, 2.8 h) in pH 7 buffer medium, indicating that cocrystals are more stable compared to the reference

drug. The intrinsic dissolution rate (IDR) profile of TMZ–oxalic acid and TMZ–succinic acid cocrystals is comparable to that of TMZ whereas cocrystals with malic acid and salicylic acid dissolved faster than TMZ. Among the Temozolomide cocrystals examined, those with succinic acid, oxalic acid and salicylic acid exhibited improved stability and comparable or faster dissolution rate than the reference drug. Even TMZ-succinic acid cocrystals are stable in accelerated humidity conditions (40°C and 75% RH) upto 28 weeks, whereas TMZ transformed to hydrate after 2 weeks and then converted to decomposed AIC hydrate after 5 weeks, confirmed from PXRD (Figure 5).

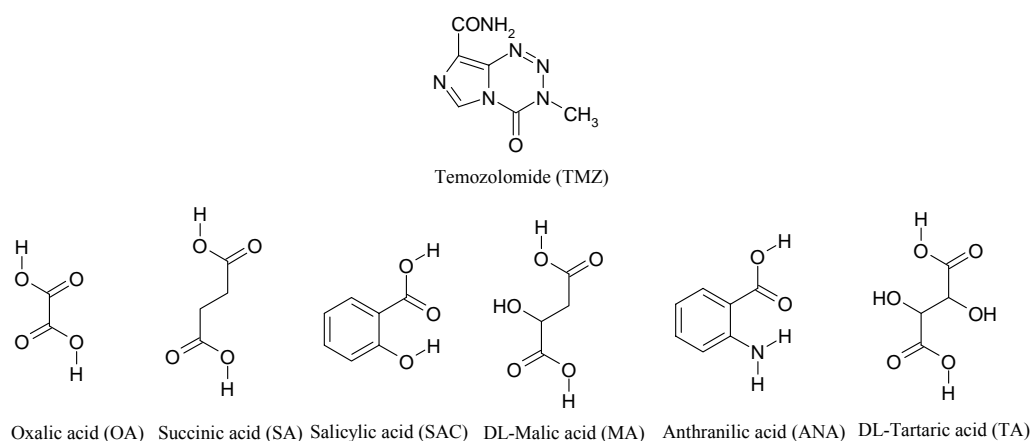


Figure 4 Chemical structures of antitumor prodrug TMZ and GRAS coformers organic acid used as pH adjuster.

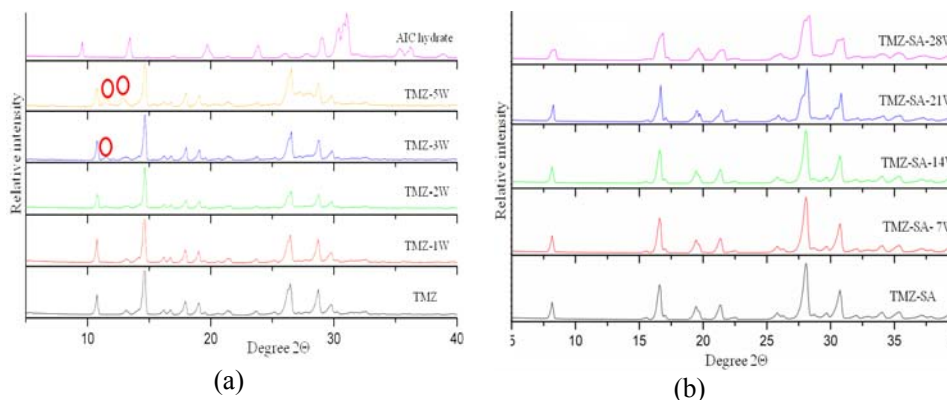


Figure 5 XRPD stack of TMZ and (b) TMZ–SA cocrystals kept at 40 °C and 75% RH, indicates that cocrystals is stable without degradation to TMZ or decomposed AIC even

after 28 weeks, but TMZ transformed to monohydrate within 2 weeks and started to decompose within 5 weeks.

CHAPTER SIX

Pharmaceutical Cocrystals of Niclosamide

Niclosamide (NCL, Figure 6) is an anthelmintic BCS class II drug having low solubility, but high permeability. To improve the solubility of niclosamide, pharmaceutical cocrystals were prepared with GRAS molecules e.g. caffeine (CAF), urea (URE), p-aminobenzoic acid (PABA), theophylline (THPH), nicotinamide (NCT) and isonicotinamide (INA) etc. Neat grinding, wet-ganulation and slow evaporation methods were employed to synthesize niclosamide cocrystals. All the crystalline forms were characterized by FT-IR, X-ray diffraction to confirm purity of the bulk phases. Crystal structures of niclosamide and its cocrystals were characterized by single crystal X-ray diffraction to know the structural aspects and hydrogen bonding in the molecular structure. The presence of intermolecular O–H···O hydrogen bond from hydroxyl to carbonyl group in niclosamide was replaced by acceptor atom of coformer in the cocrystalline phases. Cocrystals with nicotinamide and isonicotinamide were further characterized by ^{13}C ss-NMR spectroscopy. All the cocrystals, except NCL–PABA, showed better powder dissolution rate than the reference API. Niclosamide–theophylline acetonitrile (NCL–THPHS) complex showed highest dissolution rate among all crystalline forms (Figure 7). But acetonitrile is a class II solvent of limited toxicity and permissible concentration limit of 410 ppm in drugs. Comparatively NCL–THPH cocrystals showed moderate solubility and stability against hydration. Equilibrium solubility measurement showed that all the niclosamide cocrystals along with API converted to monohydrate within 24 h slurry experiment in 40% isopropanol-water medium.

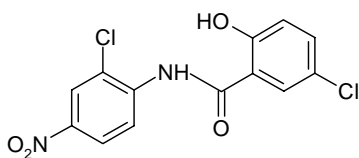


Figure 6 Chemical structure of niclosamide

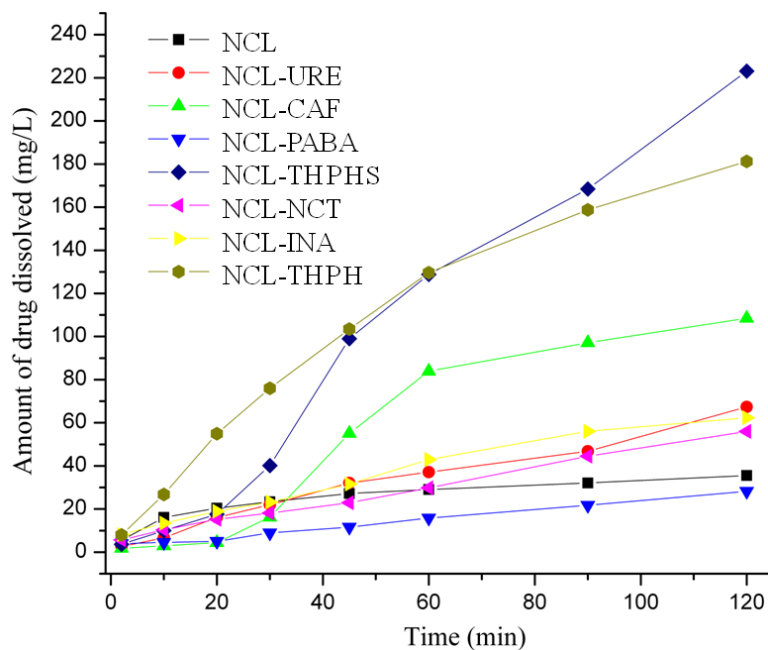


Figure 7 Dissolution curves of niclosamide and its cocrystals

CHAPTER SEVEN

High Solubility Piperazine Salts of NSAID Meclofenamic Acid

Meclofenamic acid (MFA, Figure 8) is the most potent anti-inflammatory drug among the fenamic acids. In this thesis are presented (1) two cocrystals of MFA with isonicotinamide (INA) and 4,4'-bipyridine (BPY); (2) polymorphs of MFA and piperazine (PPZ) 1:1 salt (orthorhombic $P2_12_12_1$ and monoclinic $P2_1/c$), MFA–PPZ 1:1:1 salt hydrate, MFA–PPZ 2:1 salt; and (3) MFA and 2-aminopyridine (2-APY) 1:1 salt, MFA and 4-aminopyridine (4-APY) 1:1:1 salt hydrate. Sublimation of meclofenamic acid gave single crystals for X-ray diffraction which provided good quality data for refinement and all atomic coordinates. The cocrystal and salt structures are assembled via neutral $O-H\cdots O$, $O-H\cdots N$, $N-H\cdots O$, $N-H\cdots N$ and ionic $O-H\cdots O^-$, $N^+-H\cdots O^-$ hydrogen bonds. The disorder of methyl group in meclofenamic acid crystal structure is absent in the cocrystal and salt structures, which contain different conformers (A or B) of methyl group orientation. The solubility of meclofenamic acid–isonicotinamide (1:1) and meclofenamic acid–4,4'-bipyridine (1:0.5) cocrystals is 2.9 and 7.6 times higher than that

of MFA at 37 °C in 50% EtOH–water. Interestingly, MFA–PPZ 1:1 salt and its 1:1:1 hydrate are 2724 and 1334 fold more soluble than meclofenamic acid. Both these salts transformed in 50% EtOH–water slurry at 37 °C to 2:1 MFA–PPZ salt after 24 h, which in turn transformed to meclofenamic acid after another 24 h of slurry stirring. Remarkably, the dissolution rate of MFA–PPZ (1:1) salt in water is just slightly lower than that of marketed sodium meclofenamate.

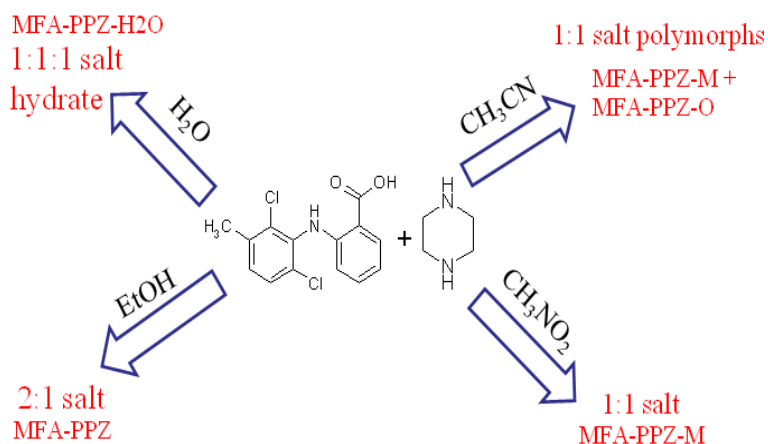


Figure 8 Different stoichiometric piperazinium meclofenamate salts obtained by liquid-assisted grinding.

CHAPTER EIGHT

Conclusion and Future Prospects

More than 40% of the marketed drugs failed to satisfy minimum solubility criteria (>100 mg/L) and 60-70% API are in the pipeline never brought to the market because of their low solubility issue. Dosage form modifications through polymorphs, amorphous phases or cocrystals/salts can be alternate formulation for poor soluble APIs. Polymorphs and cocrystals have enormous importance in pharmaceutical field because of their different physicochemical properties, e.g. solubility, stability and bioavailability etc. Generally solubility ratio of fast to slow dissolving polymorphs is 2-4 times, whereas cocrystals can improve solubility by 4-20 times than the API. Again salt is more soluble than cocrystals, but salts are more prone to be hygroscopic than cocrystals. For API

having no ionizable (acid/base moieties) functional groups, cocrystals is a logical option to improve physical properties without altering the chemical structure. The crystallization of metastable polymorphs of nimesulide and curcumin obtained during attempted cocrystallization experiments and as expected metastable forms of higher solubility are discussed in Chapter 2 and 3. Novel pharmaceutical cocrystals of low soluble herbal spice curcumin and APIs e.g. temozolomide and niclosamide and their better solubility and stability improvement than the reference API were discussed in Chapter 4, 5 and 6. It is possible to tune both solubility and stability of an API via cocrystals in the same solid form. Chapter 7 deals with both cocrystals and salts of NSAID meclofenamic acid and much better solubility of piperazine salts compared to cocrystals and reference API.

Stabilizing the metastable form and amorphous phase of API by addition of polymer, excipients etc. are an alternative to solubility manipulation. Nutraceutical is a food or food product that reportedly provides health and medical benefits, including the prevention and treatment of chronic disease in addition to the basic nutritional value found in foods. Resveratrol (grapes), flavanoids e.g. catechin (green tea), quercetin (fruits), ellagic acid (strawberries), caffeine (coffee), theobromine (dark chocolates), anthocyanins (berries), citric acid (lemon), Curcumin (turmeric), pyrogallol (amla) are well known nutraceuticals. Nutraceutical foods exhibit generally low solubility, and hence poor bioavailability and difficult to formulate as tablets or capsules. For e.g. Curcumin (8.7 mg/L), resveratrol (30 mg/L), quercetin (2 mg/L) are poorly soluble nutraceuticals. Aqueous solubility of these Nutraceuticals could be enhanced by particle size reduction, lyophilization, micelles, additives, and also new crystalline forms such as polymorphs, salts, or cocrystals.

CONTENTS

Certificate	v
Declaration	vii
Acknowledgement	ix-x
Synopsis	xi - xx

Chapter One

Introduction	1-32
1.1 Solid State Chemistry.....	3
1.2 Solid form of Active Pharmaceutical ingredients.....	4
1.2.1 Polymorphs.....	5
1.2.2 Thermodynamic relationships in Polymorphs.....	9
1.3 Multi-component systems.....	12
• Host-guest compounds, salts and cocrystals.....	12
1.3.1 Pharmaceutical cocrystals.....	14
1.3.2 Pharmaceutical salts.....	15
1.4 Solubility and dissolution rate.....	16
1.4.1 Type of dissolution.....	18-20
• Planar Surface Dissolution	
• Intrinsic Dissolution rate	
• Powder dissolution	
1.4.2 Spring and Parachute model.....	22
1.5.2 Stability issue of pharmaceutical cocrystals.....	24
1.6 References.....	27

Chapter Two

Phase Transformation in Conformational Polymorphs of NSAID Nimesulide	33-64
2.1 Introduction	35
2.2 Type of polymorphs.....	36
2.2.1 Methods of crystallization of polymorphs.....	37
2.3 Problems of choosing best solid form.....	39

2.4	Nimesulide.....	39
2.5	Result and discussion.....	40
2.5.1	Crystal structural analysis.....	41
2.5.2	Powder X-ray diffraction.....	44
2.5.3	Thermal analysis.....	45
2.5.4	Grinding and slurry experiment.....	48
2.5.5	FT-IR, FT-Raman and ss-NMR spectroscopy.....	49
2.5.6	Solubility study of nimesulide polymorphs.....	53
2.6	Conclusion.....	55
2.7	Experimental section.....	56
2.8	References.....	59

Chapter Three

New Polymorphs of Curcumin and their Faster Dissolution rates		65-98
3.1	Introduction.....	67
3.2	Curcumin.....	69
3.3	Problems and promises of Curcumin.....	70
3.4	Results and discussion.....	71
3.4.1	X-ray crystals structure solution and refinement.....	72
3.4.2	Characterization of new solid forms.....	78
3.4.2.1	Powder X-ray diffraction.....	78
3.4.2.2	Thermal Analysis.....	79
3.4.2.3	FT-IR and FT-Raman spectroscopic analysis.....	81
3.4.2.4	Solid state NMR spectroscopy.....	83
3.4.3	Solubility and dissolution study of curcumin polymorphs.....	85
3.4.4	Conclusion.....	89
3.5	Experimental Section.....	90
3.6	References.....	93

Chapter Four

Fast Dissolving Curcumin Co-crystals	99-130
---	---------------

4.1	Introduction.....	101
4.2	Curcumin.....	103
4.3	Results and discussion.....	104
4.3.1	Crystal structure analysis.....	105
4.3.2	Thermal analysis.....	110
4.3.3	Powder X-ray diffraction.....	111
4.3.4	FT-IR, FT-Raman and ss-NMR spectroscopy.....	113
4.3.5	Dissolution experiments.....	117
4.3.6	Conclusion.....	123
4.4	Experimental section.....	123
4.5	References.....	126

Chapter Five

Crystal Engineering of stable Temozolomide Cocrystals 131-166

5.1	Introduction.....	133
5.2	Temozolomide.....	135
5.3	Cocrystals of Temozolomide with acid partners.....	138
5.3.1	Crystal structure analysis.....	141
5.4	FT-IR spectroscopy.....	152
5.5	Hydrolytic stability and dissolution rate.....	152
5.6	Conclusion.....	160
5.7	Experimental Section.....	161
5.8	References.....	163

Chapter Six

Pharmaceutical Cocrystals of Niclosamide 167-196

6.1	Introduction.....	169
6.2	Niclosamide.....	170
6.3	Result and discussion.....	172
6.3.1	Crystal structure description.....	172
6.3.2	Powder X-ray diffraction.....	179

6.3.3	Thermal stability of niclosamide and its cocrystals.....	181
6.3.4	FT-IR spectroscopy.....	182
6.3.5	Solid state NMR spectroscopy.....	184
6.3.6	Solubility of niclosamide and its cocrystals.....	185
6.3.7	Relative humidity study.....	188
6.4	Conclusion.....	192
6.5	Experimental section.....	192
6.6	Reference.....	194

Chapter Seven

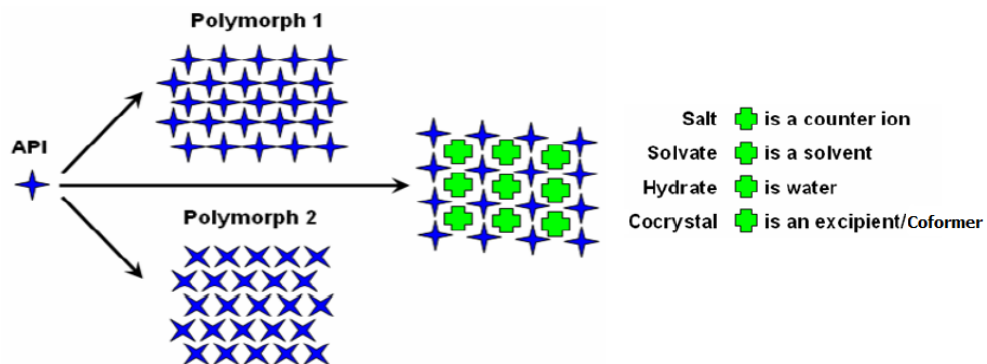
High solubility Piperazine Salts of NSAID Meclofenamic Acid		197-230
7.1	Introduction.....	199
7.2	Meclofenamic acid.....	200
7.3	Results and Discussion.....	201
7.3.1	Crystal Structure description.....	201
7.3.2	Powder X-ray diffraction.....	213
7.3.3	Thermal Analysis.....	214
7.3.4	FT-IR Spectroscopy.....	215
7.3.5	Solid State NMR Spectroscopy.....	216
7.3.6	Solution Mediated Phase Transformation.....	217
7.3.7	Solubility and Dissolution Experiments.....	221
7.4	Conclusion.....	224
7.5	Experimental Section.....	224
7.6	References.....	227

Chapter Eight

Conclusion and Future Prospects		231-242
About the Author.....		245
List of Publications.....		247

Chapter One

Introduction



Multiple crystalline solid-state forms of an active pharmaceutical ingredient; blue symbol is API and green symbol is second component, which may be neutral (crystalline solid, cocrystals, solvates, hydrates) or ionic state (salt).

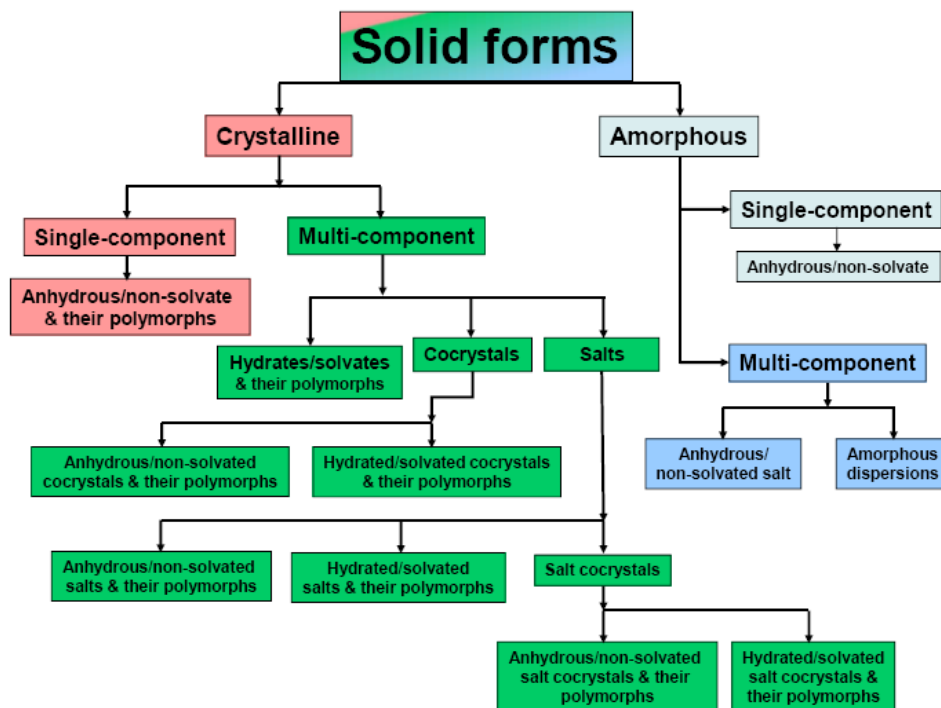
“Probably every substance is potentially polymorphic. The only question is whether it is possible to adjust the external conditions in such a way that polymorphism can be realized or not.” Maria Kuhnert-Brandstätter, *Pharm. Z.* **1975**, *4*, 131.

1.1 Solid State Chemistry

Solid State Chemistry is the study of the synthesis, structure, and properties of solid phase materials. It has a strong overlap with Physics, mineralogy, crystallography, ceramics, metallurgy, thermodynamics, materials science and electronics with a focus on the synthesis of novel materials and their characterization. The design of organic crystalline materials requires understanding of non-covalent interactions between molecules. There have been major advances in solid state and materials chemistry in the last two decades and contributed that are an integral part of life.¹ The properties of a crystalline solid depends not only on the constituent molecules, but also on their interactions in the crystal lattice. An understanding of the factors that determine crystal packing arrangement and the role of physicochemical properties is a challenging topic. Solid state chemistry is concerned with the development of new methods of synthesis, identifying and characterisation of new materials by advanced techniques for the control of useful properties.²

Active pharmaceutical ingredients (APIs) are frequently delivered to the patient in the solid-state as part of dosage forms³ (e.g. tablets, capsules, granules, powders, etc) because of their easy uptake in the bodies. No matter whether as pure drug substances or in formulated products, APIs can exist in various solid forms, such as polymorphs, pseudopolymorphs (solvates and hydrates), salts, co-crystals and amorphous solids. Polymorphs are possible for each of these solid forms (Scheme 1).^{2d} Along with crystalline materials, amorphous solids having short range order of periodicity, are also important in drug development because of their high free energy and hence solubility. Each form may possess its own unique mechanical, thermal, physical and chemical properties that can remarkably affect the solubility, bioavailability, hygroscopicity, melting point, stability, compressibility and other performance characteristics of the drug.^{2c} A thorough understanding of the relationship between the particular solid form and its functional properties are crucial for selecting the most suitable form of the API

for scale up, formulation activities, clinical trials and finally manufacturing. This exercise requires inputs about crystallization, pharmacology and formulation.



Scheme 1 Schematic representation of the structures of solid forms of APIs and for each solid form there is a possibility of polymorphs, culled from ref. 2d.

1.2 Solid forms of Active pharmaceutical Ingredients

At present nearly 40% of the new chemical entities being discovered have poor water solubility drugs, which is a serious drawback for drug formulation and so many new potential drugs fail in the formulation stages because of poor aqueous solubility. More than 80% drugs are marketed as solid formulations and 90% of them are crystalline in nature. Remaining 10% are marketed as gel, injected form etc. An enhancement of drug solubility of therapeutic agents can possibly improve their bioavailability. Identifying the optimum solid form of an active pharmaceutical ingredient (API) is always desirable for clinical use.⁴ Frequently, the API exhibits low solubility, and it might be appropriate to use its more soluble amorphous phase or a more soluble multicomponent form, such as a salt form – for ionizable APIs – or cocrystal form for neutral APIs. Furthermore, APIs are typically amenable to formation of multiple component crystals such as solvates and hydrates.

1.2.1 Polymorphs

Polymorphism⁵ is defined as the ability of a compound to exist more than one crystalline arrangement in the solid state. Polymorph is a solid crystalline phase of a given compound resulting from the possibility of at least two different crystalline arrangements of the molecule of that compound in the solid state (McCrone 1965). The number of crystalline forms or polymorphs of a compound are proportional to the time and resources dedicated to investigate to them (McCrone 1963). Allotropes and polymorphs are closely related. Polymorphism is used in general to refer to structural diversity of molecular compounds, whereas allotropy is the structural diversity of elements. For example, carbon has four allotropes diamond, graphite, fullerene and carbon nanotube.^{5e} The carbon atom is the same in four crystal structures; however the arrangement of atoms is different in different crystal structures, which consequently lead to the differences in their properties like hardness and conductivity (Figure 1). Polymorphs may have different conformations (conformational polymorphism), packing (packing polymorphism) and supramolecular synthons (synthon polymorphism) in the crystal lattice.⁶ The different types of polymorphs has been displayed in Scheme 2. Conformationally flexible molecules have greater scope for polymorphic occurrence because of large number of degrees of freedom as the energy differences between conformational polymorphs generally lies in a small energy window of 0.5-3 kcal mol⁻¹. A metastable conformation may be stabilized by stronger hydrogen bonds in the crystal structure while a stable conformer may not be able to form strong hydrogen bonds. The overall stability of a polymorph is accounted by the conformation energy and lattice energy (total) for a given polymorphic system. The energy compensation towards overall energy minimization in a polymorphic system is referred to as ‘systematic effect’. This phenomenon was recently reviewed by Nangia^{6a} with several examples of conformational polymorphs. Polymorphism in drugs like nimesulide (chapter 2), furosamide, tolbutamide, ritonavir, chlortalidone and biologically active compound curcumin (chapter 3) are examples of conformational polymorphs.

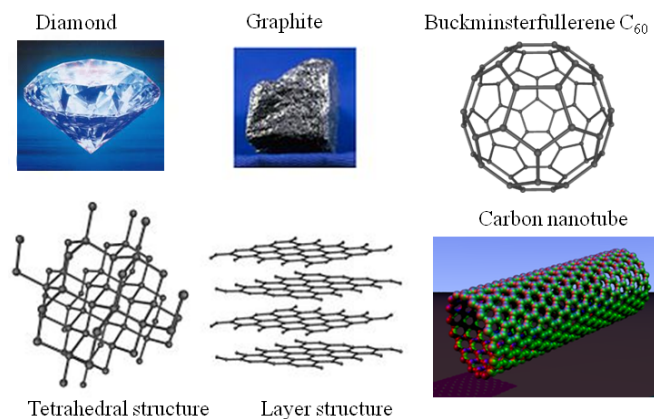
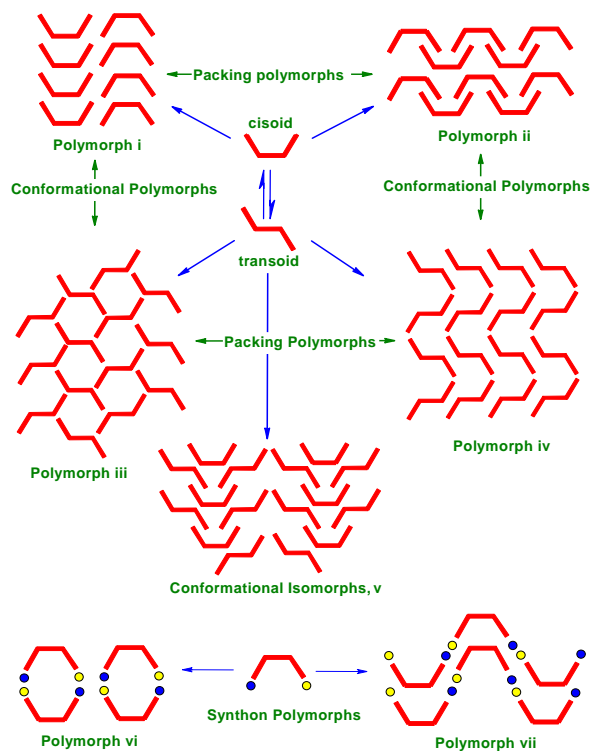


Figure 1 Four allotropes of carbon, graphite (layered), diamond (tetrahedron), buckminsterfullerene C₆₀ (spherical) and carbon nanotube (cylindrical structure) culled from ref. 5e.



Scheme 2 Schematic illustrations of different arrangements of molecules in the crystalline lattice that lead to different kinds of polymorphism, taken from ref. 6a.

Polymorphism in organic solids is of fundamental importance because of its ability to alter physicochemical properties in different crystal structures, such as melting

point, density, dipole moment, hardness, compressibility, solubility, dissolution rates and bioavailability.^{2c,7} These differences impact on drug formulation and processing of the drug, due to which it has received particular attention in pharmaceutical industry. Stability is an important concern while dealing with polymorphs. Because their energy differences are relatively small, form inter-conversion is common. For e.g. Antitumor prodrug temozolomide exists as three crystalline polymorphs (with 3D coordinates) as form 1, 2 and 3 and their stability order is form 1>form 2>form 3.^{6c} Grinding of metastable form 2 for half an hour in mortar pestle or in presence of small amount of acetonitrile transforms to stable form 1. The metastable nature of form 2 is ascribed to hydrogen-bonding differences in the two crystal structures. The amide syn NH moiety forms N–H···O hydrogen bonds in both structures. The anti NH moiety forms N–H···N hydrogen bonds in form 1, whereas the donor is not intermolecularly H-bonded in form 2 (Figure 2). Therefore risks of marketing a drug product without awareness and recognition of the thermodynamically most stable form are very high. Getting the right polymorph is not only important for drugs and pharmaceuticals but also for speciality chemicals like explosives, dyes, pigments, flavours and confectionery products. For example, anthelmintic drug mebendazole (Figure 3) exists in three polymorphic forms (A, B, C).⁸ Form A is the most stable polymorph, whereas form B and C are metastable ones. The solubility order of the three polymorphs in 0.03M hydrochloric acid is A<C<B. However, due to the increased toxicity of the highly soluble form B, form C is clinically preferred because its solubility is sufficient to ensure optimal bioavailability. This is important because polymorph A has no anthelmintic activity alone or when present above 30% in polymorphic mixtures. But form C has tendency to convert into stable inactive for A. So it is desirable to stabilize form C by additive, polymer, excipients or cocrystal coformers (CCF).⁹

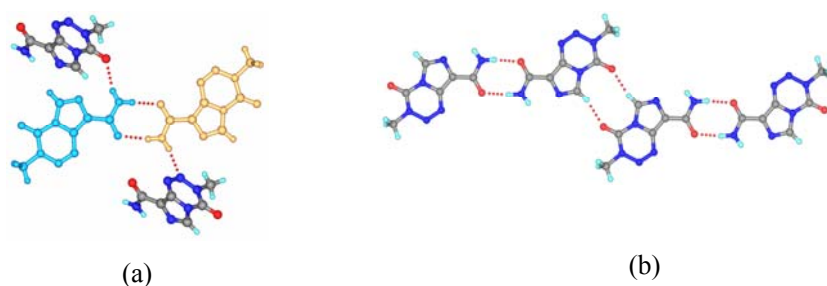


Figure 2 (a) The carboxamide dimer of crystallographic unique molecules (shaded differently) in TMZ Form 1. Anti N–Hs are involved in N–H···O and N–H···N bonds. (b)

N–H···O and C–H···O dimers assemble in a tape motif in form 2. The anti NH of CONH₂ makes only intramolecular hydrogen bond in this crystal structure (taken from ref. 6c).

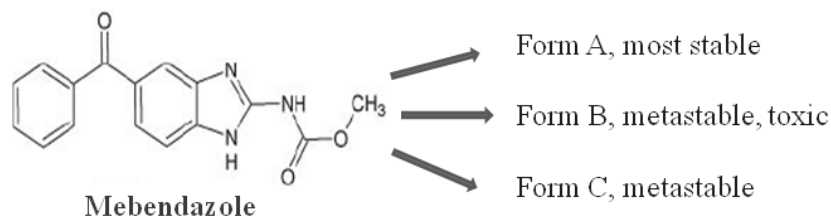
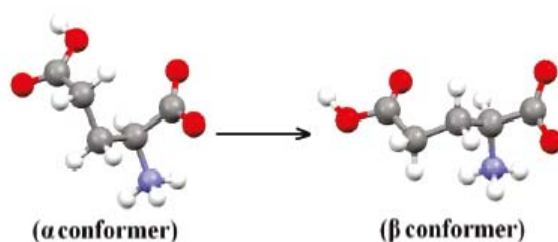


Figure 3 Three polymorphic forms of anthelmintic drug mebendazole, among them metastable form C is therapeutically active.

The transformation to the undesired polymorph may take place through a solvent mediated phase transformation¹⁰ during manufacturing process. On the other hand, recognition of such processes may lead to its utilization to obtain a desired polymorph. For example L-glutamic acid have two polymorphs; metastable α and stable β form (Scheme 3).¹¹ L-glutamic acid, later converted to the monosodium salt used for taste enhancement in food additive industry. It is crucial to obtain α polymorph rather β form. The latter can lead to a situation in which crystallization slurry coagulates into a gel and can no longer be processed.^{11b} Garti et al^{11c} showed the addition of selected surface active agents can lead to the preferential crystallization of the α polymorph of L-glutamic acid. Trimesic acid and transglutonic acid, which conformationally mimic α form of glutamic acid, selectively inhibit crystallization of β form and stabilize metastable α form.



Scheme 3 Polymorphic Transformation of L-Glutamic acid from Conformation α to β

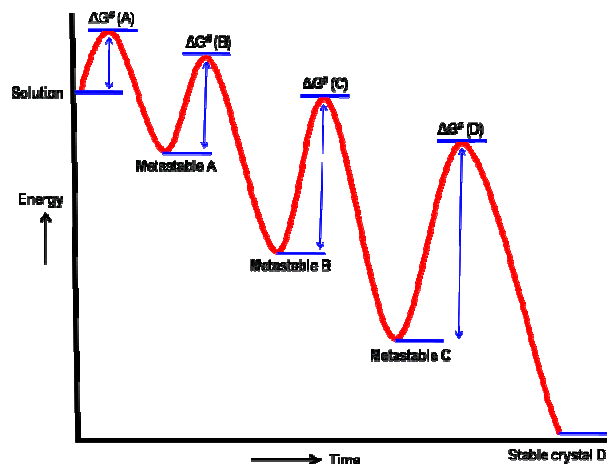
Drugs that were previously known to exist only one form are now shown to have various polymorphic forms. This has perplexed pharmaceutical companies and now they have investigated crystal polymorphism in order to optimize the physical properties of a pharmaceutical solid before the drug development. Otherwise late-stage phase

transitions to a new polymorph can become a big setback for the company like anti HIV drug ritonavir.¹² To obtain exclusively metastable forms are recent techniques such as, crystallization with structurally related additives, epitaxial growth, laser induced nucleation, crystallization in capillaries, confinement within porous materials, using polymers as heteronuclei, mechanical grinding, using supercritical liquids, gels etc..¹³ High-throughput crystallization screens have been developed using a combinatorial approach to capture crystal form diversity.¹⁴

1.2.2 Thermodynamic relationships in polymorphs

crystallization occurs in two processes, (i) nucleation and (ii) crystal growth. Although the exact mechanism of nucleation is not clear, a plausible mechanism is supported partly by some experimental evidence.¹⁵ From the thermodynamic point of view, a solution is an entropy-dominated situation and a crystal is largely the enthalpically determined outcome. In solution various clusters involving both solute molecules and solvent molecules are formed using intermolecular interactions. This brings elements of short range order in solution. These clusters are continuously breaking, forming and rearranging prior to nucleation stage. At supersaturation these clusters become larger in size and more short range order enters in the system. At this stage nucleation occurs either by homogeneous nucleation (no effect of any external factor) or by heterogeneous nucleation (effect due to foreign particle, physical disturbance, scratched surface of vessel etc.) and solvent molecules from solute-solvent clusters exit into the bulk solvent simultaneously forming the crystal, which is characterised by long range order.¹⁶

Ostwald rule¹⁷ states that a system moves to equilibrium from an initial high-energy state through minimal changes in free energy. Therefore the structure that crystallizes first is the one which has the lowest energy barrier (highest energy, kinetically metastable). This form would then transform to the next lower energy state until a thermodynamically stable state (lowest energy) is reached, the so-called Ostwald's Law of Stages (Scheme 1.4).



Scheme 1.4 Ostwald's Rule of Stages. Initial high-energy state (metastable A) through minimal changes in free energy crystallizes first and is the one which has the lowest energy barrier. Metastable form A will then transform to the next lower energy polymorph (metastable B) and so on (metastable C) until thermodynamically stable crystal D appears, culled from ref. 17.

From thermodynamic consideration polymorphic pairs can be divided as monotropic and enantiotropic systems.¹⁸ Monotropic systems are defined as systems where a single form is more stable than others regardless of temperature. Enantiotropic systems are defined as systems where the relative stabilities of the two forms invert at some transition temperature before melting. Again heat of transition rule suggest that if an endothermic phase change is observed at a particular temperature, the transition point lies below that temperature, and the two polymorphs are enantiotropically related. If an exothermic transition is observed, then there is no phase transition point below that transition temperature. This can occur when two forms are monotropically related or when they are enantiotropically related and the thermodynamic transition point is higher than the measured transition temperature. Heat of fusion rule states that in an enantiotropic system the higher melting polymorphs will have the lower heat of fusion. If the higher melting polymorph has a higher heat of fusion, the two are monotropically related.

Several analytical techniques are used to establish the thermodynamic behaviour of polymorphs, e.g. Optical and/ or Hot Stage Microscopy (HSM), Differential Scanning Calorimetry (DSC) etc. HSM can be used to obtain qualitative information on polymorphic behaviour by visualising the morphology change under optical microscope.

However thermal analysis (DSC or DTA) provides quantitative information about the relative stability of polymorphic modifications, the energies involved in phase changes between them and the monotropic and enantiotropic nature of those transitions. Tolbutamide, an oral hypoglycaemic agent exists in five polymorphic modifications.¹⁹ The thermogram of Form I^L showed two peaks; a small endotherm at 40 °C followed by another endotherm at 128 °C. The first peak was ascribed to a kinetically reversible polymorphic transition to Form I^H and the second peak corresponds to melting of Form I^H. Polymorph I^H is stable at high temperature and phase transition from polymorph II, III, and IV can clearly be described by DSC thermograms (Figure 4). Transitions II→I^H, III→I^H, IV→I^H show those polymorph pairs are enantiotropically related. Enantiotropic and monotropic relation between polymorphs in several instances are observed and discussed in Chapter 2 and 3. HSM, DSC and X-ray diffractions measurements are analyzed. Spectroscopic methods include Fourier Transformed Infrared (FT-IR), Near Infrared (FT-NIR) and Raman spectroscopy etc., thermal analysis (DSC, TGA, HSM etc) and finally X-ray diffractions (single crystal and powder X-ray diffraction) are generally used to characterization of polymorphs.

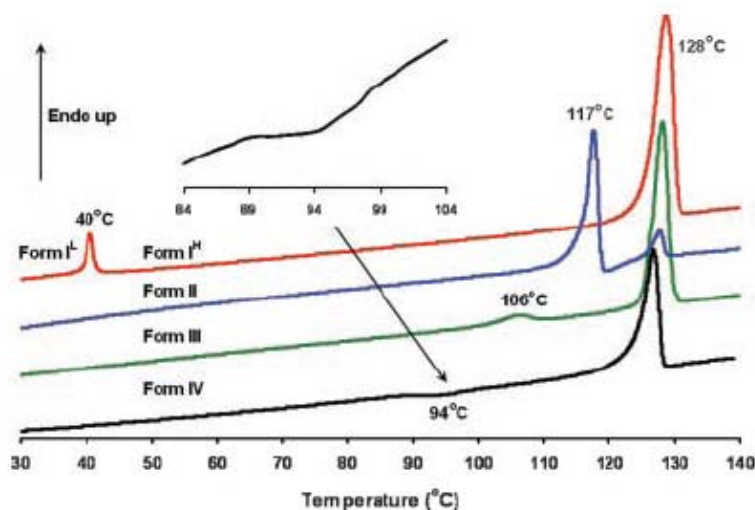


Figure 4 DSC thermogram of Tolbutamide polymorphs at heating rate of 10°/min. The polymorph conversions from other forms to form I (Ref. 19b).

Powder X-ray diffraction (PXRD) method is one of the most reliable methods for identification and characterization of polymorphs based on line profile by taking a safe threshold of $\Delta 2\theta > \pm 0.2^\circ$. Traditionally PXRD have been used for the qualitative

identification of individual polymorphic phases or mixture of phases and considered as fingerprint pattern. As polymorphs comprise different solids with different unit cells and different arrangements of the molecules within the unit cell they have different fingerprints. For e.g. Chlorpropamide, anti-diabetic drug crystallizes as five polymorphs; α , β , γ , δ and ϵ .²⁰ The PXRD of five polymorphs of chlorpropamide showed clear indication of at least five different solid phases of the API (Figure 5).

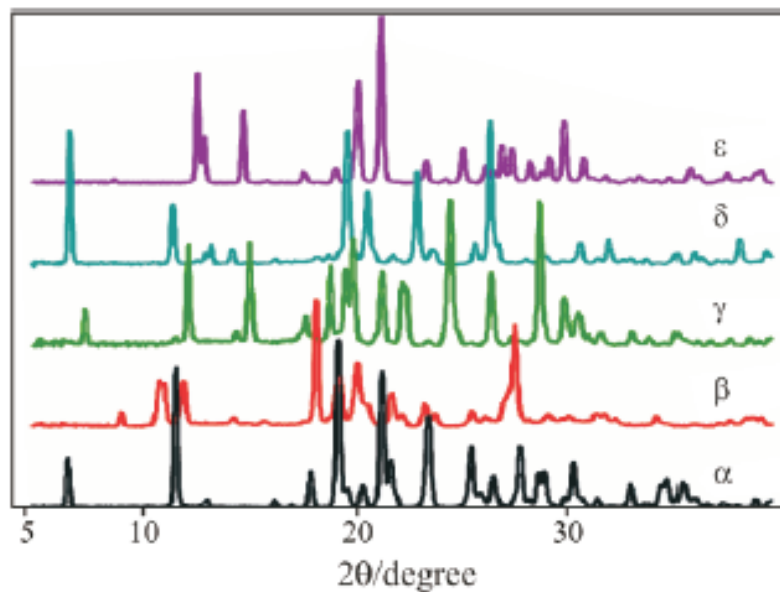


Figure 5 PXRD patterns of five polymorphs of chlorpropamide suggesting at least five different solid forms exists, taken from ref. 22a.

1.3 Multi-component system

• Host-guest compounds, salts and cocrystals

Multi-component system can be divided into host-guest compounds, molecular salts and cocrystals. The inclusion of small guest molecules in the open framework of a host molecule constitutes a host-guest compound. Some common host molecules are cyclodextrins, calixarenes, cucurbiturils, porphyrins, crown ethers, cryptophanes, bisphenols and zeolites etc.²¹ The difference between a host-guest adduct $H \cdot G$ and a binary molecular complex $A \cdot B$ is that, in a host guest adduct there are either no $H \cdots H$ and $G \cdots G$ interactions, or $H \cdots H$ interactions along with weak $H \cdots G$ association stabilizing the structure. But in case of binary molecular complex $A \cdot B$, there is a definite $A \cdots B$ interaction comparable in strength to $A \cdots A$ or $B \cdots B$ aggregation. When the guest molecule is a solvent of crystallization and present in the cavity of a crystal lattice, the

structure is referred to as solvate or pseudopolymorph. When the guest molecule present in the crystal structure is water, it is referred to as hydrate.

Solvates, hydrates (pseudopolymorphs)²² are of great importance in the pharmaceutical industry. The drug development process exposes active pharmaceutical ingredients (APIs) to various organic and aqueous solvents during crystallization, wet granulation, storage and dissolution can lead to the formation of pseudopolymorphs. The most important point is that some APIs form solvates while others do not. The propensity of an API molecule to form solvates has been related to molecular structural features, hydrogen bond patterns, donor-acceptor imbalance and crystal packing. About one third of the drugs are able to form hydrate. Generally hydrates are less soluble than anhydrous compound because of repulsion of water molecules present in the crystal lattice and external solvent molecules. But interestingly norfloxacin hydrate and tegaserod mono hydrate showed better solubility than its corresponding anhydrous forms.^{22f,g} Hence hydration plays an important role in altering solubility and stability of a drug. Some important drugs which are marketed as solvates are Indinavir sulphate ethanolate (Crixivan), Darunavir ethanolate, Doxycycline HCl ethanolate, Mirtazapine hemihydrate (Remeron), Paroxetine HCl hemihydrate (Paxil), Atorvastatin calcium trihydrate (Lipitor) and Cephadrine dihydrate (Velocef).²³

A cocrystal can be defined as multi-component assembly of two or more solid crystalline materials involving in noncovalent interactions in a definite stoichiometric ratio results homogeneous phase and solid at ambient conditions.²⁴ Co-crystals can be constructed through several types of non-covalent interactions, including hydrogen bonding, π stacking, and vander Waals forces. Again salt is defined as multi-component system where proton is transferred from acidic to the basic moiety. Salts and cocrystals are the extreme cases of proton position between an acid and a base in multi-component crystals. At the salt end the proton transfer is complete, and on the opposite end proton transfer is absent in cocrystals where the acid ionization constant (pK_a) governs the formation of a salt or cocrystal.²⁵ Both of them are very useful for alteration of physicochemical properties of an API. Salts of API are used in pharmaceutical industry for the past many decades but pharmaceutical cocrystals are still in the pipeline and much widely studied in the last decade.²⁶

1.3.1 Pharmaceutical cocrystals

Pharmaceutical cocrystal is a subclass of cocrystals that are formed between an Active Pharmaceutical Ingredient (API) and generally regarded as safe (GRAS) molecule²⁷ or biologically acceptable to the human body. Cocrystallization is a process to combine together different molecular species within one periodic crystalline lattice by noncovalent interactions without making or breaking of covalent bonds. As a result, it is expected that API should retain its biological activity as before cocrystal formation. During cocrystallization, two things can happen: interacting molecules may separate yielding individual solids or crystallize together as a cocrystal. During falling apart of individual component may crystallize into metastable forms also.²⁸ The goal of the recrystallization is to obtain homogeneous phase, whereas cocrystallization produces a heteromeric product or a binary phase (Figure 6). The most common method of obtaining cocrystals is to dissolve the components in a suitable solvent system and allowing for crystallization to take place. Gentle warming is necessary to dissolve the solids and sometimes an anti-solvent is added or the solution is subjected to sonication to accelerate crystallization. This empirical, trial-and-error method is referred as solution crystallization. Jones²⁹ showed that by adding a few drops of solvent during grinding/kneading, referred to as solvent-drop or solvent-assisted grinding, one can accelerate adduct formation due to lubrication. Again recently utilizing Kofler mixed fusion method,^{29c} nicotinamide cocrystals with seven active pharmaceutical ingredients were prepared. Here higher melting point component (A) melted and recrystallized before molten component (B) is brought into contact with it, creating a zone of mixing, shown in Figure 6.

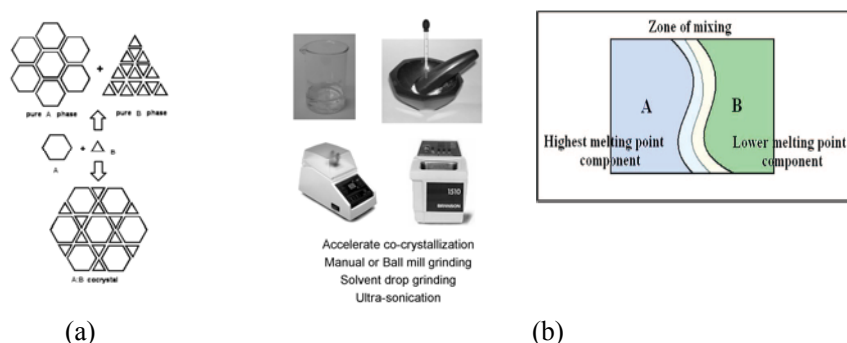


Figure 6. (a) Events that take place during co-crystallization. Two components may fall apart yielding individual phases or obtain as a cocrystal. (b) Various methods (solution, slurry, grinding, ball milling or melt) used to prepare

cocrystals.

1.3.2 Pharmaceutical salts

Salt formation is a useful method for isolation and purification of substances. The formation of a pharmaceutical salt can modify the physicochemical as well as the biological properties of an ionizable drug, which cannot be predicted from the properties of the parent drug and of the counter ion. Salt formation is an acid base reaction and a compound having an acidic or basic group can participate in salt formation. Improvement of solubility and dissolution rate of weakly acidic or basic drug having poor water solubility is the primary reason for preparation of pharmaceutical salt forms.³⁰ In addition salt formation also influences many other properties like melting point, hygroscopicity, chemical stability, solution pH, crystal form, and mechanical properties. An estimated half of the drugs in the market are administered in the salt form. It is easier to select a salt forming agent by knowing the acid ionization constant (pK_a) value of each ionizable group present in API. It is generally accepted that reaction of an acid with a base will be expected to form a salt if the ΔpK_a ($\Delta pK_a = pK_a(\text{conjugate acid of base}) - pK_a(\text{acid})$) is greater than 3.²⁵ Nangia^{25b} and coworkers noted that a smaller ΔpK_a (less than 0) will almost exclusively result in cocrystal formation, the parameter is inappropriate for accurately predicting salt formation in the solid state when ΔpK_a is between 0 and 3, as some examples are there where partial proton transfer is the case. Salt former selection is an important aspect in preparing pharmaceutical salts from toxicological and pharmacological point of view. Salt formers can be subdivided into a number of categories, depending upon their functionality and purpose. Some of the most frequently used pharmaceutical salts are listed in Table 1.

Table 1 Classification of some common pharmaceutical salts (ref. 30g)

Salt Class	Examples
Anions	
Inorganic acids	hydrochloride, hydrobromide, sulfate, nitrate, phosphate.
Sulfonic acids	mesylate, esylate, isethionate, tosylate, napsylate, besylate.
Carboxylic acids	acetate, propionate, maleate, benzoate, salicylate, fumarate.
Anionic amino acids	glutamate, aspartate.
Hydroxyacids	citrate, lactate, succinate, tartrate, glycollate.

Fatty acids	hexanoate, octanoate, decanoate, oleate, stearate.
Insoluble salts	paemoate (embonate), polystyrene sulfonate (resinate).
Cations	
Organic amines	triethylamine, ethanolamine, triethanolamine, meglumine, ethylenediamine, choline.
Metallic	sodium, potassium, calcium, magnesium, zinc.
Cationic amino acids	arginine, lysine, histidine.

1.4 Solubility and dissolution rate

According to the simplest definition, the thermodynamic solubility of a compound in a solvent is the maximum amount of the most stable crystalline form of the compound that can remain in solution under equilibrium conditions. Aqueous solubility is essential for drug candidates. Poor aqueous solubility is likely to result in poor absorption, even if the permeation rate is high, since the flux of a drug across the intestinal membrane is proportional to the concentration gradient between the intestinal lumen and the blood. The FDA regulations concerning oral medications require more extensive investigation of compounds with low solubility, and it may have an even greater impact in the case of its dosage forms. Again high concentrations of poorly soluble drugs in organisms may result in crystallization and acute toxicity, as in the case of uric acid and gout. Overall, poor solubility of drug candidates has been identified as the cause of numerous drug development failures.³¹ The traditional approach of salt formulation to improve drug solubility is unsuccessful with molecules that lack ionisable functional groups, have sensitive moieties that are prone to decomposition/racemization, and/or are not sufficiently acidic/basic to enable salt formation. Cocrystals are preferred over salts because of stability towards hydration of the former. Cocrystals have the ability to tune physicochemical properties e.g. solubility, stability, bioavailability etc. which are the major concern in most APIs.

According to the Biopharmaceutics Classification System (BCS),³² drugs are classified into four categories depending on their solubility and permeability parameters (Table 2). The seminal work of Amidon^{32b} showed that drug absorption in the gastrointestinal (GI) tract is controlled by membrane permeability and solubility/dissolution rate. Permeability is measured as the partitioning of the drug

molecule in its uncharged or neutral state between n-octanol and water, represented by log P. The reference standard for defining high or low permeability boundary is the n-octanol/water partition coefficient for metoprolol (log P 1.72). Drugs having log P > 1.72 are categorized as high-permeability because metoprolol is known to be 95% absorbed in the GI tract. High/low solubility is defined with reference to the Dose number, Do, which is the ratio of the highest drug dose strength in the administered volume (taken as 250 mL = a glass of water) to the saturation solubility of that drug in water (measured in mg/L). A Do value of <1 means a highly soluble drug whereas Do is >1 for low solubility compounds. In simple terms, Do is the number of glasses of water required to dissolve the tablet at its highest dose. Do values of 25-100 are considered low solubility drugs and this number can even exceed 1000. The serious problem posed by low solubility drugs was highlighted in recent articles,³³ over 80% drugs are sold as tablets. About 40% of marketed drugs have low solubility problems. More alarming is double the percentage of drug candidates in the R&D pipeline (80-90%) which could fail due to solubility problems (Table 3).

Table 2 The Biopharmaceutics Classification System of drugs (ref. 34) according to intestinal absorption and oral administration parameters.

<p>Class I – High solubility, High permeability</p> <p>Propafenolol, Metoprolol, Diltiazem, Verapamil, Theophylline, Paracetamol, Pseudoephedrine sulfate, Metformin hydrochloride</p>	<p>Class II – Low solubility, High permeability</p> <p>Danazol, Ketoconazole, Mefenamic acid, Nifedipine, Nifedipine, Nicardipine, Felodipine, Alovagoume, Guisecofulvin, Troglitazone, Glibenclamide, Carbamazepine</p>
<p>Class III – High solubility, Low permeability</p> <p>Acyclovir, Neomycin, Captopril, Enalaprilate, Alendronate, Atenolol, Cimetidine, Ranitidine</p>	<p>Class IV – Low solubility, Low permeability</p> <p>Chlorothiazine, Furosemide, Tobramycin, Cefuroxime, Itraconazole, Cyclosporin</p>

Table 3 Low Solubility Drugs in the Market and in the Development Pipeline According to the Biopharmaceutics Classification System (ref. 35).

BCS Class	Solubility	Permeability	% drugs on market	% drugs in R & D pipeline
I	high	high	35	5-10
II	low	high	30	60-70
III	high	low	25	5-10
IV	low	low	10	10-20

The solubility and dissolution are related to each other. The concentration of the solute in the solvent, at which the rate of molecules leaving the bulk solute surface becomes equal to the rate of redeposition, is the thermodynamic solubility. The rate at which this equilibrium is achieved is defined as the dissolution rate. Therefore solubility is an equilibrium process while dissolution is a kinetic phenomenon. According to Noyes–Whitney,³⁴ dissolution rate of a solute in a solvent is directly proportional to its solubility described by the equation

$$\text{Dissolution rate} = \frac{dQ}{dt} = \frac{DA}{h} (C_s - C_b)$$

where,

dQ/dt is the rate of mass transfer

D is the diffusion coefficient (cm^2/sec)

A is the surface area of the drug (cm^2)

h is the diffusion layer thickness (cm)

C_s is the saturation solubility of the drug

C_b is bulk solution concentration.

When particles dissolve by pure diffusion, the concentration at every point away from the solid-liquid interface increases, but the concentration gradient decreases with time. Therefore overall dissolution rate decreases and becomes constant with time and a pseudo-steady state is reached. Noyes and Whitney proposed the diffusion layer model.^{34a} When surface area is constant, the dissolution rate is proportional to the difference between solubility and the bulk solution concentration.

$$\text{Dissolution rate} = k(C_s - C_b)$$

where, k is a constant (mass transfer coefficient)

1.4.1 Types of Dissolution

There are two different types of experimental dissolution methods (1) Planar surface dissolution and (2) Powder dissolution.

• Planar Surface Dissolution

For experimental determination of dissolution rate the planar surface model is the simplest one having simple mathematics for calculation. For calculating dissolution rate the Noyes-Whitney equation can be used. Generally for pharmaceutical solids

measuring dissolution rate from a well defined surface is a popular way, for that intrinsic dissolution rate (IDR) determination is one example.

• Intrinsic Dissolution Rate

When agitation intensity and surface area are fixed, dissolution rate can be considered as a property of solid. This loosely defined property is called the Intrinsic Dissolution Rate (IDR). Due to the close relation between IDR and solubility, it can be used as a method of solubility estimation, when equilibrium solubility cannot be obtained experimentally. For the intrinsic model the container shape, agitation intensity (rotation per minute, rpm), bulk solvent volume, temperature of the medium etc. are kept constant to calculate the dissolution rate. The rotating disk apparatus for measuring IDR and the liquid flow are shown in the Figure 7.³⁵

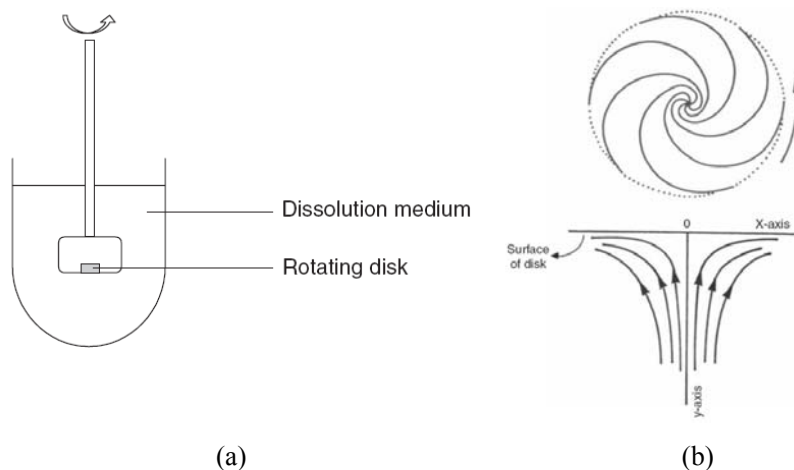


Figure 7 (a) Rotating disk apparatus for measuring IDR. (b) Liquid flow pattern around the rotating disk apparatus (ref. 35c).

• Powder Dissolution

To calculate dissolution rate experimentally the planar surface model is useful but in a real sense the drug dissolution involves solid particles and is very complicated process as the total surface area changes during dissolution. Powder dissolution³⁶ is based on the real dissolution phenomenon occurs inside the body. In this model the effect of particle size and shape play a crucial role. Generally for high soluble APIs, intrinsic dissolution experiment is better than powder dissolution because it provides dissolution rate in 4-5 h period, which is critical time for a fast dissolving drug. The drug will act accordingly in the biological system and it is preferred as tablet formulation. But for low

soluble APIs, powder dissolution experiment is more appropriate to obtain maximum solubility with respect to time and capsule formulation is better approach here. To improve solubility of specially BCS class II and IV APIs, cocrystals design approach is a preferred option. Recent examples of cocrystals of anti-depressant drug, fluoxetine hydrochloride, anti-fungal drug itraconazole (Sporanox), chronic pain killer AMG 517, and anti-epileptic drug lamotrigine (Lamictal) and carbamazepine showed better solubility than the API.³⁷ Antifungal drug Itraconazole extremely water insoluble and administered both orally and intravenously. The oral formulation of itraconazole is the amorphous form coated on the surfaces of sucrose beads, and marketed as the Sporanox® capsule. Interestingly, no crystalline salt of itraconazole has been reported in the patent literature, even though salt formation using itraconazole and an acidic salt former would seem to be a logical approach to improve the absorption properties of the API. Remener et al.^{37a} prepared stable pharmaceutical cocrystals and especially itraconazole–L-malic acid cocrystal, exhibits a similar dissolution profile to that of the sporanox beads in 0.1 (N) HCl medium, is an alternative to the existing amorphous formulation (Figure 8). The cocrystals improved the solubility 4-20 fold higher concentration than the crystalline drug form and the peak values were maintained for up to 8 h.

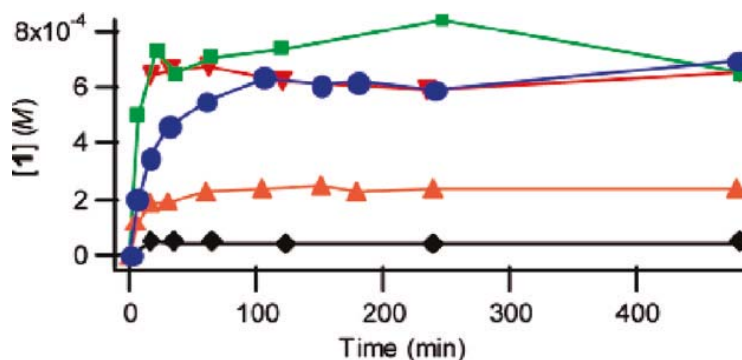
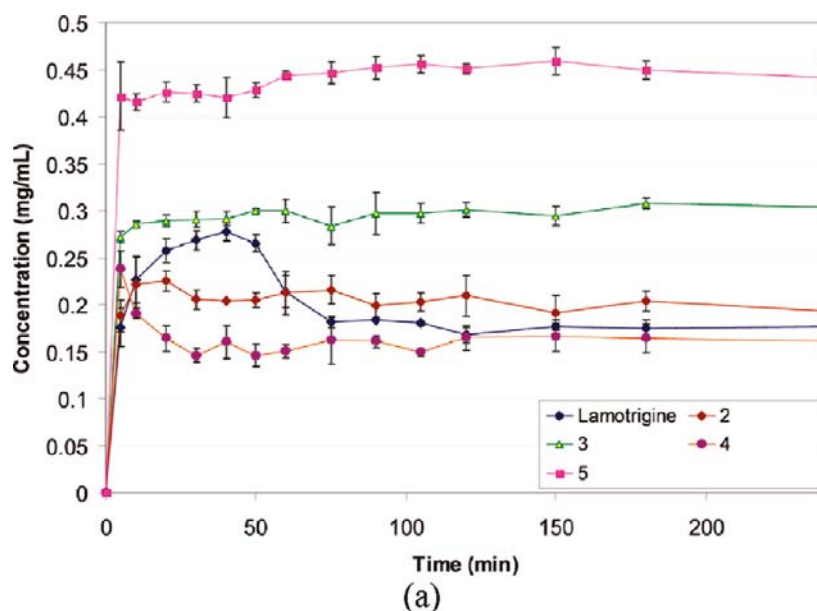


Figure 8 Dissolution curves in 0.1 N HCl at 25°C. Sporanox capsule amorphous form (■), crystalline itraconazole (◆), L-malic acid cocrystals (▼), tartaric acid cocrystal (●), and succinic acid cocrystal (▲) (ref. 37a).

Again epileptic drug Lamotrigine^{37b} showed possibility of cocrystals with methyl paraben, nicotinamide and salt with saccharin. The saccharinate salt exhibited the

highest concentration in water and maintained its peak profile for 4 h (Figure 9a). The decrease in pH from 5.5 to 5.1 was attributed as a reason for the highest dissolution rate of the saccharinate salt. The increase in the solubility of lamotrigine is higher in acidic medium compared to pure water by about 10%, it being a basic drug. The methyl paraben cocrystal had the highest dissolution profile in acidic medium and maintained its level for 4 h (Figure 9b). Nicotinamide cocrystal had the second highest concentration profile in neutral medium whereas its hydrate form was higher in acidic solution. Rodríguez-Hornedo³⁸ recently proposed that cocrystal solubility is directly proportional to the solubility of its components. However, the available data on lamotrigine cocrystals discussed above shows mixed results. Nicotinamide has the highest solubility (1 g/mL); it is used as a hydrotrope for solubility improvement, but its cocrystals exhibited the second highest solubility after saccharinate and methyl paraben in neutral and acidic medium, respectively. It appears that the theoretically expected linear relationship between the solubility ratio of the components plotted against the solubility of the cocrystal former divided by the solubility of the API³⁸ will be realized only when the crystal structures have similar hydrogen bonding and molecular packing. This results showed clearly that solubility/dissolution is pH dependent.



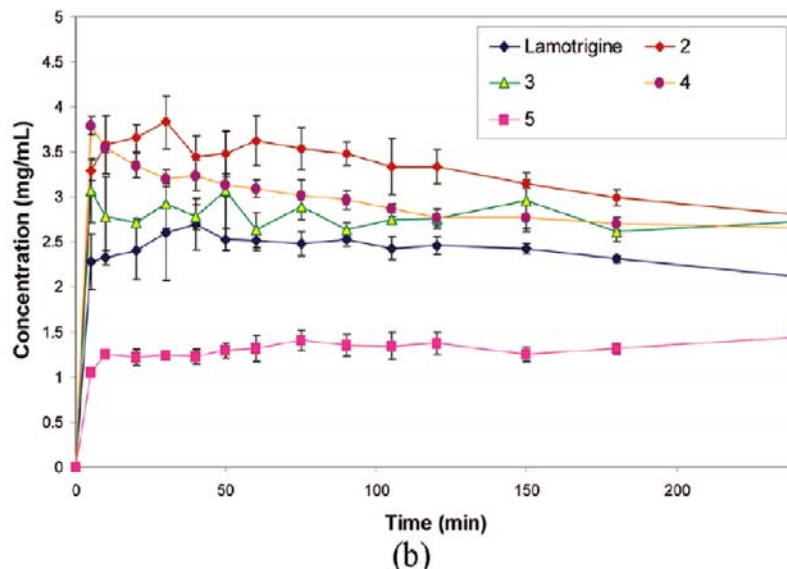


Figure 9 Dissolution profile of lamotrigine crystal forms in (a) water and (b) pH 1 buffer. Lamotrigine, 2 = lamotrigine–methyl paraben (form II), 3 = lamotrigine–nicotinamide (anhydrate), 4 = lamotrigine–nicotinamide (monohydrate), and 5 = lamotrigine–saccharinate salt (ref. 37b).

1.4.2 Spring and Parachute model

Recently Nangia et al.³⁹ explained the reason behind the solubility enhancement of pharmaceutical cocrystals which are bound through weak intermolecular interaction through Spring and Parachute model. The enhanced solubility of drug cocrystals is similar to the supersaturation phenomenon characteristic of amorphous drugs. However, in contrast to the metastable nature of amorphous phases, cocrystals are stable owing to their crystalline nature. Yet, cocrystals can exhibit dramatic solubility advantage over the stable crystalline drug form; often comparable to amorphous pharmaceuticals.^{39a} The “spring and parachute” concept for amorphous drug dissolution is adapted to explain the solubility advantage of pharmaceutical cocrystals. Thus (1) the cocrystal dissociates to amorphous or nanocrystalline drug clusters (the spring), which (2) transform via fast dissolving metastable polymorphs to the insoluble crystalline modification following the Ostwald’s Law of Stages, to give (3) high apparent solubility for cocrystals and optimal drug concentration (the parachute) in the aqueous medium (Figure 10). They proposed possible mechanism for the solubility advantage of pharmaceutical cocrystals (Figure 11). The dissociation of the hydrogen bonded cocrystals in the aqueous medium liberates the more soluble coformer into the solution, whereas the less soluble drug molecules

aggregate as an amorphous phase because of the sudden crashing out from solution. These aggregates lack the long-range order and periodicity characteristic of the crystalline state. The amorphous phase gives peak drug solubility for a short period (the spring), which will gradually transform to metastable polymorph(s) and thereby extend the metastable zone width (the parachute effect). Finally, the drug will transform to the stable, insoluble polymorph, but by this time the bulk of the drug has been absorbed through the fast dissolving metastable state(s). The Ostwald's Law of Stages could stretch the metastable zone width to several hours. If the amorphous phase directly transforms to the stable crystalline form without the intermediacy of metastable polymorphs (dash arrow), the drug will exhibit spring effect only.

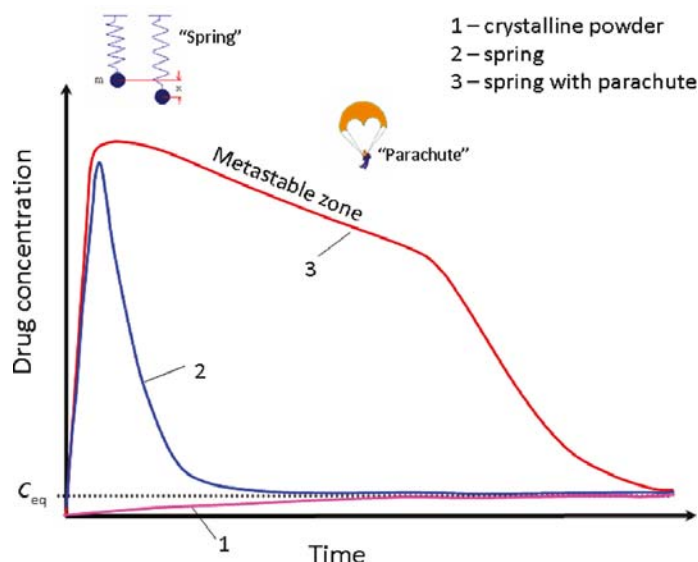


Figure 10 The spring and parachute concept to achieve high apparent solubility for insoluble drugs. (1) The crystalline (stable) form has low solubility. (2) A short-lived metastable species (i.e., amorphous phase) shows peak solubility but quickly drops (within minutes to an hour) to the low solubility of the crystalline form. (3) Highly soluble drug forms are maintained for a long enough time (usually hours) in the meta zone (ref. 39).

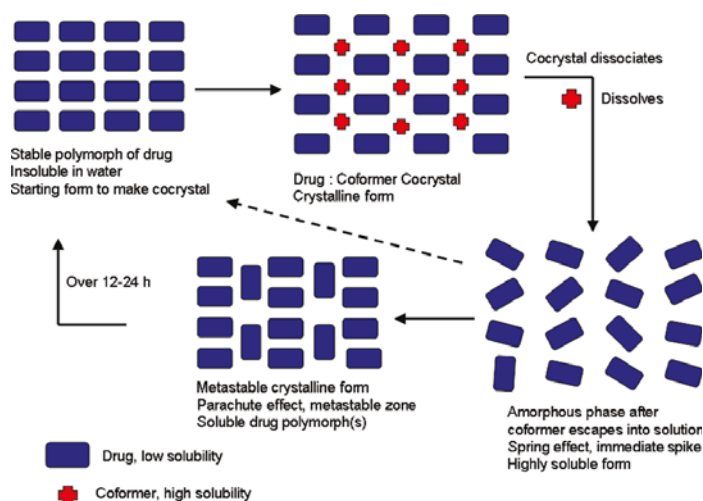


Figure 11 Possible mechanisms of pharmaceutical cocrystals in dissolution medium (ref. 39) Dissolution experiments of pharmaceutical cocrystals of biologically active molecule curcumin (chapter 4), antitumor prodrug temozolomide (chapter 5) and anthelmintic niclosamide (chapter 6) will be discussed.

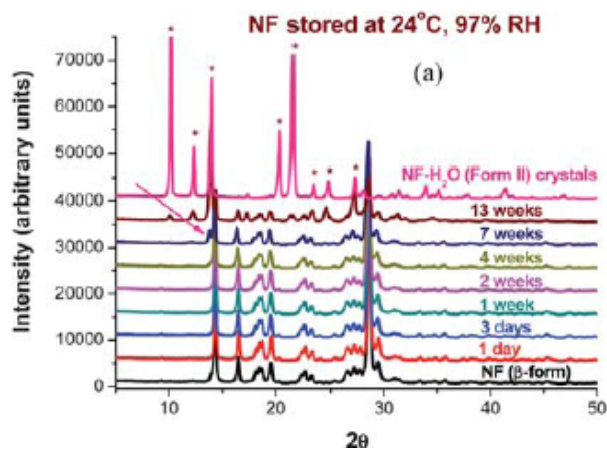
1.5 Stability issue of pharmaceutical cocrystals

The stability of a solid drug substance in the presence of atmospheric moisture is of concern to the pharmaceutical industry as it has practical implications for processing, formulation, packaging, and storage. It is sometimes the case that an anhydrous crystal form is stable below a certain critical relative humidity (RH), but at higher RH it is converted to a crystalline hydrate.⁴⁰ In these cases, solid form selection is often employed to search for a polymorph or cocrystal form that exhibits greater stability at high RH values. According to International Conference on Harmonization (ICH) guidelines,⁴¹ three storage conditions for APIs are 25°C and 60% RH; 30°C and 65% RH and 40°C and 75% RH (Table 4). The choice of test conditions defined in this guideline is based on an analysis of the effects of climatic conditions in the three regions of the EC, Japan and the United States. In general, a drug substance should be evaluated under storage conditions (with appropriate tolerances) that test its thermal stability and, if applicable, its sensitivity to moisture. For long-term studies, frequency of testing should be sufficient to establish the stability profile of the drug substance. For APIs with a proposed re-test period of at least 12 months, the frequency of testing at the long term storage condition should normally be every 3 months over the first year, every 6 months over the second year, and annually thereafter through the proposed re-test period.

Table 4 Different storage conditions according to ICH guidelines (ref. 41)

Study	Storage condition	Minimum time period covered by data at submission
Long term*	25°C ± 2°C/60% RH ± 5% RH or 30°C ± 2°C/65% RH ± 5% RH	12 months
Intermediate**	30°C ± 2°C/65% RH ± 5% RH	6 months
Accelerated	40°C ± 2°C/75% RH ± 5% RH	6 months

For e.g. Nitrofurantoin (NF) is a well known antibacterial drug extensively used as an oral treatment for urinary tract infections.⁴² The physical stability of NF-4HBA (1:1) co-crystal was tested against that of NF (β -form) at various relative humidity (RH) and temperature conditions recommended by the ICH guidelines for pharmaceutical stability testing.^{42d} Incubated samples were analyzed by PXRD at designated time points. There were no detectable changes with NF (β -form) stored at 24 °C and RH (<10, 33, 57, 75%) and at 40 °C and 75% RH as per the PXRD. However, NF anhydrous (β -form) converted to NF hydrate (Form II) at 24 °C and 97% RH in 7 weeks whereas at 40 °C and 96% RH, phase transformation was rapid and it occurred within one week. Figure 12 shows the PXRD patterns analyzed for stored samples of NF (β -form) and NF-4HBA at 24 °C and 97% RH up to 13 weeks and compared against native samples and pure NF-H₂O (Form II). The start of phase transformation was observed at 7 weeks for NF (β -form) in PXRD. Interestingly, NF-4HBA was robust and was found to remain unchanged in all the tested stress conditions.⁴³ Stability study of antitumor prodrug temozolomide (chapter 5) and anthelmintic niclosamide (chapter 6) and their pharmaceutical cocrystals will be discussed.



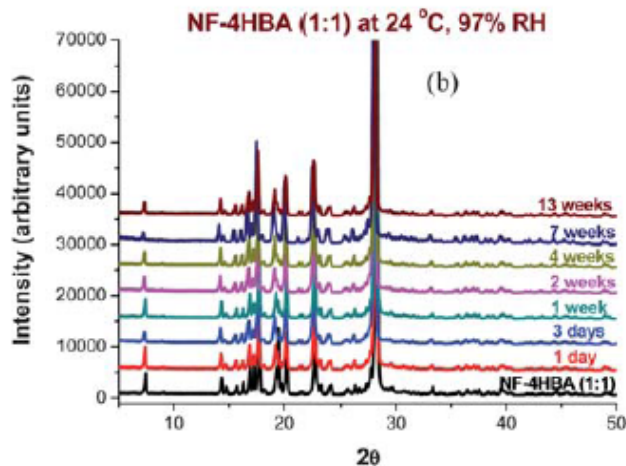


Figure 12 PXRD patterns of (a) NF (β -form), and (b) NF-4HBA incubated at 24 °C and 97% RH. While NF changed to NF-H₂O (Form II) by 7 weeks, the co-crystal remained intact (ref. 42).

To summarize, solid form selection is an important aspect of drug development. Although polymorph screening is required, preformulation activity, the scopes and experimental breadths of screens vary. It is important to do experiments as many as possible to obtain all possible crystalline forms before marketing the most stable API with optimum solubility, bioavailability and stability for further development. A metastable polymorph often has higher solubility and hence it is the desired polymorph for better bioavailability. In balance, however, the practical advantage of greater stability takes precedence over a more soluble but metastable polymorph. Using additive, polymer, excipients, stabilising metastable polymorphs will be good option for marketing. Again through the last decade, pharmaceutical cocrystals proved betterment of solubility, bioavailability, compressibility, stability etc. for an API. Still not a single cocrystal is marketed till clinical trials and dissociation of cocrystals to API to be confirmed before reaching the target side. To conclude, Solid State Chemistry has immense potential in the pharmaceutical Industry. Different solid forms of APIs (polymorphs, cocrystals, salts, hydrates, solvates etc.) can provide drugs with improved physicochemical properties.

1.6 References

1. (a) M. Jansen, *Angew Chem Int Ed.*, **2002**, *41*, 3746. (b) F. J. Disalvo, *Pure Appl Chem.*, **2000**, *72*, 1799. (c) R. Bishop, F. Toda and D. D. MacNicol, *Solid-State Supramolecular Chemistry: Crystal Engineering* Vol.6, in *Comprehensive Supramolecular Chemistry*, Pergamon, Chichester (UK), **1996**.
2. (a) M. G. Kanatzidis and K. R. Poeppelmeier (Organizers), *Prog. in Solid State Chem.*, **2007**, *36*, 1. (b) R. Hilfiker, F. Blatter, and M. V. Raumer, Relevance of Solid-state Properties for Pharmaceutical Products, **2007**, pp. 1-20. (c) S. R. Byrn.; R. R. Pfeiffer.; J. G. Stowell, *Solid-State Chemistry of Drugs*, SSCI: West Lafayette, **1999**. (d) D. Braga, F. Grepioni and L. Maini, *Chem. Commun.* **2010**, *10*, 6232.
3. S. L. Morissette.; Ö. Almarsson.; M. L. Peterson.; J. F. Remenar.; M. J. Read.; A. V. Lemmo.; S. Ellis.; M. J. Cima.; C. R. Gardner, *Adv. Drug Deliv. Rev.*, **2004**, *56*, 275.
4. (a) C. Lipinski, *Am. Pharm. Rev.* **2002**, *5*, 82. (b) S. R. Vippagunta.; H. G. Brittain.; D. J. W. Grant, *Adv. Drug Delivery Rev.* **2001**, *48*, 3-26. (c) S. R. Byrn.; R. R. Pfeiffer.; J. G. Stowell, *Solid-State Chemistry of Drugs*, 2nd ed.; SSCI, Inc.: West Lafayette, IN, **1999**.
5. (a) W. C. McCrone, *Phys. Chem. Org. Solid State*, **1965**, *2*, 725. (b) J. Bernstein, *Polymorphism in Molecular Crystals*, Clarendon, Oxford, **2002**. (c) R. Hilfiker, *Polymorphism in the Pharmaceutical Industry*, Wiley-VCH, Weinheim, **2006**. (d) H. G. Brittan, *Polymorphism in Pharmaceutical Solids*, Marcel Dekker, New York, **1999**. (e) http://en.wikipedia.org/wiki/Allotrope_of_carbon.
6. (a) A. Nangia, *Acc. Chem. Res.*, **2008**, *41*, 595. (b) N. J. Babu, S. Cherukuvada, R. Thakuria and A. Nangia, *Cryst. Growth Des.* **2010**, *10*, 1979. (c) N. J. Babu, L. S. Reddy, S. Aitipamula, and A. Nangia, *Chem. Asian J.* **2008**, *3*, 1122. (d) D. E. Braun, T. Gelbrich, V. Kahlenberg, R. Tessadri, J. Wieser, U. J. Grisser, *J. Pharm. Sci.* **2009**, *98*, 2010.
7. (a) T. L. Threlfall, *Analyst* **1995**, *120*, 2435. (b) B. Rodríguez-Spong, C. P. Price, A. Jayashankar, A. J. Matzger, N. Rodríguez-Hornedo, *Adv. Drug. Del. Rev.* **2004**, *56*, 241. (c) J. Bernstein, R. J. Davey, J. O. Henck, *Angew. Chem., Int. Ed.* **1999**, *38*, 3440.
8. (a) E. Swanepoela.; W. Liebenberga.; M. M. de Villiers, *Eur. J. Pharm & Biopharm.*, **2003**, *55*, 345. (b) F. T. Martins.; P. P. Neves.; J. Ellena.; G. E. Cami', E.

- V. Brusau, G. E. Narda. *J. Pharm. Sci.*, **2009**, 98, 2336. (c) J. Costa, M. Fresno, L. Guzman, A. Igual, M. Pujol, *Circ. Farm.* **1991**, 415. (d) M. Brits.; W. Liebenberg, M. M. De Villiers. *J. Pharm. Sci.*, **2010**, 99, 1138.
9. (a) J. P. Lakshman, Y. Cao, J. Kowalski, and A. T. M. Serajuddin, *Mol. Pharmaceutics* **2008**, 5, 994. (b) E. H. Lee, and S. R. Byrn, *J. Pharm. Sci.*, **2010**, 99, 4013.
 10. (a) F. Tian, T. Rades, and N. Sandler, *AAPS PharmSciTech*, **2008**, 9, 390. (b) P. Sanphui, B. Sarma and A. Nangia, *J. Pharm. Sci.*, **2011**, 100, 2287. (c) S. Maruyama and H. Ooshima, *Chem. Eng. J.* **2001**, 81, 1.
 11. (a) E. S. Ferrari and R. J. Davey, *Cryst. Growth & Des.* **2004**, 4, 1061. (b) Y. –H. Sugita, *Agric. Biol. Chem.*, **1988**, 52, 3081. (c) N. Garti and H. Zour, *J. Cryst. Growth*, **1997**, 172, 486.
 12. S. R. Chemburkar, J. Bauer, K. Deming, H. Spiwek, K. Patel, J. Morris, R. Henry, S. Spanton, W. Dziki, W. Porter, J. Quick, P. Bauer, J. Donaubauer, B. A. Narayanan, M. Soldani, D. Riley, K. McFarland, *Org. Process Res. Dev.* **2000**, 4, 413.
 13. (a) E. H. Lee.; S. R. Byrn. and M. T. Carvaja, *Pharm Res.* **2006**, 23, 10. (b) C. A. Mitchell, L. Yu, M. D. Ward, *J. Am. Chem. Soc.* **2001**, 123, 10830. (c) X. Sun, B. A. Garetz, A. S. Myerson, *Cryst. Growth Des.* **2006**, 6, 684. (d) J. L. Hilden, C. E. Reyes, M. J. Kelm, J. S. Tan, J. G. Stowell, K. R. Morris, *Cryst. Growth Des.* **2003**, 3, 921. (e) G. Di Profio, S. Tucci, E. Curcio, E. Drioli, *Cryst. Growth Des.* **2007**, 7, 526. (f) V. López-Mejías.; J. W Kampf.; A. J. Matzger, *J. Am. Chem. Soc.* **2009**, 131, 4554. (g) A. V. Trask, N. Shan, W. D. S. Motherwell, W. Jones, S. Feng, R. B. H. Tan, K. J. Carpenter, *Chem. Commun.* **2005**, 880.
 14. S. L. Morissette, Ö. Almarsson, M. L. Peterson, J. F. Remenar, M. J. Read, A. V. Lemmo, S. Ellis, M. J. Cima, C. R. Gardner, *Adv. Drug. Del. Rev.* **2004**, 56, 275.
 15. (a) A. S. Myerson and P. Y. Lo, *J. Cryst. Growth*, **1991**, 110, 26. (b) A. S. Myerson and R. M. Ginde, *Handbook of Industrial Crystallization*, A. S. Myerson, Ed.; Butterworth-Heinemann: Stoneham, MA, **1992**. (c) I. Weissbuch, V. Y. Torbeev, L. Leiserowitz and M. Lahav, *Angew. Chem., Int. Ed.*, **2005**, 44, 3226.
 16. (a) A. C. Zettlemoyer, *Nucleation*, Dekker: New York, **1969**. (b) B. Lewis, *Nucleation and Growth Theory: Crystal Growth*, Ed.; B. R., Pamplin, Pergamon: Oxford, **1980**. (c) R. J. Davey and J. Garside, *From Molecules to Crystallizers*, Oxford University Press: Oxford, U.K., **2000**. (d) R. J. Davey, N. Blagden, S.

- Righini, H. Alison, M. J. Quayle and S. Fuller, *Cryst. Growth Des.*, **2001**, *1*, 59. (e) G. R. Desiraju, *Angew. Chem. Int. Ed.*, **2007**, *46*, 8342.
17. W. F. Ostwald, *Z. Phys. Chem.*, **1897**, *22*, 289.
 18. A. Burger, R. Ramberger, *Mikrochim Acta* II, **1979**, 259.
 19. (a) K. Kimura, F. Hirayama and K. Uekama, *J. Pharm. Sci.*, **1999**, *88*, 385. (b) S. Thirunahari.; S. Aitipamula.; P. S. Chow.; R. B. H. Tan, *J. Pharm. Sci.*, **2010**, *99*, 2975. (c) N. K. Nath and A. Nangia, *CrystEngComm*, **2011**, *13*, 3232.
 20. (a) V. A. Drebuschak.; T. N. Drebuschak.; N. V. Chukanov and E. V. Boldyreva, *J. Therm. Anal. & Calorimetry* **2008**, *93*, 343. (b) Y. A. Chesalov.; V. P. Baltakhinov.; T. N. Drebuschak.; E. V. Boldyreva.; N.V. Chukanov.; V.A. Drebuschak, *J. Mol. Struct.* **2008**, *891*, 75. (c) T. N. Drebuschak.; A. A. Ogienkoc and E. V. Boldyreva, *CrystEngComm*, **2011**, *13*, 4405.
 21. (a) J. W. Steed and J. L. Atwood, *Supramolecular Chemistry*, 2nd Ed., John Wiley & Sons, Ltd., **2009**. (b) W. M. Nau and X. Zhang, *J. Am. Chem. Soc.*, **1999**, *121*, 8022. (c) M. L. Singleton, J. H. Reibenspies and M. Y. Darensbourg, *J. Am. Chem. Soc.*, **2010**, *132*, 8870. (d) J. W. Lee, S. Samal, N. Selvapalam, H.-J. Kim and K. Kim, *Acc. Chem. Res.*, **2003**, *36*, 621. (e) C. Márquez, R. R. Hudgins and W. M. Nau, *J. Am. Chem. Soc.*, **2004**, *126*, 5806.
 22. (a) T. L. Threlfall, *Org. Proc. Res. Dev.*, **2000**, *4*, 384. (b) S. Garnier, S. Petit and G. Coquerel, *J. Thermal Anal. & Calorimetry*, **2002**, *68*, 489. (c) Y.-S. Kim and R. W. Rousseau, *Cryst. Growth Des.*, **2004**, *4*, 1211. (d) T. Hosokawa, S. Datta, A. R. Sheth, N. R. Brooks, V. G. Young and D. J. W. Grant, *Cryst. Growth Des.* **2004**, *4*, 1195. (e) M. R. Caira, T. le-Roex, L. R. Nassimbeni, J. A. Ripmeester and E. Weber, *Org. Biomol. Chem.*, **2004**, *2*, 2299. (f) A. V. Katdare, J. F. Bavitz, *Drug Dev. Ind. Pharm.* **1984**, *10*, 789. (g) R. Srivijaya, P. Vishweshwar, B. R. Sreekanth and K. Vyas, *CrystEngComm*, **2008**, *10*, 283.
 23. (a) R. Srivijaya, P. Vishweshwar, B. R. Sreekanth and K. Vyas, *CrystEngComm*, **2008**, *10*, 283. (b) A. V. Kadare, J. F. Bavitz, *Drug Dev. Ind. Pharm.* **1984**, *10*, 789. (c) R. K. Khankari, W. D. J. Grant, *Thermochim. Acta* **1995**, *248*, 61. (d) E. Tiekink, J. Vittal and M. Zaworotko (Eds.), *Organic Crystal Engineering: Frontiers in Crystal Engineering*, 1st Ed., John Wiley & Sons, Ltd., **2010**.
 24. (a) M. C. Etter, *J. Phys. Chem.*, **1991**, *95*, 4601. (b) J. D. Dunitz, *CrystEngComm*, **2003**, *4*, 506. (c) G. R. Desiraju, *CrystEngComm*, **2003**, *5*, 466. (d) B. R. Bhogala

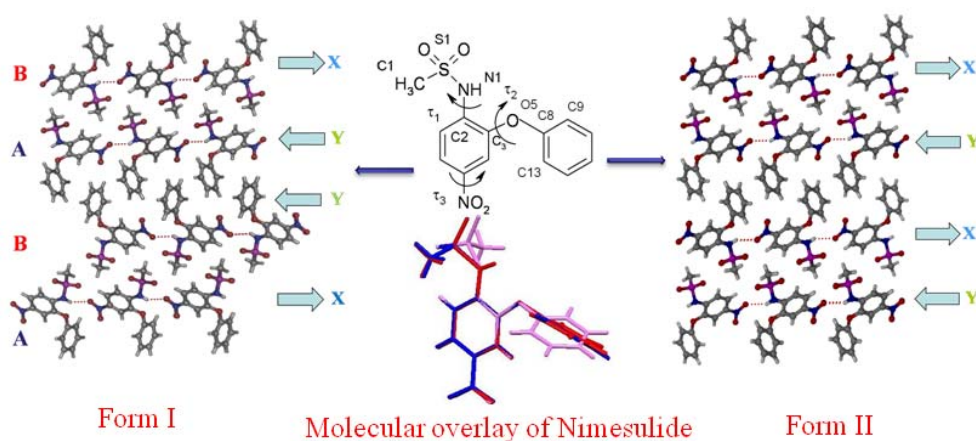
- and A. Nangia, *New J. Chem.*, **2008**, 32, 800. (e) S. L. Childs and K. I. Hardcastle, *Cryst. Growth Des.*, **2007**, 7, 1291. (f) W. Jones, W. D. Motherwell and A. V. Trask, *MRS Bull.*, **2006**, 341, 875. (g) J. A. McMahon, J. A. Bis, P. Vishweshwar, T. R. Shattock, O. L. McLaughlin and M. J. Zaworotko, *Z. Kristallogr.* **2005**, 220, 340. (h) C. B. Aakeröy, J. Desper, M. Fasulo, I. Hussain, B. Levin and N. Schultheiss, *CrystEngComm*, **2008**, 10, 1816.
25. (a) B. Sarma, N. K. Nath, B. R. Bhogala and A. Nangia, *Cryst. Growth Des.*, **2009**, 9, 1546. (b) C. B. Aakeröy, M. E. Fasulo and J. Desper, *Mol. Pharmaceutics* **2007**, 4, 317. (c) S. L. Childs, G. P. Stahly and A. Park, *Mol. Pharmaceutics*, **2007**, 4, 323. (d) S. Mohamed, D. A. Tocher, M. Vickers, P. G. Karamertzanis and S. L. Price, *Cryst. Growth Des.*, **2009**, 9, 2881. (e) P. Sanphui, G. Bolla, A. Nangia, *Cryst. Growth Des.*, **2012**, DOI: 10.1021/cg300002p.
26. (a) Ö. Almarsson and M. J. Zaworotko, *Chem. Commun.*, **2004**, 1889. (b) S. L. Childs, L. J. Chyall, J. T. Dunlap, V. N. Smolenskaya, B. C. Stahly, G. P. Stahly, *J. Am. Chem. Soc.*, **2004**, 126, 13335. (c) M. B. Hickey, M. L. Peterson, L. A. Scoppettuolo, S. L. Morrisette, A. Vetter, H. Guzmán, J. F. Remenar, Z. Zhang, M. D. Tawa, S. Haley, M. J. Zaworotko and Ö. Almarsson, *Eur. J. Pharm. Biopharm.*, **2007**, 67, 112. (d) A. V. Trask, W. D. S. Motherwell and W. Jones, *Cryst. Growth Des.*, **2005**, 5, 1013. (e) A. Nangia, N. Rodríguez-Hornedo, *Cryst. Growth Des.*, **2009**, 9, 3339. (f) N. Schultheiss, S. Bethune and J.-O. Henck, *CrystEngComm*, **2010**, 12, 2436. (g) C. B. Aakeröy, S. Forbes and J. Desper, *J. Am. Chem. Soc.*, **2009**, 131, 17048. (h) R. D. B. Walsh, M. W. Bradner, S. Fleischman, L. A. Morales, B. Moulton, N. Rodríguez-Hornedo and M. J. Zaworotko, *Chem. Commun.*, **2003**, 186. (i) N. Rodríguez-Hornedo, *Mol. Pharmaceutics*, **2007**, 4, 299.
27. EAFUS: A Food Additive Database, <http://vm.cfsan.fda.gov/~dms/eafus.html>
28. (a) G. M. Day, A. V. Trask, W. D. S. Motherwell and W. Jones, *Chem. Commun.*, **2006**, 54. (b) J. Li, S. A. Bourne and M. R. Caira, *Chem. Commun.*, **2011**, 47, 1530. (c) P. Sanphui, N. R. Goud, U. B. R. Khandavilli, S. Vanoth and A. Nangia, *Chem. Commun.*, **2011**, 47, 5013.
29. (a) A. V. Trask, W. Jones, *Top. Curr. Chem.* **2005**, 254, 41. (b) T. Frišćić, L. Fábíán, J. C. Burley, W. Jones, W. D. S. Motherwell, *Chem. Commun.* **2006**, 5009. (c) A. Jayasankar, A. Somwangthanaroj, Z. J. Shao, N. Rodríguez-Hornedo, *Pharma. Res.* **2006**, 23, 2381. (d) A. Delori, T. Frišćić and W. Jones, *CrystEngComm* **2012**, 14,

2350. (e) D. J. Berry.; C. C. Seaton.; W. Clegg.; R. W. Harrington.; S. J. Coles.; P. N. Horton.; M. B. Hursthouse.; R. Storey.; W. Jones, T. Frišćić and N. Blagden, *Cryst. Growth Des.*, **2008**, 8, 1697.
30. (a) P. H. Stahl and C. G. Wermuth (Eds.), *Handbook of Pharmaceutical Salts: Properties, Selection, and Use*; Wiley-VCH, **2002**. (b) L. D. Bighley, S. M. Berge and D. C. Monkhouse, *Salt Forms of Drugs and Absorption*, in: J. Swarbrick, J. Boylan (Eds.), *Encyclopaedia of Pharmaceutical Technology*, vol. 13, Dekker, New York, **1996**, p 453–499. (c) A. T. M. Serajuddin, *Adv. Drug Deliv. Rev.*, **2007**, 59, 603. (d) A. V. Trask, D. A. Haynes, W. D. S. Motherwell and W. Jones, *Chem. Commun.*, **2006**, 51. (e) J. F. Remenar, J. M. MacPhee, B. K. Larson, V. A. Tyagi, J. H. Ho, D. A. McIlroy, M. B. Hickey, P. B. Shaw and Ö. Almarsson, *Org. Proc. Res. Dev.*, **2003**, 7, 990. (g) R. J. Bastin, M. J. Bowker and B. J. Slater, *Org. Proc. Res. Dev.*, **2000**, 4, 427.
31. (a) Y. W. Alelyunas, J. R. Empfield, D. McCarthy, R. C. Spreen, K. Bui, L. Pelosi-Kilby, C. Shen, *Bioorg. Med. Chem. Lett.* **2010**, 20, 7312. (b) S. N. Bhattachar, L. A. Deschenes, J. A. Wesley, *Drug Discovery Today* **2006**, 11, 1012.
32. (a) G. L. Amidon, H. Lennernas, V. P. Shah, J. R. Crison, *Pharm. Res.* **1995**, 12, 413. (b) A. Dahan, J. M. Miller, G. L. Amidon, *AAPS J.* **2009**, 11, 740. (c) T. Takagi, C. Ramachandran, M. Bermejo, S. Yamashita,; L. X. Yu, G. L. Amidon, *Mol. Pharmaceutics* **2006**, 3, 631.
33. (a) A. M. Thayer, *Chem. Eng. News* **2007**, 85, 17. (b) A. M. Thayer, *Chem. Eng. News*, **2010**, 88, 13.
34. (a) A. A. Noyes and W. R. Whitney, *J. Am. Chem. Soc.*, **1897**, 19, 930. (b) W. E. Hamlin, J. I. Northam and J. G. Wagner, *J. Pharm. Sci.*, **1965**, 54, 1651.
35. (a) V. G. Levich, *Physicochemical Hydrodynamics*, 2nd Ed., Prentice-Hall, Englewood Cliffs, New Jersey, **1962**, p 61–72. (b) D. J. W. Grant and H. G. Brittain, *Physical Characterization of Pharmaceutical Solids*, H. G. Brittain. (Ed.), Marcel Dekker, Inc, New York, p. 359. (c) Y. Qiu, Y. Chen, G. G. Z. Zhang, L. Liu and W. R. Porter (Eds.), *Developing Solid Oral Dosage Forms: Pharmaceutical Theory and Practice*, 1st Ed., Elsevier, **2009**.
36. (a) P. J. Niebergall, G. Milosovich and J. E. Goyan, *J. Pharm. Sci.*, **1963**, 52, 236. (b) W. I. Higuchi, E. L. Rowe and E. N. Hiestand, *J. Pharm. Sci.*, **1963**, 52, 162.

37. (a) J. F. Remenar, S. L. orisette, M. L. Peterson, B. Moulton, J. M. MacPhee, H. R. Guzmán, Ö. Almarsson, *J. Am. Chem. Soc.* **2003**, *125*, 8456. (b) M. K. Stanton, A. Bak, *Cryst. Growth Des.* **2008**, *8*, 3856. (c) M. K. Stanton, S. Tufekcic, C. Morgan, A. Bak, *Cryst. Growth Des.* **2009**, *9*, 1344. (d) D. P. McNamara.; S. L. Childs.; J. Giordano.; A. Iarriccio.; J. Cassidy, M. S. Shet.; R. Mannion, E. O'Donnell and A. Park. *Pharm. Res.* **2006**, *23*, 1888. (e) J. Galcera, E. Molins, *Cryst. Growth Des.* **2009**, *9*, 327. (f) M. L. Cheney, N. Shan, E. R. Healey, M. Hanna, L. Wojtas, M. J. Zaworotko, V. Sasa, S. Song, J. R. Sanchez-Ramos, *Cryst. Growth Des.* **2010**, *10*, 394. (g) B. H. Magali, L. P. Matthew, A. S. Lisa, L. M. Sherry, A. Vetter, G. Hector, *Eur. J Pharm. Biopharm.* **2007**, *67*, 112.
38. (a) D. Good, N. Rodríguez-Hornedo, *Cryst. Growth Des.* **2009**, *9*, 2252. (b) S. J. Bethune, N. Huang, A. Jayasankar, N. Rodríguez-Hornedo, *Cryst. Growth Des.* **2009**, *9*, 3976. (c) D. Good, N. Rodríguez-Hornedo, *Cryst. Growth Des.* **2010**, *10*, 1028.
39. N. J. Babu, and A. Nangia, *Cryst. Growth Des.* **2011**, *11*, 2662.
40. (a) R. K. Khankari, D. J. W. Grant, *Thermochim. Acta* **1995**, *248*, 61. (b) S. R. Byrn, R. R. Pfeiffer, J. G. Stowell, *Solid-State Chemistry of Drugs*; 2nd ed.; SSCI, Inc.: West Lafayette, Indiana, **1999**. (c) M. D. Ticehurst, R. A. Storey, C. Watt, *Int. J. Pharm.* **2002**, *247*, 1. (d) A.V. Trask, W.D.S. Motherwell, W. Jones, *Cryst. Growth Des.* **2005**, *5*, 1013.
41. (a) http://www.ema.europa.eu/docs/en_GB/document_library/Scientific_guideline/2009/09/WC500002651.pdf. (b) ICH harmonized guideline, Q1A (R2) stability testing of new drug substances and products, 2003.
42. (a) M. R. Caira, E. W. Pienaar and A. P. Lötter, *Mol. Cryst. Liq. Cryst.*, **1996**, *279*, 241. (b) E. W. Pienaar, M. R. Caira and A. P. Lötter, *J. Crystallogr. Spectrosc. Res.*, **1993**, *23*, 739. (c) E. W. Pienaar, M. R. Caira and A. P. Lötter, *J. Crystallogr. Spectrosc. Res.*, **1993**, *23*, 785. (d) V. R. Vangala, P. S. Chowa and R. B. H. Tan, *CrystEngComm* **2011**, *13*, 759.

Chapter Two

Phase Transformation in Conformational Polymorphs of NSAID Nimesulide



Two conformational polymorphs of nonsteroidal anti-inflammatory drug nimesulide and their molecular overlay. Nimesulide Polymorphs arise from the torsional degrees of freedom at secondary sulfonamide group and phenoxy ring.

2.1 Introduction

Long-range periodicity of molecules in crystalline solids results in substantial differences in physical and chemical properties.¹ Majority of drugs (>90%) are administered as solids and preferred in their crystalline forms because of superior purity and stability over amorphous solids. Crystal structure, polymorphism, morphology, shape and size have economical and practical impact on active substances at all stages of development from research to commercialization. Crystalline forms of solid compounds may either exist as single molecular entities or multi-component species. The contribution from various possible intermolecular interactions like van der Waals, ionic, hydrogen bonding etc. will be different in different polymorphs. As a result their physical and chemical properties will be different. ‘Polymorphism’ comes from the Greek word, *Polus*=many, *morph*=form. Polymorphism² is defined as the phenomenon by which a given compound may exist in more than one distinct crystal structure, an extremely important phenomenon in single and multi-component species. Multi-component crystals include salts, hydrates, solvates and cocrystals of a molecule where a second component (counter-ion, water, solvent or a cocrystal former respectively) is incorporated into the crystalline lattice. After the accidental discovery of less soluble form of the anti-HIV drug Ritonavir, Abbott Laboratory suffered commercial loss of almost \$800 billion.³ Growing a new and selective crystalline form, understanding polymorphism and phase transformations between polymorphs is important specially in pharmaceutical developments.⁴ Thus it is essential to screen all possible polymorphs (all crystalline forms) of a drug molecule and choose the right candidate preferably the most stable polymorph. This led to an increased interest in developing methods to control the outcome of crystallization in producing desired polymorphs. Control over the formation of different polymorphic structures during production is desirable, especially to avoid concomitant polymorphism^{4e}. A mixture of polymorphs is chemically pure but it is not pure in a crystallographic sense as it consists of crystals with different packing arrangement. The relative stability of polymorphs is defined by thermodynamics, but the structure that will actually form, depends also on kinetics, that is, competitive nucleation and growth rates. The focus of the current chapter as well as the next one is on different

crystallization conditions which has a direct impact on the resulting polymorphic outcome.

2.2 Types of polymorphism

Polymorphism is a major challenge in the fundamental understanding of crystallization and received immense practical importance in pharmaceuticals as each polymorph can exhibit different chemical and physical properties including dissolution rate, oral absorption, bioavailability, stability, melting point, solubility, tableting, optical and mechanical properties, vapor pressure, etc.² When different conformers (flexible torsions) of the same molecule occur in different crystal forms, the phenomenon is termed as conformational polymorphism.⁵ Polymorphism perhaps tends to be prominent in molecules that contain multifunctional groups, thereby forming multiple supramolecular synthons known as synthon polymorphs. Polymorphism in isomeric hydroxybenzoic acids^{6d} is an example of synthon polymorphism.⁶ When polymorphism arises only because of different packing arrangement of molecules with the presence of same synthon or similar conformation, then it represents a case of packing polymorphism.⁷ The simultaneous appearance of polymorphs of a substance under identical conditions are called concomitant polymorphs. Near equal lattice energy or stability of various polymorphs of a compound is usually a prerequisite for observing concomitant polymorphism.⁸ Though polymorphs can be differentiated using this classification, yet there are cases where two or more types of polymorphism exist in the same polymorphic system. Polymorphism in Furosemide (brand name Lasix), a diuretic drug, is due to both conformational and synthon differences (Figure 1).^{9a} Pyrazinamide^{9b} is also a similar case where both synthon and packing polymorphism was observed. Again Clonixin (chemical name 2-(2-methyl-3-chloroanilino) nicotinic acid)^{9c}, a nonsteroidal anti-inflammatory drug was crystallized as three neutral polymorphs (form I, III and IV) and one zwitterionic form. Here polymorphs arise because of robust acid-pyridine synthon in form I, carboxylate-pyridinium ionic hydrogen bond and acid-acid dimer synthon (Figure 2). But carboxylic acid dimer synthon is present in both forms III and form IV. Thus clonixin is a good example of synthon polymorphs.

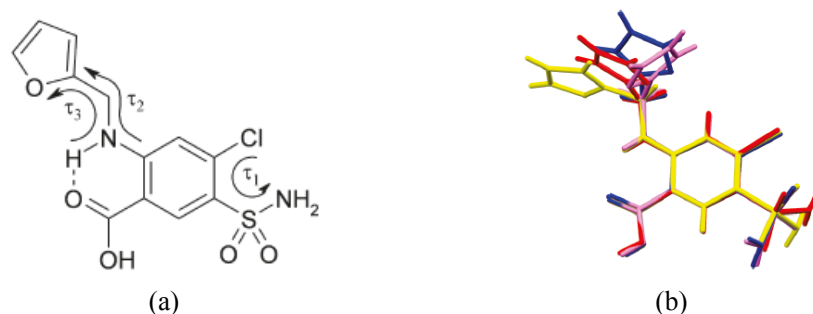


Figure 1 (a) The three torsion parameters in Furosemide^{9a}: $\tau_1 = \text{C-C-S-N}$, $\tau_2 = \text{C-N-C-C}$, $\tau_3 = \text{N-C-C-O}$. The anthranilic acid moiety is locked in an intramolecular hydrogen bond. (b) Overlay of four conformations in Furosemide crystal structures. Form 1 conformers (magenta and blue) have similar τ_1 but different τ_2 and τ_3 values, whereas all three torsion angles are different in form 2 and 3 conformers (yellow and red).

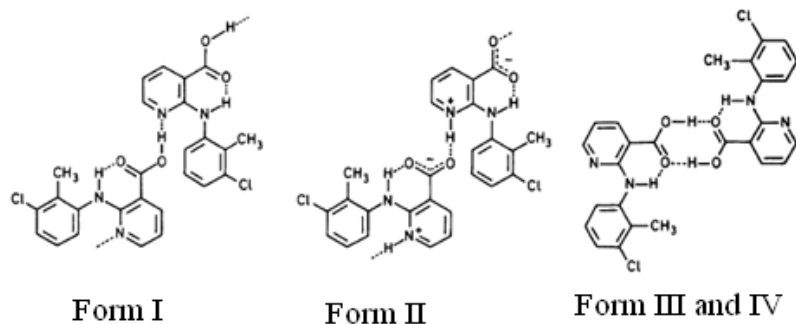


Figure 2 Synthon polymorphs of clonixin: Carboxylic acid-pyridine heterosynthon is present in form I. Form II (zwitterionic) consists of carboxylate-pyridinium ionic hydrogen bond. Again acid-acid dimer synthon is present in both form III and IV (culled from ref. 9c)

2.2.1 Methods of crystallization of polymorphs

During nucleation, millions of molecules must aggregate to form a crystal. In this process, if there are energetically viable pathways, molecules may choose any of these depending upon the crystallization conditions. This leads to the crystallization of different polymorphs. Thus formation of a large aggregate (i.e. nucleation) is an important step in the formation of a polymorph. Selective growth of a particular polymorph is an important goal for the pharmaceutical chemist. This led to an increased interest on developing methods to control the outcome of crystallization in producing desired polymorphs. In anti-solvent crystallization,¹⁰ a solution of the compound that has

to be crystallized is mixed with an antisolvent. Mixed solvent lowers the solubility of the compound compared to the original solution which creates a driving force for supersaturation by changing the interfacial energy between solution and crystal. The increase in supersaturation ratio results in a decrease of the nucleation, while the increase of the interfacial energy results in an increase of the nucleation. For example anti-solvent crystallization of L-Histidine^{10c} from aqueous solution with ethanol as anti-solvent the polymorphic fraction of the metastable polymorph B increased with increasing supersaturation ratio. Rapid cooling and different cooling rates can also results in new polymorphic modification. The use of structurally similar additives that direct the nucleation process of a synthon through habit modification in the supersaturated solution has been recognized as a new entry toward manipulating new crystalline modification and growth. Additive induced polymorphism or cocrystallization is explored recently and there are many instances of new polymorphs being discovered as unintended outcomes of cocrystallization experiments. Polymorphs of mefenamic acid, benzidine, acridine, pentafluorophenol are some interesting examples of additive induced polymorphism.¹¹ Structurally related compound, flufenamic acid stabilizes the metastable form of mefenamic acid against solid state polymorphic transformation. It was shown that flufenamic acid attached on the (100) face of crystals or was incorporated into mefenamic acid crystals. Stabilization could be achieved by inhibiting nucleation of the new phase and by decreasing the energy difference between the polymorphs.^{11a} Kofler contact method, change in pH can also lead to a new polymorphic outcome.¹² Solution crystallization by slow vaporization at different temperature condition is default crystallization technique to screen for new polymorphic modifications.¹³ More common and current approaches for discovery and selection of polymorphic forms of a compound include crystallization with tailor made soluble additives,¹⁰ polymer induction, epitaxial growth, laser induced nucleation, crystallization in capillaries, confinement within porous materials, and more traditional methods, such as varying solvent, temperature, and extent of supersaturation.¹⁴ High throughput polymorph generation is limited to combinatorially changing solvent, temperature, and supersaturation conditions.^{14h}

2.3 Problems of choosing best solid form

Drugs can exist in different crystalline forms depending upon various interactions possible from the synthon point of view. In the literature, there are many example of suitability of using one crystalline form over the other.¹⁵ However; a limit exists in the use of metastable forms because of their higher free energy¹⁶ and reactivity than the stable form, with adverse effects on their physicochemical stability. Crystal modifications can also appear during the formulation phase, or even during the normal shelf-life of tablet. Changes in crystal form could be a consequence of some common technological process such as wet granulation, melting, spray drying, compression, milling¹⁷ that are required to produce the final dosage form. The possible incidence of these phenomena must be discovered and studied. Therefore detection and the full characterization of all the possible polymorphs or solvates that can be formed are of paramount importance. In addition, the use of organic solvents, can give important problems on the residual solvent content, especially when they remain in high amount in the crystalline drug structure. Hence, solvent must be removed by desiccation and the efficacy of the process must be demonstrated.

2.4 Nimesulide

Nimesulide (chemical name, 4-nitro-2-phenoxyethanesulfonamide) is a non-steroidal anti-inflammatory drug (NSAID) that is particularly selective towards a preferential Cyclooxygenase-2 (COX-2) inhibition.¹⁸ Nimesulide is widely used as solid oral formulations (100 mg tablet dose). It has analgesic, anti-inflammatory and antipyretic properties with moderate incidence of gastric side effects and high therapeutic index. It is an inhibitor of prostaglandin synthetase and of platelet aggregation. Nimesulide possesses a much lower risk for gastroduodenal lesions compared to classical NSAIDs. It is also safe in aspirin-sensitive asthmatic patients. Nimesulide also showed suppression of aromatase activity and expression in several breast cancer lines.^{18f,g} effects. Nimesulide is a BCS (Biopharmaceutical Classification System) class II drug with poor aqueous solubility (10 mg/L) and dose number D_0 40 and high permeability ($\log P=2.56$).^{18h,i} Some literature of increasing solubility of nimesulide by encapsulation

of sodium nimesulide and precursors in β -cyclodextrin, evaluation of nimesulide lyophilized orally disintegrating tablets, using polymer nanocomposites crospovidone, CD complexes with L-lysine etc. are reported.¹⁹ The active drug is used as a tablet formulation loaded into crospovidone along with lactose and cellulose. Differential scanning calorimetry (DSC) and X-ray powder diffraction (PXRD) pattern of crospovidone-loaded Nimesulide^{19c,f} showed a mixture of two polymorphic modifications; the native material (form I) and the phase reported on ICDD and CSD databases (form II). The crystal structure of metastable form II (CSD refcode WINWUL) was reported in 1995 by Dupont et. al.²⁰ but the crystal structure of form I (native or reference material) is not reported to our knowledge. Nimesulide undergoes polymorphic modification from form II to I during formulation.^{26c} Despite the commercial importance of this drug, polymorphism and stability studies of Nimesulide are not available in the published literature. We report the X-ray crystal structure of the stable form I of Nimesulide and phase stability relationships characterized by IR, Raman, ss-NMR, PXRD and DSC. Furthermore solubility and intrinsic dissolution experiments were carried out on both polymorphs.

2.5 Result and Discussion

Nimesulide (Figure 1) was purchased from Sigma-Aldrich and used without further purification. The compound was also extracted from the marketed drug Nimulid (India) using methanol or acetone solvent and its chemical structure was confirmed by NMR, IR and Raman spectroscopy and melting point. Nimesulide polymorphs were crystallized concomitantly from EtOH and MeOH, and they were easily identified by the difference in their morphology. Crystals with acicular and prismatic morphology were characterized as form II, and rod-shape morphology is associated with form I. Form II was crystallized exclusively from THF and acetone. When Nimesulide was crystallized with succinic acid as a co-crystallization additive²¹ in EtOH solvent, rod-shape crystals of form I appeared concomitantly with form II, but now the former being in larger quantity. The pure form I could be generated by solvent crystallization, slurry grinding,²² and solvent-drop grinding (discussed later).

2.5.1 Crystal structural analysis

Single crystal X-ray reflections were collected on a rod-shaped crystal. The structure of form I was solved and refined in the orthorhombic space group $Pca2_1$ with two molecules in the asymmetric unit ($Z' = 2$). X-ray data on form II is matched with the reported space group $C2/c$ ($Z' = 1$).²⁰ The newly reported X-ray structure of form I and reported form II were both collected at 100 K for better comparison. We note that their unit cells (see Table 1) are similar having the relationship $a_I \approx c_{II}$, $b_I \approx b_{II}$, and $c_I \approx a_{II}$, i.e. b -axis is identical, but a and c -axes are interchanged.

The two molecules (A and B) form individual tapes mediated through N–H \cdots O hydrogen bonds along $[-1\ 0\ 0]$ or $[1\ 0\ 0]$ (Figure 2). Conformer A has stronger hydrogen bond (N1–H1 \cdots O3, 2.09 Å, 3.001(6) Å, 148°) compared to conformer B (N3–H2 \cdots O9, 2.28 Å, 3.079(6) Å, 135°). These molecular tapes are C–H \cdots O hydrogen-bonded (C19–H19 \cdots O6, 2.45 Å, 3.463(6), 155° and C6–H6 \cdots O1, 2.39 Å, 3.420(6) Å, 159°) to the sulfonyl oxygen from the relatively acidic phenyl CH ortho to the NO₂ group. The absence of crystallographic symmetry between A and B molecules means that the crystal system is non-centrosymmetric and polar ($Pca2_1$). Form II crystallizes in the centrosymmetric space group $C2/c$. The molecular tapes are again formed via intermolecular N–H \cdots O hydrogen bond (N2–H1 \cdots O3, 2.14 Å, 3.044(2) Å, 148°) that run in opposite direction for adjacent tapes. In effect, the difference between the two polymorphs is in the N–H \cdots O chain direction and associated molecular arrangement: it is XYYX in form I but XYXY in form II (where X denotes the N–H \cdots O chain going from left to right and Y is in the opposite directions). Neutron normalized hydrogen bond parameters calculated in Platon are listed in Table 2. The presence of torsional degrees of freedom in the Nimesulide molecule (Figure 1) indicates the possibility of conformational polymorphism. The two conformers of form I (blue and pink, Figure 3) have very similar torsion angles whereas the molecule in form II (red) has different torsion angles at the phenoxy and sulfonamide groups (Table 3).

Z denotes the number of molecules in the unit cell while Z' is the number of independent molecules in the asymmetric unit. Z' is the number of formula units in the unit cell divided by the number of independent general positions. Approximately 10% of all molecular crystals have $Z' > 1$.²³ These structures are of particular interest to crystal engineers. They represent special cases in which crystal packing is not ideal; they could

arise from frustration between two or more competing factors (say optimization of hydrogen bonds versus shape packing) during nucleation process. Systems exhibiting $Z' > 1$ are frequently polymorphic. $Z' > 1$ structures may be regarded as a special case of cocrystallization of chemically identical species. Generally high Z' structures are representative of the fastest growing crystal nucleus, say a metastable polymorph.^{5c,23} But for Nimesulide polymorphs, thermodynamic form I is the high Z' structure ($Z'=2$) whereas kinetic form II is lower Z' structure ($Z'=1$). These are not the first case of high Z' as stable polymorphs, Other examples are. 3,5-dihydroxybenzoic acid, furosemide.^{6d,9a}

The density and packing fraction calculated from the crystal data (at 100 K) are very similar for the two polymorphs (1.538, 1.533 g cm⁻³; 71.7, 71.5%), making it difficult to deduce their relative stability. Crystal lattice and molecular conformer energies were calculated²⁴ in Cerius² (Dreiding force field) and Gaussian 03 (DFT, B3LYP/6-31G (d,p)) for the two polymorphs (Table 4). When both intra- and intermolecular energies are accounted for (100 K crystal data sets), form I is more stable by 2.1 kcal mol⁻¹. Such calculations are reliable only from accurate crystal structure data determined under identical conditions.

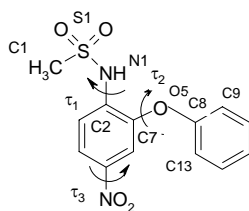


Figure 1 Torsional degrees of freedom in Nimesulide molecule lead to conformational polymorphism for this drug. The conformers at the sulfonamide group (τ_1 , C1–S1–N1–C2) and the phenoxy group (τ_2 , C7–O5–C8–C9) are different, but not at the nitro group (τ_3). Atom numbering at the two flexible torsion angles is shown.

Table 1 Single crystal data of form I and form II of Nimesulide

Nimesulide	Form I	Form II
Emp. Formula	C ₁₃ H ₁₂ N ₂ O ₅ S	C ₁₃ H ₁₂ N ₂ O ₅ S
Formula wt.	308.31	308.31
a (Å)	16.1268 (19)	33.231 (2)
b (Å)	5.0411 (6)	5.0720 (4)
c (Å)	32.761 (4)	15.8736 (12)
α (°)	90	90
β (°)	90	92.712 (2)

γ (°)	90	90
V (Å ³)	2663.4 (5)	2672.46
D_{calc} / g cm ⁻³	1.538	1.533
Z / Z'	8/2	8/1
R_1 [$I > 2 \sigma(I)$]	0.0654	0.0341
wR_2 (all)	0.1519	0.0889
GOF	1.066	1.081

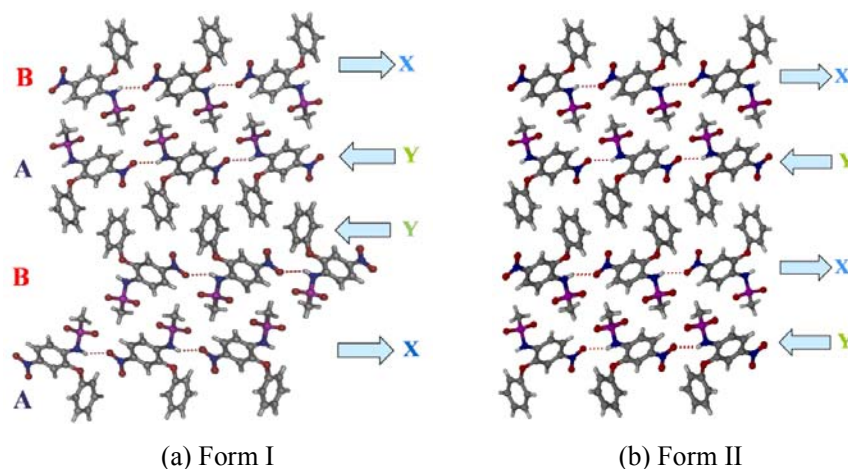


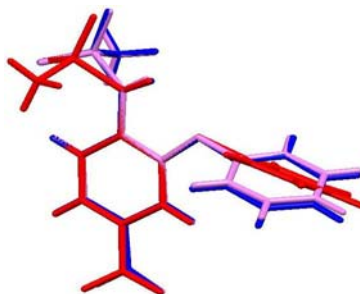
Figure 2 Molecular packing differences. (a) View of form I along the b -axis to show symmetry-independent A and B molecules arranged in the tape sequence XYXX. (b) View of form II along the b -axis shows the tape sequence XYYX between inversion related molecules in adjacent tapes.

Table 2 Neutron normalized hydrogen bond parameters for two polymorphs of Nimesulide

Nimesulide	Interaction	d (H \cdots A) (Å)	D (D \cdots A) (Å)	θ (\angle D–H \cdots A) (°)
Form I	N1–H1 \cdots O5	2.15	2.615 (6)	106
	N1–H1 \cdots O3	2.09	3.001(6)	148
	N3–H2 \cdots O9	2.28	3.079(6)	135
	C6–H6 \cdots O1	2.39	3.420(6)	159
	C7–H7 \cdots O2	2.29	3.034(6)	124
	C19–H19 \cdots O6	2.45	3.463(6)	155
	C20–H20 \cdots O7	2.30	3.029(6)	123
Form II	N1–H1 \cdots O5	2.15	2.591(1)	104
	N1–H1 \cdots O3	2.14	3.044(2)	148
	C7–H7 \cdots O2	2.31	3.047 (2)	124
	C4–H4 \cdots O1	2.37	3.377 (2)	154
	C10–H10 \cdots O4	2.51	3.250 (2)	125

Table 3 Torsion angles (τ , °) in molecular conformers of Nimesulide

Nimesulide	<C1–S1– N1–C2(°)	<S1–N1– C2–C3(°)	<N1–C2– C3–O5(°)	<C2–C3– O5–C8(°)	<C3–O5– C8–C9(°)	<C3–O5– C8–C13 (°)
Form I	61.1(5)	154.2(4)	0.2(6)	170.0(5)	67.0(6)	115.6(5)
	60.2(5)	155.0(4)	0.8(7)	170.0(4)	70.1(6)	113.2(5)
Form II	58.33(12)	155.00(10)	0.41(18)	176.59(12)	109.62(14)	74.51(17)

**Figure 3** Molecular overlay diagram of the three conformers of nimesulide in polymorphs I (blue and pink) and II (red).**Table 4** Lattice and conformational energies of two polymorphs of nimesulide were computed in Cerius² Dreiding 2.21 and Gaussian03 (DFT, B3LYP/6-31G (d,p)).

Nimesulide	E_{latt} (kcal mol ⁻¹)	E_{conf} (kcal mol ⁻¹)	$E_{\text{total}} = E_{\text{latt}} + E_{\text{conf}}$ (kcal mol ⁻¹)
Form I	–33.589	0	–33.589
Form II	–33.689	+ 2.209	–31.480

2.5.2 Powder X-ray diffraction

X-ray powder diffraction²⁵ is a diagnostic tool to differentiate between polymorphs based on line profile by taking a safe threshold of $\Delta 2\theta > \pm 0.2^\circ$. The PXRD traces of the two polymorphs of Nimesulide match the calculated X-ray patterns from the crystal structures, confirming the purity of the bulk phases. There are noticeable differences in the peak positions of form I and form II (Figure 4). Sometimes there is very close similarity in powder X-ray diffraction between polymorphs, (e.g. caffeine, aspirin, β -lactum, Curcumin),²⁶ in that case further characterization by solid state NMR will be appropriate to differentiate between polymorphs. The powder X-ray diffraction of stable form I exhibits characteristic reflections at about 2θ 11.99, 19.40, 21.69, 23.12,

24.04 and $24.39 \pm 0.2^\circ$. Again metastable form II exhibits characteristic reflections at about 2θ 12.35, 12.51, 18.87, 19.67, 22.15 and $24.18 \pm 0.2^\circ$.

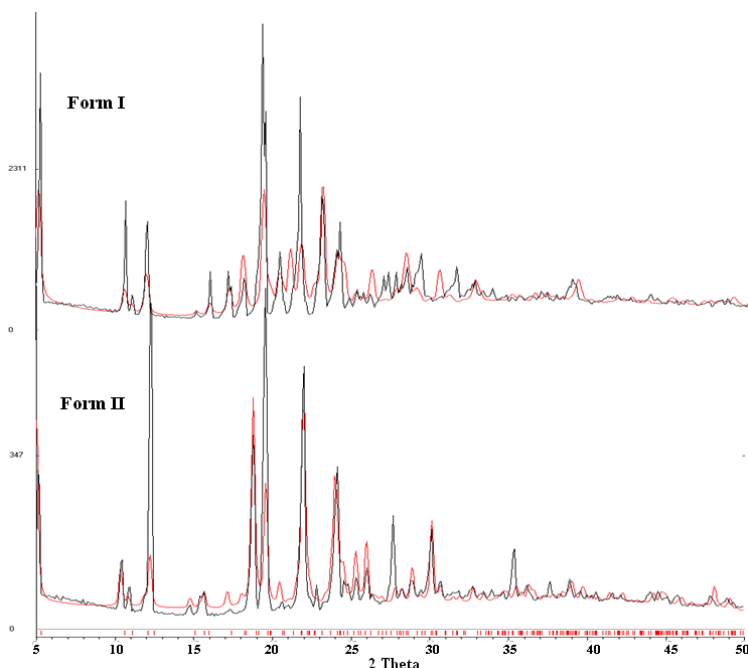


Figure 4 Overlay of the PXR D pattern recorded for Form I and Form II (black trace) along with their calculated X-ray lines (red trace). Similar x-ray pattern also support the similarity in packing.

2.5.3 Thermal analysis

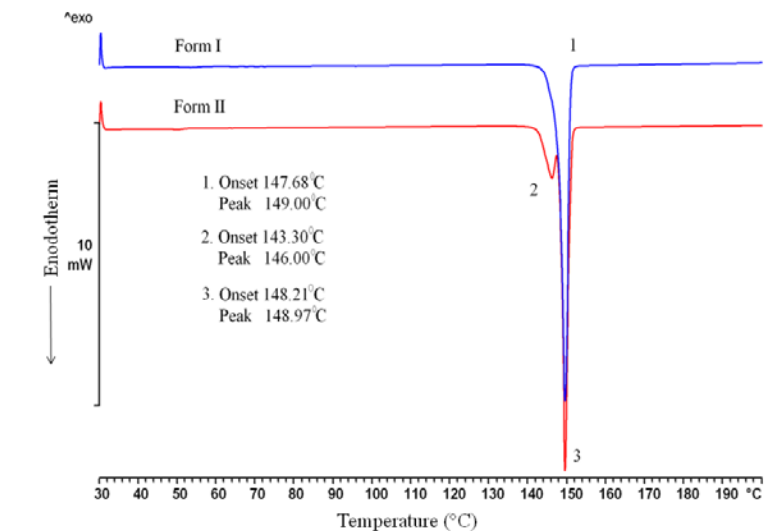
Differential scanning calorimetry measurements indicate the thermal characteristics of the polymorphs (Figure 5a). DSC of Form I showed one endotherm at $147.7^\circ\text{C}/149.0^\circ\text{C}$ (peak #1) for its melting point. Form II showed two endotherms at onset temperature of 143.3°C and 148.2°C . The broad small endotherm ($T_{\text{onset}} 143.3^\circ\text{C}$, $T_{\text{peak}} 146.0^\circ\text{C}$, peak #2) for Form II corresponds to the melting of this material. There is large endotherm at $148.2^\circ\text{C}/148.9^\circ\text{C}$ (#3), indicating that a phase transition has occurred to the stable polymorph I that is now melting. The thermograms confirm greater stability of Form I compared with Form II. The heat of fusion values of form II are not reliable for the first phase transformation to Form I immediately thereafter and then melts at 148.9°C . The closeness of the two endotherms and the absence of baseline separation make it difficult to use the ΔH_f numbers to apply the heat of fusion rule²⁷. To

obtain the actual enthalpy of fusion value for form II, DSC was recorded further at 10 °C and 20 °C/min heating rate.^{28a} With increasing heating rate, 1st endotherm (transition temperature) of form II slowly vanished and one single endotherm correspond to stable form I appeared (Figure 5b). Now it is easy to calculate enthalpy of fusion (Table 5) for both forms and can be compared. We speculated from DSC that Form II starts to melt at 143.3 °C and then immediately undergoes transformation to Form I at 148.2 °C, and the freshly formed Form I then melts at 148.9 °C. The phase transition²⁸ to Form I occurs immediately after melting of Form II and hence this is not a true solid-to-solid phase change. The higher melting Form I is stable over the temperature range studied (40 °C–200 °C), whereas Form II is stable up to 143.3 °C but converts to Form I at 148.2 °C, making nimesulide an enantiotropic system. The phase transformation was confirmed in an independent experiment. These phase transitions were also visualized under a hot stage microscope (HSM). Crystals of form I do not show any change before melting, but form II crystals melt at 145 °C, transform to Form I at 146 °C and resolidify, then finally Form I melts at 147 °C (Figure 6). Form II crystals were kept at 140 °C in the oven for 2–3 h, and then PXRD was recorded; the line trace matched with that of Form I and no peaks for Form II could be detected.

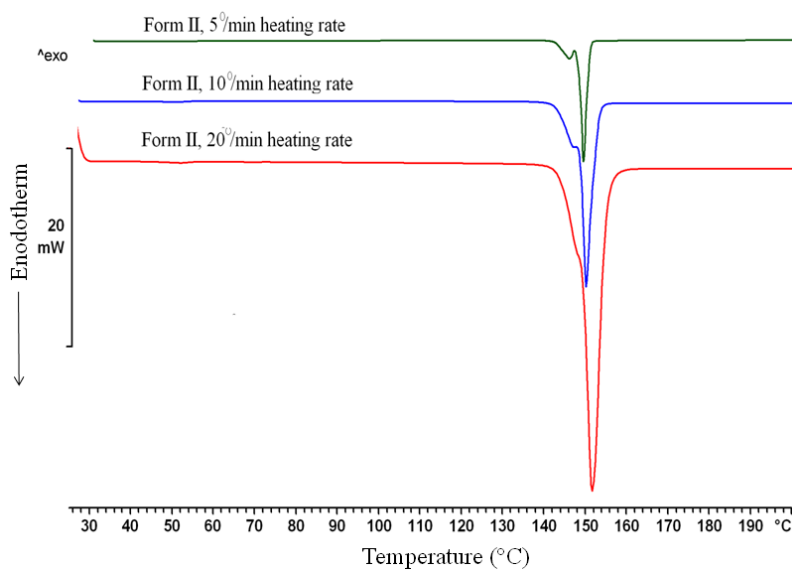
Two endotherms were observed in previous thermal measurements on nimesulide polymorphs,¹⁹ and the system was described as monotropic even though the lower melting Form II was noted to be metastable by DSC. However, the nature of the structure transformation event at 145 °C–146 °C was not investigated. The PXRD of trace of Form I obtained after keeping Form II at this temperature suggests an enantiotropic relationship for the dimorphs, and not a monotropic behavior. Desolvation of the dioxane solvate^{19c} of nimesulide at 120 °C, or keeping the same material at ambient conditions for a long time (1 year), or melting it at 145 °C transformed it to the stable Form I.

Table 5 Melting Point (onset, peak), Enthalpy of fusion (ΔH_{fus}).

Nimesulide	Form I	Form II
$T_{\text{onset/peak}}$ (°C)	147.7/ 149.0	143.3/146.0
ΔH_{fus} (kJ mol ⁻¹)	33.76 (05)	32.55 (05)



(a)



(b)

Figure 5 (a) Two endotherms at onset value 143 °C and 148 °C for Form II indicate a phase transition from Form II to Form I as the second peak is exactly matching with the melting endotherm of Form I. DSC of Form I have a single melting endotherm. (b) DSC of form II at different heating rate indicates, 1st endotherm (small) disappeared slowly and single endotherm (2nd endotherm) became predominant. Melting point of form II increased with increasing heating rate.

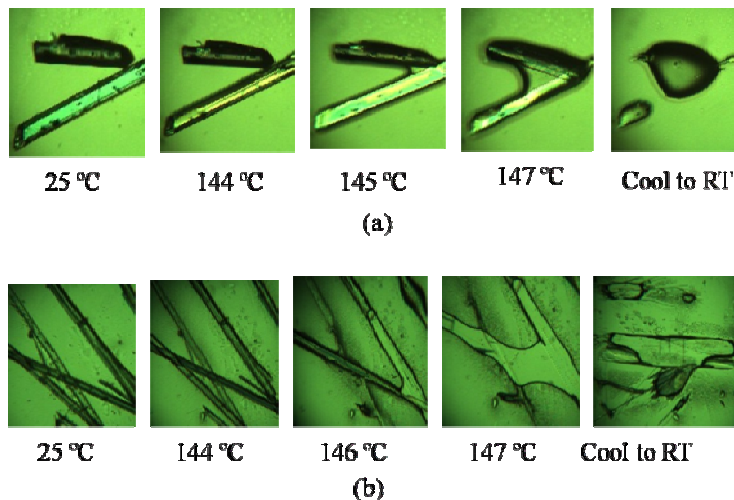


Figure 6 Hot-stage microscopy snapshots of nimesulide polymorphs. (a) Form I showed melting as the only event at 147 °C. (b) Form II showed change of needle morphology to thick plate in the sequence melting at 145 °C, transformation to Form I at 146 °C and resolidification, and finally melting of Form I at 147 °C. The presence of stable Form I upon cooling was confirmed by PXRD in an independent experiment.

2.5.4 Grinding and slurry experiments

The stable form I can be obtained exclusively by grinding of form II in tetrahydrofuran (THF), a solvent that was used to obtain the same polymorph. THF was added drop wise while grinding for 30 min to afford pure form I. Pure form II crystals were obtained by crystallization from THF or acetone. Slurry-grinding experiments on polymorphs of Nimesulide were carried out in THF for 24 h by continuous stirring. The starting material was either a mixture of form I and II, or pure form II. The product residue after slurry grinding was the stable form I, as confirmed by PXRD (Figure 7) and spectroscopy (see next). A solvent-mediated phase transformation²⁹ can proceed in three steps: (1) dissolution of the metastable form; (2) nucleation of the stable form; (3) crystal growth of the stable phase. The same sequence seems to occur in the case of Nimesulide.

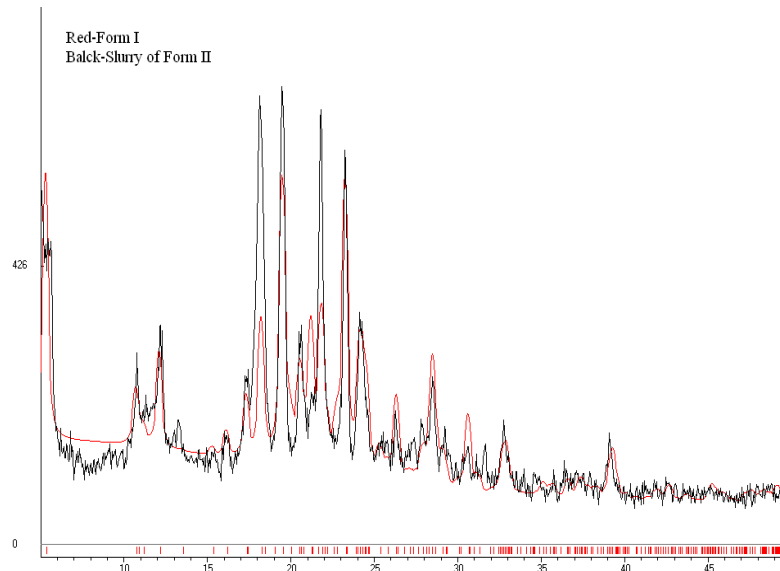


Figure 7 PXRD of Form I generated after slurry grinding of form II for 24 h in THF solvent (black trace) matches with the calculated X-ray pattern for Form I (red).

2.5.5 FT-IR, FT-Raman and ss-NMR spectroscopy

Infrared and Raman spectroscopy³⁰ provide useful information about the vibrational modes of a compound, and these change due to the physical state of the sample and because of hydrogen bonding and molecular conformations. Raman and IR bands are likely to be active for virtually all the bonds, but their relative intensities will differ, the more symmetric ones give higher Raman intensities, while the asymmetric modes exhibit higher IR intensities. In the spectra of the solid sample, symmetric and asymmetric N–H stretching vibrations are observed in the range 3279–3229 cm^{-1} and 3390–3323 cm^{-1} due to hydrogen bonding. Secondary sulphonamides show strong N–H stretching bands near 3265 cm^{-1} in the solid state. Asymmetric and symmetric stretch S=O Vibrational frequencies appear as strong absorption peaks between 1344 to 1317 and 1187 to 1147 cm^{-1} , respectively as well as S–N stretch at 924 to 906 cm^{-1} . The phenoxy group exhibits C–O stretch at 1200–1250 cm^{-1} . Nimesulide Form I and Form II show very little difference in N–H stretch, SO_2 symmetric stretch, and S–N bands (Figure 8). There is negligible difference in the stretching frequency because the same N–H \cdots O₂N hydrogen bond is present in both forms. Thus, Form I and Form II have very similar IR spectra. Even their Raman spectra exhibit marginal differences (Figure 9),

which is surprising because the molecules have very different conformations in the two crystal structures. The IR and Raman frequencies are listed in Table 6 and 7. The microstructures of nimesulide/crospovidone matrix were studied by electron and Raman microscopies.^{19f}

Solid-state ^{13}C NMR spectroscopy³¹ provides structural information on differences in hydrogen bonding, molecular conformations, and molecular mobility. It studies chemical environment of the nuclei which is different in polymorphs because of magnetic non-equivalence. Resonance peak for the magnetically nonequivalent nuclei will differ in different polymorphs and can provide useful information. It is expected that crystal structures with two molecules in the asymmetric unit will show at least a few doubled peaks in the ^{13}C ss-NMR spectrum. Differences in the two crystal structures of Nimesulide were analyzed by ^{13}C cross-polarization and magic-angle spinning (CP-MAS) ss-NMR.³² The crystallographic units of form I and II were easily identified by their distinguishable chemical shifts of identical carbon peaks at δ 106 (C6), 129 (C3) and 150 (C8) ppm (Figure 10). These δ values have been compared with solution NMR spectrum in CDCl_3 as reference (Table 8). The multiplicity of ^{13}C peaks for form I is due to two independent molecules in the crystallographic asymmetric unit. It appears that grinding form II solid for sample preparation causes partial conversion to form I, as seen by the shoulder peaks due to form I in the spectrum of form II.

Table 6 FT-IR frequency of two polymorphs of nimesulide

Nimesulide	N–H stretch (cm^{-1})	SO_2 asym stretch (cm^{-1})	SO_2 sym stretch (cm^{-1})	C–O stretch (cm^{-1})	S–N stretch (cm^{-1})
Form I	3284.9	1342.0	1153.6	1248.7	907.4
Form II	3287.9	1342.2	1152.2	1247.3	913.7, 905.1

Table 7 FT-Raman frequency two polymorphs of nimesulide

Nimesulide	N–H bend (cm^{-1})	SO_2 asym stretch (cm^{-1})	SO_2 sym stretch (cm^{-1})	lattice vibrations (cm^{-1})
Form I	1596.8	1335.3	1155.2	182.8, 199.2
Form II	1598.4	1336.5	1159.3	177.2, 200.5

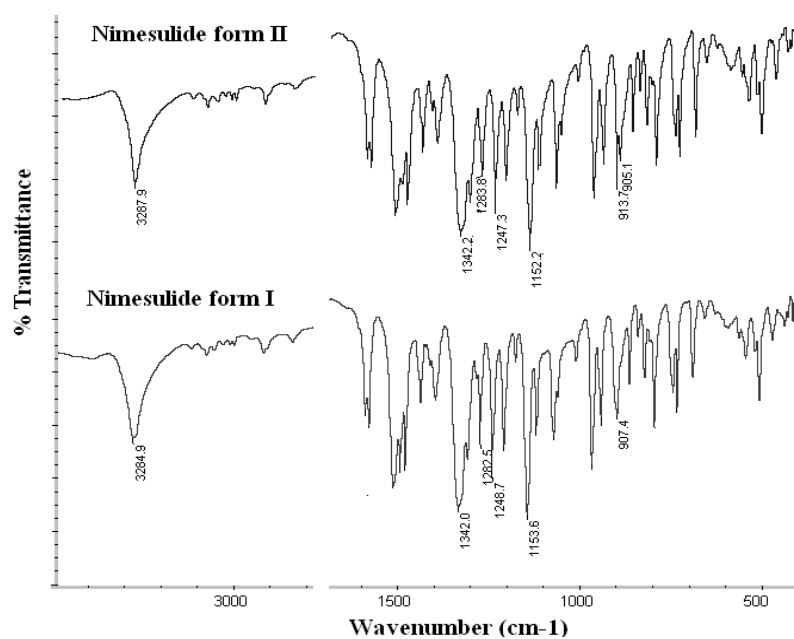


Figure 8 Comparison of FT-IR spectra of nimesulide polymorphs.

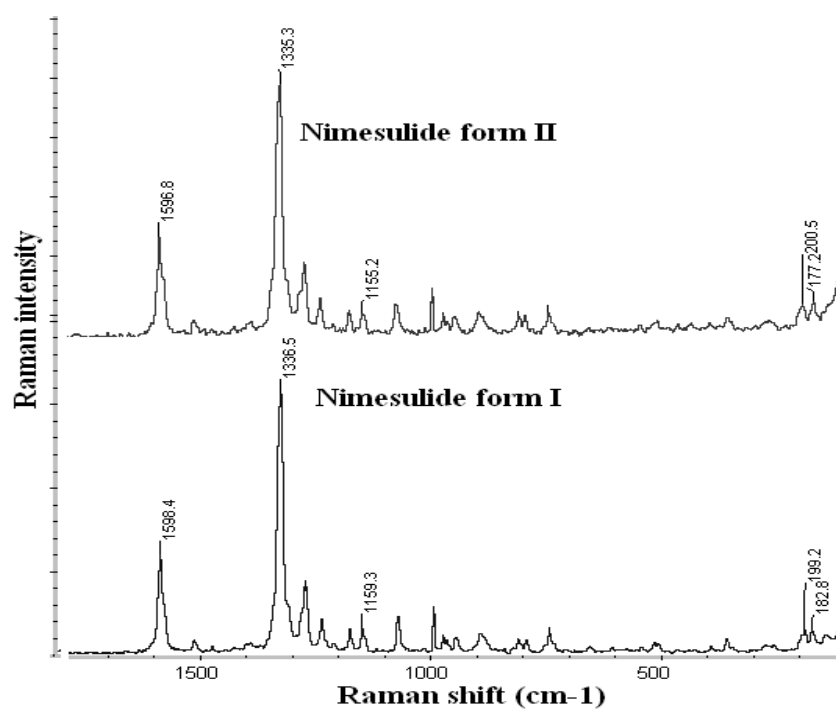


Figure 9 Comparison of FT-Raman spectra of nimesulide polymorphs.

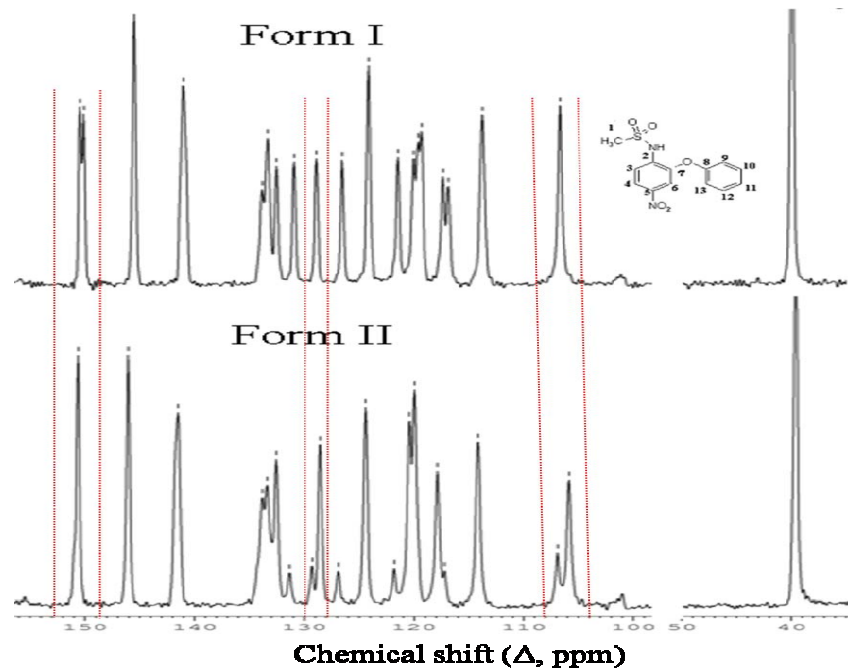


Figure 10 ^{13}C CP-MAS NMR spectra of Nimesulide polymorphs at 25 °C. The vertical red lines point to the regions where there are clear differences.

Table 8 Comparison of solid state ^{13}C NMR spectra of nimesulide polymorphs with the solution spectrum. See Figure 10 for atom numbering.

^{13}C peak	Form I	Form II	Nimesulide (CDCl_3)
1	39.68	39.59	40.56
2	141.46	141.51	143.70
3	129.26	129.28, 128.55	125.93
4	134.23, 133.72	133.82, 133.37	134.0
5,7	145.98	146.04	146.38
6	106.90	106.91, 105.86	111.91
8	150.96, 150.61	150.60	154.18
9,13	121.77, 120.33	121.80, 120.40	119.71, 119.40
10,12	132.91, 131.32	132.53, 131.33	130.68
11	124.48	124.40	117.41

2.5.6 Solubility study of nimesulide polymorphs

Solubility of a solid substance is the concentration at which the solution phase is in equilibrium with a given solid phase at a stated temperature and pressure. Under these conditions the solid is neither dissolving nor continuing to crystallize. When a substance exists in more than one crystalline form, only least soluble of these at a given temperature is considered the most physically stable form at that temperature and all others are considered to be metastable forms. In given cases, a solution of a substance may be in apparent equilibrium with one of these metastable phases for a long time, in which case the system is in metastable equilibrium and is expressing the thermodynamic solubility of that solid form. Always there is a possibility of transformation of metastable form to the most stable form in a certain solvent. To be sure, the time it takes to express this tendency depends on kinetic factors and may be quite variable; but in any event, a less soluble form never converts to the more soluble form under rigorously defined conditions. Generally phase transformation will be faster in high soluble solvent than less ones. So equilibrium solubility or dissolution experiments purpose one should choose low soluble solvent to avoid phase transformation. For e.g. diuretic drug furosemide exists as three crystalline forms, and DMF and dioxane solvates. Matsuda et al.³³ showed there is no phase transformation for furosemide polymorphs upto 6h at various pH ranging from 2.2-5.6, though meta stable form III showed highest solubility and stable form I showed lowest in all buffer solutions. But Nangia et al.^{9a} showed metastable form II of furosemide converted to stable form I within a few minutes in acetonitrile solvent, in which furosemide is highly soluble. So phase transformation is solvent dependent.

Nimesulide like other NSAIDs, has very poor aqueous solubility (10 mg/L) that imposes bioavailability problem. The aqueous solubility of the commercial (or reference form I) sample is reported as 14.8 mg/L (20 °C, pH 6.8) and 18.2 mg/L (37 °C, pH 7.4).³⁴ To increase the solubility of nimesulide, there are salt formations of nimesulide with Na⁺, L-arginine, L-lysine with β -CD complex; orally disintegrating tablets, solid dispersion techniques are used in literature.³⁵ Certainly nimesulide is more soluble in alkaline medium than acidic medium as sodium salt of nimesulide is soluble in water. Yet nimesulide is directly marketed in the brand name as Nimulid, Nicip, Nice etc. (100 mg tablets), which is stable form I, confirmed from PXRD. Two polymorphs of Nimesulide directly taken in pH 7 buffer medium and equilibrium solubility were

obtained after 48 h continuous stirring at 37 °C. Extinction coefficient of form I and II of Nimesulide are 13.91 ($\text{mM}^{-1}\text{cm}^{-1}$) and 9.53 ($\text{mM}^{-1}\text{cm}^{-1}$), obtained from the plot of five known concentrated solution of each form using Lambert-Beer's law. Solubility of form I and form II are 16.4 and 71.0 mg/L in pH 7 buffer medium and there was no phase transformation between them after slurry experiments. So equilibrium solubility suggest that metastable form II is 4.3 times more soluble than commercial form I. This kind of dramatic enhancement in solubility between the polymorphs of a drug is uncommon. In general, the ratio of polymorph solubility among drug polymorphs is less than 2. An exception to the rule is the anti-HIV drug Ritonavir, whose form II is 4.7 times more soluble than form I.³⁶

The rate of dissolution and the solubility of a drug in aqueous solvents are important aspects of the solid state Chemistry of drugs. The dissolution rate and solubility of different polymorphs of the same drug can be different. Before finalizing dosage form, one should confirm it has proper dissolution rate and also solubility. Intrinsic dissolution rate (IDR) can be defined as amount of drug dissolved per minute per unit surface area in a certain solvent medium at constant temperature. Intrinsic dissolution experiments of two polymorphs of nimesulide were determined at 37°C in pH 7 aqueous buffer medium. The amount of nimesulide dissolved (mg L^{-1}) versus time (h) is plotted in Figure 11 and the solubility values and intrinsic dissolution rates are listed in Table 9. The IDR of Form I and Form II is 5.7 and 13.6 $\mu\text{g}/(\text{cm}^{-2} \text{ min}^{-1})$, respectively, that is, Form II dissolves 2.4 times faster than Form I in pH 7 buffer solution. Linearity of the both forms indicates that there is no phase transformation upto 48h of dissolution experiments. Actually ratio of IDR between polymorphs should be higher always than that solubility. Form II showed more linear curve, where as stable form I get plateau region after 48h i.e. saturation point reached. May be another 24h dissolution experiments could give actual IDR values. So both solubility and IDR experiments suggest, form II is better candidate for formulation than stable form I.

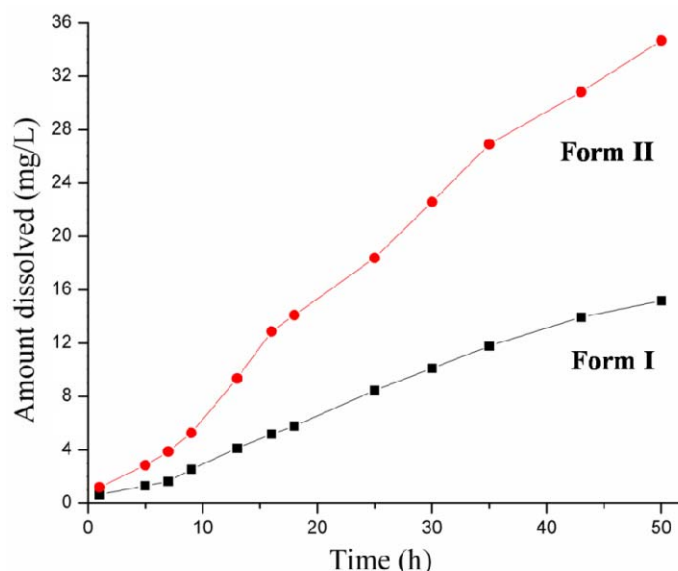


Figure 11 Intrinsic dissolution profile of nimesulide Form I and Form II in pH 7 buffer

Table 9 Solubility and dissolution rate of Nimesulide polymorphs at 37 °C in pH 7 buffer.

Nimesulide	Absorption coefficient, ϵ , $\text{mM}^{-1}\text{cm}^{-1}$	Equilibrium Solubility at 48h (mg L^{-1})	Intrinsic dissolution rate ($\mu\text{g cm}^{-2} \text{min}^{-1}$)
Form I	13.91	16.4	5.76
Form II	9.53	71.0	13.67

2.6 Conclusion

Knowledge of the stable polymorph of a drug is an obligatory step in the pharmaceutical industry for Drug regulatory reasons and manufacturing. Moreover, late-stage phase transitions to a new polymorph can become a big setback for the company. On the contrary, a metastable polymorph often has higher solubility and hence it is the desired polymorph for better bioavailability. In balance, however, the practical advantage of greater stability takes precedence over a more soluble but metastable polymorph. The marketed or reference Form I of nimesulide is the stable polymorph in all our experiments. Structural, phase stability, slurry experiments, and thermal measurements demonstrate the thermodynamic nature of polymorph I. Hydrogen bonding is similar for both forms, but packing wise they are different. Spectroscopic techniques, specially ss-NMR is useful to differentiate between polymorphs of Nimesulide. The significantly

enhanced bioavailability of nimesulide Form II suggests that the search for additives, coformers, excipients, and polymers to stabilize the metastable polymorph will be a rewarding exercise.

2.7 Experimental Section

Nimesulide was purchased from Sigma-Aldrich, Hyderabad, India and used directly for experiments. Nimesulide (brand name Nicip, Nimulid) was purchased from local medicine store to check what form of nimesulide is marketed in the tablet form. Nimesulide was extracted from MeOH after stirring for 1h and confirmed the purity with ^1H NMR and m.p.

2.7.1 Crystallization

The commercial material obtained from Sigma-Aldrich matched with Form I by PXRD. Form I was obtained exclusively after solid state grinding of Form II for 30 min in a mortar-pestle or slurry grinding for 24 h. The slurry solvent was either acetonitrile or THF. 100 mg of pure Form II was ground and added to 3 mL of THF and stirred continued for 24 h. The residue was collected and PXRD trace of the solid material matched with the calculated X-ray pattern of Form I. Form II was obtained exclusively by crystallization from THF solvent. The quality of single crystals of Form I was superior when the compound was crystallized in the presence of succinic acid (1:1 equiv). The quality of Form I in the absence of this additive was not so good, and very thin plate or twin crystals not suitable for X-ray diffraction were obtained.

2.7.2 X-ray crystallography

Reflections were collected on a Bruker SMART CCD diffractometer. Mo-K α ($\lambda = 0.71073 \text{ \AA}$) radiation was used to collect X-ray reflections on all crystal structures. Data reduction was performed using Bruker SAINT software.³⁷ Intensities were corrected for absorption using SADABS. Structures were solved and refined using SHELXL-97³⁸ with anisotropic displacement parameters for non-H atoms. Hydrogen atoms on N were experimentally located and all C-H atoms were fixed geometrically using the HFIX command in SHELX-TL.³⁹ X-Seed⁴⁰ was used to prepare the figures and packing diagrams. A check of the final CIF file using PLATON⁴¹ did not show any missed

symmetry. Hydrogen bond distances in Table 3 are neutron-normalized to fix the D–H distance to its accurate neutron value in X-ray crystal structures (N–H 1.009 Å, C–H 1.083 Å).

2.7.3 X-ray powder diffraction

Powder XRD patterns of all samples were recorded on a PANalytical 1830 (Philips Analytical) diffractometer using Cu-K α X-radiation ($\lambda = 1.54056$ Å) at 35 kV and 25 mA. Diffraction patterns were collected over the 2θ range of 5–50° at scan rate of 1 °/min. The program Powder Cell 2.3⁴² was used for overlaying the experimental PXRD pattern on the calculated X-ray lines from the crystal structure.

2.7.4 Vibrational spectroscopy

A Nicolet 6700 FT-IR spectrometer with a NXR FT-Raman Module was used to record IR and Raman spectra. IR spectra were recorded on samples dispersed in KBr pellets. Raman spectra were recorded on samples contained in standard NMR diameter tubes or on compressed samples contained in a gold-coated sample holder.

2.7.5 ¹³C Nuclear magnetic resonance spectroscopy

Solid-state ¹³C NMR (SS-NMR) spectroscopy provides structural information about differences in hydrogen bonding, molecular conformations, and molecular mobility in the solid state. The solid-state ¹³C NMR spectra were obtained on a Bruker Ultrashield 400 spectrometer (Bruker BioSpin, Karlsruhe, Germany) utilizing a ¹³C resonant frequency of 100 MHz (magnetic field strength of 9.39 T). Approximately 100 mg of sample was lightly packed into a zirconium rotor with a Kel-F cap. The cross polarization, magic angle spinning (CP-MAS) pulse sequence was used for spectral acquisition. Each sample was spun at a frequency of 5.0±0.01 kHz and the magic angle setting calibrated by the KBr method. Each data set was subjected to a 5.0 Hz line broadening factor and subsequently Fourier transformed and phase corrected to produce a frequency domain spectrum. The chemical shifts were referenced to TMS using glycine ($\delta_{\text{glycine}} = 43.3$ ppm) as an external secondary standard.

2.7.6 Thermal analysis

DSC was performed on a Mettler Toledo DSC 822e module. 4-6 mg of the sample was placed in a crimped but vented aluminum pan in the temperature range was 30-200 °C at heating rate of 5 °C min⁻¹. For nimesulide form II, DSC was recorded at 10° and 20 °C/min also to calculated exact enthalpy of fusion value. The sample was purged by a stream of dry nitrogen flowing at 150 mL min⁻¹.

2.7.7 Computations

Conformer energies were calculated in Gaussian 03 (B3LYP/6-31G (d,p)). Since the observed conformation in the crystal structure is usually different from the gas phase minimized conformer and often higher in energy, constrained optimization of the crystal conformer was carried out by keeping bond distances and angles fixed. Lattice energies were computed in Cerius² using the DREIDING force field. Crystal structures were minimized (U_{latt}) by allowing small variations in cell parameters but not gross differences between the calculated and experimental crystal lattice.

2.7.8 Dissolution experiments

A calibration curve was obtained for Form I and Form II of Nimesulide by plotting absorbance vs. concentration curve of UV-Vis spectra for known concentrated solutions in pH 7 aqueous buffer medium. The slope of the plot gave the molar extinction coefficient (ϵ) by using the Beer-Lambert's law. To obtain the equilibrium solubility, 200 mg Nimesulide was stirred for 48 h in 5 mL pH 7 aqueous buffer solutions at 37 °C, and the absorbance was measured at 397 nm. The concentration of the saturated solution was calculated at 48 h, which is the equilibrium solubility of that polymorph. PXRD of the solid residue (from slurry experiments) confirmed that there was no phase transformation between the polymorphs.

For intrinsic dissolution study, 200 mg of each polymorph was made into a pellet using hydraulic press at a pressure of 4 ton for 5 min. The pellet was compressed to provide a flat surface at one end and the other end was sealed. Then the pellet was dipped into 500 mL aqueous pH 7 buffer solutions at 37 °C with the paddle rotating at 150 rpm. At regular interval of 1 h, 5 mL of the dissolution medium was withdrawn and replaced by an equal volume of fresh medium to maintain a constant volume. Samples

were filtered through 0.2 μm nylon filter and assayed for drug content spectrophotometrically at 397 nm. The amount of drug dissolved in each time interval was calculated using the calibration curve.

2.8 References

1. S. R. Byrn, R. R. Pfeiffer, J. G. Stowell, *Solid-State Chemistry of Drugs*; SSCI: West Lafayette, IN, 1999.
2. (a) J. Bernstein, *Polymorphism in Molecular Crystals*; IUCR Monographs on Crystallography 14; Oxford Science Publications: OUP, Oxford, U.K. 2002. (b) W. C. McCrone, Polymorphism. In *Physics and Chemistry of the organic solid state*. Wiley Interscience, New York, USA, 1965.
3. J. Bauer, S. Spanton, R. Henry, J. Quick, W. Dziki, W. Porter, J. Morris, *Pharm. Res.* **2001**, *18*, 859.
4. (a) R. Hilfiker, *Polymorphism in the Pharmaceutical Industry*, Wiley-VCH, Weinheim, Weinheim, 2006. (b) H. G. Brittan, *Polymorphism in Pharmaceutical Solids*, Marcel Dekker, New York, 1999. (c) T. L. Threlfall, *Analyst* **1995**, *120*, 2435; (d) B. R. Spong, C. P. Price, A. Jayashankar, A. J. Matzger, N. Rodríguez-Hornedo, *Adv. Drug. Del. Rev.* **2004**, *56*, 241. (e) I. S. Lee, A. Y. Lee, A. S. Myerson, *Pharm. Res.* **2008**, *25*, 4.
5. (a) J. Bernstein, R. J. Davey, J. -O. Henck. *Angew. Chem. Int. Ed.* **1999**, *38*, 3440; (b) A. Nangia, *Acc. Chem. Res.* **2008**, *41*, 595. (c) B. Sarma, S. Roy, A. Nangia, *Chem. Commun.* **2006**, 4918.
6. (a) R. K. R. Jetti, R. Boese, J. A. R. P. Sarma, L. S. Reddy, P. Vishweshwar and G. R. Desiraju, *Angew. Chem., Int. Ed.*, **2003**, *42*, 1963. (b) B. R. Sreekanth, P. Vishweshwar and K. Vyas, *Chem. Commun.* **2007**, 2375. (c) P. Sanphui, B. Sarma, and A. Nangia, *Cryst. Growth Des.*, **2010**, *10*, 4550. (d) B. Sarma, P. Sanphui and A. Nangia, *Cryst. Growth Des.*, **2010**, *10*, 2388.
7. S. R. Vippagunta, H. G. Brittain and D. J. W. Grant, *Adv. Drug Deliv. Rev.*, **2001**, *48*, 3.
8. (a) A. Lemmerer, N. B. Báthori, C. Esterhuysen, S. A. Bourne and M. R. Caira, *Cryst. Growth Des.*, **2009**, *9*, 2646. (b) N. K. Nath, S. Nilapwar, A. Nangia, *Cryst. Growth Des.*, **2012**, *12*, 1613.

9. (a) N. J. Babu, S. Cherukuvada, R. Thakuria and A. Nangia, *Cryst. Growth Des.*, **2010**, *10*, 1979. (b) S. Cherukuvada, R. Thakuria and A. Nangia, *Cryst. Growth Des.*, **2010**, *10*, 3931. (c) M. Takasuka, H. Nakai, M. Shiro, *J. Chem. Soc. Perkin Trans. II* **1982**, 1061.
10. (a) W. Beckmann, *J. Cryst. Growth* **1999**, *198*, 1307. (b) J. Toth, A. K. Fodor, S. H. Peterfi, *Chem. Eng. Process.* **2004**, *44*, 193. (c) C. P. M. Roelands, S. Jiang, M. Kitamura, J. H. Horst, H. J. M. Kramer, P. J. Jansens, *Cryst. Growth Des.* **2006**, *6*, 955.
11. (a) E. H. Lee, S. R. Byrn, and M. T. Carvajal, *Pharm. Res.* **2006**, *23*, 2375. (b) M. Rafilovich, J. Bernstein, *J. Am. Chem. Soc.* **2006**, *128*, 12185. (c) X. Mei, C. Wolf, *Cryst. Growth Des.* **2004**, *4*, 1099. (d) M. T. Kirchner, D. Bläser, R. Boese, G. R. Desiraju, *CrystEngComm* **2009**, *11*, 229. (e) N. J. Babu, A. Nangia, *Cryst. Growth Des.* **2006**, *6*, 1995. (f) G. Mehta, S. Sen and K. Venkatesan, *CrystEngComm*, **2007**, *9*, 144.
12. (a) L. Kofler, E. Lindpaintner, *Mikrochemie* **1938**, *24*, 52. (b) I. S. Lee, K. T. Kim, A. Y. Lee, A. S. Myerson, *Cryst. Growth Des.* **2008**, *8*, 108.
13. (a) D. E. Braun, T. Gelbrich, R. K. R. Jetti, V. Kahlenberg, S. L. Price, U. J. Griesser, *Cryst. Growth Des.* **2008**, *8*, 1977. (b) R. J. Davey, N. Blagden, S. Righini, H. Alison, E. S. Ferrari, *J. Phys. Chem. B* **2002**, *106*, 1954. (c) C. Cashell, D. Corcoran, B. K. Hodnett, *Chem. Commun.* **2003**, 374, 375; (d) E. S. Ferrari, R. J. Davey, *Cryst. Growth Des.* **2004**, *4*, 1061.
14. (a) C. P. Price, A. L. Grzeiak, A. Matzger, *J. Am. Chem. Soc.* **2005**, *127*, 5512. (b) V. López-Mejías, J. W. Kampf and A. J. Matzger, *J. Am. Chem. Soc.* **2009**, *131*, 4554. (c) A. L. Grzeiak and A. J. Matzger, *J. Pharm. Sci.* **2007**, *96*, 2978. (d) S. J. Bonafede, M. D. Ward, *J. Am. Chem. Soc.* **1995**, *117*, 7853. (e) C. A. Mitchell, L. Yu, M. D. Ward, *J. Am. Chem. Soc.* **2001**, *123*, 10830. (f) J. Zaccaro, J. Matic, A. S. Myerson, B. A. Garetz, *Cryst. Growth Des.* **2001**, *1*, 5. (g) L. J. Chyall, J. M. Tower, D. A. Coates, T. L. Houston, S. L. Childs, *Cryst. Growth Des.* **2002**, *2*, 505. (h) J. M. Ha, J. H. Wolf, M. A. Hillmyer, M. D. Ward, *J. Am. Chem. Soc.* **2004**, *126*, 3382. (i) M. L. Peterson, S. L. Morissette, C. McNulty, A. Goldsweig, P. Shaw, M. LeQuesne, J. Monagle, N. Encina, J.

- Marchionna, A. Johnson, J. Gonzalez-Zugasti, A. V. Lemmo, S. J. Ellis, M. J. Cima, O. Almarsson, *J. Am. Chem. Soc.* **2002**, *124*, 10958.
15. (a) J. Haleblan, W. McCrone, *J. Pharm. Sci.* **1969**, *58*, 911. (b) E. Joiris, P. Di Martino, C. Berneron, A. M. Guyot-Hermann, J. C. Guyot, *Pharm. Res.* **1998**, *15*, 1122. (c) M. Bartolomei, P. Bertocchi, M. C. Ramusino, N. Santucci, L. Valvo, *J. Phar. Biomed. Anal.* **1999**, *21*, 299. (d) S. Changquan, D. J. W. Grant, *Pharm. Res.* **2001**, *18*, 274. (e) J. M. Rollinger, E. M. Gstrein, A. Burger, *J. Pharm. Biopharm.* **2002**, *53*, 75.
16. B. C. Hancock, G. Zografi, *J. Pharm. Sci.* **1997**, *86*, 1
17. (a) M. Otsuka, H. Hasegawa, Y. Matsuda, *Chem. Pharm. Bull.* **1999**, *47*, 852. (b) P. Di Martino, P. Conflant, M. Drache, J. P. Huvenne, A. M. Guyot-Hermann, *J. Therm. Anal. Calorim.* **1997**, *48*, 447. (c) P. Di Martino, M. Scoppa, E. Joiris, G. F. Palmieri, C. Andr s, Y. Pourcelot, S. Martelli, *Int. J. Pharm.* **2001**, *213*, 209. (d) H. K. Chan, E. Doelker, *Drug Dev. Ind. Pharm.* **1985**, *11*, 315. (e) A. Bauer-Brandl, *Int. J. Pharm.* **1996**, *140*, 195.
18. (a) L. Bicarini, L. Patoia and A. Del Favero, *Drugs Today*, **1988**, *24*, 23. (b) A. K. Singla, M. Chawla and A. Singh, *J. Pharm. Pharmacol.*, **2000**, *52*, 467. (c) G. G. I. Moore, J. K. Harrington, Belgian Patent 801,812, US Patent 3,840,597, **1974**. (d) K. F. Swingle, G. G. I. Moore, *Drugs Exp. Clin. Res.* **1984**, *10*, 587. (e) L. Biscarin, L. L. Patoia, A. D. Favero, *Drugs Today*, **1988**, *24*, 23. (f) E. S. Diaz-Cruz, C. L. Shapiro, R. W. Brueggemeier, *J. Clin. Endocrinol. Metab.* **2005**, *90*, 2563. (g) B. Su, R. Tian, M. V. Darby, and R. W. Brueggemeier, *J. Med. Chem.* **2008**, *51*, 1126. (h) G. L. Amidon, H. Lennern s, V. P. Shah, J. R. Crison, *Pharm Res.* **1995**, *12*, 413. (i) F. Meriani, N. Cocceani, C. Sirotti, D. Voinovich, M. Grassi, *J. Coll. Inter. Sci.* **2003**, 263 590.
19. (a) S. S. Braga, P. Ribeiro-Claro, M. Pillinger, I. S. Gon alves, F. Pereira, A. C. Fernandes, C. C. Rom o, P. B. Correia, and J. J. C. Teixeira-Dias, *Org. Biomol. Chem.*, **2003**, *1*, 873. (b) B. N. Nalluri, K. P. R. Chowdhary, K. V. R. Murthy, V. Satyanarayana, A. . Hayman and G. Becket, *J. Inclu. Phenom. & Macro. Chem.* **2005**, *53*, 103. (c) P. Bergese, E. Bontempi, I. Colombo, D. Gervasoni, L. E. Depero, *Composites Sci. & Techno.* **2003**, *63*, 1197. (d) G. Piel, B. Pirotte, I. Delneuve, P. Neven, G. Llabres, J. Delarge and L. Delattre, *J. Pharm. Sci.*

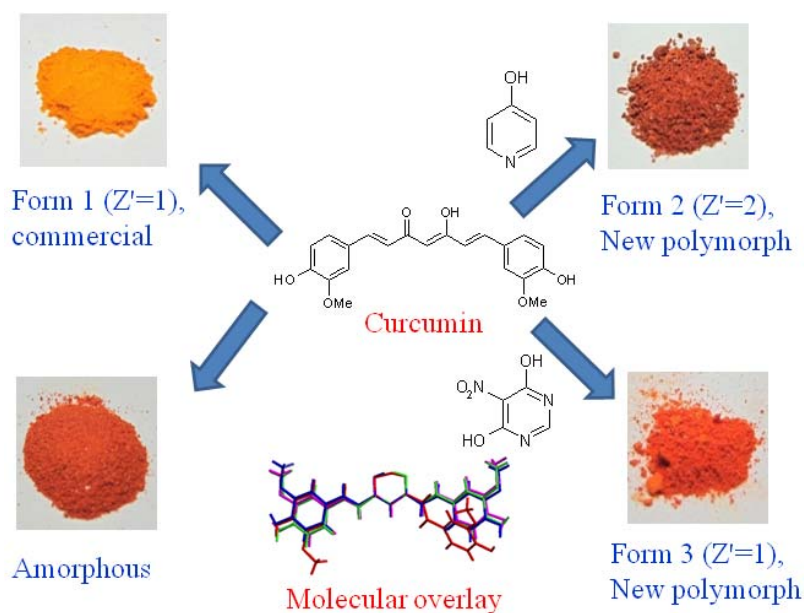
- 1997**, 86, 475. (e) P. D. Martino, R. Censi, C. Barthelemy, R. Gobetto, E. Joiris, A. Masic, P. Odou and S. Martelli. *Int. J. Pharm.* **2007**, 342, 137. (f) P. Bergese, I. Alessandri, I. Colombo, N. Coceani, L. E. Depero, *Compos Part A* **2005**, 36, 443.
20. L. Dupont, B. Pirrotte, B. Masereel, J. Delarge and J. Geczy, *Acta Cryst.* **1995**, C51, 507.
21. P. Sanphui, B. Sarma, A. Nangia, *J. Pharm. Sci.* **2011**, 100, 2287. (b) R. J. Davey, N. Blagden, G. D. Potts, R. Docherty, *J. Am. Chem. Soc.* **1997**, 119, 1767. (c) X. He, J. G. Stowell, K. R. Morris, R. R. Pfeiffer, H. Li, G. P. Stahly, S. R. Byrn, *Cryst. Growth Des.* **2001**, 1, 305. (d) J. Li, S. A. Bourne and M. R. Caira, *Chem. Commun.* **2011**, 47, 1530. (e) M. Karanam, S. Dev, A. R. Choudhury, *Cryst. Growth Des.*, **2012**, 12, 240.
22. (a) S. Maruyama, H. Ooshima, J. Kato, *Chem. Eng. J.* **1999**, 75, 193. (b) C. H. Gu, Jr. V. Young, D. J. W. Grant, *J Pharm. Sci.* **2001**, 90, 1878. (c) E. S. Ferrari, R. J. Davey, *Cryst. Growth Des.* **2004**, 4, 1061.
23. (a) J. W. Steed, *CrystEngComm*, **2003**, 5, 169. (b) G. R. Desiraju, *CrystEngComm*, **2007**, 9, 91. (c) S. Roy, R. Banerjee, A. Nangia, and G. J. Kruger, *Chem. Eur. J.* **2006**, 12, 3777.
24. Cerius² Materials studio and Gaussian 03, version 6.0.
25. (a) R. B. Gandhi, J. B. Bogardus, D. E. Bugay, R. K. Perrone, M. A. Kaplan, *Int. J. Pharm.* **2000**, 201, 221. (b) X. J. Gu and W. Jiang, *J Pharm. Sci.* **1995**, 84, 1438. (c) M. Tiwari, G. Chawla, A. K. Bansal, *J Pharm Biomed Anal* **2007**, 43, 865.
26. (a) L. Seton, D. Khamar, I. J. Bradshaw, and G. A. Hutcheon, *Cryst. Growth Des.*, **2010**, 10, 3879. (b) L. Fábán, A. Kálmán, G. Argay, G. Bernáth and Z. Cs. Gyarmatib, *Chem. Commun.*, **2004**, 2114. (c) P. Sanphui, N. R. Goud, U. B. R. Khandavilli, S. Bhanoth and A. Nangia, *Chem. Commun.*, **2011**, 47, 5013.
27. A. Burger, R. Ramberger, *Mikrochim Acta II* **1979**, 259
28. (a) S. Roy, P. M. Bhatt, A. Nangia and G. J. Kruger, *Cryst. Growth Des.* **2007**, 7, 476. (b) K. Kimura, F. Hirayama and K. Uekama, *J Pharm. Sci.* **1999**, 88, 385. (c) L. M. Katrincica, Y. T. Sunb, R. A. Carltonb, A. M. Diedericha, R. L. Muellerb, F. G. Vogtb, *Int. J. Pharm.* **2009**, 366, 1.

29. (a) J. M. Rollinger, E. M. Gstrein, A. Burger, *Eur. J. Pharm. & Biopharm.* **2002**, 53, 75. (b) Y. H. Sugita, *Agric. Biol. Chem.* **1988**, 52, 3081.
30. (a) A. L. Grzesiak, M. Lang, K. Kim, A. J. Matzger, *J. Pharm. Sci.* **2003**, 92, 2260. (b) A. M. Tudor, S. J. Church, P. J. Hendra, M. C. Davies and C. D. Melia, *Pharm. Res.* **1993**, 10, 1772. (c) F. Vrečer, M. Vrbinc, A. Meden. *Int. J. Pharm.* **2003**, 256, 3. (d) Y. A. Chesalov, P. Baltakhinov, T. N. Drebuschak, E. V. Boldyreva, N. V. Chukanov, V. A. Drebuschak. *J. Mol. Struct.* **2008**, 891, 75.
31. (a) S. M. Reutzel-Edens, J. K. Bush, P. A. Magee, G. A. Stephenson and S. R. Byrn, *Cryst. Growth Des.* **2003**, 3, 897. (b) K. Kimura, F. Hirayama and K. Uekama, *J. Pharm. Sci.* **1999**, 88, 385. (c) N. Zencirci, T. Gelbrich, D. C. Apperley, R. K. Harris, V. Kahlenberg and U. J. Grisser, *Cryst. Growth Des.* **2010**, 10, 302. (d) S. Tothadi, B. R. Bhogala, A. R. Gorantla, T. S. Thakur, R. K. R. Jetti, G. R. Desiraju, *Chem. Asian J.* **2012**, 7, 330.
32. (a) P. A. Tishmack, D. E. Bugay and S. R. Byrn, *J. Pharm. Sci.* **2003**, 92, 441. (b) D. D. Laws, H. -ML Bitter, and A. Jerschow, *Angew Chem. Int. Ed.* **2002**, 41, 3096
33. Y. Matsuda, E. Tatsumi, *Int. J. Pharm.* **1990**, 60, 11.
34. (a) A. K. singla, M. Chawla, A. singh, *J. Pharm. Pharmacol.*, **2000**, 52, 467. (b) B. Pirrote, G. Piel, P. Neven, I. Delneuveille and J. Geczy. US patent **1998**, 5,756,546.
35. (a) M. Moneghinia, I. Kikicb, B. Perissuttia, E. Franceschinisa, A. Cortesi, *Eur. J. Pharm. & Biopharm.* **2004**, 58, 637. (b) L. Magarotto, s. Bertini, C. Cosentino, G. Torri, *Mat. Sci. Forum* **2001**, 360, 643. (c) R. A. Shoukri, I. S. Ahmed, R. N. Shamma, *Eur. J. Pharm. & Biopharm.* **2009**, 73, 162.
36. (a) M. Pudipeddi, A. T. M. Serajuddin, *J Pharm. Sci.* **2005**, 94, 929. (b) J. Bauer, S. Spanton, R. Henry, J. Quick, W. Dziki, W. Porter, and J. Morris, *Pharm. Res.*, **2001**, 18, 859.
37. SAINT-Plus, version 6.45, Bruker AXS Inc., Madison, WI, 2003.
38. G. M. Sheldrick, SHELXS-97 and SHELXL-97, University of Göttingen, 1997.
39. SMART (Version 5.625) and SHELX-TL (Version 6.12), Bruker AXS Inc., Madison, WI, 2000.

40. L. J. Barbour, X-Seed, Graphical interface to SHELX-97 and POV-Ray, University of Missouri-Columbia, 1999.
41. A. L. Spek, PLATON, A multipurpose crystallographic tool, Utrecht University, Utrecht, 2002.
42. Powder Cell, A program for structure visualization, powder pattern calculation and profile fitting.

Chapter Three

New Polymorphs of Curcumin and their Faster Dissolution rates



New crystalline polymorphs (form 2 and 3) and one stable amorphous phase of Curcumin were obtained during attempted cocrystallization and melt crystallization experiments. Different colors of the polymorphs may be due to greater planarity in the structure of metastable form 2 and 3 compared to stable form 1.

3.1 Introduction

Crystalline solids have regular arrangements of molecules that repeat in three dimensions, whereas amorphous solids lack long-range order and periodicity. The differences in molecular arrangement can result in substantially different physical and chemical properties of crystalline and amorphous solids in pharmaceutical substances.¹ Although amorphous solids often have desirable properties such as faster dissolution rates than their crystalline counterparts, they are not marketed as widely as crystalline forms because of their lower physicochemical stability and their frequent tendency to crystallize in the stable form. Most of the marketed pharmaceuticals are preferred in crystalline stable forms as tablet dose. The arrangement of the molecules in a crystal determines its physical and chemical properties, i.e. stability, solubility, bioavailability of the particular drug. At the supramolecular level, variation in the crystalline forms of a solid material is possible. They may either exist as single molecular entities or multi-component species. For both cases molecular solids can show polymorphism,² which is defined as the ability of a substance to exist in two or more crystalline phases that have different arrangements and/or conformations of molecules in the crystal lattice without undergoing changes in its chemical composition.

The structural differences between polymorphs originate through three crystalline arrangements, namely, packing, synthon and conformational polymorphism. Packing polymorphism is a phenomenon by which molecules that are conformationally rigid can be packed into different three-dimensional structures. Again synthon polymorphism arises from synthon differences. For example, the anti-bacterial drug Nitrofurantoin is a dimorphic substance.³ Form 1 contains amide dimer N–H···O hydrogen bonds, whereas form 2 arises from different packing arrangements of molecules connected by infinite chain of N–H···O hydrogen bonds or an amide catemer (Figure 1). Pyrazinamide, Carbamazepine, Paracetamol are other examples of APIs having packing differences.⁴ Conformational polymorphism on the other hand arises from different conformers that can pack into different crystal structures. For example, anti-diabetic drug Tolbutamide⁵ crystallizes into five polymorphs (forms I–V) which differ in their mode of packing and in molecular conformation but with similar hydrogen bonding synthon (urea tape motif), shown in Figure 2. Venlafaxine hydrochloride,

Phenobarbital, Temozolomide, Furosemide, Chlortalidone, Indomethacin, ritonavir etc. are well known examples of conformational polymorphs.⁶

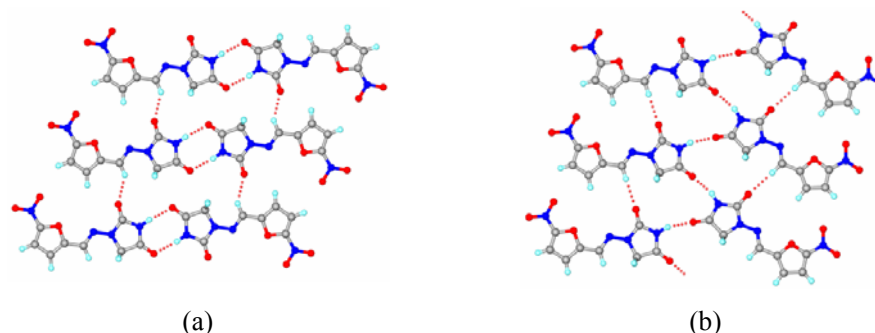


Figure 1 Polymorphs of Nitrofurantoin drug.³ (a) form 1. (b) form 2. The amide molecule forms amide dimer in form 1 whereas it forms catemer motif in form 2. Polymorphism arises due to different modes of amide packing arrangements.

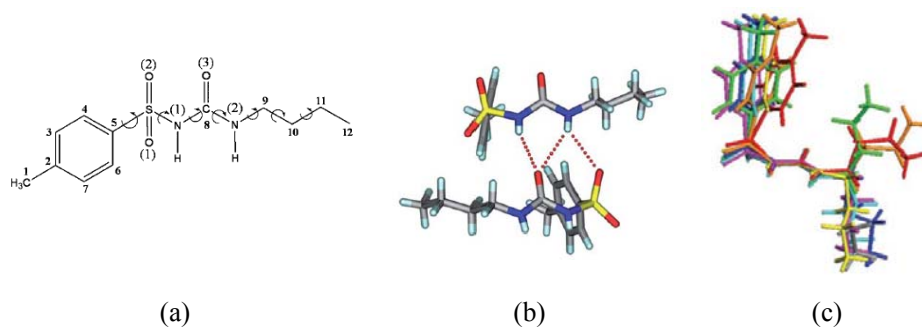


Figure 2 (a) Chemical structure of Tolbutamide (TB) with several rotational degrees of freedom. (b) Common urea motif present in all the forms in tobutamide. (c) Molecular overlay of four polymorphs of Tolbutamide indicates molecular flexibility in the n-butyl chain (culled from ref. 5).

There has been substantial research activity in the field of polymorphism driven by both fundamental scientific discovery and their importance across a wide range of industries like agrochemicals, dyes, foodstuffs and especially in the pharmaceutical industry. Recent books by Hilfiker, Brittain, Bernstein and Byrn¹ highlighted the importance of polymorphism in pharmaceuticals.⁷ There are numerous special issues of journals⁸ dedicated to this particular topic and several annual reviews⁹ and patents are published in the last decade. Despite its potential implications, the phenomenon of polymorphism is still not properly understood, and even after many decades of research there is no clear answer to what type of molecules will exhibit polymorphism. Even

sometimes it is very difficult to reproduce certain polymorphs, which have appeared initially and characterized, called disappearing polymorphs.¹⁰ Some drug molecules easily form polymorphs but some molecules like meclofenamic acid, niflumic acid¹¹ do not show any sign of polymorphism even after extensive research. In 2006 a new polymorph II of maleic acid^{12a} was discovered during attempted co-crystallization experiments with Caffeine, 124 years after the first crystal form was studied. However there are difficulties in reproducing form II crystallization of maleic acid.^{12b} Similarly a second polymorph of Aspirin^{12c} was obtained in the presence of an additive Levetiracetam. Recently Caira et al^{12d} obtained new polymorphs of nicotinamide and isonicotinamide during attempting cocrystallization experiments with an anti-tubercular API. These experiments show that additives can induce the appearance of polymorphic forms. It has been reported that changing the crystallization conditions such as solvents and temperature, pseudoseeding, adding impurities, additives or polymer etc.¹³ yielded novel polymorphs in the literature. Impurities somehow block the crystallization process of stable form and favour metastable form processing. Of these methods, the induced nucleation or pseudoseeding with the adequate seed crystals of the form to be reproduced is the most straightforward and promising to get the desired polymorph by inhibiting the nucleation or the crystal growth of other undesired polymorphs.

3.2 Curcumin

Curcumin (chemical name diferuloylmethane) is present in turmeric as a mixture with three of its analogues, viz. demethoxycurcumin, bis-demethoxycurcumin and cyclocurcumin, together known as curcuminoids (Figure 3). But Curcumin is the active ingredient in the traditional herbal remedy and dietary spice turmeric (*Curcuma longa*). This vibrant yellow spice, derived from the rhizome of the plant¹⁴, has a long history of use in traditional medicines of China and India. The rhizome of turmeric has been crushed into a powder and used in Asian cookery, medicine, cosmetics, and fabric dying for more than 2000 years. As part of the ancient Indian medical system Ayurveda, a poultice of turmeric paste is used to treat common eye infections, and to dress wounds, treat bites, burns, acne and various skin diseases. Powdered turmeric is taken with boiled milk to cure cough and related respiratory ailments. In food and manufacturing, curcumin is currently used in perfumes and as a natural yellow coloring agent, as well as

an approved food additive (nutraceutical) to flavor various types of curries and mustards.¹⁵

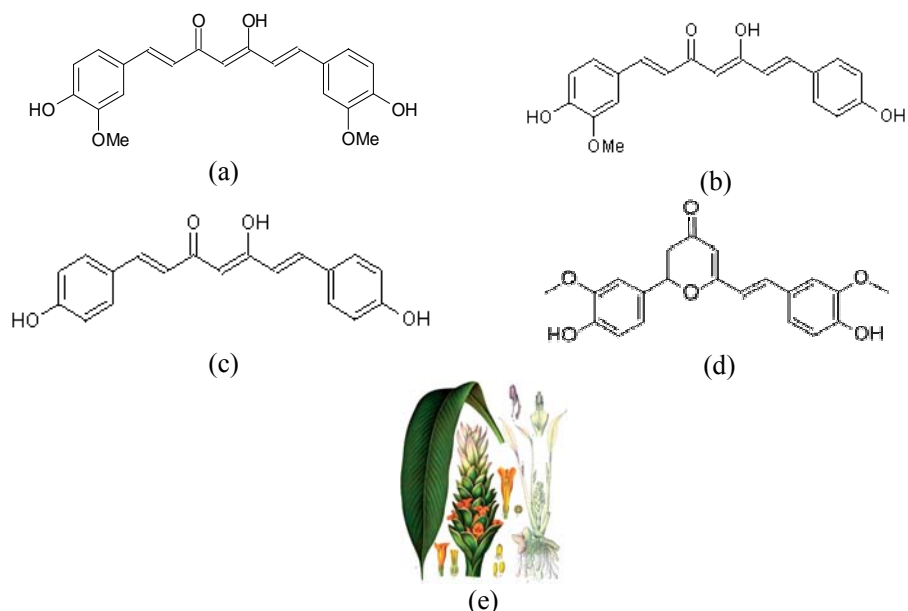


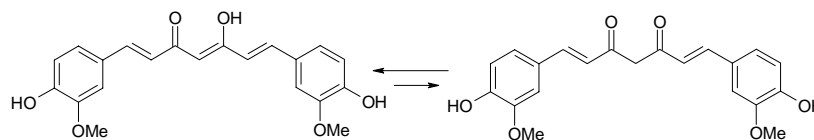
Figure 3 Chemical structure of (a) Curcumin, (b) demethoxycurcumin, (c) bis-demethoxycurcumin, (d) cyclocurcumin and (e) *Curcuma longa* (from Koehler's medicinal plant), culled from ref.^{14c}

3.3 Problems and promises of Curcumin

Curcumin (chemical name diferuloylmethane) is a hydrophobic polyphenol with diverse pharmacological effects including anti-inflammatory, antioxidant, antiproliferative and antiangiogenic activities.¹⁶ Phase I clinical trials have shown that curcumin is safe even at high doses (12 g/day) in humans but exhibits poor bioavailability. Major reasons contributing to the low plasma and tissue levels of curcumin appear to be due to poor absorption, rapid metabolism, and rapid systemic elimination. Once absorbed orally, Curcumin is subjected to conjugations like sulfation and glucoronidation. Metabolised products have reduced biological activity than curcumin. Liver is main responsible for metabolism of Curcumin.¹⁷ It has very low solubility in water, maximum solubility after heating for 10 minutes in water is 7.4 mg/L. A solution to the problem of bioavailability would be to increase the solubility of curcumin by heating. Heat solubilised Curcumin or turmeric should be considered for oral administration to patients in clinical trials because Curcumin's full pharmacological

potential is limited to its extremely limited solubility in water. There is no effect of heat on the activity of Curcumin. However, 98.5% Curcumin and 94.7% turmeric is still insoluble even after heating.¹⁸ Again Curcumin has stability problem in neutral or alkaline medium. It is stable in acidic medium, but when it was incubated in 0.1 M Phosphate buffer and serum free medium, pH 7.2 at 37 °C, more than 90% curcumin decomposed within 30 min.¹⁹ Tonnesen et al.^{19b} identified degradation products including ferulic acid and feruloylmethane, and studied the kinetics in a MeOH/aqueous buffer medium (1:9). Hence, despite its efficacy and safety, curcumin is still not approved as a therapeutic agent. The stability and bioavailability of curcumin has been improved by several methods, e.g. by (1) adding adjuvants such as piperine to block the metabolic pathways of curcumin, (2) novel drug delivery platforms such as nanoparticles, liposomes, micelles, phospholipid complexes, and (3) concomitant administration of lecithin, quercetin, genistein, eugenol, terpinol etc. to increase the bioavailability.¹⁷ The aqueous solubility of curcumin was enhanced 38 fold in the presence of 1-10% (w/v) rubusoside. The bioavailability of curcumin in water and lipid medium was enhanced by complexation with phosphatidyl choline in equimolar ratio.²⁰ Polymorph screening is another method to improve solubility of a drug.²¹

Curcumin was first isolated by Vogel in 1842 and structurally characterized by Lampe and Milobedeska in 1910. It was synthesized and confirmed in 1913.²² The molecule exists as keto-enol tautomers (Scheme 1), being present predominantly in the keto form in acidic and neutral solution while the enol tautomer is stable in alkaline medium.

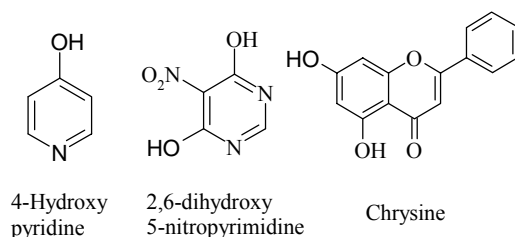


Scheme 1 Enol and keto tautomers of Curcumin

3.4 Results and Discussion

The first crystal structure of Curcumin was reported in 1982 in the monoclinic space group $P2_1/n$.^{23a} There are four subsequent reports of Curcumin structure, all in space group $P2_1/n$ ($Z = 4$, $Z' = 1$) having improved crystal data quality and structure refinement parameters.²³ No polymorphs are known for this biologically active ingredient

despite its ancient origin and current thrust to improve its stability and bioavailability. To obtain a new solid form having better solubility and bioavailability, polymorph screening was performed by solution crystallization, addition of coformers or additive, melting, sublimation etc.²⁴ Commercial curcumin (Sigma-Aldrich material) matched with the known stable form 1 by X-ray powder diffraction pattern (PXRD). Crystallization from several common laboratory solvents at room temperature routinely gave crystals that matched with the same unit cell and PXRD lines. Single crystals of a new polymorph 2 were crystallized in the orthorhombic space group $Pca2_1$ ($Z = 8$, $Z' = 2$) upon attempted cocrystallization of curcumin with 4-hydroxypyridine in EtOH at room temperature. The same form 2 was obtained from DMSO solution at room temperature and also from a saturated solution of curcumin in EtOH kept at 10 °C in refrigerator for 2 days. Again form 3 can be obtained in presence of Chrysine and 4,6-dihydroxy, 5-nitro pyrimidine (Scheme 2) and crystallized in the space group $Pbca$ ($Z=8$, $Z' = 1$). The crystallographic parameters for curcumin polymorphs are summarized in Table 1. An amorphous phase of Curcumin was obtained after melting the compound at ~185°C cooling to room temperature or freeze cooling. Amorphous phase is unusually stable at ambient conditions of temperature (20-35 °C) and humidity (40-70 %) in the sealed sample vial for at least 6 months.



Scheme 2 Coformers used to obtain form 2 and 3 of Curcumin

3.4.1 X-ray crystal structure solution and refinement

Single crystal X-ray data were collected at 100K to compare the structure of Curcumin polymorphs. The crystal structure of Curcumin form 1 was solved in monoclinic $P2_1/n$ space group with one molecule in the asymmetric unit ($Z' = 1$) in its enol tautomer. The molecule has a curved, slightly twisted conformation in form 1. Phenyl rings are slightly twisted from each other in form 1. Strong intramolecular

hydrogen bond (O4–H4A···O3, 1.51 Å, 2.441(2) Å, 155.7°) is present in the enol tautomer. Normalized hydrogen bonds for curcumin polymorphs are summarized in Table 2. Curcumin molecules are aggregated into infinite chains linked through intermolecular phenolic OH and the enolic OH (O1–H1A···O4, 2.28 Å, 2.904(2) Å, 119.8°) along the *a*-axis. In polymorph 1 there are phenol O–H···O hydrogen bonds on both sides to different molecules which are in turn connected to a fourth curcumin molecule in a macrocyclic hydrogen bond ring of $R^4_5(42)$ graph set²⁵ (Figure 4a). Weak C–H···O interactions also play an important role in the overall molecular aggregation. There is a bifurcated C–H···O hydrogen bond involving phenolic O–H acceptor with aromatic hydrogen (C3–H3···O5: 2.58 Å, 3.544(2) Å, 149.6°) and olefinic hydrogen (C8–H8···O5: 2.54 Å, 3.528 (2) Å, 154.5°) donors. The molecular packing was compared in the three polymorphs by considering 6 nearest neighbor molecules. Adjacent molecules are connected by O–H···O hydrogen bonds and such neighboring tapes make bifurcated C–H···O motif of $R^1_2(7)$ ring in form 1 (Figure 4b).

The crystal structure of Curcumin form 2 was solved in orthorhombic space group $Pca2_1$ with two molecules in the asymmetric unit ($Z' = 2$). Both the symmetry-independent molecules (A and B) have intramolecular O–H···O hydrogen bond in the enol tautomer. Molecule A (ball & stick model) forms intermolecular O–H···O hydrogen bond (O7–H7A···O9: 1.71 Å, 2.626(3) Å, 154.0°) with another molecule through enolic carbonyl and phenolic OH group along the *c*-axis. In contrast, Molecule B (capped stick model) forms an intermolecular O–H···O hydrogen bond (O1–H1A···O12: 2.23 Å, 2.834(3) Å, 119.0°). In addition B type molecules are connected intermolecularly by O–H···O hydrogen bond (O5–H5A···O1, 2.14 Å, 2.905(3) Å, 134.0°) between phenolic OH groups in a zigzag chain along the *a*-axis. The two crystallographically independent molecules are connected by $R^1_2(6)$ ring and C–H···O interaction (Figure 5a). The A molecules form O–H···O hydrogen bond (O11–H11A···O8: 1.96 Å, 2.896(3) Å, 159.0°) with the methoxy acceptor also along the *a*-axis. A and B type molecules are interconnected through bifurcated C–H···O interaction (C33–H33···O5: 2.32 Å, 3.288(3) Å, 148.0° and C31–H31···O5: 2.67 Å, 3.487(3) Å, 144.7°) from olefinic hydrogens to phenolic OH. There are C–H···O interactions from methoxy group of molecule B (C20–H20A···O11: 2.43 Å, 3.464(4) Å, 159.0° and C20–H20B···O2: 2.44 Å, 3.288(4) Å, 134.4°).

Form 3 crystal structure also solved in orthorhombic space group *Pbca* with one molecule in the asymmetric unit. Strong intramolecular hydrogen bond (O4–H4A···O3: 1.59 Å, 2.490 (6) Å, 149.6°) is present in the enol tautomer. Form 3 molecules aggregate intermolecularly into infinite chains through phenolic OH and carbonyl oxygen forming O–H1···O hydrogen bond (O1–H1···O3: 1.69 Å, 2.666(5) Å, 167.9°) along the *a*-axis. In addition a weaker O–H···O hydrogen bond (O5–H5A···O2: 2.17 Å, 2.975(6) Å, 137.8°) exists between phenolic OH and methoxy group along the *c*-axis. There is C–H···O interaction (C20–H20B···O4: 2.41 Å, 3.192 (7) Å, 127.6°) from methoxy hydrogen to hydroxyl acceptor (Figure 5b).

However, macrocyclic hydrogen bond ring $R^4_5(42)$ could be dissected in the crystal structure of form 2 or 3 due to the linear molecular shape. The crystallographic parameters of curcumin polymorphs listed in Table 1 show that the unit cell parameters of forms 2 and 3 are different from that of form 1. There is some closeness between the orthorhombic cells of non-centrosymmetric form 2 and centrosymmetric structure 3, but number of molecules in the asymmetric unit (*Z'*) is different in both forms. Similarities and subtle differences in the molecular packing of Curcumin forms 2 and 3 are shown in Figure 6.

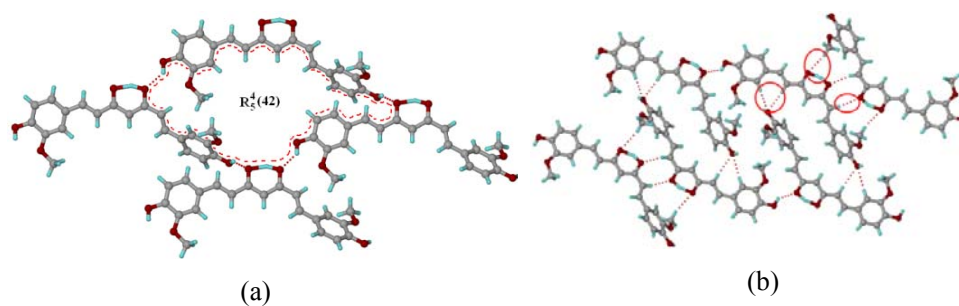


Figure 4 (a) Hydrogen bond ring of $R^4_5(42)$ graph set notation in the crystal structure of form 1. (b) Hydrogen bonding and molecular packing in curcumin form 1. Molecules are interacted via O–H···O hydrogen bonds along with $R^1_2(7)$ and $R^2_2(8)$ motifs of C–H···O interactions.

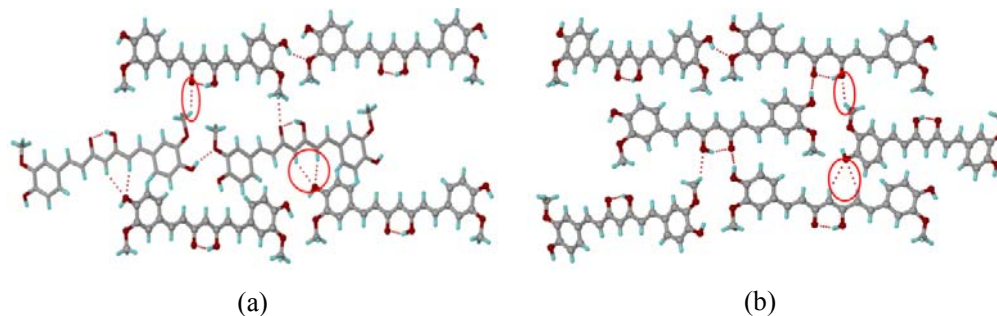


Figure 5 (a) Hydrogen bonding and molecular packing in curcumin form 2. Symmetry-independent molecules (shaded differently) organized via O–H···O hydrogen bonds are connected through $R_2^1(6)$ C–H···O motif. (b) Hydrogen bonding and molecular packing in curcumin form 3. The O–H···O and C–H···O motifs are similar to form 2 but the relative orientation of the keto-enol fragment in neighboring molecules is different.

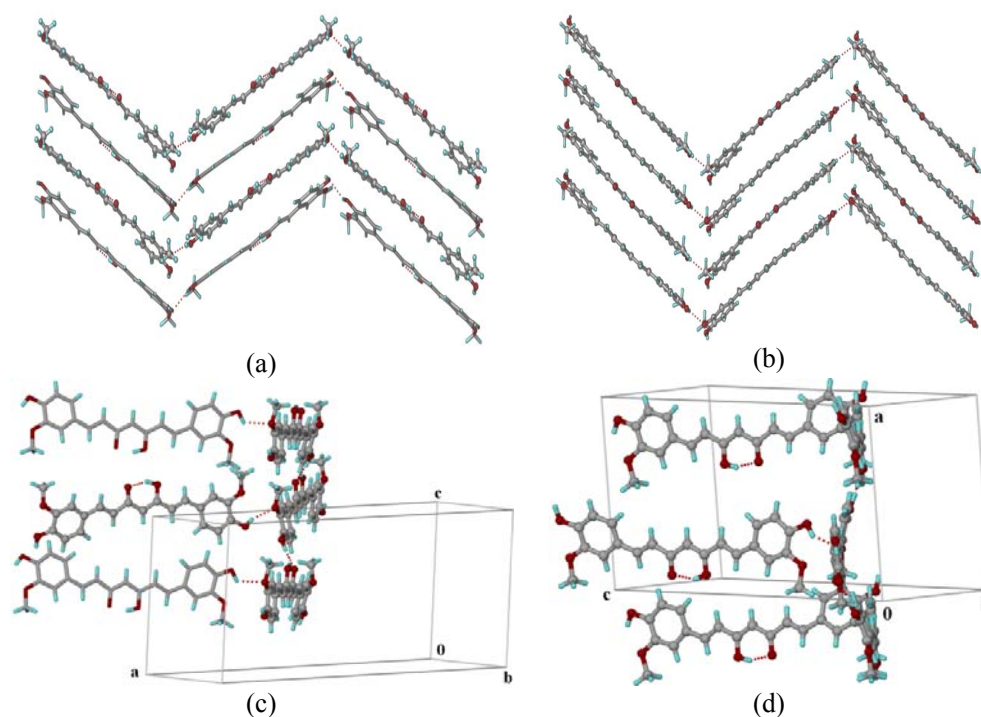


Figure 6 Similarities and subtle differences in the molecular packing of Curcumin forms 2 and 3. (a) O–H···O(OMe) hydrogen bond of symmetry-independent molecules along [100] in form 2. (b) Chain of O–H···O (OMe) hydrogen bonds along [001] in form 3. (c) A cluster of six molecules in form 2. (d) Similar cluster in form 3. Note that the keto-enol group orientation for the middle molecule is different. The b -axis of the two orthorhombic unit cells are similar and a - and c -axes are interchanged (dimensions are approximately equal).

Curcumin exists in the β -keto-enol tautomer in all crystal structures (Scheme 1) but the extent of symmetrization in the fragment varies (Table 3). Phenyl rings are slightly twisted from each other in form 1. The dihedral angle between the least-square planes passing through C4/C7/C8/C9/C10/C11 and C12/C13/C14 is 20.63° . In form 2, among the two asymmetric molecules, one is almost planar (dihedral angle between two phenyl rings, 9.42°), but another one is twisted (dihedral angle, 17.02°) like form 1 molecule. Again the dihedral angle between these planes is 11.69° in form 3. Torsion between two phenyl rings in four asymmetric molecules suggests that Curcumin exist as conformational polymorphs. Molecular overlay of four asymmetric molecules of curcumin were displayed in Figure 7. The density and packing fraction (calculated from the crystal data) are very similar for the three polymorphs ($1.390, 1.404, 1.417 \text{ g cm}^{-3}$; $72.5, 72.6, 72.7\%$), making it difficult to deduce their relative stability. Density, packing fraction calculation suggest the stability order as form 3>form 2>form 1. According to Kitaigorodskii,^{26a} more the dense crystal packing corresponds to a more stable polymorphic form (“density rule”). But there are examples that do not follow the density rule.^{26bc} But DSC endotherm and slurry grinding experiments (discussed later) suggest that form 1 is the thermodynamically stable form.

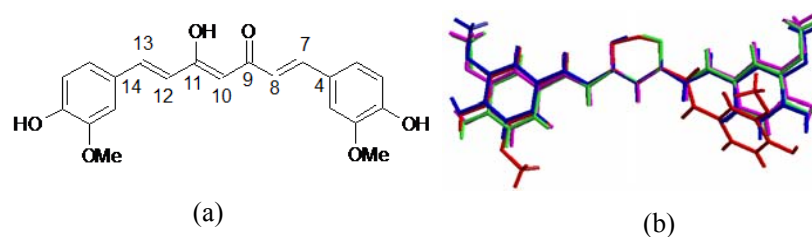


Figure 7 (a) Atom numbering in curcumin and (b) molecular overlay of four asymmetric molecules (Red-form 1), (Blue, magenta-form 2) and (green-form 3) of Curcumin, suggests conformational polymorphs.

Table 1 Crystallographic parameters of curcumin polymorphs

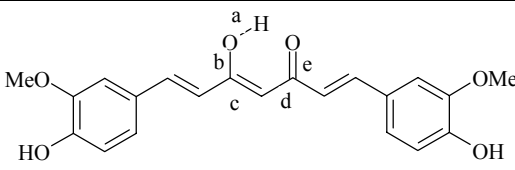
Curcumin	Form 1	Form 2	Form 3
Emp. Formula	C ₂₁ H ₂₀ O ₆	C ₂₁ H ₂₀ O ₆	C ₂₁ H ₂₀ O ₆
Formula wt.	368.37	368.37	368.37
Space group	<i>P2₁/n</i>	<i>Pca2₁</i>	<i>Pbca</i>
a (Å)	12.5676(11)	35.417(3)	12.536(3)
b (Å)	7.0425(6)	7.7792(7)	7.9916(17)
c (Å)	19.9582(18)	12.6482(11)	34.462(7)

α (°)	90	90	90
β (°)	94.987(1)	90	90
γ (°)	90	90	90
V (Å ³)	1759.8(3)	3484.7(5)	3452.3(13)
$D_{\text{calc}} / \text{g cm}^{-3}$	1.390	1.404	1.417
Z / Z'	4/1	8/2	8/1
$R_1 [I > 2 \sigma(I)]$	0.0435	0.0513	0.0893
wR_2 (all)	0.1163	0.1218	0.1681
GOF	1.054	1.083	0.930

Table 2 Hydrogen bonds in crystal structures (neutron-normalized distances)

Crystal Form	Interaction	H...A / Å	D...A / Å	$\angle \text{D-H...A} / ^\circ$
Form 1	O1–H1A...O2	2.14	2.667(2)	111.5
	O1–H1A...O4	2.28	2.904(2)	119.8
	O4–H4A...O3	1.51	2.441(2)	155.7
	O5–H5A...O6	2.23	2.695(2)	107.4
	O5–H5A...O3	1.89	2.793(2)	150.1
	C7–H7...O3	2.37	2.779(2)	100.0
	C3–H3...O5	2.58	3.544(2)	149.6
	C8–H8...O5	2.54	3.528(2)	154.5
	C7–H7...O6	2.38	3.449(2)	166.9
	C19–H19...O1	2.46	3.492(2)	157.3
	C20–H20A...O3	2.49	3.557(2)	166.5
Form 2	O1–H1A...O2	2.02	2.655(3)	120.0
	O1–H1A...O12	2.23	2.834(3)	119.0
	O3–H3A...O4	1.58	2.498(3)	154.0
	O5–H5A...O6	2.07	2.646(3)	115.0
	O5–H5A...O1	2.14	2.905(3)	134.0
	O7–H7A...O9	1.71	2.626(3)	154.0
	O10–H10A...O9	1.64	2.528(3)	147.0
	O11–H11A...O12	2.27	2.711(3)	106.0
	O11–H11A...O8	1.96	2.896(3)	159.0
	C20–H20A...O11	2.43	3.464(4)	159.0
	C20–H20B...O2	2.44	3.291(4)	135.0
	C33–H33...O5	2.32	3.289(3)	147.8
Form 3	C41–H41B...O4	2.38	3.032(3)	116.6
	O1–H1...O3	1.69	2.666(5)	167.9
	O4–H4A...O3	1.59	2.490(6)	149.6
	O5–H5A...O6	1.99	2.685(6)	124.8
	O5–H5A...O2	2.17	2.975(6)	137.8
	C13–H13...O4	2.34	2.754(8)	100.7
	C20–H20B...O4	2.41	3.192(7)	127.6

Table 3 Comparison of bond lengths to estimate extent of symmetrization in keto-enol fragment.^a

						
Bond type	A (O-H in Å)	b (C-O in Å)	e (C=O in Å)	c (C=C in Å)	d (C-C in Å)	Symmetry/asymmetry
Form 1	1.07	1.30	1.30	1.40	1.38	Sym
Form 2 A	0.94	1.31	1.27	1.37	1.42	Asym
Form 2 B	0.95	1.33	1.27	1.37	1.41	Asym
Form 3	0.83	1.33	1.28	1.36	1.43	Asym

^a Chemical symmetrization is defined as near equality of C-C and C-O bond lengths in keto-enol fragment.²⁷

3.4.2 Characterization of new solid forms

Since polymorphs represent different crystal structures essentially every physical and chemical property vary among the polymorphic structures of a material. Some techniques are more sensitive to differentiate the polymorphs and many cases these are preferred in detecting and characterizing polymorphs. New polymorphs and amorphous phase were characterized by powder X-ray diffraction, thermal analysis (DSC and HSM), and spectroscopy (FT-IR, FT-Raman and ss-NMR). Polymorph for drug formulation should be highly pure and should not show phase transformation during clinical trials or storage conditions. In that case desirable property of the polymorph may change during the application. Following are the usual analytical technology to differentiate between polymorphs and also amorphous phase.

3.4.2.1 Powder X-ray Diffraction

Powder X-ray diffraction²⁸ is a standard method for the characterization of solid-state forms, especially polymorphs based on line profile by taking a safe threshold of $\Delta 2\theta > \pm 0.2^\circ$ between polymorphs. The formation of amorphous phase was monitored by the appearance of characteristic hump in the PXRD plot. The crystalline form was monitored by the appearance of new diffraction peaks. Comparison of experimental and calculated X-ray patterns (Figure 8) suggests that minimum three crystalline polymorphs

exist and bulk amount of each form are pure enough for further characterization. The calculated powder XRD lines are visibly different even though there is some degree of overlap, but this is not uncommon for polymorphs.²⁹ The powder X-ray diffraction of Curcumin form 1 exhibited characteristic reflections at about 2θ 8.68, 17.16, 18.01, 24.39, 25.38 and $27.20 \pm 0.2^\circ$. The powder X-ray diffraction of Curcumin form 2 exhibits characteristic reflections at about 2θ 13.80, 17.71, 21.32, 25.19, 26.25 and $27.31 \pm 0.2^\circ$. The powder X-ray diffraction of Curcumin form 3 exhibited characteristic reflections at about 2θ 13.72, 17.79, 25.32, 26.47, 26.90 and $27.20 \pm 0.2^\circ$.

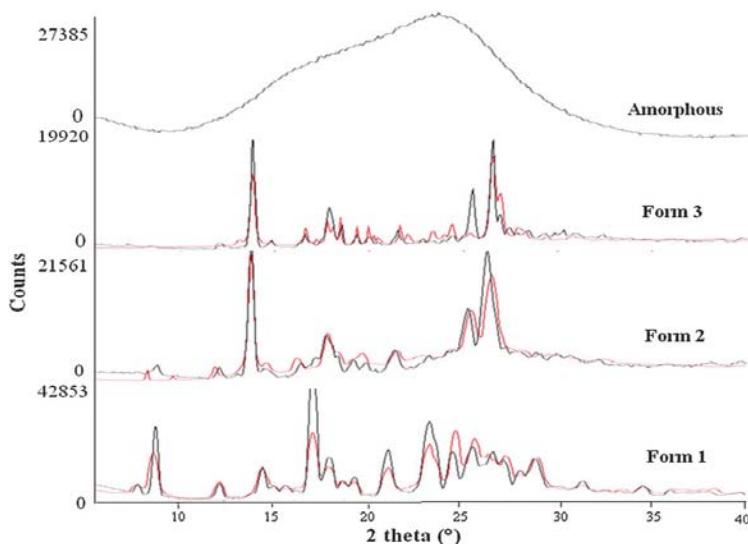


Figure 8 PXRD profiles of curcumin polymorphs 1, 2, 3 and the amorphous phase. Experimental XRD (black) and calculated lines from the crystal structure (red).

3.4.2.2 Thermal Analysis

Differential scanning calorimetry (DSC) measurements indicate the thermal characteristics of the polymorphs (Figure 9). DSC of form 1 showed one endotherm at onset of 177°C . The sharp endotherm ($T_{\text{onset}} 177.5^\circ\text{C}$, $T_{\text{peak}} 181.4^\circ\text{C}$, peak #1) for Form 1 corresponds to the melting of this material. But Form 2 showed two endotherms at $171.9 / 175.1^\circ\text{C}$ (peak #2) and $179.81/182.22^\circ\text{C}$ (peak#3). First and second endotherm corresponds to melting of form 2 and form 1 respectively. There is a phase transition at 171.9°C when form 2 transformed to stable Form 1. Again form 3 showed single endotherm at $168.3/172.8^\circ\text{C}$ (peak#4). The thermograms confirm the stability of form 1 over forms 2 and 3 based on high melting temperature of form 1. Again Curcumin

Amorphous phase having glass transition temperature (T_g) at 52.1 °C (peak#5), crystallization temperature at 118.0 °C (peak#6), finally converted to crystalline form 1 and shows sharp endotherm (T_{onset} 173.8 °C, T_{peak} 178.8 °C, peak #7), corresponds to melting, which is in between the onset melting of Form 1 and Form 2. Enthalpy of fusion for polymorphs are 37.19, 34.98 and 31.31 KJ mol⁻¹, this suggest that stable form having higher enthalpy of fusion. According to heat of fusion rule^{30a}, Form 1, 2 and 3 are monotropically related and stability order of three forms is form 1> form 2>form 3> amorphous phase. But as there is transition from Form 2 to Form 1 at 172 °C (1st endotherm) and at 180 °C (2nd endotherm) represents the melting of Form 1, according heat of transition rule^{30b} Form 1 and Form 2 are monotropically related. Phase transition from form 2 to form 1 was further confirmed by Hot Stage Microscopy (HSM) snapshots of form 2 (Figure 10) which displayed after melting at 168 °C, crystallized during cooling at 120 °C. There is no such recrystallization happened during cooling after melt of forms 1 and 3. The distinction between forms 2 and 3 is somewhat complicated by the fact that their powder XRD lines are very close. Interestingly, forms 2 and 3 have higher crystal density than form 1, but their melting endotherms occur at lower temperature in DSC.

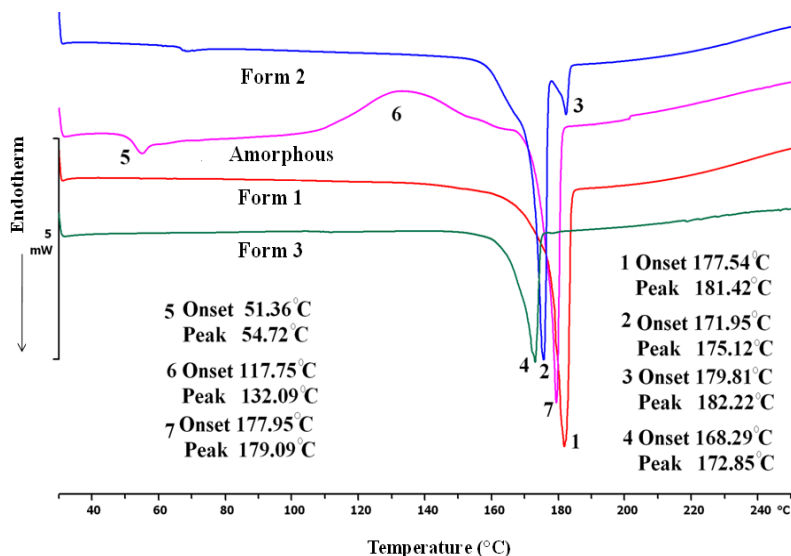


Figure 9 DSC of three crystalline polymorphs and amorphous phase of Curcumin. There is small amount of form 1 seen in the DSC of form 2 possibly due to a phase transition upon heating.

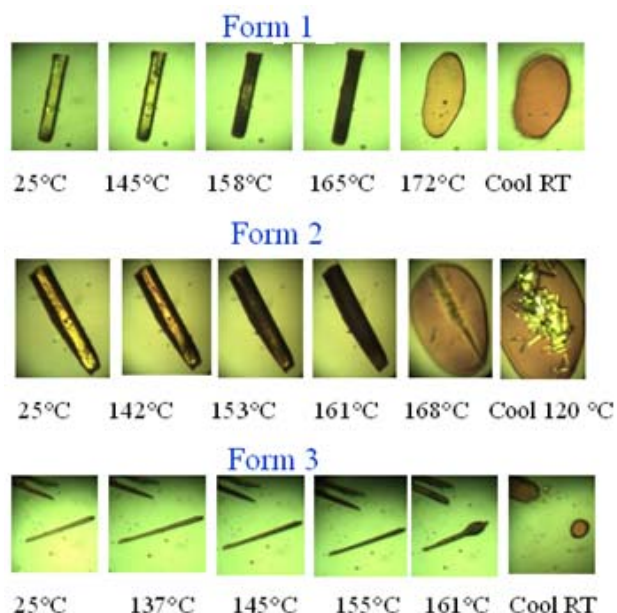


Figure 10 HSM snapshots of three crystalline polymorphs of Curcumin. Form 2 showed recrystallization after cooling from melt at 168 °C, confirmed as form 1. But there was no such event for form 1 and 3 after melt, provided form 1 converted to amorphous phase after melt.

3.4.2.3 FT-IR and FT-Raman spectroscopy analysis

Infrared and Raman spectroscopy³¹ provide useful information about the vibrational modes of a compound, and these changes due to the physical state of the sample and hydrogen bonding and molecular conformations. IR and Raman bands are likely to be active for virtually all the bonds, but their relative intensities will differ, the more symmetric ones give higher Raman intensities, while the asymmetric modes exhibit higher IR intensities. Generally hydroxyl group of phenol absorbs strongly in the stretching frequencies 3700-3584 cm^{-1} regions. Intermolecular hydrogen bonding increases as the concentration of the solution increases, and additional bands start to appear at lower frequencies, 3550-3200 cm^{-1} . There are two types of C–O stretching, one is phenolic and other is olefinic in curcumin. Again C–O stretching vibration in alcohol and phenol produce strong band in the 1260-1000 cm^{-1} and 1430-1410 cm^{-1} region in the IR spectrum respectively. Vibrational stretching frequency comparison for four forms of curcumin was displayed in Figure 11 and listed in Table 4. IR spectra of four forms

mainly differ in the C=O as well as C–O stretching frequency region. Similarly Raman spectroscopy shows differences between four forms in carbonyl stretch, phenolic as well as olefinic C–O stretch (Figure 12). FT-Raman vibrational stretching frequency comparison of four forms was listed in Table 5.

Table 4 FT-IR vibrational modes frequency (cm^{-1}) of three polymorphs and amorphous phase of curcumin

Curcumin	O–H	C=O	Aromatic C=C	Phenol C–O	Enol C–O
Form 1	3510.9	1627.5	1602.6	1429.0	1281.2
Form 2	3401.2 (broad), 3254.1	1651.6, 1626.7	1588.1, 1601.4	1427.3	1282.6, 1263.5
Form 3	3440.9 (broad)	1626.8	1587.3	1416.7	1262.1
Amorphous	3440.6 (broad)	1629.9	1588.4	1428.5	1280.7, 1262.8

Table 5 FT-Raman vibrational modes frequency (cm^{-1}) of three polymorphs and amorphous phase of curcumin.

Curcumin	C=O	Aromatic C=C	Phenol C–O	Enol C–O
Form 1	1626.2	1600.4	1430.2	1249.3
Form 2	1638.9	1591.1, 1602.3	1415.6	1233.1
Form 3	1637.9	1591.4	1415.2	1234.4
Amorphous	1630.5	1599.3	1428.8	1243.2

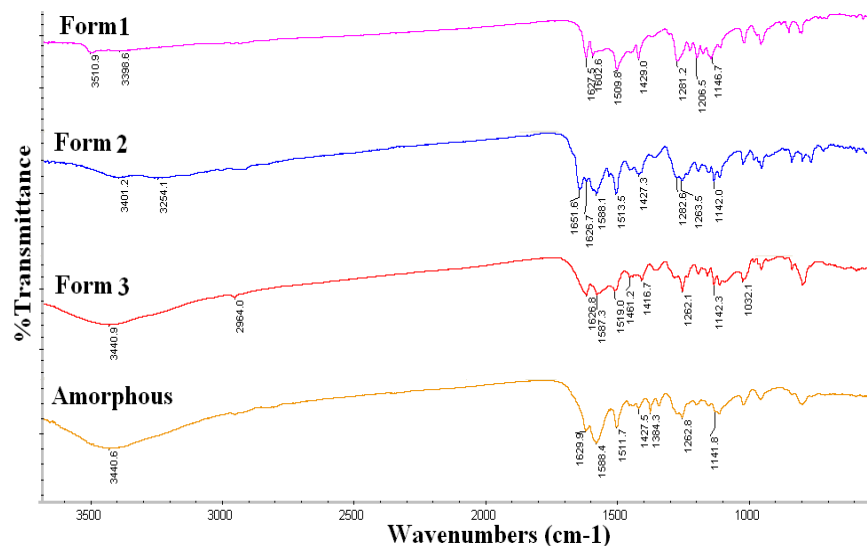


Figure 11 FT-IR spectra comparison of Curcumin three polymorphs and amorphous phase. Change in frequency in C=O region is characteristic of individual polymorphs.

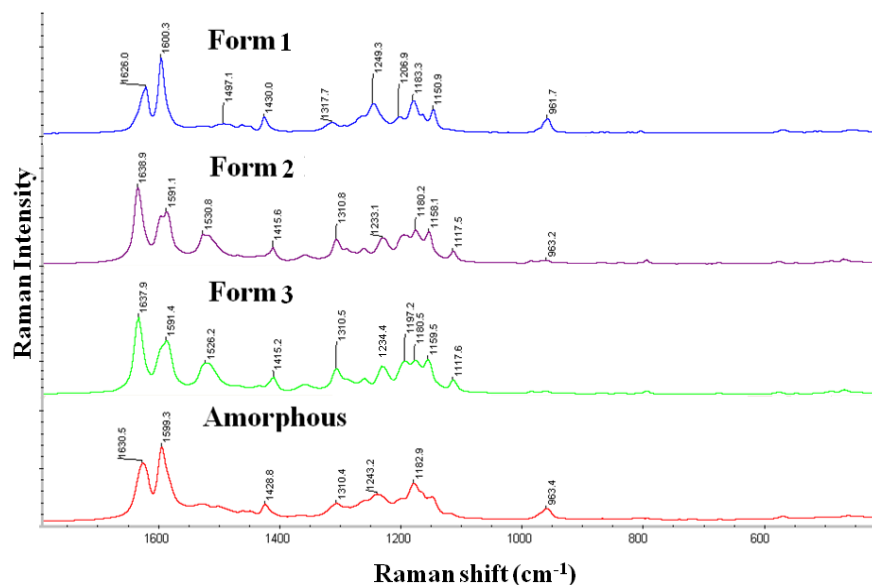


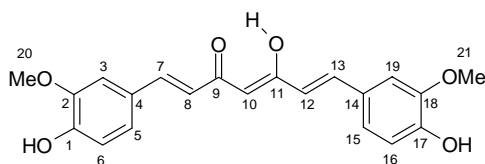
Figure 12 FT-Raman spectra comparison of Curcumin three polymorphs and amorphous phase. Change in frequency in C=O region is characteristic of individual polymorphs.

3.4.2.4 Solid state NMR spectroscopy

Solid-state ^{13}C NMR (SSNMR) spectroscopy³² provides structural information on differences in hydrogen bonding, molecular conformations, and molecular mobility. The peaks of the crystalline Curcumin spectrum were sharp while the peaks of the amorphous phase were diffuse indicating a more heterogeneous environment typical of disordered materials that lack crystallinity (order). SSNMR has proved to be a useful analytical tool to differentiate between crystalline and noncrystalline solids.^{32d} It is expected that crystal structures with two molecules in the asymmetric unit will show at least a few doubled peaks in ss-NMR. Differences in the four forms of Curcumin were analyzed by ^{13}C cross-polarization and magic-angle spinning (CP-MAS) ss-NMR. Curcumin exists as keto form in solution and enol form in solid state (Scheme 1). ^{13}C NMR spectrum (in d_6 -DMSO solvent) of keto form of curcumin shows 11 peaks for 11 nonequivalent carbon atoms, but as in the solid state, enol tautomer is present, NMR spectrum becomes more complex. Besides the signal of the methoxy group (~53 ppm) the spectrum shows the signal of aromatic region (100-150 ppm) and carbonyl carbon (~180-190 ppm). The crystallographic units of form 1, 2 and 3 were easily identified by

their distinguishable chemical shifts of identical carbon peaks at δ 53 (C21), 146 (C2) and 183 (C9) ppm (Figure 13). These δ values have been compared with solution NMR spectrum as reference (Table 6). The multiplicity of ^{13}C peaks for form 2 is due to two independent molecules in the crystallographic asymmetric unit. The slightly broadened NMR peaks for form 2 imply that the degree of crystallinity for the bulk material is less and that its amorphous content is higher than other polymorphs. Since PXRD lines of forms 2 and 3 of curcumin are very close, ss-NMR proved to be useful technique to distinguish between them.

Table 6 ^{13}C NMR chemical shifts of Curcumin three polymorphs and amorphous phase in the solid-state and solution spectrum. Atom numbering has been shown below.



^{13}C peak	Form 1	Form 2	Form 3	Amorphous	Curcumin (d ₆ DMSO)
1, 17	156.753, 157.703	163.589 152.618	163.557, 159.906, 156.038	157.564	153.203, 154.546
2, 18	146.910	144.812	145.904	146.782	145.953, 145.614
3, 19	106.949	103.351	102.772	103.140	116.17
4, 14	128.283, 127.732	127.111	127.397	126.263	128.341
5, 15	108.614, 107.293	104.028	114.114	106.522 (broad)	126.297
6, 16	113.437, 113.023	113.630 109.387	116.668	113.995	116.477
7, 13	139.105, 138.649	133.519	139.030	139.218	131.548
8, 12	123.664, 121.338	120.308	125.190	122.294	121.127, 120.907
9, 11	184.496, 182.223	193.409, 187.572 (broad), 183.102	188.074, 184.673, 180.771, 177.530	177.237, 189.242 (broad)	188.417
10	97.540	96.235 (broad)	93.123, 97.851	97.326	106.063
20, 21	55.576, 53.693	60.812	56.150, 54.592	53.884	60.898

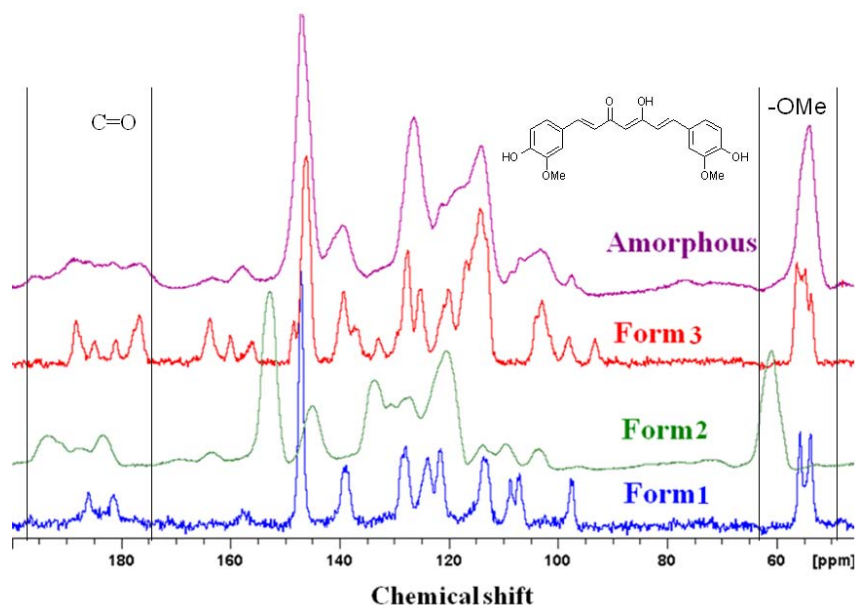


Figure 13 ^{13}C CP-MAS ss-NMR spectra of Curcumin polymorphs. The difference between polymorphs 2 and 3 is clearly visible in $-\text{OMe}$ and $\text{C}=\text{O}$ region.

3.4.3 Solubility and dissolution study of curcumin polymorphs

Aqueous solubility is one of the key physicochemical properties in drug discovery.³³ High solubility in intestinal fluid provides the concentration gradient that drives the absorption of orally administered drugs and subsequent distribution to the site of action to elicit a pharmacological response. For intravenously administered agents, sufficiently high solubility in plasma is critical to minimize undesirable precipitation in the systematic circulation. Generally, poor aqueous solubility leads to formulation challenges in development, raising costs during this phase. Aqueous solubility data facilitate the interpretation of biological assay results. Poor aqueous solubility can lead to problems in vivo, such as incomplete absorption following oral administration, variable bioavailability, fed/fasting effects, and difficulties in establishing a sufficient safety margin following dose escalation studies.³⁴ Moreover, poor solubility is relatively difficult to modulate in the later stage of a discovery project, where the core structure of the lead series is more or less defined. Enabling formulations, such as nanoparticle technology or polymer dispersion, solid crystal suspension, additives/complexation with cyclodextrins, surfactants as microemulsions, solid state modifications using salt

formulations, solid state stabilization of amorphous state, particle size reduction etc.³⁵ may provide enhanced dissolution rate of poor soluble APIs.

Curcumin shows negligible aqueous solubility (8.7 mg/L).²⁰ It is also low soluble in acidic or neutral pH. At pH 7.2 buffer, 90 % of Curcumin decomposes within 30 min. Comparatively Curcumin is soluble in EtOH, acetone, dioxane etc. and stable also. It was reported previously that drugs³⁶ had a higher solubility in cosolvent-water systems than in water alone. For e.g. form 1 of poorly water soluble anti-HIV drug ritonavir^{36a} showed ~ 5 times more soluble than form 2 in 95% EtOH-water mixture. Again intrinsic dissolution experiments of anthelmintic drug niclosamide^{36b} and two monohydrate polymorphs were performed in 40% isopropanol-water medium, as the API is not sufficiently soluble in water to calculate the intrinsic dissolution rate. Intrinsic dissolution rates (IDR) have been defined as “the rate of dissolution of a pure pharmaceutical active ingredient when conditions such as surface area, temperature, agitation or stirring speed, pH, and ionic strength of the dissolution medium are kept constant”. Generally IDR experiments are performed by paddle rotation method.³⁷ In this method, API is made into a thin circular pellet of 0.5 cm² surface using hydraulic press and then pasted on the one side of the paddle so that only one surface area will be exposed to dissolution medium with the rotation of paddle. IDR experiments of Curcumin form 1, metastable form 2 and amorphous phase were performed in 40% EtOH-water medium in which the solubility is higher (1.21 g/L) to compare intrinsic dissolution rate and carried out the experiments upto 7h by USP certified intrinsic dissolution apparatus. Unfortunately metastable form 3 was not reproducible and so it was excluded from the experiments. Here amount of Curcumin (mg/L) dissolved vs time (min) were plotted in Figure 14. Equilibrium solubility and intrinsic dissolution rates for three forms were summarized in Table 7. Since IDR experiments were carried out over a 6–7 hour run, the profile represents a good indication of the improved uptake of form 2 compared to form 1. When the higher solubility polymorph dissolves faster it indicates that the polymorph is stable under the dissolution experiment conditions. Initially molar absorption coefficient of the corresponding form was calculated from the slope of the linear region of the absorbance (A) vs known concentrated (c) solutions using Lambert-Beer's law ($A = \epsilon cl$, ϵ =absorption coefficient, l = UV cell length through which light is absorbed by the sample solution). The intrinsic dissolution rate of form 1 and form 2 are

7.956×10^{-3} and 25.264×10^{-3} mg/cm²/min respectively i.e. form 2 dissolves 3.2 times faster than that of form 1 in 40% EtOH-water mixture. Amorphous phase showed intermediate dissolution rate between stable form 1 and metastable form 2.³⁸ As form 3 is least stable forms among polymorphs, so it is expected that form 3 should show highest dissolution rate. In general, there is an inverse relation between stability and solubility among polymorphic crystals, and the less stable polymorph is more soluble/has faster dissolution rate. Generally for polymorphs, the solubility ratio will be 2-3 times, which cases being exceptional acetaminophen (4.7 times), Ritonavir (5 times), premarin (23 times) etc.^{38b}

Again solubility may be defined as the amount of a substance that dissolves in a given volume of solvent at a specified temperature. Generally maximum solubility (or saturation point) of an API will be reached within 24 h, sometimes for low soluble APIs 48 h or 72 h time may be required. For equilibrium solubility experiments, 100 mg curcumin was slurried in 5 mL of 40% aqueous EtOH for 24 h at 37 °C and maximum solubility obtained for form 1 was 1.21g/L and there was no phase transformation for the stable phase. However phase transformation of form 2 to stable modification after 24 h on slurry experiments was observed. The amorphous phase was more stable, ~90% of amorphous phase converted to form 1 and remaining converted to metastable form 2 of curcumin after 24 h of slurry experiments in 40% EtOH-water, confirmed by matching of PXRD with the calculated lines from the X-ray crystal structure of stable form 1 (Figure 15 and 16). There is a possibility of phase transition from amorphous phase to metastable form 2 and then to stable form 1. In case of phase transformation equilibrium solubility is not appropriate method since that value corresponds to the stable phase. Here one should consider apparent solubility,³⁹ defined as the concentration of solid material at apparent equilibrium (supersaturation) and is distinct from true thermodynamic solubility, which is reached at infinite equilibrium time.

The Apparent Solubility of a metastable polymorph is calculated using the equation.

$$\text{Solubility}_{\text{metastable}} = \text{Solubility}_{\text{stable}} (\text{IDR}_{\text{metastable}} / \text{IDR}_{\text{stable}}).$$

So apparent solubility and intrinsic dissolution rates are proportional to each other for dissolution studies of an API. Apparent solubilities of metastable form and amorphous phase are summarized in Table 7.

Table 7 Absorption coefficient (ϵ), solubility and intrinsic dissolution rate of Curcumin polymorphs.

Curcumin	Absorption coefficient (ϵ , /mM/cm)	Solubility by dispersion, at 24 h (g/L)	IDR over 7 h, mg /($\text{cm}^2 \cdot \text{min}$)	Apparent solubility, calculated (g/L)
Form 1	46.21	1.21	7.96×10^{-3}	---
Form 2	43.99	$2.12 (\times 1.75)$	25.26×10^{-3}	$3.84 (\times 3.17)$
Amorphous	38.75	$2.16 (\times 1.78)$	14.65×10^{-3}	$2.23 (\times 1.84)$

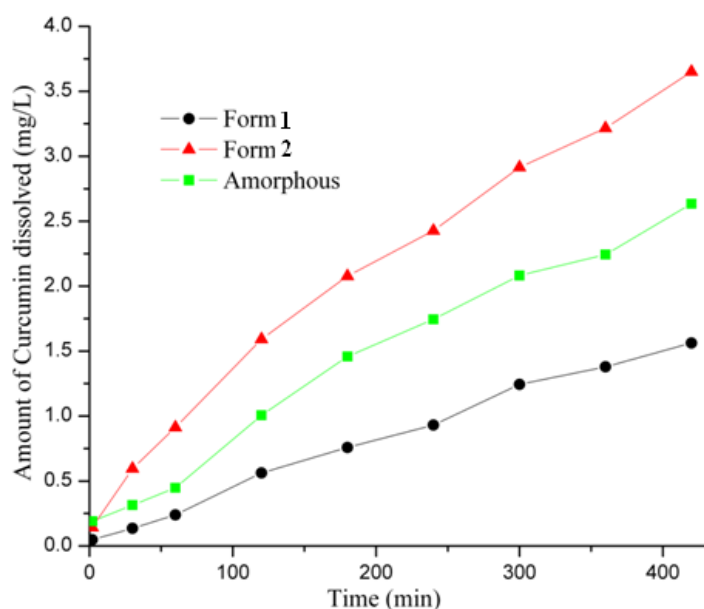


Figure 14 Dissolution experiments of Curcumin polymorphs in 40% EtOH-water at 37 °C. There was no phase transformation for metastable form or amorphous phase during 7 h IDR experiments.

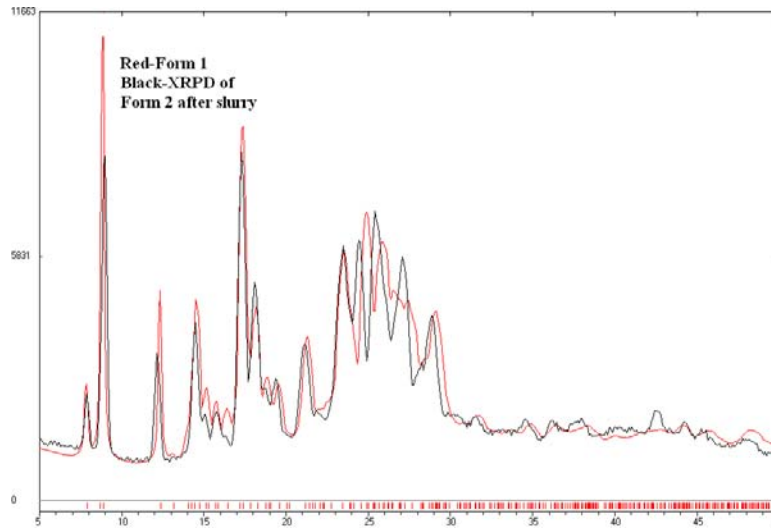


Figure 15 PXRD of form 2 (black) after slurry experiment for 24h with the calculated X-ray lines of form 1 from the crystal structure shows that it has transformed to form 1.

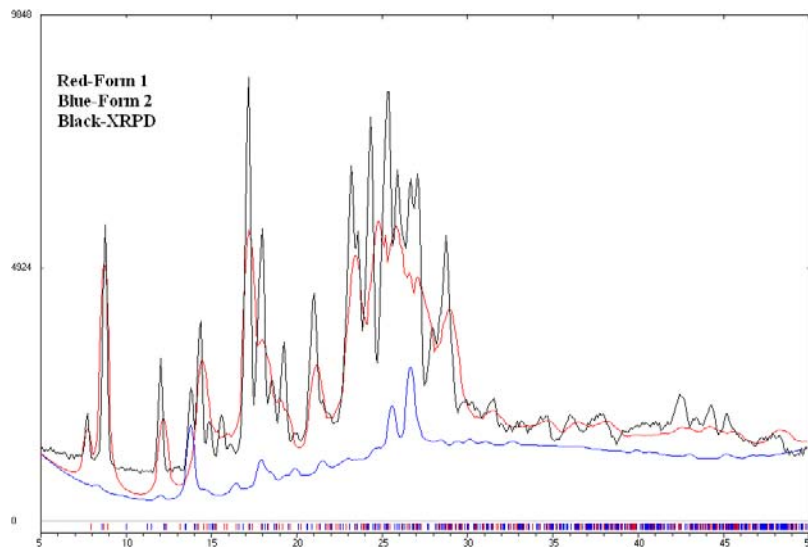


Figure 16 PXRD of the amorphous solid after 24 h slurry grinding (black) matched with the calculated X-ray lines of form 1 (red) and form 2 (blue) of Curcumin. Rietveld refinement gave an estimate of 90% form 1 and 10% form 2 in the sample.

3.4.4 Conclusion

Before launching a new drug into market, high throughput polymorph screening is necessary, otherwise a sudden outbreak of a new form can become a big setback for

the pharmaceutical industry. On the other hand, a metastable polymorph often has higher solubility and hence it is the desired polymorph for better bioavailability. In balance, however greater stability takes precedence over higher solubility. Curcumin is very low soluble active ingredient of natural turmeric. Because of its poor solubility and bioavailability, so far curcumin is not marketed as capsule or tablet formulation in spite of its diverse pharmacological activities. The marketed (or Sigma-Aldrich) form 1 of curcumin is the stable polymorph in all our experiments. The crystal structure of form 1 contains one molecule in the asymmetric unit in the centrosymmetric space group $P2_1/n$, whereas new metastable form 2 crystal structure contains two symmetry independent molecules in the noncentrosymmetric space group $Pca2_1$. Again novel form 3 crystal structure was solved in orthorhombic $Pbca$ with one molecule in the asymmetric unit. This observation is very intuitive⁴⁰ since most crystallographers and structural chemists tend to believe that among polymorphic structures, the crystal structure with the lower Z' (typically $Z' = 1$ for low symmetry drug molecules) is the more stable modification. FT-IR and FT-Raman spectroscopy supports hydrogen bond similarity between form 1 and form 3 and similar packing or conformational flexibility between forms 2 and 3. Interestingly molecular overlay diagram of curcumin polymorphs showed that metastable forms have more planar structure than angular curcumin form 1 and former showed better solubility and IDR than latter. Though there is inverse relationship between planarity and solubility.⁴¹ PXRD of forms 2 and 3 are very close, solid state ^{13}C NMR spectra were able to differentiate and characterize between all the four forms. Since IDR experiments were carried out over a 6–7 hour run, the profile represents a good indication of the improved uptake of form 2 compared to form 1. When the higher solubility polymorph dissolves faster it indicates that the polymorph is stable under the dissolution experiment conditions. The stabilization of form 2 and the amorphous phase through additives, excipients, polymers, etc. could lead to the development of curcumin as a more bioavailable active ingredient.

3.5 Experimental Section

Curcumin was purchased from Sigma–Aldrich (Hyderabad, Andhra Pradesh, India) and used directly for experiments. All other chemicals including solvents were of analytical or chromatographic grade.

3.5.1 Crystallization conditions for Curcumin polymorphs

Pure Curcumin (Sigma-Aldrich) was confirmed as form 1 by X-ray powder diffraction. This material was used without further purification. Experimental conditions to obtain each polymorph and also amorphous phase of curcumin are summarized in Table 8.

Table 8 Experimental techniques used to obtain polymorphs of curcumin.

Curcumin	Crystallization conditions	Time (days)
Form 1	Commercial sample or Sigma-Aldrich material. Good quality crystals were obtained from recrystallization of 200 mg Curcumin in 10 mL isopropanol.	2-3
Form 2	(a) 200 mg (0.54 mmol) Curcumin and 52 mg (0.54 mmol) of 4-hydroxy pyridine were ground in mortar-pestle for 30 min after adding 5 drops of EtOH, and then kept for crystallization in 25 mL EtOH. The coformer 4-hydroxypyridine was obtained as precipitate at the bottom of the conical flask. Curcumin has low solubility in EtOH and crystallized faster and appeared as thick rod crystals.	3-4 1-2
	(b) 200 mg Curcumin was dissolved in 10 ml EtOH in 250 mL beaker and heated to make supersaturated solution and then kept for crystallization in temperature controlled refrigerator at 10 °C.	
	(c) 200 mg Curcumin was dissolved in 5 mL DMSO in 25 ml beaker heated to make supersaturated solution and then kept at room temperature (30°C).	4-5
Form 3	100 mg Curcumin (0.27 mmol) and 42 mg (0.27 momol) of 4,6-dihydroxy-5-nitropyrimidine were ground in mortar-pestle for 30 min after adding 5 drops of EtOH, and then kept for crystallization in 10 mL EtOH. The coformer 4,6-dihydroxy-5-nitropyrimidine was obtained as precipitate at the bottom of the conical flask. Curcumin crystallized	2-3

	faster and appeared as starry aggregate of thin needle crystals. Form 3 crystals were difficult to obtain and sometimes what crystallized was Form 1.
Amorphous phase	100 mg Curcumin was melted at 190 °C and then immediately cooled to room temperature or dipped in ice to cool down to a glassy state.

3.5.2 Dissolution and solubility experiments

Intrinsic dissolution rate (IDR) and solubility measurements were carried out on a USP-certified Electrolab TDT-08 L Dissolution Tester (Electrolab, Mumbai, MH, India). A calibration curve was obtained for curcumin forms 1, 2 and amorphous phase by plotting absorbance vs. concentration UV-Vis spectra curves on a Thermo Scientific Evolution EV300 UV-Vis spectrometer (Waltham, MA, USA) for known concentration solutions in 40% EtOH-water medium. The mixed solvent system (EtOH-water) was selected for its higher solubility of curcumin in this medium. The slope of the plot from the standard curve gave the molar extinction coefficient (ϵ) by applying the Beer-Lambert's law. Equilibrium solubility was determined in 40% EtOH-water medium using shake-flask method.⁴² To obtain the equilibrium solubility, 100 mg of each solid material was stirred for 24 h in 5 mL 40% EtOH-water at 37 °C, and the absorbance was measured at 430 nm. The concentration of the saturated solution was calculated at 24 h, which is referred to as the Equilibrium solubility of the stable solid form (C_s). The Apparent solubility (C_m) is more appropriate for metastable forms/amorphous phase because they were found to transform to the stable form 1 of curcumin under the solubility measurement conditions. The Apparent solubility (C_m) of a metastable phase is calculated using the equation

$$C_m = C_s \times (J_m / J_s)$$

where J_s and J_m are the dissolution rates of the stable and metastable forms. The dissolution rates J_s and J_m are obtained from the IDR experiments.

100 mg of the each polymorph was taken in the intrinsic attachment and compressed to a 0.5 cm² pellet using a hydraulic press at a pressure of 2.5 ton/inch² for 2 min. The pellet was compressed to provide a flat surface on one side and the other side

was sealed. Then the pellet was dipped into 900 mL of 40% EtOH-water medium at 37 °C with the paddle rotating at 150 rpm. At regular interval of 10 min, 5 mL of the dissolution medium was withdrawn and replaced by an equal volume of fresh medium to maintain a constant volume. Samples were filtered through 0.2 µm nylon filter and assayed for drug content spectrophotometrically at 430 nm on a Thermo-Nicolet EV300 UV-Vis spectrometer. The amount of drug dissolved in each time interval was calculated using the calibration curve. The linear region of the dissolution profile was used to determine the intrinsic dissolution rate (IDR) of the curcumin (= slope of the curve, i.e. amount of drug dissolved divided by the surface area of the disc (0.5 cm²) per minute).

3.6 Reference

1. S. R. Byrn, R. R. Pfeiffer and J. G. Stowell, *Solid-State Chemistry of Drugs*; SSCI: West Lafayette, IN, **1999**.
2. W. C. McCrone, in *Physics and Chemistry of the Organic Solid State*, Vol. 2, eds. D. Fox, M. M. Labes and A. Weissberger, Wiley Interscience, New York, **1965**, pp. 725-767.
3. E. W. Pienaar, M. R. Caira, A. P. Lotter, *J. Cryst. Spectro. Res.* **1993**, 23, 785.
4. (a) S. Cherukuvada, R. Thakuria, and A. Nangia, *Cryst. Growth Des.* **2010**, 10, 3931. (b) A. L. Grzesiak, M. Lang, K. Kim, A. J. Matzger, *J. Pharm. Sci.*, **2003**, 92, 2260. (c) G. L. Perlovich, T. V. Volkova and A. Bauer-Brandl, *J. Therm. Anal. & Calorimetry*, **2007**, 89, 767.
5. (a) S. Thirunahari, S. Aitipamula, P. S. Chow, R. B. H. Tan. *J. Pharm. Sci.*, **2010**, 99, 2975. (b) N. K. Nath, A. Nangia, *CrystEngComm*, **2011**, 13, 47.
6. (a) J. Bauer, S. Spanton, R. Henry, J. Quick, W. Dziki, W. Porter, J. Morris, *Pharma. Res.* **2001**, 18, 856. (b) S. R. Chemburkar, J. Bauer, K. Deming, H. Spiwek, K. Patel, J. Morris, R. Henry, S. Spanton, W. Dziki, W. Porter, J. Quick, P. Bauer, J. Donaubauer, B. A. Narayanan, M. Soldani, D. Riley, K. McFarland, *Org. Process Res. Dev.* **2000**, 4, 413. (c) S. Roy, P. M. Bhatt, A. Nangia, G. J. Kruger, *Cryst. Growth Des.* **2007**, 7, 476. (d) C. Platteau, J. Lefebvre, S. Hemon, C. Baetz, F. Danede, D. Prevost, *Acta. Crystallogr.* **2006**, B61, 80. (e) N. J. Babu, L. S. Reddy, S. Aitipamula, A. Nangia, *Chem Asian J.* **2008**, 3, 1122. (f) N.

- J. Babu, S. Cherukuvada, R. Thakuria and A. Nangia, *Cryst. Growth Des.*, **2010**, *10*, 1979. (g) F. T. Martins, M. D. Bocelli, R. Bonfilio, M. B. de Araújo, P. V. de Lima, P. P. Neves, M. P. Veloso, J. Ellena and A. C. Doriguetto, *Cryst. Growth Des.*, **2009**, *9*, 3235. (h) X. Chen, K. R. Morris, U. J. Griesser, S. R. Byrn, and J. G. Stowell, *J. Am. Chem. Soc.* **2002**, *124*, 15012.
7. (a) R. Hilfiker, *Polymorphism in the Pharmaceutical Industry*, Wiley-VCH, Weinheim, **2006**. (b) H. G. Brittan, *Polymorphism in Pharmaceutical Solids*, Marcel Dekker, New York, **1999**. (c) J. Bernstein, *Polymorphism in Molecular Crystals*, Clarendon, Oxford, **2002**.
 8. Special Issue: Facets of Polymorphism in Crystals. (a) *Cryst. Growth Des.* **2008**, *8*, 1-362. (b) *Cryst. Growth Des.* **2003**, *3*, 867-1040. (c) *Cryst. Growth Des.* **2004**, *4*, 1087-1441. (d) *Adv. Drug. Del. Rev.* **2001**, *48*, 1-136. (e) *Adv. Drug. Del. Rev.* **2004**, *56*, 241-414.
 9. (a) T. L. Threlfall, *Analyst* **1995**, *120*, 2435. (b) J. Bernstein, R. J. Davey, J. -O. Henck, *Angew. Chem. Int. Ed.* **1999**, *38*, 3440. (c) H. G. Brittan, *J. Pharm. Sci.*, **2007**, *96*, 705. (d) J. Bernstein, *Chem. Commun.* **2005**, 5007. (e) B. Rodríguez-Spong, C. P. Price, A. Jayashankar, A. J. Matzger, N. Rodríguez-Hornedo, *Adv. Drug. Del. Rev.* **2004**, *56*, 241. (f) G. P. Stahly, *Cryst. Growth Des.* **2007**, *7*, 1007.
 10. (a) J. D. Dunitz, J. Bernstein, *Acc. Chem. Res.*, **1995**, *28*, 193. (b) J. M. Rubin-Preminger and J. Bernstein, *Cryst. Growth Des.* **2005**, *5*, 1343. (c) N. Blagden, R. J. Davey, R. Rowe and R. Roberts, *Int. J. Pharm.* **1998**, *172*, 169.
 11. (a) H. M. K. Murthy, M. Vijayn, *Acta Cryst. B* **1980**, *37*, 1102. (b) H. M. K. Murthy, M. Vijayn, *Acta Cryst. B* **1979**, *35*, 262.
 12. (a) G. M. Day, A. V. Trask, W. D. S. Motherwell, W. Jones, *Chem. Commun.* **2006**, 54. (b) K. Guo, G. Sadiq. C. Seaton, R. Davey, and Q. Yin, *Cryst. Growth Des.* **2010**, *10*, 269. (c) P. Vishweshwar, J. A. McMahon, M. Oliveira, M. L. Peterson, M. J. Zaworotko, *J. Am. Chem. Soc.* **2005**, *127*, 16802. (d) J. Li, S. A. Bourne and M. R. Caira, *Chem. Commun.*, **2011**, 47, 1530. (e) G. Mehta, S. Sen and K. Venkatesan, *CrystEngComm*, **2007**, *9*, 144.
 13. (a) S. Khoshkoo, J. Anwar, *J. Phys. D. Appl. Phys.* **1993**, *B90*, 26. (b) J. D. Dunitz, J. E. Bernstein, *Acc. Chem. Res.* **1995**, *28*, 193. (c) I. Weissbuch, M. Lahav, L. Leiserowitz, *Cryst. Growth Des.* **2003**, *3*, 125. (d) P. K. Thallapally, R.

- K. R. Jetti, A. K. Katz, H. L. Carrell, K. Singh, K. Lahiri, S. Kotha, R. Boese, G. R. Desiraju, *Angew. Chem. Int. Ed.* **2004**, *4*, 1149. (e) J. M. Kelleher, S. E. Lawrence, H. A. Moynihan, *CrystEngComm* **2006**, *8*, 327. (f) V. López-Mejías, J. W. Kampf, and A. J. Matzger *J. Am. Chem. Soc.* **2009**, *131*, 4554. (g) M. Karanam, S. Dev, A. R. Choudhury, *Cryst. Growth Des.*, **2012**, *12*, 240.
14. (a) H. Ammon, and M. A. Wahl, *Planta Med.* **1991**, *57*, 1. (b) H. Hatcher, R. Planalp, J. Chob, F. M. Tortia, and S. V. Tortic, *Cell. Mol. Life Sci.* **2008**, *65*, 1631.
15. (a) R. Thakur, H. S. Puri and A. Husain, Major medicinal plants of India, Central Institute of Medicinal and Aromatic Plants, Lucknow, **1989**. (b) J. Tilak, M. Banerjee, H. Mohan, and T. P. A. Devasagayam, *Phytother. Res.* **2004**, *18*, 798. (c) S. Shishodia, G. Sethi and B. B. Aggarwal, *Ann. N. Y. Acad. Sci.* **2005**, *1056*, 206.
16. (a) O. P. Sharma, *Biochem. Pharmacol.* **1976**, *25*, 1811. (b) A. J. Ruby, G. Kuttan, K. D. Babu, K. N. Rajasekharan, R. Kuttan, *Cancer Lett.* **1995**, *94*, 79. (c) Y. Sugiyama, S. Kawakishi, T. Osawa, *Biochem. Pharmacol.* **1996**, *52*, 519. (d) R. C. Srimal, B. N. Dhawan, *J. Pharm. Pharmacol.* **1973**, *25*, 447. (e) W. C. Jordan, C. R. Drew, *J. Natl. Med. Assoc.* **1996**, *88*, 333. (f) G. B. Mahady, S. L. Pendland, G. Yun, Z. Z. Lu, *Anticancer Res.* **2002**, *22*, 4179. (g) G. Liang, S. Yang, H. Zhou, L. Shao, K. Huang, J. Xiao, Z. Huang, X. Li, *Eur. J. Med. Chem.* **2009**, *44*, 915.
17. P. Anand, A. B. Kunnumakkara, R. A. Newman, and B. B. Agarwal, *Mol. Pharmaceutics* **2007**, *4*, 807.
18. (a) B. T. Kurien *Assay Drug Dev. Technol.* **2007**, *5*, 567. (b) B. T. Kurien and R. H. Scofield, *Trends in Pharmacological Sci.* **2009**, *30*, 334. (c) B. B. Agarwal, *Trends in Pharmacological Sci.* **2009**, *30*, 335.
19. (a) Y. -J. Wang, M.-H. Pan, A.-L. Cheng, L.-I. Lin, Y.-S. Ho, C.-Y. Hsieh, J.-K. Lin, *J. Pharmaceutical & Biomed. Anal.* **1997**, *15*, 1867. (b) H. H. Tonnsen, J. Kirlsen, *Z. Lebensm. Unters Forsch* **1985**, *180*, 132.
20. (a) F. Zhang, G. K. Koh, D. P. Jeanson, J. Hollingworth, P. S. Russo, G. Vicente, R. W. Stout, Z. Liu. *J. Pharm. Sci.* **2011**, *100*, 2778. (b) N. K. Gupta, V. K. Dixit, *J. Pharm. Sci.* **2011**, *100*, 1987.

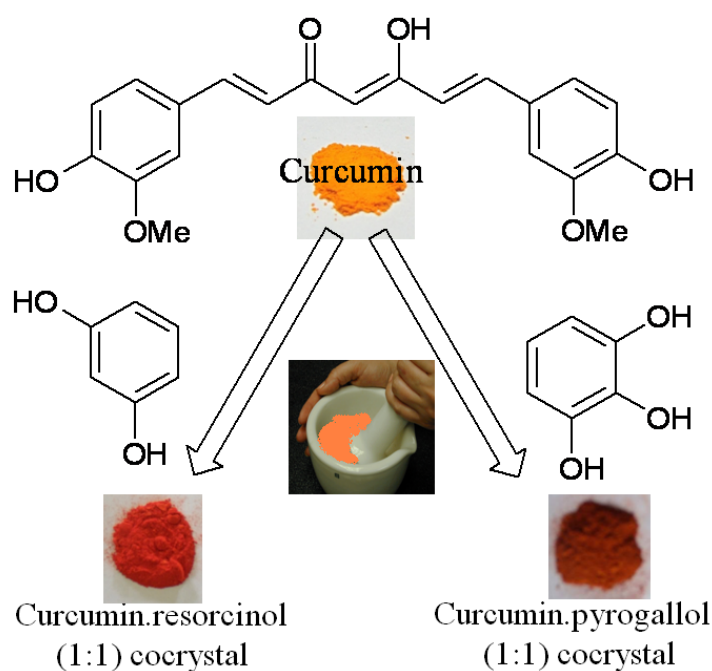
21. (a) S. Romero, B. Escalera, P. Bustamante, *Int. J. Pharm.* **1999**, 178, 193. (b) P. Sanphui, B. Sarma, Ashwini Nangia, *J. Pharm. Sci.* **2011**, 100, 2287. (c) B. C. Hancock and M. Parks, *Pharm. Res.*, **2000**, 17,397.
22. (a) J. Milobedzka, S. Kostanecki and V. Lampe, *Ber. Dtsch. Chem. Ges.* **1910**, 43, 2163. (b) V. Lampe, J. Milobedzka, *Ber. Dtsch. Chem. Ges.* **1913**, 46, 2235.
23. (a) H. H. Tonnesen, J. Karlsen, and A. Mostad, *Acta Chem. Scand. B*, **1982**, 36, 475. CCDC refcode BINMEO. (b) Y. Ishigami, M. Goto, T. Masuda, Y. Takizawa, and S. Suzuki, *Shikizai Kyokaishi (Jap.)*, **1999**, 72, 71. (c) Q.-L. Suo, Y.-C. Huang, L.-H. Weng, W.-Z. He, C.-P. Li, Y.-X. Li, and H.-L. Hong, *Shipin Kexue (Beijing) (Chin.) (Food Sci. (Beijing))*, **2006**, 27, 27. (d) S. P. Parimita, Y. V. Ramshankar, S. Suresh, and T. N. Guru Row, *Acta Cryst.*, **2007**, E63, o860. (d) F. R. Fronczek, Private Communication, **2008**. CCDC refcode BINMEO01, 02, 03, 04.
24. (a) J. P. Lakshman, Y. Cao, J. Kowalski, and A. T. M. Serajuddin, *Mol. Pharmaceutics*, **2008**, 5, 994. (b) E. H. Lee, and S. R. Byrn, *J. Pharm. Sci.*, **2010**, 99, 4013. (c) A. Nangia, and G.R. Desiraju, *Chem. Commun.*, **1999**, 605.
25. (a) J. Bernstein, R. E. Davis, L. Shimoni, and N.-L. Chang, *Angew. Chem., Int. Ed. Engl.*, **1995**, 34, 1555. (b) M. C. Etter, and J. C. Macdonald, *Acta Crystallogr.*, **1990**, B46, 256.
26. (a) A. I. Kitaigorodskii, *Organic Chemical Crystallography*, Consultants Bureau, New York, 1961. (b) G. L. Perlovich, T. V. Volkova and A. Bauer-Brandl, *J. Therm. Anal. Calorim.*, **2007**, 89, 767. (c) Y. V. Nelyubina, I. V. Glukhov, M. Y. Antipin and K. A. Lyssenko, *Chem. Commun.*, **2010**, 46, 3469.
27. F. H. Herbstein, B. B. Iverson, M. Kapon, F. K. Larson, G. K. H. Madsen and G. M. Reisner, *Acta Cryst.*, **1999**, B55, 767.
28. (a) V. A. Drebuschak.; T. N. Drebuschak.; N. V. Chukanov and E. V. Boldyreva, *J. therm. anal. & Calorimetry* **2008**, 93, 343. (b) A. V. Trask, N. Shan, W. D. S. Motherwell, W. Jones, S. Feng, R. B. H. Tan and K. J. Carpenter, *Chem. Commun.*, **2005**, 880. (c) G. C. Viscomi, M. Campana, M. Barbanti, F. Grepioni, M. Polito, D. Confortini, G. Rosini, P. Righi, V. Cannataa and D. Braga, *CrystEngComm*. **2008**, 10, 1074.

29. (a) L. Seton, D. Khamar, I. J. Bradshaw and G. A. Hutcheon, *Cryst. Growth Des.*, **2010**, *10*, 3879; (b) L. Fábán, A. Kálmán, G. Argay, G. Bernáth and Z. Cs. Gyarmatib, *Chem. Commun.*, **2004**, 2114.
30. (a) A. Burger, R. Ramberger, *Mikrochim Acta II*, **1979**, 259. (b) A. Burger, R. Ramberger, *Mikrochim Acta II*, **1979**, 273.
31. (a) L. Johnson and K. A. Rumon, *J. Phys. Chem.*, **1965**, *69*, 74. (b) B. H. Stuart, *Infrared Spectroscopy: Fundamentals and Applications*, **2004**, John-Wiley, UK
(c) R. L. McCreery, *Raman Spectroscopy for Chemical Analysis*, John-Wiley, 2000, UK; E. Smith and G. Dent, *Modern Raman Spectroscopy - A Practical Approach*, John-Wiley, 2005, UK. (d) Y. A. Chesalov, P. Baltakhinov, T. N. Drebuschak, E. V. Boldyreva, N. V. Chukanov, V. A. Drebuschak, *J. Mol. Struc.* **2008**, *891*, 75. (d) T. M. Kolev, E. A. Velcheva, B. A. Stamboliyska, M. Spitteller, *Int. J. Quantum Chem.*, **2005**, *102*, 1069.
32. (a) S. M. Reutzel-Edens, J. K. Bush, P. A. Magee, G. A. Stephenson and S. R. Byrn, *Cryst. Growth Des.* **2003**, *3*, 897. (b) K. Kimura, F. Hirayama and K. Uekama, *J. Pharm. Sci.* **1999**, *88*, 385. (c) N. Zencirci, T. Gelbrich, D. C. Apperley, R. K. Harris, V. Kahlenberg and U. J. Grisser, *Cryst. Growth Des.* **2010**, *10*, 302. (d) J. Lu, S. Rohani, *Curr. Med. Chem.*, **2009**, *16*, 884. (e) S. Tothadi, B. R. Bhogala, A. R. Gorantla, T. S. Thakur, R. K. R. Jetti, G. R. Desiraju, *Chem. Asian J.* **2012**, *7*, 330.
33. (a) C. A. Lipinski, F. Lombardo, B. W. Dominy, and P. J. Feeney, *Adv. Drug Del. Rev.*, **2001**, *46*, 3. (b) E. Kerns, *J. Pharm. Sci.*, **2001**, *90*, 1838.
34. (a) L. Di and E. H. Kerns, *Adv. Drug Del. Rev.*, **2006**, *11*, 446. (b) S. L. McGovern, E. Caselli, N. Grigorieff, and B. K. Shoichet, *J. Med. Chem.*, **2002**, *45*, 1712.
35. (a) B. V. Eerdenbrugh, J. Vermant, J. A. Martens, L. Froyen, J. V. Humbeeck, G. V. den Mooter, and P. Augustijns, *Mol. Pharmaceutics*, **2010**, *7*, 1858. (b) P. S. Mohanachandran, P. G. Sindhumol and T. S. Kiran, *Pharmacie Globale (IJCP)* **2010**, *4*, 1. (c) M. Thommes, D. R. Ely, M. T. Carvajal, and R. Pinal, *Mol. Pharmaceutics*, **2011**, *8*, 727. (d) D. C. Bibby, N. M. Davies, I. G. Tucker, *Int. J. Pharm.* **2000**, *197*, 1. (e) M. E. Matteucci, J. C. Paguio, M. A. Miller, R. O. Williams III, and K. P. Johnston, *Mol. Pharmaceutics*, **2009**, *6*, 375.

36. (a) E. C. Vantonder, T. S. P. Maleka, W. Liebenberg, M. Song, D. E. Wurster, M. M. D. Villers, *Int. J. pharm.* **2004**, 269, 417. (b) S. Romero, B. Escalera, P. Bustamante, *Int. J. Pharm.* **1999**, 178, 203.
37. (a) T. X.Viegas, R. U.Curatella, L. L. V. Winkle, and G. Brinker, *Pharm. Techno.* **2011**, 44. (b) J. Mauger, J. Ballard, R. Brockson, S. De, V. Gray, and D. Robinson. *Dissol. Techno.* **2003**, 6.
38. (a) P. Sanphui, N. R. Goud, U. B. R. Khandavilli, S. Vanoth and A. Nangia, *Chem.Comm.* **2011**, 47, 5013. (b) M. Pudipeddi and A. T. M. Serajuddin, *J. Pharm. Sci.*, **2005**, 94, 929.
39. M. Otsuka, R. Teraoka and Y. Matsuda, *Chem. Pharm. Bull.*, **1991**, 39, 2667. (b) V. M. Rao, R. Sanghvi and H. Zhu, in *Developing Solid Oral Dosage Forms, Pharmaceutical Theory and Practice*, Y. Qiu, Y. Chen and G. G. Z. Zhang (Eds.), 1st Ed., **2009**, Burlington: Elsevier, pp. 3-24. (c) J. H. Fagerberg, O. Tsinman, N. Sun, K. Tsinman, A. Avdeef, and C. A. S. Bergström, *Mol. Pharmaceutics*, **2010**, 7, 1419.
40. (a) A. Gavezzotti, *CrystEngComm.*, **2008**, 10, 389. (b) G. R. Desiraju, *CrystEngComm*, **2007**, 9, 91. (c) J. W. Steed, *CrystEngComm*, **2003**, 5, 169. (d) T. S. Thakur, R. Sathishkumar, A. G. Dikundwar, T. N. Guru Row and G. R. Desiraju, *Cryst. Growth Des.* **2010**, 10, 4246. (d) B. Sarma, S. Roy and A. Nangia, *Chem. Commun.*, **2006**, 4918.
41. M. Ishika, Y. Hashimoto, *J. Med. Chem.* **2011**, 54, 1439.
42. A. Glomme, J. Marz, J. B. Dressman, *J. Pharm. Sci.* **2005**, 94, 1.

Chapter Four

Fast Dissolving Curcumin Cocrystals



Cocrystals of Curcumin with resorcinol and pyrogallol obtained through EtOH assisted solvent drop grinding resulted in solubility enhancement by 5 and 12 times in 40% EtOH-water medium compared to Curcumin. Color changes from yellow in Curcumin to dark red or brown in cocrystals are due to more effective conjugation and planarity. Presence of water soluble phenolic cofomers may be a reason for the improved aqueous solubility of curcumin.

4.1 Introduction

The physical and chemical properties of any particular crystalline form of a drug depend on the internal arrangement of molecules in the crystals. Since different inter- and intramolecular interactions such as hydrogen bonds, halogen interactions, π -stacking and van der Waals interactions are present in different crystalline forms, they will have different free energies and therefore exhibit different properties. Single component crystals exhibit polymorphism as discussed in chapter 2 and 3. Even multi-component crystals exist as polymorph, hydrate, solvate, cocrystal and salt. While selecting a crystalline form in pharmaceutical industry for drug development, one has to consider two important factors i.e. solubility/bioavailability and stability. Accordingly the standard screening¹ in pharmaceutical industry involves searching for all possible crystalline forms initially and then selecting the best crystalline form of Active Pharmaceutical Ingredient (API), with optimal solubility and greater stability for further development. It could be a polymorph (e.g. Mebendazole), hydrate (e.g. Amoxicillin trihydrate), solvate (e.g. Indinavir sulphate ethanolate), or a salt (e.g. Fluoxetine hydrochloride). In addition to these established crystalline API modifications, pharmaceutical cocrystals² or crystalline molecular complexes of an API with another pharmaceutically acceptable molecule have recently attracted the attention of pharmaceutical chemists. Multi-component crystals possess a distinct physicochemical profile (e.g. solubility, bioavailability, stability or tableting properties etc), potentially enabling improvements in the properties of existing API for drug formulations. At present more than 80% drugs are sold as tablets and about 40% of marketed drugs have low solubility. More alarming is double the percentage of drug candidates in the R&D pipeline (80-90%) which could fail due to solubility problems.³ In the last decade Pharmaceutical Chemists have proved that pharmaceutical cocrystals can improve solubility, stability, bioavailability, tableting, chiral resolutions etc. using crystal engineering approach.

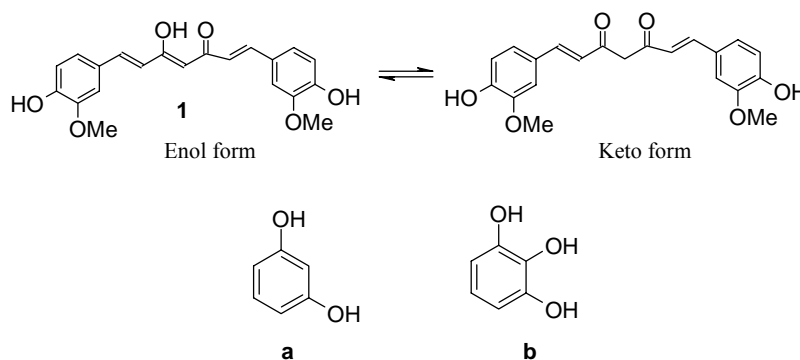
A cocrystal may be defined as a multi-component neutral molecular complex in a definite stoichiometric ratio that are solid at ambient conditions, interact through non-covalent interactions, predominantly hydrogen bonds. Again salt is an ionic species consists of cation and anion, held together by ionic interaction or columbic forces.

Generally to improve solubility of an API, salt is preferred than cocrystals because of their ionic nature and higher aqueous solubility. However salts possess some inherent drawbacks. It is normally targeted to one acidic or basic moiety in the molecule and therefore requires minimum of one ionizable center on the API of interest. Also it has inherent tendency to convert to corresponding hydrate, which poses stability problem. Furthermore non-ionizable pharmaceutical molecules are incapable of salt formation. On the other hand, pharmaceutical cocrystals² which are emerging as a new class of solid forms can address multiple functional groups and aggregate as complexes with neutral APIs that do not have ionizable groups, APIs that are not sufficiently acidic/ basic enough to form salts, and including those of salts. In pharmaceutical cocrystals, one of the components is an investigational or marketed drug molecule (the active pharmaceutical ingredient or API) and the second component (the coformer) is a safe chemical for human consumption selected from the GRAS list of the US-FDA (Generally Regarded As Safe additive chemicals by the Food and Drugs Administration).⁴ Such substances include food additives, preservatives, pharmaceutical excipients, vitamins, minerals, amino acids and other bio-molecules, as well as other APIs. In addition, the space is not limited for binary combinations since ternary and quaternary cocrystals are realistic possibilities.⁵ In recent years cocrystals have been found to offer an attractive platform to improve the solubility and dissolution rate of pharmaceuticals without compromising on the stability of the solid form. Remenar et al.^{2h} reported cocrystals of itraconazole with carboxylic acids that exhibited 4-20 fold higher concentration than the insoluble, crystalline drug form. The best examples of the 2:1 cocrystals of L-tartaric acid and L-malic acid with itraconazole were able to achieve and sustain dissolution profiles comparable to the marketed amorphous form as Sporanox capsule. The main advantages of cocrystals over the alternate method of amorphous drugs for solubility improvement is that the former adducts being crystalline in nature are relatively stable and less prone to phase transformations. Secondly, the large number of GRAS coformers makes it possible to explore several cocrystals for the same API.⁶ High solubility is a necessary condition for good oral absorption of an active drug to ensure optimal delivery, which is related to issues such as bioavailability, biopharmaceutical classification, biowaivers, and bioequivalence.

4.2 Curcumin

Curcumin, a hydrophobic phenol, an active ingredient of popular Indian spice turmeric is included in the list of nutraceutical compounds.⁷ Nutraceutical is the term used to describe a medicinal component which is present in food, plant or any natural occurring material, used for improvement of health by preventing diseases. Nutraceuticals includes wide range of products such as polyphenols such as curcumin from turmeric, epigallocatechin gallate (ECGE) from tea or resveratrol from red grapes, vitamins, oils from fish and flax, theobromine from cacao tree, caffeine from coffee leaves etc. Nutraceuticals are popularly available in forms of tablets, capsules, softgels, soft chews etc.⁷ Curcumin is derived from the rhizome of the herb *Curcuma longa*.⁸ Curcumin possesses diverse pharmacological activities such as anti-inflammatory, antioxidant, antiproliferative, antiangiogenic, anticancer, etc.⁹ The molecule exists as keto-enol tautomers (Scheme 1), being present predominantly in the keto form in acidic and neutral solution whereas the enol tautomer is stable in alkaline medium. Curcumin is safe even at high doses of 12 g/day¹⁰ in animal and human trials but its effectiveness is limited by low aqueous solubility (7.8 mg/L) and poor bioavailability in the aqueous medium. The poor bioavailability of curcumin is due to its low absorption, rapid metabolism in the liver and intestinal wall and fast systemic elimination from the biological system.¹¹ Curcumin is almost insoluble in acidic or neutral medium, comparatively better soluble in alkaline medium. But it has stability problems in alkaline medium. Curcumin decomposes rapidly in neutral and alkaline medium, >90% decomposition occurs within 30 min in pH 7.4 buffer medium.¹² Hence, despite its efficacy and safety, curcumin is still not approved as a therapeutic agent. The stability and bioavailability of curcumin has been improved by several methods, e.g. by (1) adding adjuvants such as piperine to block the metabolic pathways of curcumin, (2) novel drug delivery platforms such as nanoparticles, liposomes, micelles, phospholipid complexes, and (3) concomitant administration of lecithin, quercetin, genistein, eugenol, terpinol etc. to increase the bioavailability.^{11c,13} The aqueous solubility of curcumin was enhanced 38 fold in the presence of 1-10% (w/v) rubusoside. The bioavailability of curcumin in water and lipid medium was enhanced by complexation with phosphatidyl choline in equimolar ratio.¹⁴

The instability of curcumin at physiological pH may be ascribed to the β -diketone linker in the seven carbon chain of curcumin. We reasoned that the reactivity of the keto-enol group could be modified through hydrogen bonding with phenolic cofomers in cocrystals, which in turn might provide more soluble and stable curcumin solid-state forms. A few examples of pharmaceutical cocrystals involving a phenol API or cofomer were reported¹⁵ while our work was in progress. Cocrystals can alter the physicochemical properties (e.g. stability, solubility, bioavailability and tableting etc.) of drugs in a controlled manner.¹⁶ We recently reported novel polymorphs of curcumin which exhibited superior dissolution rate compared to the known crystalline modification.¹⁷ However, the metastable nature of such fast dissolving polymorphs observed in follow-up experiments could pose a serious concern for further development. A solid form screen of curcumin with phenolic cofomers¹⁸ afforded novel cocrystals with resorcinol and pyrogallol (Scheme 1). These curcumin cocrystals were characterized by X-ray diffraction, spectroscopy and thermal techniques. Resorcinol is a safe cofomer molecule from the GRAS list,⁴ and pyrogallol and its derivatives¹⁹ exhibit anticancer activity. Pyrogallol is an active ingredient of *Embllica officinalis* (amla), which has the potential to develop as nontoxic anti-cancer agent.



Scheme 1 Chemical structure of curcumin (keto and enol tautomers) and cofomers resorcinol and pyrogallol.

4.3 Results and discussions

The cocrystallization of curcumin–resorcinol **1a** and curcumin–pyrogallol **1b** was attempted by solid-state and liquid-assisted grinding methods. The main advantage

of solid-state grinding technique is that it overcomes complications due to possible solvent / water inclusion during solution crystallization, but a drawback is that the product is often microcrystalline and hence not suitable for single crystal X-ray diffraction. Addition of few drops of a solvent as lubricant (here EtOH) to accelerate molecular mobility during grinding/ kneading, referred to as liquid-assisted grinding,²⁰ facilitated quantitative formation of the product cocrystals. Curcumin–resorcinol **1a** (1:1) and curcumin–pyrogallol **1b** (1:1) cocrystals were obtained by liquid-assisted manual grinding of the individual solid components for 30 min in a mortar pestle after adding 5–6 drops of EtOH. The starting materials were consumed and new peaks observed in the powder X-ray diffraction pattern. Diffraction quality single crystals of **1a** and **1b** were obtained by slow crystallization of the components in 1:1 molar ratio from benzene–EtOH solvent mixture (see Experimental Section). The cocrystal composition and stoichiometry was confirmed from the crystal structure. The crystallographic parameters for both the cocrystals are listed in Table 1. Among the 1,3-diketone and β -keto-enol tautomers of curcumin **1**, the keto-enol tautomer is more stable by 6.7 kcal/mol in the gas phase, and this tautomer is present in its crystal structures.²¹

4.3.1 Crystal structure analysis

The asymmetric unit of **1a** in the monoclinic space group $P2_1/c$ contains one molecule each of curcumin and resorcinol. The curcumin molecule is almost planar, similar to that present in the metastable polymorphs of curcumin.¹⁷ In contrast, the stable crystalline modification of curcumin has a twisted conformation.²² The dihedral angle between the least squares planes passing through C4–C7–C8–C9–C10–C11 and C12–C13–C14 atoms of curcumin is 4.9° in cocrystal **1a** (the values in polymorph 2 and 3 of curcumin are 9.4° and 17.0°, 11.7° respectively). There is an intramolecular hydrogen bond (O4–H4A...O3, 1.79 Å, 2.569(5) Å, 132.9°) in the enol tautomer. Curcumin molecules form an intermolecular O–H...O hydrogen bond (O1–H1...O6, 2.57 Å, 3.506(6) Å, 159.3°) between the phenol O–H donor and OMe acceptor. The resorcinol molecules are inclined at a dihedral angle of 64.9° to curcumin. Two resorcinol molecules donate O–H...O hydrogen bonds along the *a*-axis to the carbonyl group of curcumin (O7–H7A...O3, 1.81 Å, 2.773(6) Å, 165.4°; O8–H8A...O3, 2.09 Å, 2.921(6) Å, 140.4°) (Figure 2a). Weak C–H...O and C–H... π interactions play an

auxiliary role in structure stabilization (Figure 2b). Neutron normalized Hydrogen bonds are summarized in Table 2.

The asymmetric unit of **1b** in the monoclinic space group $P2_1/n$ contains one molecule each of curcumin and pyrogallol. The curcumin molecule is almost planar: the dihedral angle between the least squares planes in curcumin is 6.7° . There is an intramolecular hydrogen bond (O4–H4A \cdots O3, 1.76 Å, 2.552(5) Å, 135°) in the enol tautomer. Two pyrogallol molecules form hydrogen bond along the *a*-axis to the carbonyl oxygen of the β -keto group (O7–H7B \cdots O3, 1.91 Å, 2.748(5) Å, 141° ; O8–H8A \cdots O3, 1.78 Å, 2.665(5) Å, 148°). Curcumin molecules are arranged in infinite chains linked through intermolecular O–H \cdots O hydrogen bond between the phenolic OH groups of adjacent molecules (O5–H5A \cdots O1, 1.98 Å, 2.724(5) Å, 130°). An O–H \cdots O hydrogen-bonded trimer (O1–H1 \cdots O9, 1.97 Å, 2.814(5) Å, 142° ; O9–H9 \cdots O5, 1.83 Å, 2.681(5) Å, 143°) is formed between the phenol OH of two curcumin molecules with pyrogallol oxygen acceptor forms a ring motif of $R_3^3(6)$ graph set notation²³ (Figure 3a). A few crystal structures having the O–H \cdots O trimer synthon extracted from the Cambridge Structural Database are HESKOF, QEXXEW, SEFRIE and XEFSIK (six alphabet CSD REFCODEs).²⁴ Weak C–H \cdots O and C–H $\cdots\pi$ interactions stabilize the overall packing of cocrystal structure **1b** (Figure 3b).

The molecular overlay of curcumin in polymorphs 1-3, curcumin–resorcinol **1a**, and curcumin–pyrogallol **1b** displays the almost planar conformation of curcumin molecule in its metastable polymorphs and cocrystals, but the molecule is twisted in the stable modification (Figure 4). The cocrystal of curcumin with resorcinol is a pharmaceutical cocrystal because resorcinol has GRAS status, and curcumin–pyrogallol may be classified as a drug–drug cocrystal,²⁵ given the lung cancer and tumor growth inhibition activity of pyrogallol.¹⁹ Attempts to make cocrystals of curcumin with other phenols such as catechol, orcinol, phloroglucinol, hydroquinone, etc. were unsuccessful. Instead of obtaining cocrystals, both curcumin and phenolic coformers were separated from solution crystallization. There were no new metastable phases of curcumin obtained in our cocrystallization experiments.

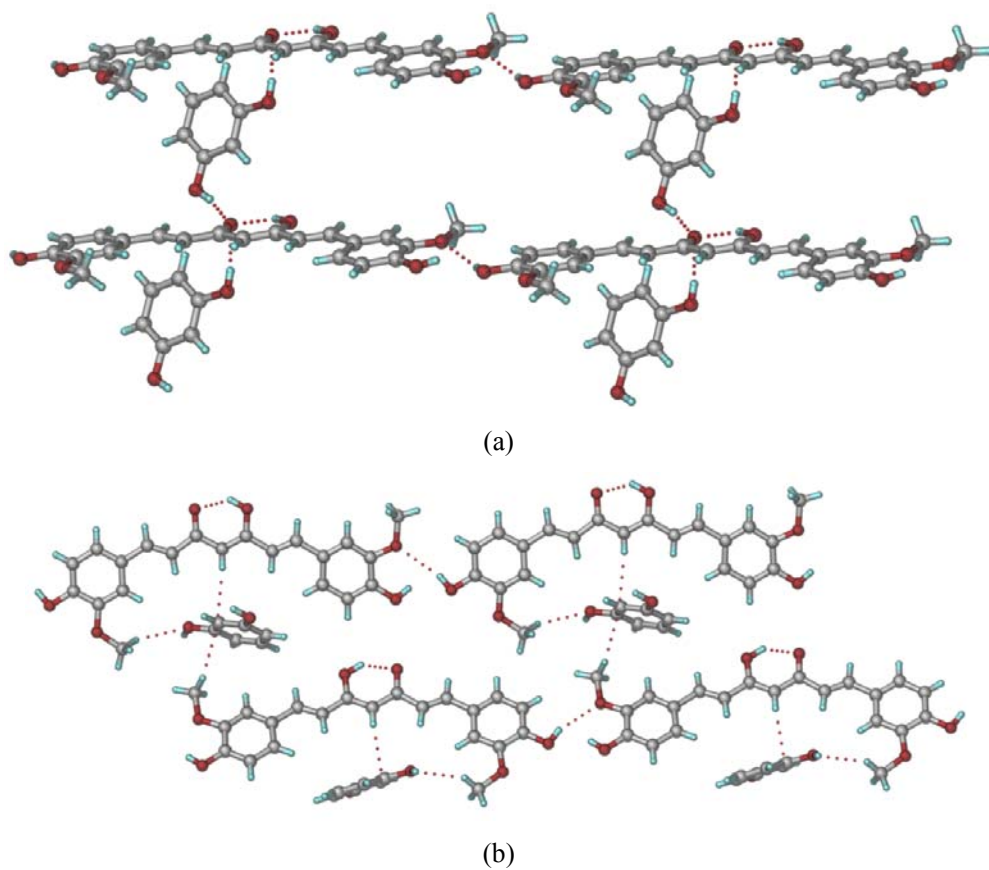


Figure 1 (a) O–H \cdots O hydrogen bond between curcumin and resorcinol along the *a*-axis in cocrystal **1a**. (b) O–H \cdots O, C–H \cdots O and C–H \cdots π interactions between curcumin and resorcinol molecules in the crystal structure.

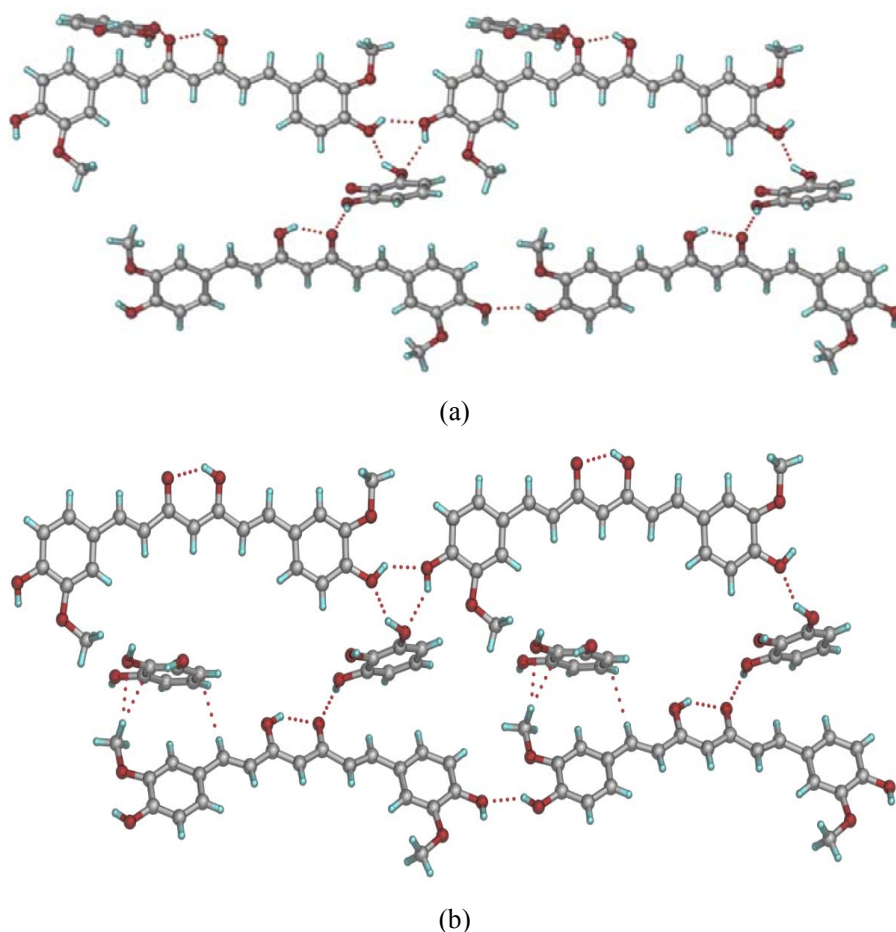


Figure 2 (a) O-H...O trimer between two curcumin and one pyrogallol in cocrystal **1b**. (b) O-H...O, C-H...O and C-H... π interactions between curcumin and pyrogallol molecules in the crystal structure.

Table 1 Crystallographic data for curcumin cocrystals **1a** and **1b**

Crystal Data	Curcumin–resorcinol 1a	Curcumin–pyrogallol 1b
Emp. Formula	C ₂₁ H ₂₀ O ₆ , C ₆ H ₆ O ₂	C ₂₁ H ₂₀ O ₆ , C ₆ H ₆ O ₃
Formula wt.	478.48	494.48
Crystal system	Monoclinic	Monoclinic
Space group	<i>P</i> 2 ₁ / <i>c</i>	<i>P</i> 2 ₁ / <i>n</i>
<i>T</i> [K]	298(2)	100(2)
<i>a</i> [Å]	7.7321(9)	7.3706(6)
<i>b</i> [Å]	16.1990(19)	15.8001(10)
<i>c</i> [Å]	19.558(3)	19.8972(14)

α [deg]	90	90
β [deg]	101.095(12)	92.933(7)
γ [deg]	90	90
Z	4	4
Volume [\AA^3]	2403.9(5)	2314.1(3)
D_{calc} [g/cm^3]	1.322	1.419
R_1 [$I > 2\sigma(I)$]	0.0687	0.0923
wR_2	0.2029	0.2867
GOF	0.983	1.030

Table 2 Hydrogen bonds in crystal structures (neutron-normalized distances).

Crystal forms	Interaction	H \cdots A / \AA	D \cdots A / \AA	\angle D–H \cdots A / $^\circ$	Symmetry code
Curcumin–resorcinol (1a)	O1–H1 \cdots O6	2.57	3.506(6)	159	$-1+x, y, -1+z$
	O4–H4A \cdots O3	1.79	2.569(5)	133	Intramolecular
	O5–H5A \cdots O1	2.01	2.750(8)	130	$1+x, y, 1+z$
	O5–H5A \cdots O6	2.13	2.648(9)	111	Intramolecular
	O7–H7A \cdots O3	1.81	2.773(6)	166	$2-x, 1-y, -z$
	O8–H8A \cdots O3	2.10	2.921(6)	140	$1-x, 1-y, -z$
	C21–H21A \cdots O8	2.68	3.414(6)	133	$x, 1/2-y, 1/2+z$
Curcumin–pyrogallol (1b)	O1–H1 \cdots O2	2.16	2.620(5)	106	Intramolecular
	O4–H4A \cdots O3	1.76	2.552(5)	135	Intramolecular
	O5–H5A \cdots O1	1.98	2.724(5)	130	$x, y, 1+z$
	O1–H1 \cdots O9	1.97	2.814(5)	142	$3/2-x, 1/2+y, 1/2-z$
	O9–H9 \cdots O5	1.83	2.681(5)	143	$3/2-x, 1/2+y, 1/2-z$
	O7–H7B \cdots O3	1.91	2.748(5)	141	$-2+x, y, z$
	O8–H8A \cdots O3	1.78	2.665(5)	148	$x, y, -1+z$
	C8–H8 \cdots O7	2.66	3.738(6)	171	$1-x, 1-y, -z$
	C20–H20C \cdots O8	2.41	3.366(6)	146	$1-x, 1-y, -z$
	C7–H7 \cdots O9	2.41	3.480(6)	168	$x, y, -1+z$
	C23–H23 \cdots O9	2.25	3.310(6)	165	$-1+x, y, z$

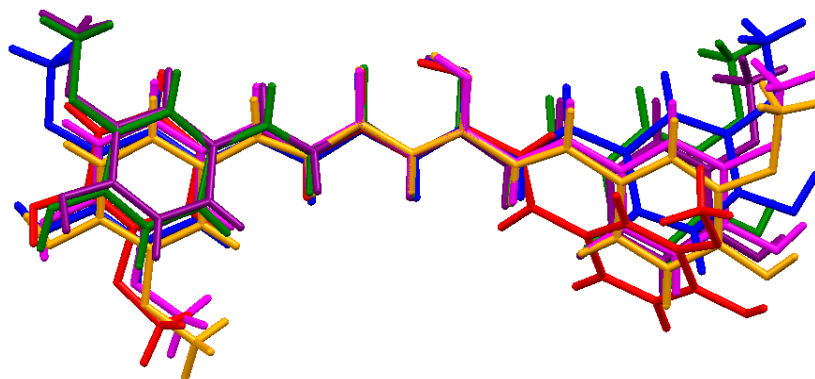


Figure 3 Molecular overlay of curcumin in Form 1 (red), Form 2 (blue, magenta), Form 3 (green), curcumin–resorcinol cocrystal **1a** (orange), and curcumin–pyrogallol cocrystal **1b** (pink). The two aryl side arms are nearly coplanar to the central β -keto-enol group in all crystal structures except the stable commercial polymorph 1 of curcumin in which one aryl group is twisted.

4.3.2 Thermal analysis

The thermal stability of curcumin cocrystals **1a** and **1b** was examined by differential scanning calorimetry (DSC) (Figure 4). They exhibited a single endotherm peak at 166 °C and 158 °C, respectively, indicative of a homogeneous solid phase. The melting point of both cocrystals is in between that of curcumin and the coformer¹⁶ (curcumin 177 °C, resorcinol 110 °C, and pyrogallol 131 °C). The higher onset temperature of cocrystal **1a** compared to **1b** does not correlate with coformer melting point. There is inverse relationship between solubility and melting point. By decreasing melting point of the curcumin cocrystals, we were able to increase the solubility (will be discussed later).

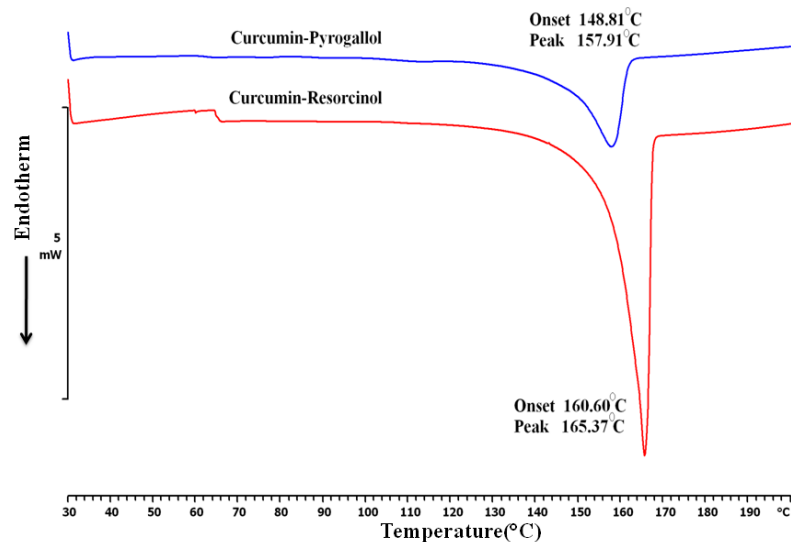
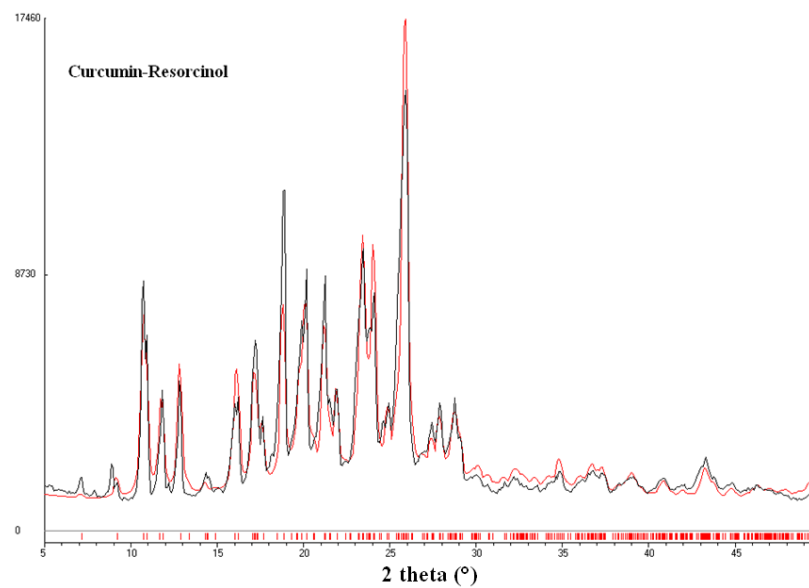


Figure 4 DSC endotherm of cocrystal **1a** and **1b**. The single endotherm at a temperature different from the melting points of the pure components is indicative of a homogeneous cocrystal phase. Melting point of curcumin is 177 °C, resorcinol 110 °C, and pyrogallol 131 °C.

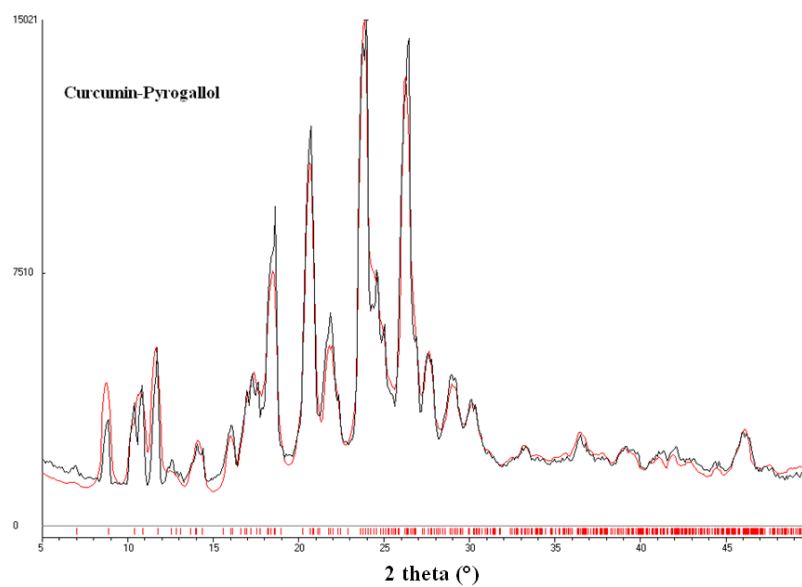
4.3.3 Powder X-ray diffraction

Powder X-ray diffraction is a fingerprint characterization method for solid phases, such as cocrystals and salts.²⁶ If the resulting PXRD of the solid product after grinding the pure solid compounds (the API and the coformer) is different from that of the reactants, then it may be inferred that a new solid phase has formed. The unexpected formation of a new polymorph for one of the components during grinding and/or due to the presence of a coformer as an additive is another possibility.^{17,27} The presence of both the molecular components and their stoichiometry was ascertained by ¹H NMR spectroscopy. The bulk material appeared to be pure and homogeneous cocrystal composition by PXRD, which was confirmed by matching the experimental PXRD patterns with the calculated diffraction lines from the X-ray crystal structures (Figure 5). The powder X-ray diffraction of curcumin–resorcinol **1a** exhibited characteristic reflections at about 2θ 10.91, 18.81, 20.12, 23.39, 24.05 and $25.82 \pm 0.2^\circ$. Curcumin–pyrogallol **1b** exhibited characteristic reflections at about 2θ 10.57, 11.96, 18.78, 20.97, 24.11, 24.69 and $26.66 \pm 0.2^\circ$. Both cocrystals were found to be stable for up to six months in our laboratory ambient conditions of 25–35 °C and 40–60% relative humidity. A systematic check under ICH accelerated stability conditions of 40 °C and

75% RH in a controlled humidity oven showed no sign of degradation or dissociation of cocrystals to curcumin at three months (13 weeks).



(a)



(b)

Figure 5 Experimental PXRD plots (black trace) of (a) curcumin–resorcinol and (b) curcumin–pyrogallol match nicely with the calculated X-ray diffraction lines from the crystal structures (red), indicating excellent purity of the bulk phases

4.3.4 FT-IR, FT-Raman and ss-NMR spectroscopy

Infrared and Raman spectroscopy provide useful information about the vibrational modes of a molecule resulting from changes in the physical state of the sample and differences in hydrogen bonding and molecular conformations.²⁸ Hydroxyl groups absorb strongly in the 3700-3584 cm⁻¹ region. Phenolic and olefinic C–O stretching vibrations occur between 1260-1000 cm⁻¹ and 1430-1410 cm⁻¹ respectively. IR spectra of cocrystals **1a** and **1b** alongside those of curcumin and the coformer are displayed in Figure 6. The changes in the O–H and C=O stretching frequencies of the cocrystals compared to the coformers suggested the formation of new compounds. Similarly the Raman spectra exhibited diagnostic differences in the carbonyl stretch, phenol, and olefinic C–O stretch regions (Figure 7). A comparison of IR and Raman stretching frequencies is summarized in Table 3 and 4. Together with ss-NMR spectroscopy (discussed next) the formation of new cocrystals of curcumin was confirmed in the bulk phase.

Solid-state ¹³C NMR spectroscopy²⁹ (ss-NMR) provides structural information about differences in hydrogen bonding, molecular conformation, molecular mobility, and short range environment in crystalline and amorphous solids. The sharp peaks in the spectra of cocrystals **1a** and **1b** indicated their crystalline nature. Differences in the cocrystals of curcumin from the starting materials were analyzed by ¹³C cross-polarization, magic-angle spinning (CP-MAS) ss-NMR (Figure 8). The upfield chemical shift of the OMe carbon (δ ~55 ppm) and downfield shift movement of the carbonyl carbon atom of curcumin (δ ~185 ppm) provided additional characterization of new solid materials **1a** and **1b**. The chemical shift values are summarized in Table 5.

Table 3 FT-IR stretching vibration modes wavenumber (ν_s , cm⁻¹) for curcumin cocrystals compare to coformers.

	O–H	C=O	Aromatic C=C	Enol C–O	Phenol C–O
Curcumin	3510.9	1627.5	1602.6	1429.0	1281.2
Curcumin- pyrogallol	3427.2 (broad)	1624.6	1573.1	1435.3	1281.1
Curcumin- resorcinol	3439.7	1625.5	1603.3, 1577.0	1430.7	1283.8
Pyrogallol	3527.4	---	1621.9	---	1285.3

Resorcinol	3257.3 (broad)	---	1608.3	---	1297.3
------------	-------------------	-----	--------	-----	--------

Table 4 FT-Raman stretching vibration modes wavenumber (ν_s , cm^{-1}) for curcumin cocrystals compare to coformers.

	C=O	Aromatic C=C	Enol C-O	Phenol C-O
Curcumin Form I	1626.0	1600.3	1430.0	1183.3
Curcumin-pyrogallol	1638.3	1591.6	1428.0	1184.6
Curcumin-resorcinol	1639.0	1601.3, 1585.4	1426.2	1185.4
Pyrogallol	---	1624.9	---	1156.7
Resorcinol	---	1606.4	---	1084.6

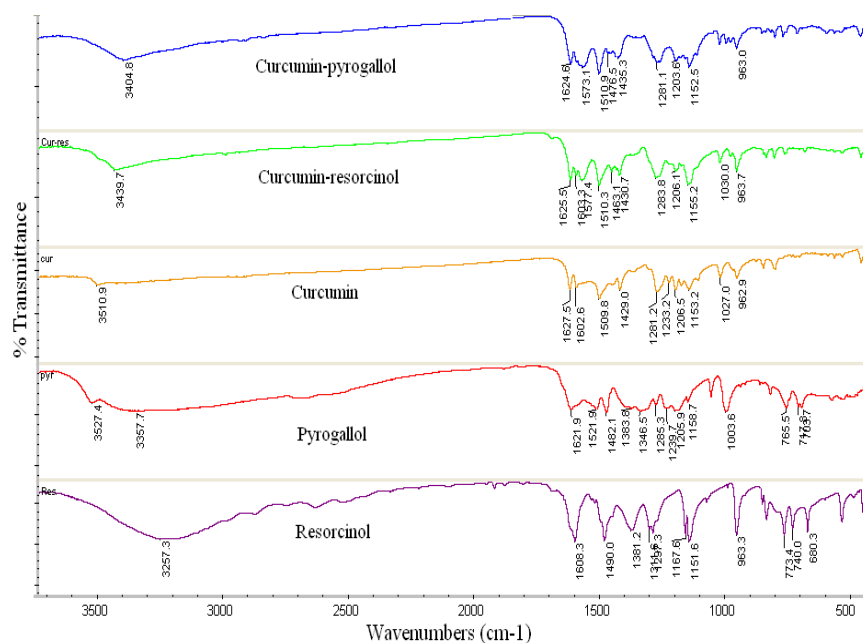


Figure 6 IR spectra of curcumin-resorcinol and curcumin-pyrogallol and the pure components.

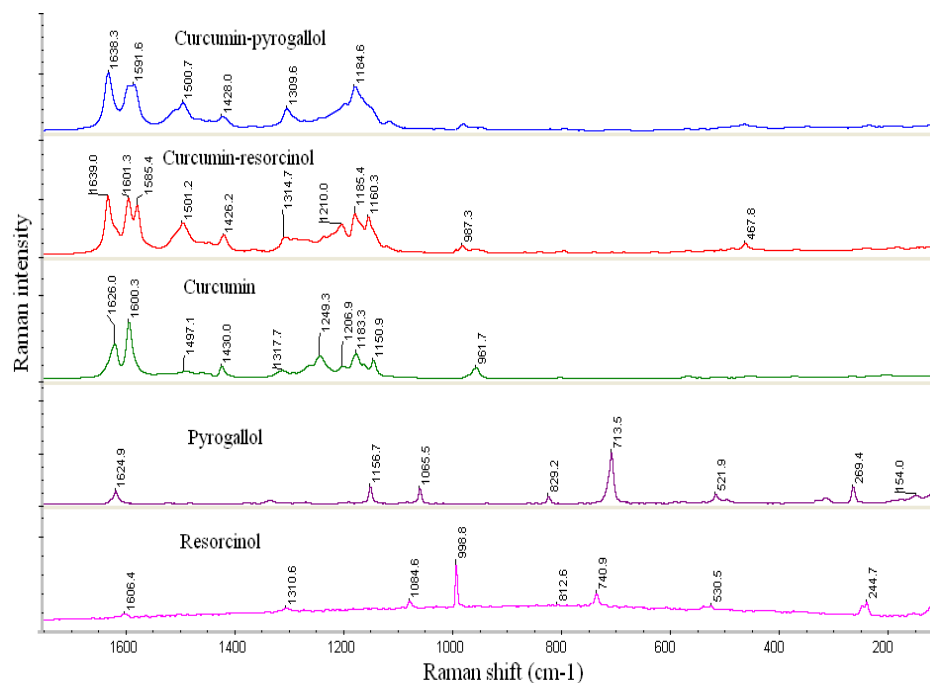
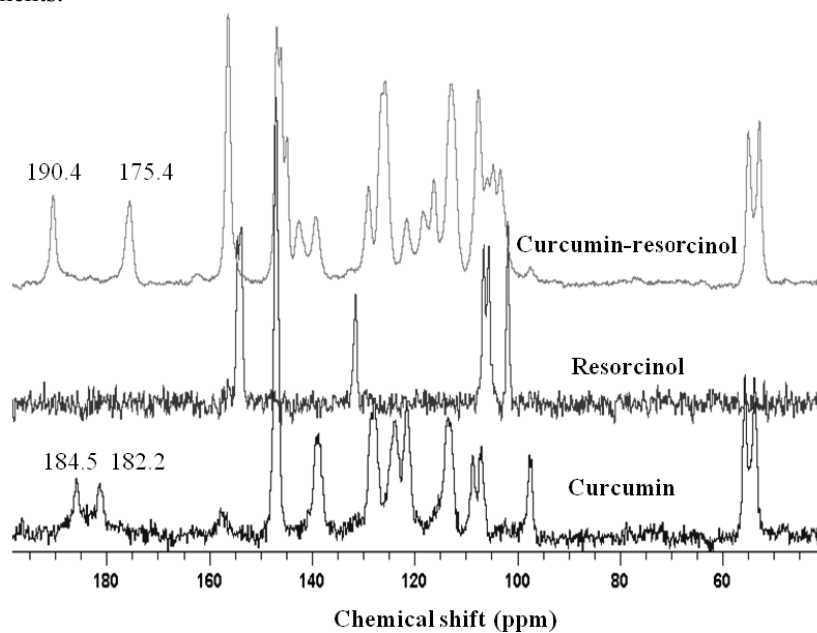


Figure 7 Raman spectra of curcumin–resorcinol and curcumin–pyrogallol and the pure components.



(a)

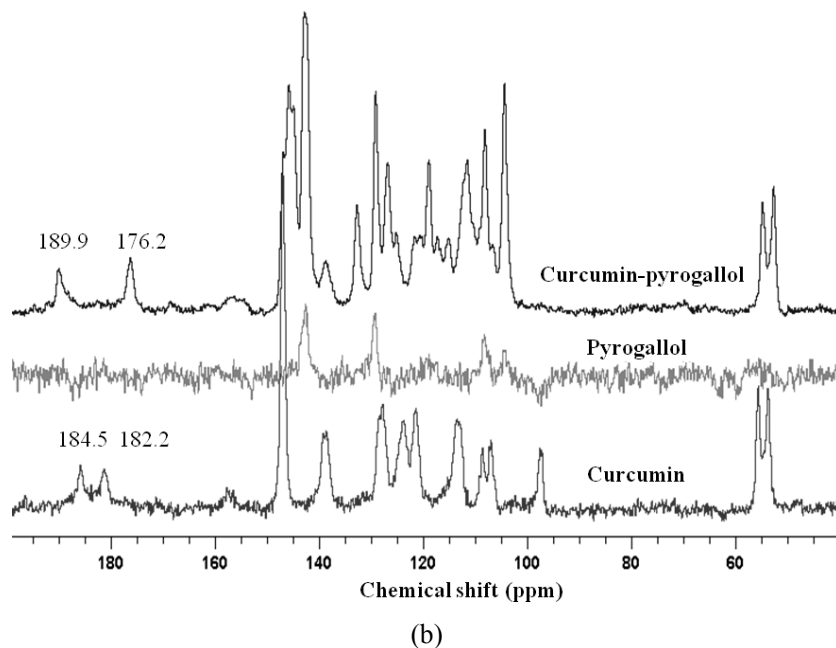


Figure 8 Solid state ^{13}C NMR spectra of (a) curcumin–resorcinol **1a** and (b) curcumin–pyrogallol **1b** cocrystals along with the pure components. The peaks in the cocrystal are shifted relative to the pure components. See the difference in the C=O chemical shift region.

Table 5 ^{13}C solid-state NMR chemical shifts (δ , ppm) for curcumin cocrystals **1a** and **1b** and curcumin polymorph 1. Atom numbering was shown below.

^{13}C peak atom #	Curcumin– resorcinol 1a	Curcumin– pyrogallol 1b	Curcumin polymorph 1
1, 17	146.79, 146.02	145.75, 144.90	156.75, 157.70
2, 18	142.54	142.77	146.91
3, 19	112.87	111.51	106.95
4, 14	128.92	129.09, 132.65	128.28, 127.73
5, 15	115.31	115.12	108.61, 107.29
6, 16	121.52	117.33, 118.85	113.44, 113.02
7, 13	139.09	138.69, 138.30	139.10, 138.65
8, 12	126.34, 125.70	125.17, 126.79	123.66, 121.34
9, 11	190.37, 175.43	189.94, 176.23	184.50, 182.22
10	---	---	97.540
20, 21	54.91, 52.77	54.73, 52.63	55.58, 53.63

1', 3'	154.34, 153.71	142.96, 142.60	---
2'	101.78	129.19	---
4', 6'	106.44, 105.42	104.16	---
5'	131.38	108.21	---

4.3.5 Dissolution experiments

More than 50% marketed drugs have very low solubility problems and consequently exhibit low bioavailability. To improve bioavailability of poorly soluble drugs, typical solubilisation techniques include cocrystal/salt formation, cosolvents, surfactants, complexation, hydrotropic agents and solid crystal suspensions were performed.³⁰ These approaches increase solubility by altering a solvating environment, making it better suited for maintaining hydrophobic solutes in aqueous solutions. However, hydrophobicity is not the sole reason for low drug solubility; rather strong crystallinity (or high melting point) is also responsible. Cocrystallization of low soluble drug molecules, showed much better solubility improvement than other techniques without changing the original drug molecule.

The aqueous solubility of curcumin is very low (8.7 mg/L).¹¹ Its solubility is lower at acidic and neutral pH and higher in basic conditions. However curcumin is unstable in the alkaline medium where 90% of curcumin decomposes at pH 7.2 buffer within 30 min. It is soluble in EtOH and acetone and is stable in these media. The dissolution rate of curcumin polymorphs was determined in 40% EtOH-water medium in which it has higher solubility (stable Form 1 = 1.21 g/L). The dissolution rate of Form 2 is about 3 times faster than that of commercial Form 1.¹⁷ The dissolution rates of curcumin cocrystals **1a** and **1b** were compared with that of the stable Form 1 at 37 °C for 5 h. The intrinsic dissolution experiment could not be run beyond 5 h because at this the time the pellet of cocrystal **1a** and **1b** started to disintegrate and a hole was observed in the center. The contact surface area of the pellet increased abruptly at this point leading to faster dissolution of cocrystals and consequent supersaturation of curcumin released suddenly into the medium causing precipitation. In contrast, the pellet of pure curcumin was intact beyond 5 h. The amount of curcumin dissolved per unit surface area (mg/cm²) was plotted against time (min) (Figure 9) and intrinsic dissolution rates were calculated (Table 6) from the slope in the linear region of the dissolution curves. Curcumin–pyrogallol (1:1) and curcumin–resorcinol (1:1) cocrystals dissolved ~12 and ~5 times

faster than curcumin, respectively. The rate of dissolution and apparent solubility are different from equilibrium solubility. The former are kinetic parameters while the latter is a thermodynamic quantity. Since most drugs exert their therapeutic effect within 4–6–8 h of oral administration, the apparent solubility of the drug is a relevant parameter for those solid-state drug forms which undergo phase transformation during the solubility experiment.

Solubility is defined as the concentration of the substance in solution that is at chemical equilibrium with an excess of the undissolved substance. The rate at which this equilibrium is reached is the dissolution rate. The solubility (after 24 h stirring, generally taken as an equilibrium value at 24–48 h) of curcumin Form 1, cocrystal **1a** and cocrystal **1b** are 1.21, 2.02 and 5.97 g/L, respectively (curcumin Form 2 = 2.12 g/L).²⁶ However, both cocrystals **1a** and **1b** were not indefinitely stable in the slurry medium of the dissolution experiment and converted to stable Form 1 of curcumin as concluded from their PXRD plots. When the solid form is not stable during the solubility experiment, as in the present case, the apparent solubility³¹ may be calculated for comparison. The apparent solubility is the rate at which the cocrystal dissolves with respect to the stable form, multiplied by the solubility of the stable form (Eq. 1).

$$C_m = C_s \times (J_m / J_s) \quad \text{Eq. (1)}$$

where C_m is the apparent solubility of the cocrystal, C_s is the solubility of the thermodynamic form, and J_m and J_s are the dissolution rates for the cocrystal and the stable species (derived from the linear region of the drug concentration vs. time plots). The apparent solubility's of curcumin–resorcinol **1a** and curcumin–pyrogallol **1b** cocrystals are 5.71 and 14.23 g/L, respectively (curcumin Form 2 = 3.84 g/L).

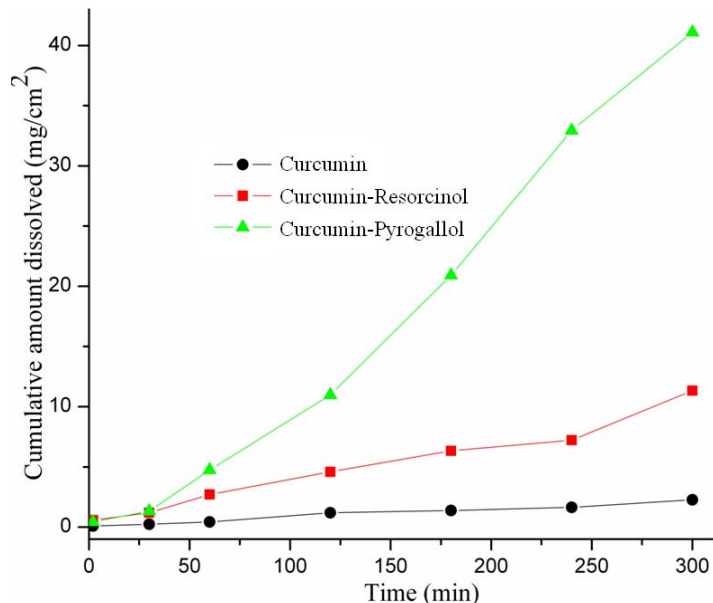


Figure 9 Intrinsic dissolution rate of curcumin Form 1 (●), curcumin–resorcinol (■) and curcumin–pyrogallol (▲) in 40% EtOH-water at 37 °C. The amount of curcumin dissolved in solution was monitored by UV-Vis spectroscopy.

Table 6 Dissolution and solubility data for curcumin polymorphs and cocrystals **1a** and **1b**. The extent of increase (× times) relative to curcumin polymorph 1 is given in bracket

Curcumin Forms	Absorption coefficient (ε), (/mM)	Solubility at 37 °C (24 h) in 40% ethanol-water (g/L)	Intrinsic dissolution rate (× 10 ⁻³) (mg/cm ²) /min	Apparent solubility ^a (g/L)
Curcumin	46.21	1.21	7.96	1.21
Curcumin–resorcinol (1a)	37.15	2.02 (× 1.67)	37.61 (× 4.72)	5.71 (× 4.72)
Curcumin–pyrogallol (1b)	52.42	5.97 (× 4.93)	93.64 (× 11.76)	14.23 (× 11.76)

^a Calculated using Eq. 1 given in text.

Powder dissolution experiments (Figure 10) were carried out on materials sieved to ~200 μm particle size to know the peak value of dissolution Vs. time. Peak solubilities were achieved at 2.5 h (Form 1 = 62 mg/L, **1a** = 119 mg/L, **1b** = 183 mg/L) and then steady state plateau concentrations were maintained until 4 h. The amount of curcumin dissolved in 4 h (AUC_{0-4 h}) of powder dissolution in 40% EtOH-water is 12.2 g h/L for form 1, 23.3 g h/L for cocrystal 1a, and 36.5 g h/L for cocrystal 1b. The fact that both curcumin-pyrogallol and curcumin-resorcinol are stable in the early phase of the

dissolution experiment (up to 2-4 h) (verified by placing 200 mg of cocrystal in 5 mL of 40% EtOH-water mixture) is an encouraging result. There was no trace of curcumin by PXRD after 2 h, but the cocrystals transformed to curcumin after 4 h (Figure 11). In contrast, the faster dissolving polymorph 2 of curcumin transformed to the stable modification in less than 1 h.

The higher apparent solubility of curcumin cocrystals 1a and 1b compared to the metastable polymorph 2 (discussed in chapter 3) is consistent with the general trend for polymorphs and cocrystals. Solubility improvement among crystalline drug polymorphs is about 2-3 times,³² with the less stable polymorph being more soluble. Cocrystal solubility can often match with that of the amorphous drug,^{2h,6} and these latter values are much higher (4-14-fold)³³ than that of the crystalline form. We noted the inverse correlation between melting point and solubility: the higher melting curcumin–resorcinol (1a) has lower solubility than the lower melting curcumin–pyrogallol cocrystal (1b). The data in Table 5 suggest that cocrystals 1a and 1b have a greater potential in solid form development for curcumin compared to the metastable polymorph because of their faster dissolution performance and improved stability. The concentration of curcumin in dissolution and solubility experiments was assayed spectrophotometrically at the 430 nm maxima from standardized concentration-intensity UV-vis plots; there was no interference from cofomers that absorb in the blue-shifted 250-270 nm UV region. We noted a structural similarity among the more soluble forms: the curcumin molecule is near-planar in the metastable polymorph 2 and cocrystals 1a and 1b, whereas it is bent in the stable polymorph. A possible explanation could be that the extended planarity³⁴ and conjugation of curcumin molecule are responsible for increased solubility. Conjugation is more effective in the planar structures because they are bright red colored compared to the deep yellow color of commercial curcumin. Another speculation is that the more soluble coformer makes O–H···O hydrogen bonds with water and thereby facilitates release of curcumin from the cocrystal into the aqueous medium.

BFDH morphology prediction using Mercury 2.4 software suggested why curcumin-pyrogallol exhibits higher solubility than curcumin-resorcinol. Considering six curcumin molecules on both sides of the predicted hexagonal crystals morphology along the *b*-axis, one hydroxyl groups of three each resorcinol molecules are exposed to the surface area, but two hydroxyl groups of three each pyrogallol molecules are exposed

(Figure 12). The solubility depends upon number of polar groups exposed on the surface and interacts with solvent molecules during dissolution experiments. This morphology prediction model explains better solubility of curcumin-pyrogallol than curcumin-resorcinol.

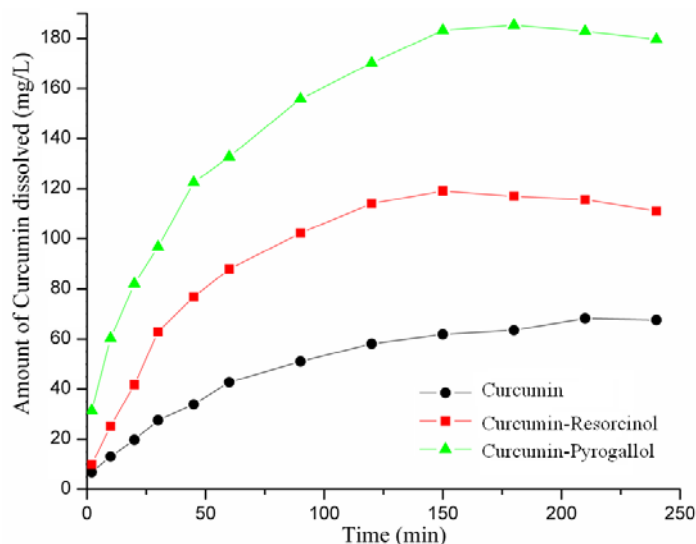
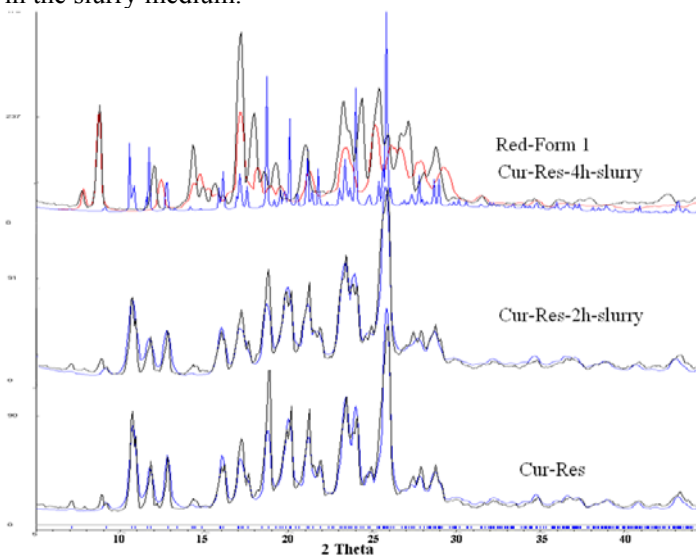
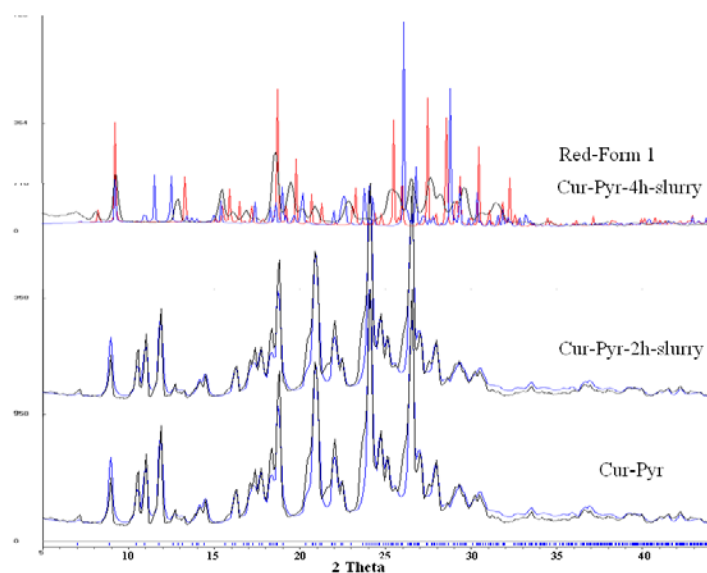


Figure 10 Powder dissolution curves for curcumin Form 1 (●), cocrystal **1a** (■) and cocrystal **1b** (▲). The curcumin concentration for cocrystals reaches a peak value at about 2.5 h and then starts decreasing slowly because of transformation to the stable polymorph 1 in the slurry medium.

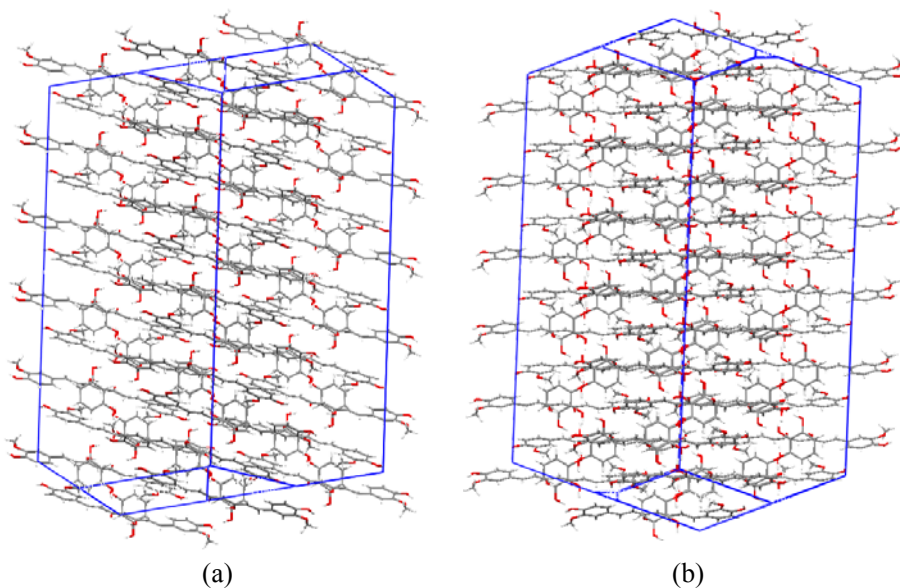


(a)



(b)

Figure 11 PXRD comparisons of (a) curcumin–resorcinol, 1a and (b) curcumin–pyrogallol, 1b with calculated X-ray lines of the respective cocrystals (blue) and curcumin (red) at 2 h and 4 h of slurry grinding in 40% EtOH-water medium. The cocrystals are stable up to 2 h but transform to curcumin after 4 h.



(a)

(b)

Figure 12 BFDH morphology predictions for curcumin–resorcinol (a) and curcumin–pyrogallol cocrystals along *b*-axis.

4.3.6 Conclusion

A major problem in the use of bioactive herbal ingredient curcumin as a therapeutic agent is its low solubility and bioavailability. The present results on more soluble cocrystals of curcumin could provide faster dissolving solid forms of curcumin that are relatively stable for drug development. These results are of general applicability in that cocrystals could offer the dual advantage of higher solubility and improved stability compared to fast dissolving polymorphs, which are often metastable. A crystal engineering approach was utilized to prepare 1:1 cocrystals of curcumin with resorcinol and pyrogallol by liquid-assisted grinding. The products 1a and 1b were characterized by IR, Raman, ss-NMR, and X-ray diffraction. In cocrystals curcumin molecules are interconnected in a chain motif where coformers resorcinol and pyrogallol situate at perpendicular positions. These are the earliest examples of curcumin cocrystals with complete structural characterization and physicochemical measurements to our knowledge. Pending in vivo clinical data, we believe that the faster dissolving curcumin cocrystals hint at improved bioavailability than pure curcumin.

4.4 Experimental section

4.4.1 Crystallization

The procedures for preparing microcrystalline powders (bulk material for measurements) and single crystals (for X-ray diffraction) of products are detailed in Table 7. The use of EtOH in liquid-assisted grinding did not show any apparent evidence of ethanol solvates as judged from the ^1H NMR spectra of products that were devoid of solvent peaks. Liquid-assisted grinding followed by solution crystallization gave single crystals, but the first stage was not mandatory; an equimolar mixture of components in solution crystallization gave similar results.

Table 7 Crystallization conditions for curcumin cocrystals

Cocrystal	Condition	Time (d)
Curcumin– resorcinol (1:1), 1a	(a) Solution crystallization for single crystals 200 mg (0.54 mmol) curcumin and 59.5 mg (0.54 mmol) resorcinol were ground in a mortar-pestle for 30 min after adding 5 drops of	3-4

	EtOH, and then kept for crystallization in EtOH-benzene mixture (18 mL + 2 mL).	
	(b) Liquid-assisted grinding method for bulk material	
	200 mg (0.54 mmol) curcumin and 59.5 mg (0.54 mmol) resorcinol were ground in a mortar-pestle for 30 min after adding of 5-6 drops of EtOH which gave the cocrystal as microcrystalline powder.	
Curcumin– pyrogallol (1:1), 1b	(a) Solution crystallization for single crystals 200 mg (0.54 mmol) curcumin and 68.1 mg (0.54 mmol) pyrogallol were ground in a mortar-pestle for 30 min after adding 5 drops of EtOH, and then kept for crystallization in EtOH-benzene mixture (18 mL + 2 mL). (b) Liquid-assisted grinding method for bulk material 200 mg (0.54 mmol) curcumin and 68.1 mg (0.54 mmol) pyrogallol were ground in a mortar-pestle for 30 min after adding 5-6 drops of EtOH to give the cocrystal as a microcrystalline powder.	3-4

4.4.2 Dissolution and solubility experiments

Intrinsic dissolution rate (IDR) and solubility measurements were carried out on a USP-certified Electrolab TDT-08 L Dissolution Tester (Electrolab, Mumbai, MH, India). A calibration curve was obtained for curcumin Form 1, and cocrystals **1a** and **1b** by plotting absorbance vs. concentration UV-Vis spectra curves on a Thermo Scientific Evolution EV300 UV-Vis spectrometer (Waltham, MA, USA) for known concentration solutions in 40% EtOH-water medium. The mixed solvent system (EtOH-water) was selected for its higher solubility of curcumin in this medium. The slope of the plot from the standard curve gave the molar extinction coefficient (ϵ) by applying the Beer-Lambert's law. Equilibrium solubility was determined in 40% EtOH-water medium using the shake-flask method.³⁵ To obtain the equilibrium solubility, 100 mg of each solid material was stirred for 24 h in 5 mL 40% EtOH-water at 37 °C, and the absorbance was measured at 430 nm. The concentration of the saturated solution was calculated at 24 h, which is referred to as the Equilibrium solubility of the stable solid form (C_s). The Apparent solubility (C_m) is more appropriate for cocrystals **1a** and **1b**

because they were found to transform to the stable Form 1 of curcumin under the solubility measurement conditions. The Apparent solubility (C_m) of a cocrystal is calculated using the equation

$$C_m = C_s \times (J_m / J_s)$$

where J_s and J_m are the dissolution rates of the stable and cocrystals forms. The dissolution rates J_s and J_m are obtained from the IDR experiments.

100 mg of the solid (drug, cocrystal, polymorph) was taken in the intrinsic attachment and compressed to a 0.5 cm² pellet using a hydraulic press at a pressure of 2.5 ton/inch² for 2 min. The pellet was compressed to provide a flat surface on one side and the other side was sealed. Then the pellet was dipped into 900 mL of 40% EtOH-water medium at 37 °C with the paddle rotating at 150 rpm and continued upto 5 h. At regular interval of 10 min, 5 mL of the dissolution medium was withdrawn and replaced by an equal volume of fresh medium to maintain a constant volume. Samples were filtered through 0.2 µm nylon filter and assayed for drug content spectrophotometrically at 430 nm on a Thermo-Nicolet EV300 UV-Vis spectrometer. There was no interference to the curcumin UV-Vis maxima at 430 nm by the coformers because resorcinol and pyrogallol absorb at 250-270 nm in the UV region. The amount of drug dissolved in each time interval was calculated using the calibration curve. The linear region of the dissolution profile was used to determine the intrinsic dissolution rate (IDR) of the compound (= slope of the curve, i.e. amount of drug dissolved divided by the surface area of the disc (0.5 cm²) per minute). The dissolution rates for Form 1 and cocrystals **1a** and **1b** of curcumin were computed from their IDR values.

For powder dissolution studies of curcumin and its cocrystals the starting solids were sieved in ASTM standard mesh sieves to provide samples with particle size of approximately 200 µm and then directly poured into 900 mL dissolution medium and the paddle rotation was fixed at 100 rpm. Dissolution experiments were continued up to 4h at 37 °C. At regular interval of 5-10 min, 5 mL of the dissolution medium was drawn and replaced by an equal volume of fresh medium to maintain a constant volume. The area under the curve for 4 h of dissolution experiment (AUC_{0-4h}) was calculated by the linear trapezoidal rule of drug bioavailability.³⁶

4.5 References

1. (a) S. R. Byrn, R. R. Pfeiffer and J. G. Stowell, *Solid-State Chemistry of Drugs*; SSCI: West Lafayette, IN, **1999**. (b) R. Hilfiker, *Polymorphism in the Pharmaceutical Industry*, Wiley-VCH, Weinheim, **2006**. (c) S. L. Morissette, Ö. Almarsson, M. L. Peterson, J. F. Remenar, M. J. Read, A. V. Lemmo, S. Ellis, M. J. Cima, C. R. Gardner, *Adv. Drug. Del. Rev.* **2004**, *56*, 275.
2. (a) N. Rodríguez-Hornedo, Guest Editor, Special Section on Pharmaceutical Cocrystals, *Mol. Pharmaceutics* **2007**, *4*, 299–434. (b) P. Vishweshwar, J. A. McMahon, M. J. Zaworotko, in *Frontiers in Crystal Engineering*, E. R. T. Tiekink and J. J. Vittal, Eds., Wiley, Chichester, **2006**, pp. 25-49. (c) Ö. Almarsson, M. J. Zaworotko, *Chem. Commun.* **2004**, 1889. (d) P. Vishweshwar, J. A. McMahon, J. A. Bis, M. J. Zaworotko, *J. Pharm. Sci.* **2006**, *95*, 499. (e) W. Jones, W. D. S. Motherwell, A. V. Trask, *Mat. Res. Soc.* **2006**, *31*, 875. (f) C. R. Gardner, C. T. Walsh, Ö. Almarsson, *Nat. Rev.* **2004**, *3*, 926. (g) M. L. Peterson, M. B. Hickey, M. J. Zaworotko, Ö. Almarsson, *J. Pharm. Pharmaceut. Sci.* **2006**, *9*, 317. (h) N. Shan, M. Zaworotko, *Drug Discovery Today* **2008**, *13*, 440. (i) J. F. Remenar, S. L. Morissette, M. L. Peterson, B. Moulton, J. M. MacPhee, H. R. Guzmán, Ö. Almarsson, *J. Am. Chem. Soc.* **2003**, *125*, 8456.
3. (a) A. M. Thayer, Form and function. *Chem. Eng. News* **2007**, *85*, 17. (b) A. M. Thayer, Finding solutions. *Chem. Eng. News* **2010**, *88*, 13.
4. Everything added to food in the United States (EUFAS) list of chemicals published by the US-FDA. Updated 10/01/2010. <http://www.accessdata.fda.gov/scripts/fcn/fcnNavigation.cfm? rpt=eafusListing>.
5. (a) B. R. Bhogala, S. Basavoju, A. Nangia, *CrystEngComm* **2005**, *7*, 551. (b) C. B. Aakeröy, D. J. Salmon, *CrystEngComm* **2005**, *7*, 439. (c) C. B. Aakeröy, A. M. Beatty, B. A. Helfrich, *Angew. Chem., Int. Ed.* **2001**, *40*, 3240. (d) B. R. Bhogala, A. Nangia, *New. J. Chem.* **2008**, *32*, 800. (e) J. N. Moorthy, P. Natarajana and P. Venugopalan, *Chem. Commun.* **2010**, *46*, 3574. (f) T. Friščić, A. V. Trask, W. Jones, and W. D. S. Motherwell, *Angew. Chem. Int. Ed.* **2006**, *45*, 7546

6. (a) S. Karki, M. Frišćić, L. Fábián, P. R. Laity, G. M. Day and W. Jones, *Adv. Mater.* **2009**, *21*, 3905. (b) S. L. Childs, N. Rodri'guez-Hornedo, L. S. Reddy, A. Jayasankar, C. Maheshwari, L. McCausland, R. Shipplett and B. C. Stahlya, *CrystEngComm*, **2008**, *10*, 856. (c) M. Viertelhaus, R. Hilfiker, F. Blatter, M. Neubu, *Cryst. Growth Des.* **2009**, *9*, 2220.
7. (a) B. Lockwood, Nutraceuticals, Pharmaceuticals Press: London, UK, **2007**. (b) L. Rapport, B. Lockwood, Nutraceuticals, London: Pharmaceutical press, **2002**.
8. (a) S. Çıkırıkcı, E. Mozioglu, H.Yılmaz, *Rec. Nat. Prod.* **2008**, *2*, 19. (b) H. Hatcher, R. Planalp, J. Cho, F. M. Torti, S. V. Torti, *Cell Mol. Life Sci.* **2008**, *65*, 1631.
9. (a) G. B. Mahady, S. L. Pendland, G. Yun, Z. Z. Lu, *Anticancer Res.* **2002**, *22*, 4179. (b) Y. Sugiyama, S. Kawakishi, T. Osawa, *Biochem. Pharmacol.* **1996**, *52*, 519. (c) A. J. Ruby, G. Kuttan, K. D. Babu, K. N. Rajasekharan, R. Kuttan, *Cancer Lett.* **1995**, *94*, 79. (d) W. C. Jordan, C. R. Drew, *J. Natl. Med. Assoc.* **1996**, *88*, 333.
10. (a) S. Qureshi, A. H. Shah, A. M. Ageel, *Planta Med.* **1992**, *58*, 124. (b) C. D. Lao, M. T. Ruffin, D. Normolle, D. D. Heath, S. I. Murray, J. M. Bailey, M. E. Boggs, J. Crowell, C. L. Rock, D. E. Brenner, *BMC Complement, Altern. Med.* **2006**, *6*, 10.
11. (a) B.T. Kurien and R. H. Scofield. *Trends Pharmacol. Sci.*, **2009**, *30*, 334. (b) S. M. H. Rahman, T. C. Telny, T. K. Ravi, S. Kuppusamy, *Ind. J. Pharm. Sci.* **2009**, *71*, 139. (c) P. Anand, A. B. Kunnumakkara, R. A. Newman, B. B. Aggarwal, *Mol. Pharmaceutics*, **2007**, *4*, 807.
12. (a) Y. J. Wang, M. H. Pan, A. L. Cheng, L. I. Lin, Y. S. Ho, C. Y. Hsieh, J. K. Lin, *J. Pharm. Biomed. Anal.* **1997**, *15*, 1867. (b) H. H. Tonnesen and J. Karlsen, *Z Lebensm Unters Forsch*, **1985**, *180*, 402. (c) Y.-J. Wang, M.-H. Pan, A.-L. Cheng, L.-I. Lin, Y.-S. Ho, C.-Y. Hsieh, J.-K. Lin, *J. Pharm. & Biomed. Anal.* **1997**, *15*, 1867.
13. (a) B. Antony, B. Merina, V. S. Iyer, N. Judy, K. Lennertz, S. A. Joyal, *Ind. J. Pharm. Sci.* **2008**, 445. (b) S. Ganta, H. Develapally, M. Amiji, *J. Pharm. Sci.* **2010**, *99*, 4630. (c) N. Kaewnopparat, S. Kaewnopparat, A. Jangwang, D. Maneenaun, T. Chuchome, and P. Panichayupakaranant, World Academy of

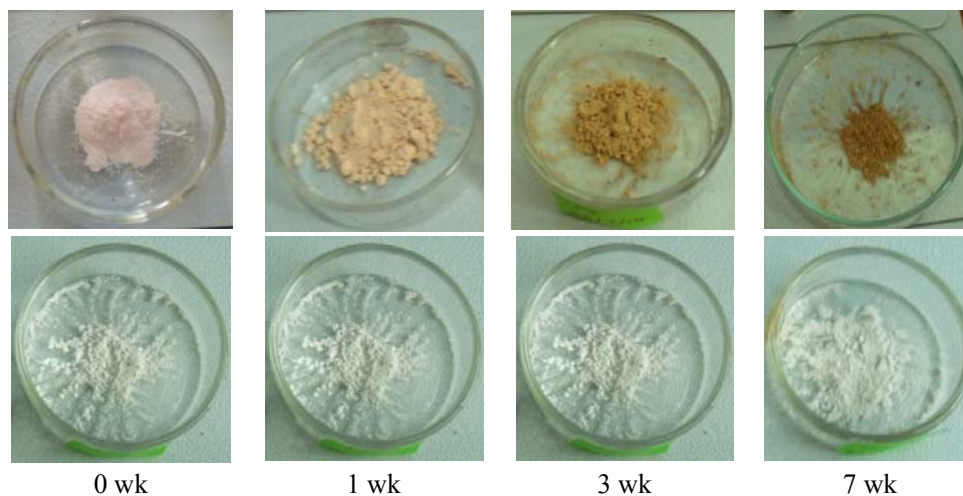
- Science, Eng. & Techno. **2009**, 55, 229. (d) G. Shoba, D. Joy, T. Joseph, M. Majeed, R. Rajendran, P. S. Srinivas, *Planta Med.* **1998**, 64, 353.
14. (a) N. K. Gupta, V. K. Dixit, *J. Pharm. Sci.* **2011**, 100, 1987. (b) F. Zhang, G. K. Koh, D. P. Jeansonne, J. Hollingworth, P. S. Russo, G. Vicente, R. W. Stout, Z. Liu, *J. Pharm. Sci.* **2011**, 100, 2778.
 15. (a) N. Schultheiss, S. Bethune, J.-O. Henck, *CrystEngComm* **2010**, 12, 2436. (b) S. Karki, T. Friščić, L. Fábián, W. Jones, *CrystEngComm* **2010**, 12, 4038. (c) S. J. Bethune, N. Schultheiss, J. -O. Henck, *Cryst. Growth Des.* **2011**, 11, 2817.
 16. (a) N. Schultheiss, A. Newman, *Cryst. Growth Des.* **2009**, 9, 2950. (b) D. P. McNamara, S. L. Childs, J. Giordano, A. Iarriccio, J. Cassidy, M. S. Shet, R. Mannion, E. O'Donnell, A. Park, *Pharm. Res.* **2006**, 23, 1888. (c) S. Karki, T. Friščić, L. Fábián, P. R. Laity, *Adv. Mater.* **2009**, 21, 3905. (d) M. K. Stanton, S. Tufekcic, C. Morgan, and A. Bak, *Cryst. Growth Des.*, **2009**, 9, 1344. (e) A. V. Trask, W. D. S. Motherwell, and W. Jones, *Cryst. Growth Des.*, **2005**, 5, 1013.
 17. P. Sanphui, N. R. Goud, U. B. R. Khandavilli, S. Bhanoth and A. Nangia, *Chem. Commun.*, **2011**, 47, 5013.
 18. (a) A. Mukherjee, P. Grobelny, T. S. Thakur, G. R. Desiraju, *Cryst. Growth Des.* **2011**, 11, 2637. (b) G. J. Kemperman, R. D. Gelder, F. J. Dommerholt, A. J. H. Klunder, B. Zwanenburg, *Eur. J. Org. Chem.* **2002**, 345. (c) P. Vishweshwar, A. Nangia, V. M. Lynch, *CrystEngComm* **2003**, 5, 164.
 19. (a) C. J. Yang, C. S. Wang, J. Y. Hung, H. W. Huang, Y. C. Chia, P. H. Wang, C. F. Weng, M. S. Huang, *Lung Cancer*. **2009**, 66, 162. (b) G. Tang, C. Y. Yang, Z. Nikolovska-Coleska, J. Guo, S. Qiu, R. Wang, W. Gao, G. Wang, J. Stuckey, K. Krajewski, S. Jiang, P. P. Roller, S. Wang, *J. Med. Chem.* **2007**, 50, 1723.
 20. (a) A. V. Trask, W. D. S. Motherwell, and W. Jones, *Chem. Commun.* **2004**, 890. (b) S. Aitipamula, P. S. Chow, R. B. H. Tan, *CrystEngComm* **2009**, 11, 889. (c) N. R. Goud, N. J. Babu, and A. Nangia, *Cryst. Growth Des.* **2011**, 11, 1930.
 21. K. Balasubramanian, *J. Agric. Food Chem.* **2006**, 54, 3512.
 22. (a) Y. Ishigami, M. Goto, T. Masuda, Y. Takizawa and S. Suzuki, Shikizai Kyokaishi (Jap.), **1999**, 72, 71; (b) Q. -L. Suo, Y.-C. Huang, L.-H. Weng, W.-Z. He, C.-P. Li, Y.-X. Li and H.-L. Hong, Shipin Kexue (Beijing, China) (Food Sci.

- (Beijing)), **2006**, 27, 27; (c) S. P. Parimita, Y. V. Ramshankar, S. Suresh and T. N. Guru Row, *Acta Crystallogr., Sect. E: Struct. Rep. Online*, **2007**, E63, o860; (d) F. R. Fronczek, Private Communication, **2008**. CCDC refcode BINMEO01, 02, 03, 04.
23. (a) J. Bernstein, R. E. Davis, L. Shimoni, N.-L. Chang, *Angew. Chem., Int. Ed. Engl.* **1995**, 34, 1555. (b) M. C. Etter and J. C. Macdonald, *Acta Crystallogr., Sect. B: Struct. Sci.*, **1990**, B46, 25.
24. (a) O. Ermer, C. Robke, *Angew. Chem., Int. Ed. Engl.* **1994**, 33, 1755. [Refcode HESKOF]; (b) M. B. Dinger, M. J. Scott, *Eur. J. Org. Chem.* **2000**, 2467. [Refcode QEXXEW]; (c) M. Parvez, S. K. Kurtz, I. Williams, *Acta Cryst.* **1990**, C46, 165. [Refcode SEFRIE]. (d) T. L. Andresen, F. C. Krebs, N. Thorup, K. Bechgaard, *Chem. Mater.* **2000**, 12, 2428 [Refcode XEFSIK].
25. (a) Z. Ma, B. Moulton, *Mol. Pharmaceutics* **2007**, 4, 373. (b) S. Aitipamula, P. S. Chowa, and R. B. H. Tan, *CrystEngComm* **2009**, 11, 1823. (c) P. M. Bhatt, Y. Azim, T. S. Thakur, and G. R. Desiraju, *Cryst. Growth Des.* **2009**, 9, 951. (d) P. Grobelny, A. Mukherjee and G. R. Desiraju, *CrystEngComm*, **2011**, 13, 4358.
26. (a) R. Thakuria, A. Nangia, *CrystEngComm*. **2011**, 13, 1759. (b) J. F. Remenar, M. L. Peterson, P. W. Stephens, Z. Zhang, Y. Zimenkov, M. B. Hickey, *Mol. Pharmaceutics* **2007**, 4, 386.
27. (a) J. Li, S. A. Bourne, M. R. Caira, *Chem. Commun.* 2011, **47**, 1530. (b) G. M. Day, A. V. Trask, W. D. S. Motherwell and W. Jones, *Chem. Commun.*, **2006**, 54.
28. (a) B. H. Stuart, *Infrared Spectroscopy: Fundamentals and Applications*, 2004, John-Wiley, UK (b) R. L. McCreery, *Raman Spectroscopy for Chemical Analysis*, John-Wiley, 2000, UK; E. Smith and G. Dent, *Modern Raman Spectroscopy - A Practical Approach*, John-Wiley, 2005, UK.
29. (a) Z. J. Li, Y. Abramov, J. Bordner, J. Leonard, A. Medek, and A. V. Trask, *J. Am. Chem. Soc.* **2006**, 128, 8199. (b) F. G. Vogt, J. S. Clawson, M. Strohmeier, A. J. Edwards, T. N. Pham, S. A. Watson, *Cryst. Growth Des.* **2009**, 9, 921.
30. (a) S. H. Yalkowsky, *Techniques of solubilization of drugs*; Marcel Dekker Inc.: New York, **1981**. (b) C. Leuner, J. Dressman, *Eur. J. Pharm. Biopharm.* **2000**,

- 50, 47. (c) M. Thommes, D. R. Ely, M. T. Carvajal, and R. Pinal, *Mol. Pharmaceutics*, **2011**, 8, 727.
31. (a) J. H. Fagerberg, O. Tsinman, N. Sun, K. Tsinman, A. Avdeef, C. A. S. Bergström, *Mol. Pharmaceutics* **2010**, 7, 1419. (b) M. Otsuka, R. Teraoka, Y. Matsuda, *Chem. Pharm. Bull.* **1991**, 39, 2667.
32. M. Pudipeddi, A. T. M. Serajuddin, *J. Pharm. Sci.* **2005**, 94, 929.
33. (a) B. C. Hancock, M. Parks, *Pharm. Res.* **2000**, 17, 397. (b) N. J. Babu, A. Nangia, *Cryst. Growth Des.* **2011**, 11, 2662.
34. T. Murashima, S. Tsujimoto, T. Yamada, T. Miyazawa, H. Uno, N. Uno, N. Sugimoto, *Tetrahedron Lett.* **2005**, 46, 113.
35. A. Glomme, J. Marz, J. B. Dressman, *J. Pharm. Sci.* **2005**, 94, 1.
36. G. C. Viscomi, M. Campana, M. Barbanti, F. Grepioni, M. Polito, D. Confortini, G. Rosini, P. Righi, V. Cannata, D. Braga, *CrystEngComm* **2008**, 10, 1074.

Chapter Five

Crystal Engineering of Stable Temozolomide Cocrystals



Solid form stability and color comparison of pure Temozolomide (top panel) and Temozolomide–succinic acid cocrystal (bottom panel) under accelerated ICH conditions of 40 °C and 75% RH. Whereas pure temozolomide turned pink to tan to dark brown in color due to degradation, its cocrystal remained white (stable) for the entire duration.

5.1 Introduction

Crystal Engineering¹ is a flourishing field of research dealing with “the understanding of intermolecular interactions in the context of crystal packing and in the utilization of such understanding in the design of new solids with desired physical and chemical properties”. Crystal Engineering has subsequently attracted general interest from a wide range of molecular scientists, in particular organic, inorganic and physical chemists, crystallographers and materials scientists. Crystal Engineering not only addresses a fundamental understanding of crystal packing, it also offers an opportunity for the design of new solids with desired structure and properties. Furthermore, supramolecular approaches to synthesis² can offer considerable advantages over traditional covalent synthesis in which compounds are generated by stepwise breaking and making of covalent bonds. In particular, supramolecular synthesis facilitates self-assembly of molecules through non-covalent interactions (e.g. hydrogen bond) without changing the chemical structure of the molecular components.

Considerable time and funds are required for the research and development and formulation of any API that is to be delivered in a solid form.³ Unfortunately, some potentially useful APIs administered as solids may never realize their maximum potential due to poor stability and bioavailability, limited by their solubility.⁴ The enhanced stability and solubility critically impacts the pharmacokinetic profile of orally delivered APIs resulting in better absorption in the gastrointestinal tract (GIT) and reduced dosage-level requirements.⁵ Thus, a number of approaches have been pursued for optimizing the solubility of APIs such as preparation of solid dispersions, microionization, the use of surfactants, self-emulsifying formulations, inclusion complexation with cyclodextrins, nanocrystals, and the use of single and multi-component molecular crystals.⁶ Recently there is heightened interest and awareness of the need to diversify the range of crystal forms exhibited by APIs. The multi-component approach that includes salts as well as cocrystals results in a set of structural variations of the same API. Salt formation indeed is a widely accepted approach to modify the physical properties of APIs,⁷ Cocrystal (as discussed in chapter 4) is a multi-component system, solid at ambient condition, held together by noncovalent interactions e.g. hydrogen bond, electrostatic, columbic interactions. However, pharmaceutical cocrystallization is a recent technology which

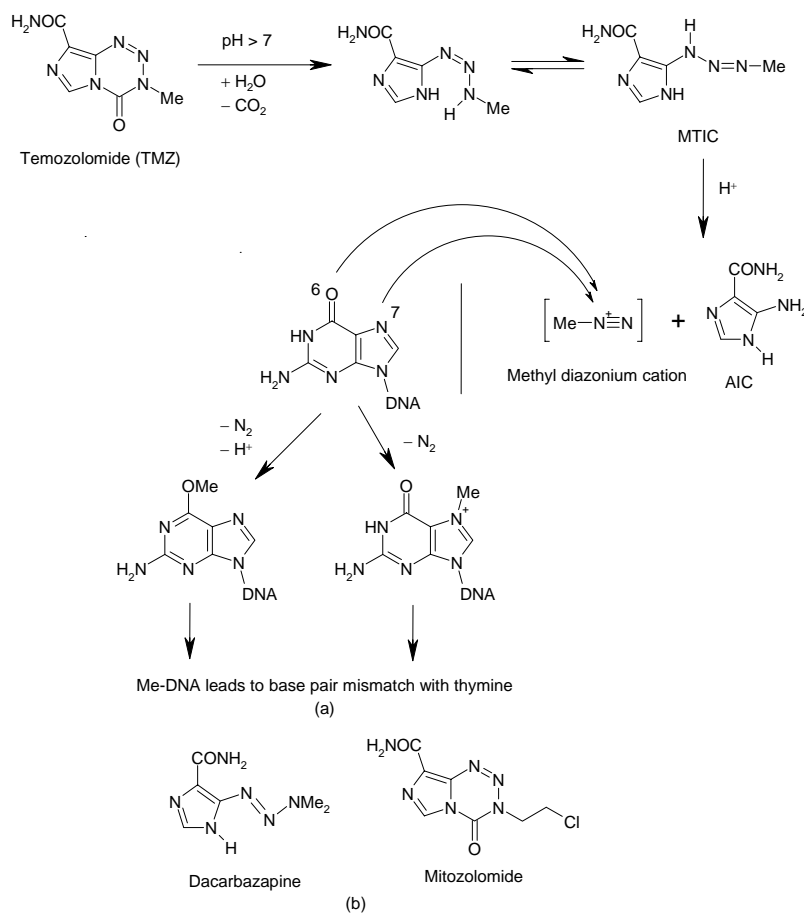
offers an alternative platform to improve the physicochemical properties of active pharmaceutical ingredients (APIs), such as the melting point, solubility, tableting, stability and dissolution rate.⁸ Whereas improvement in solubility and faster dissolution rates are the most preferred reasons for developing novel cocrystal materials, the opposite trend of reduced solubility is also possible.^{9a} Other applications of pharmaceutical cocrystals are changes in crystal morphology and isomer separation.⁹ For example, the crystal packing of paracetamol^{9b} was modified to a layer structure in a cocrystal with theophylline (1:1) that had improved compression and tableting properties compared to the stable polymorph of the drug. Difficult to separate isomers/ stereoisomers and chiral resolution of quinidine from its stereoisomer quinine was achieved via cocrystals with methyl paraben as a molecular hook.^{9c} Pharmaceutical cocrystals consists of one pharmaceutical ingredient and GRAS molecule as a cofomer. They are multiple component solids in a definite stoichiometric ratio, also represent a broad patent space since they are clearly new chemical entities, their design and preparation involve several elements of non-obviousness. Cocrystals generally have novel and useful properties.¹⁰ These are particularly relevant for APIs lacking functional groups that enable salt formation. Again the synthon¹¹ which is defined as “structural units within the molecules can be formed and/or assembled by known or conceivable synthetic operations” provides rational strategies for the construction of cocrystals and assessing the likelihood of formation of specific hydrogen bond. Normally all good hydrogen bond donors and acceptors are used in hydrogen bonding, and the best hydrogen bond donor tends to interact with the best hydrogen bond acceptor and so on, in a given crystal structure. Based on the functional groups in molecules and the hydrogen bond rules,¹² Crystal Engineering has recently gained relevance in the preparation of various stoichiometries of cocrystals. Further they can be easily prepared through solvent free or solvent reduced methods. Neat grinding, solvent-drop or liquid assisted grinding, slurry grinding, ball milling and solvent mediated cocrystal formation are few general methods used for cocrystal preparation.¹³ Cocrystals can be designed by synthon strategies, this does not mean that details of crystal structures or physical properties can be predicted before they are measured.

5.2 Temozolomide

Temozolomide (TMZ) is an anticancer agent with a broad spectrum of antineoplastic activity.¹⁴ TMZ is a monofunctional alkylating agent prodrug that is able to cross the blood-brain barrier. It is the preferred treatment of choice for some of the most malignant and intractable brain tumors. Temozolomide is the most effective drug for glioblastoma multiforme, malignant melanoma, and other advanced cancers in human patients. Temozolomide is superior to its closely related nitrogen heterocycle predecessor drug molecules, e.g. dacarbazine and mitozolomide.¹⁵ Mitozolomide was very successful in rats but produced toxic side effects in human Phase I clinical trials. The biochemically active species in all cases is 5-(3-monomethyl-1-triazeno)imidazole-4-carboxamide (MTIC), but the difference is that dacarbazine requires hepatic metabolism to generate the active intermediate species whereas temozolomide spontaneously hydrolyzes above pH 7 to MTIC which further transforms to 5-aminoimidazole-4-carboxamide (AIC) by-product. MTIC auto-degrades to the highly reactive methyldiazonium cation (CH_3N_2^+) which is the nascent alkylating agent for DNA. The most nucleophilic centers for methylation of nucleotides are O6 (5% of adducts) and N7 of guanine (70% of adducts), N1 and N3 of adenine, and N3 of cytosine (25% of adducts). Although O6 methylation is a minor site of DNA alkylation, it causes the maximum cell apoptosis and death. The mechanism of activation of TMZ^{14b,16} involves hydrolytic cleavage of the tetrazinone ring at neutral-to-basic pH conditions and release of the methylating agent (Scheme 1), which binds in the major groove of DNA. Temozolomide is an effective antitumor agent when a large population of cancer cells is actively replicating.

Several polymorphs of temozolomide are published in the patent literature and X-ray crystal structures of four of these ten polymorphs (three crystalline polymorphs and a monohydrate) were determined.^{15,17} Commercially available temozolomide matches with the powder X-ray diffraction (PXRD) pattern of Form 1. The material is crystalline and non hygroscopic. However, there is a stability problem associated with temozolomide tablets marketed under the brand name Temodar or Temodal.^{16b} Even though freshly crystallized temozolomide is obtained as a white powder, the material often turns to light tan/ pink powder upon storage. The product information leaflet of Temodar drug in the Physician Desk Reference 60th Edition¹⁸ states that the drug material is a light tan/ light pink powder. The coloration is indicative of degradation to

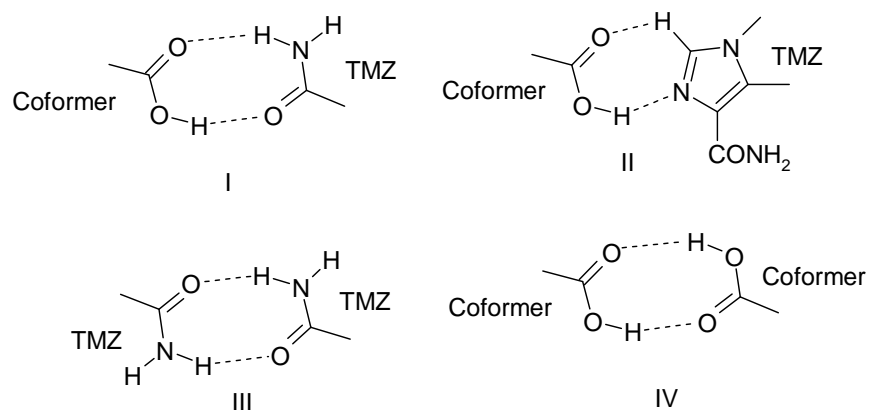
AIC during storage, thus making the prodrug less effective. Moreover, the tan brown color of tablet can also cause unnecessary scare in patients. A recent patents¹⁹ on storing temozolomide in sealed bags noted that “in view of the apparent tendency of temozolomide to degrade, as evidenced by the change in color, there exists a need for products and methods, which improve the stability and shelf life of temozolomide.” Special storage precautions such as reduced humidity, desiccants, low oxygen and light levels are specified for storing this compound. A sample containing 1.8% water decomposes faster than samples with 0.1% water over 6 months. White samples of temozolomide stored at 45% RH started to turn pink after 24 hours and the material was distinctly pink after 4 days. There is thus an urgent need for an improved solid-state form of temozolomide exhibiting superior drug stability.



Scheme 1 Mechanism of action for the anti-tumor prodrug Temozolomide by DNA methylation. MTIC = 5-(3-monomethyl-1-triazeno)imidazole-4-carboxamide, AIC = 5-

aminoimidazole-4-carboxamide. (b) Structure of dacarbazapine and mitozolomide, close analogues of temozolomide.

The kinetics of temozolomide decomposition is pH dependent: the drug is stable at acidic pH (<5) but labile at basic pH (>7).²⁰ MTIC intermediate is stable at basic pH but unstable under acidic conditions. In this background we reasoned that the decomposition of temozolomide could be inhibited or retarded by organic carboxylic acids in the pK_a range 1–5 as pH adjusters. Our objective was to bring together temozolomide and the carboxylic acid coformer into the same crystalline lattice by cocrystallization. The amide group of TMZ, and to a lesser extent the N acceptors on the heterocyclic ring, will serve as complementary functional groups to COOH donors in a cocrystal engineering strategy (Scheme 2). Normally, aromatic N, such as in pyridine, triazole, imidazole, etc. are excellent to good hydrogen bond acceptors for the COOH donor, but in temozolomide the acceptor strength of basic N atoms is attenuated because of electron-withdrawing amide and urea groups on the bicyclic core as well as an intramolecular hydrogen bond with the amide *anti* NH^{16b} (Figure 1). It was expected that the CONH₂ group of TMZ will be the first choice partner for COOH coformers.



Scheme 2 Some possible hydrogen bond synthons in cocrystal structures between TMZ with carboxylic acids. Both homo and heterosynthons are shown. Heterosynthon I between TMZ amide and coformer acid groups of N–H···O and O–H···O hydrogen bonds is expected to guide cocrystal formation.

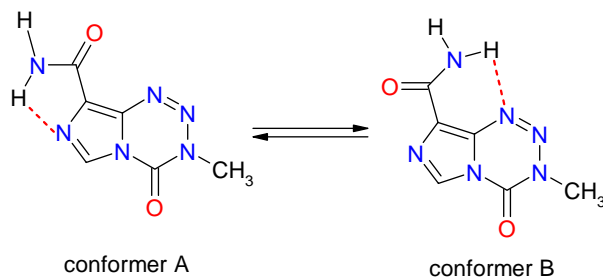


Figure 1 TMZ conformers first noted in polymorphs of the drug. Conformation A is more stable than B by 1.4 kcal/mol.^{17b}

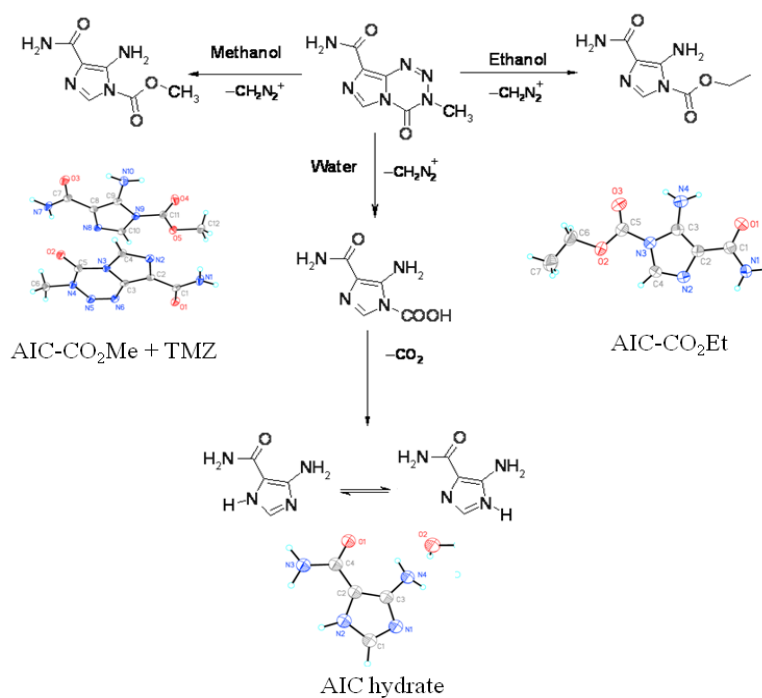
Improving drug stability to avoid discoloration of a tablet is not reported through a cocrystal strategy to our knowledge. Even as we embarked on this project we were aware that it should be implemented in certain boundary conditions to have a real impact. The carboxylic acid cofomers must be selected from the safe list of chemicals for human consumption (generally regarded as safe or GRAS and everything added to food in the US or EAFUS list of the US-FDA) so that the product temozolomide cocrystals are pharmaceutically acceptable.²¹ Secondly, whereas the decomposition of temozolomide should be inhibited to control coloration, the retardation should be just enough to stabilize the drug but not so long that the TMZ prodrug does not release the active MTIC species. The conversion of MTIC to CH_3N_2^+ is quite fast for subsequent DNA alkylation. The objective therefore was to optimize TMZ stability and active drug content release in the same cocrystal. Cocrystals presented as ideal drug candidates for the modification of temozolomide. (1) Many cocrystals can be crystallized for the same drug, thus giving an opportunity to optimize and fine tune physicochemical properties of the best cocrystal after screening. (2) Cocrystals appeared to be the only practical solution for improving temozolomide stability because the drug molecule lacks ionizable functional groups for salt formation.

5.3 Cocrystals of Temozolomide with acid partners

Temozolomide is soluble in polar solvents such as water, methanol, ethanol, propanol, acetonitrile, acetone, DMSO, DMF, etc. Crystallization from common alcoholic solvents, MeOH and EtOH, afforded the esterified by-products at ambient conditions. All such products were characterized by their X-ray crystal structures (Scheme 3). Crystallization from MeOH gave a mixture of TMZ and its hydrolysis

product AIC-CO₂Me in the crystal lattice whereas EtOH produced crystals of AIC-CO₂Et. The isolation of ester products as crystalline solids confirmed the problem of tetrazinone ring opening under alcoholic/ aqueous conditions. The colorless solution turned brownish and the structure of 5-amino-3H-imidazole-4-carboxamide (AIC) was confirmed by ¹H-NMR (Figure 2), and crystal structure of its hydrate. The hydrolysis of TMZ in different media followed a qualitative rate order: H₂O (less than 1 day) > MeOH (2-3 days) > EtOH (4-5 days). These results confirmed the hydrolytic instability of temozolomide in protic media. The color of crystallization solutions (pink, brown to black) correlated qualitatively with the presence of hydrate and decomposed products.

With the knowledge that TMZ is stable at acidic pH <5 but labile at pH >7,²⁰ it was co-crystallized with some GRAS organic acid pH adjusters^{20e} to adjust pH of solution and thereby improving drug stability during crystallization. Several cocrystals of TMZ with organic acids are prepared so that the pH of the solution is controlled and there will be lesser extent of hydrolysis in water compared to pure TMZ, and hence expected to be used as controlled release of the drug in its cocrystal form. The possibility that the cocrystals are chemically less susceptible to hydration is another factor than salt. As TMZ is neutral molecule, salt formation is unusual here. Pharmaceutical cocrystals with monocarboxylic and dicarboxylic acids e.g. anthranilic (pKa=4.95), succinic (pKa=4.2, 5.6), d,l-tartaric (pKa=3.2,4.8), d,l-malic (pKa=3.4, 5.1), oxalic (pKa=1.2, 4.2), salicylic acid (pKa=2.9) etc. and cocrystal hydrates with p-hydroxybenzoic acid (pKa=4.48), formic acid (pKa= 3.7) and acetic acid (pKa=4.7) were prepared either by solid-state or solvent-assisted grinding (Scheme 4). Generally hydrate forms of drugs are not preferred for stability reasons, hence only the six cocrystal structures with oxalic acid, succinic acid, malic acid, tartaric acid, anthranilic acid and salicylic acid are discussed broadly in this chapter. All starting materials are stable to the crystallization conditions. The crystalline solids obtained (See experimental sections, Table 6 for details) were characterized by PXRD, FT-IR, m.p. The stoichiometry of cocrystals was the same whether starting materials were taken in 1:1 or 2:1 ratio and up to 3:1 ratio of TMZ: coformer.



Scheme 3 Chemical reactions or hydrolytic cleavage of tetrazinone ring of TMZ upon dissolution in polar solvents like water, methanol and ethanol.

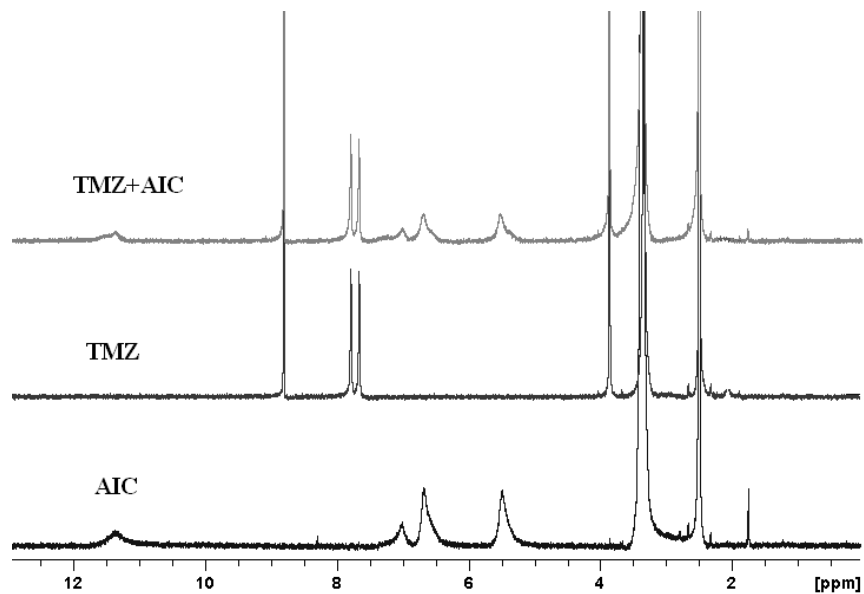
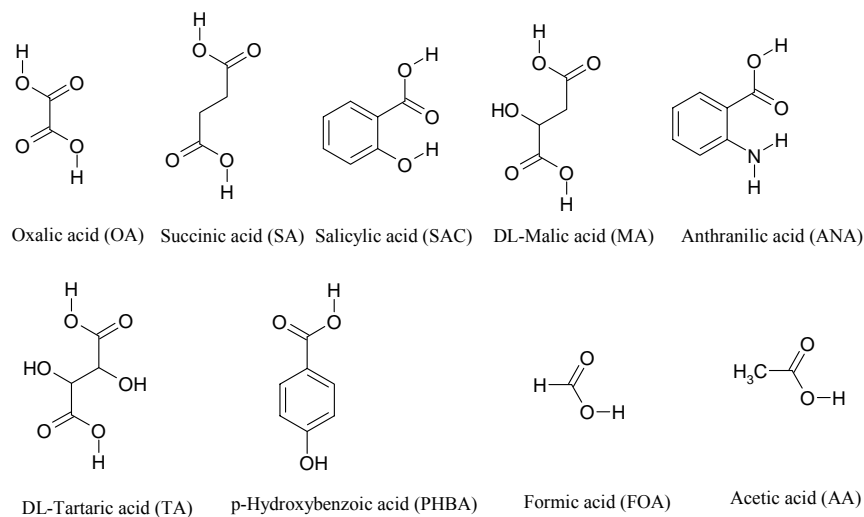


Figure 2 ¹H NMR spectrum (in d₆ DMSO solvent) is a comparison of 1:1 mixture of pure TMZ, TMZ and AIC hydrate obtained by slurrying pure TMZ in water for 2-3 h at 37 °C.



Scheme 4 Structure of cofomers (carboxylic acid) used to make TMZ cocrystals

5.3.1 Crystal Structure Analysis

A cocrystal of TMZ with each of the above cofomer acids was prepared by solid-state grinding of the individual components in a mortar-pestle for 10-15 min. The drug and the carboxylic acid were taken in a simple stoichiometric ratio of 1:1 for mono and 2:1 for dicarboxylic acids. The successful synthesis of all cocrystals was evidenced by the characteristic PXRD lines being different from the starting components. Crystallization of the ground solid from water or polar solvents (usually CH_3CN) gave single crystals after 4-5 days. An early hint of the success of our strategy was the indication that now temozolomide did not show any hydrolytic cleavage by the solvent water in co-crystallization experiments, suggesting that the pH of the solution was adjusted by the organic acid. The same cocrystals were obtained by solution crystallization of TMZ and cofomer acid upon mixing in their chemical ratio in acetonitrile solvent (without grinding). Crystallographic parameters of TMZ cocrystals are summarized in Table 1.

Cocrystal of TMZ and oxalic acid (1:0.5), TMZ–OA

The asymmetric unit contains one molecule of TMZ and half molecule of oxalic acid (residing on the inversion centre) in the monoclinic space group $C2/c$. Temozolomide can adopt two distinct conformations (A and B, Figure 1) which differ in

energy by 1.4 kcal/mol, the more stable one being TMZ_A. The carboxamide group of TMZ is hydrogen bonded to the carboxylic acid of the coformer via the amide–acid heterosynthon²² (N1–H1A···O4: 1.93 Å, 2.916(3) Å, 164.4°; O3–H3···O1: 1.59 Å, 2.557(2) Å, 166.1°; normalized hydrogen bonds are listed in Table 2). The anti NH of TMZ, which is intramolecularly bonded to the imidazole nitrogen (N1–H1B···N2: 2.28 Å, 2.735(3) Å, 105.6°) is also bonded via a longer N–H···O bond (N1–H1B···O3: 2.13 Å, 3.103(2) Å, 160.3°). The layered structure of TMZ–OA extends via stacking at 3.39 Å along the [201] direction (Figure 3).

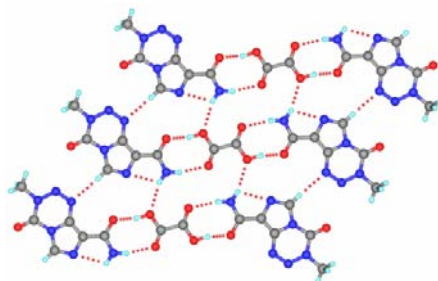


Figure 3 Amide–acid heterosynthon of N–H···O and O–H···O hydrogen bonds in TMZ–oxalic acid cocrystal (1:0.5). There are additional N–H···O and C–H···N interactions in the crystal structure. TMZ molecule is in the stable A conformation.

Cocrystal of TMZ and succinic acid (1:0.5), TMZ–SA

The 2:1 molecular stoichiometry is consistent with the diacid coformer in the monoclinic space group $P2_1/n$. TMZ participates in the amide–acid heterosynthon (N1–H1A···O3: 1.93 Å, 2.903(3) Å, 161.2°; O4–H4A···O1: 1.63 Å, 2.609(2) Å, 171.0°, Figure 4a) and the amide anti NH forms a helix along the *b*-axis via N1–H1B···O2 bonds (2.21 Å, 3.022(3) Å, 136.6°, Figure 4b). The packing of the molecules is similar to polymorph 1 of TMZ^{17b} such that the amide dimer is replaced by amide–acid synthon with succinic acid acting as a spacer in the cocrystal structure.

Cocrystal of TMZ and salicylic acid (1:1), TMZ–SAC

The crystal structure (in space group $P-1$) exhibited the amide–acid heterosynthon between TMZ (conformer B) and salicylic acid (N1–H1A···O4: 2.04 Å, 3.053(4) Å, 162.5°; O5–H5···O1: 1.50 Å, 2.544(3) Å, 169.3°). The anti NH is intramolecularly bonded to the tetrazinone nitrogen (N1–H1B···N6: 2.31 Å, 3.031(4) Å, 127.6°) and it also participates in intermolecular hydrogen bond with a TMZ molecule

via (N1–H1B \cdots N5: 2.55 Å, 3.269(4) Å, 127.8°). Ribbons of TMZ–SAC molecules form a layered structure (Figure 5).

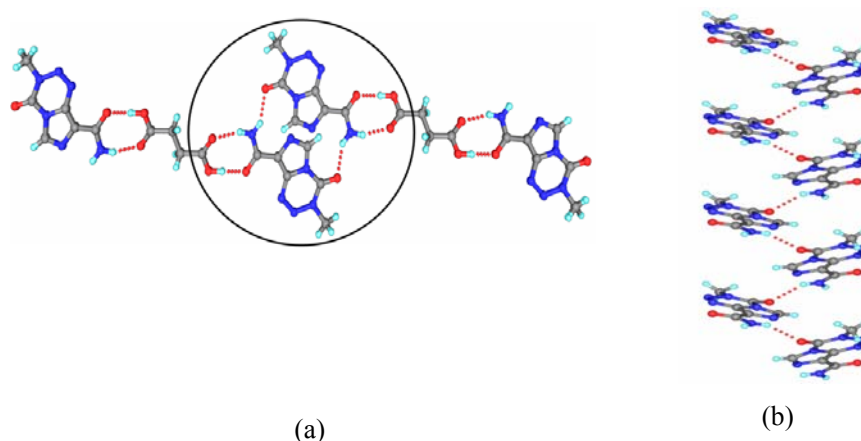


Figure 4 Amide–acid heterosynthon of N–H \cdots O and O–H \cdots O hydrogen bonds in TMZ–succinic acid cocrystal (1:0.5). The anti amide NH is bonded to tetrazinone C=O acceptor. TMZ is in the stable A conformation. (b) The encircled motif is viewed as a helix along the *b*-axis.

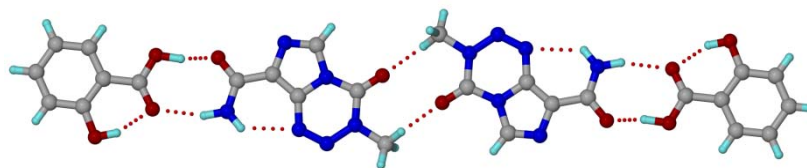


Figure 5 Amide–acid heterosynthon in TMZ–salicylic acid cocrystal (1:1). The anti NH is intramolecularly bonded to tetrazinone N (conformation B) and also intermolecularly to another TMZ via N–H \cdots N interaction (not shown).

Cocrystal of TMZ and DL-malic acid (1:0.5), TMZ–MA

The cocrystal structure in *C2/c* space group contains one molecule of TMZ and half molecule of disordered malic acid. Although malic acid contains one OH group, it is disordered over two sites with equal occupancy (Figure 6) such that the molecule now appears symmetric to give a half molecule of malic acid about the inversion center. The hydroxyl group participates in intramolecular hydrogen bonds and has no role in intermolecular association. The crystal packing is therefore very similar to succinic acid cocrystal (see Figure 4a). The recurring amide–acid heterosynthon (N1–H1A \cdots O3: 1.91 Å, 2.913(5) Å, 167.4°; O4–H4A \cdots O1: 1.62 Å, 2.589(5) Å, 167.8°) and a helix (N1–

H1B \cdots O2: 2.17 Å, 3.018(5) Å, 140.3°) along [010] direction are the main hydrogen bond motifs.

Cocrystal of TMZ and anthranilic acid (2:1), TMZ–ANA

The crystal structure in space group *P*-1 contains two crystallographically independent TMZ and one anthranilic acid molecules. In contrast to previous structures, there is no amide–acid heterosynthon; instead anthranilic acid molecules form carboxylic acid dimer (O8–H8A \cdots O7: 1.76, 2.694(4) Å, 167.6°) and are connected to TMZ through N–H \cdots O hydrogen bond (N13–H13A \cdots O3: 2.02 Å, 3.002 (4) Å, 162.7°). Symmetry-independent TMZ molecules interact through the anti NH of carboxamide via N–H \cdots N hydrogen bond (N7–H7A \cdots N8: 2.11 Å, 3.017 (4) Å, 148.3°) and the symmetry related molecules form N7–H7B \cdots O2 (2.02 Å, 3.005 (4) Å, 165.6°) in a layer motif (Figure 7).

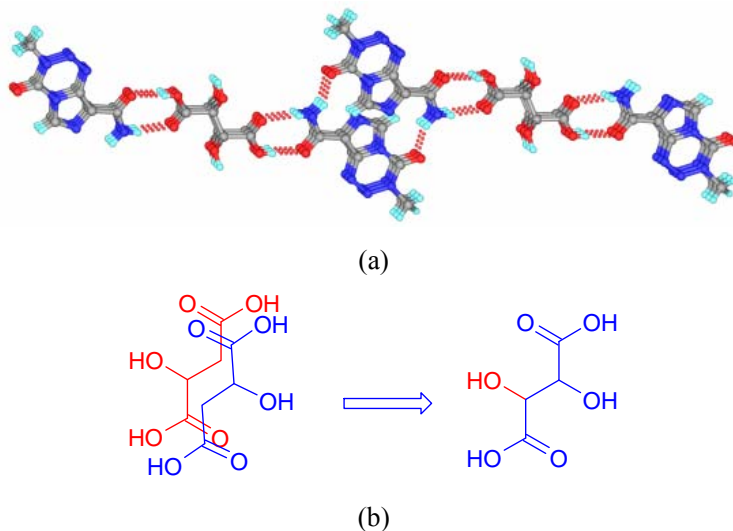


Figure 6 Crystal packing in TMZ–DL-malic acid cocrystal (1:0.5). The enantiomeric molecules of malic acid mimic a succinic acid/ tartaric acid spacer due to disorder shown in. TMZ resides in conformation A.

Cocrystal of TMZ and DL-tartaric acid (1:1), TMZ–TA

The crystal structure (in space group *P*-1) is assembled via the recurring amide–acid heterosynthon (N1–H1B \cdots O7: 2.29 Å, 3.180(4) Å, 146.1°; O8–H8 \cdots O1: 1.59 Å, 2.567(3) Å, 169.2°) and the second COOH is bonded to the tetrazinone nitrogen (O4–H4A \cdots N6: 1.92 Å, 2.897(3) Å, 172.5°). The amide anti N–H is bonded to the carbonyl group of COOH (N1–H1A \cdots O3: 2.33 Å, 3.144(4) Å, 139.4°). Even though the coformer

is a diacid, the cocrystal stoichiometry is 1:1 because the two COOH groups of TA make different hydrogen bond (acid-amide and acid-pyridine) motifs to symmetry related TMZ molecules. Tartaric acid molecules are present inside the hydrogen bonded column made by TMZ molecules parallel to the *b*-axis (Figure 8).

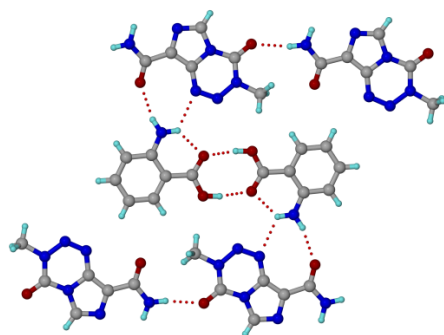


Figure 7 Crystal structure of TMZ–anthranilic acid cocrystal (2:1). Both TMZ and anthranilic acid are connected by cyclic homosynthons via O–H···O and N–H···N hydrogen bond, and such dimers are connected by N–H···O and N–H···N hydrogen bonds.

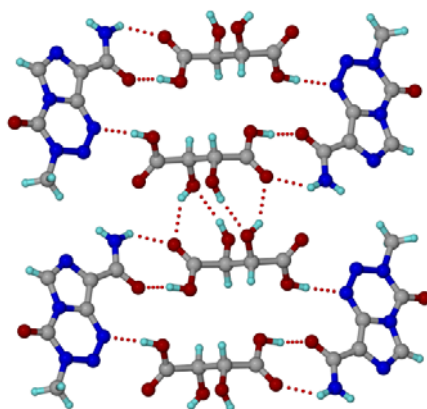


Figure 8 Crystal structure of TMZ–DL-tartaric acid (1:1) sustained via amide–acid and acid–pyridine heterosynthons with the dicarboxylic acid spacer.

Cocrystal of TMZ, *p*-hydroxybenzoic acid monohydrate (TMZ–PHBA.H₂O, 1:1:1)

It crystallized in monoclinic space group $P2_1/c$ with one molecule each of TMZ (conformer B), *p*-hydroxybenzoic acid and water. TMZ is involved in the formation of amide–acid heterosynthon with *p*-hydroxybenzoic acid (N1–H2···O5: 1.84, 2.829(2) Å, 165.9°; O4–H3···O1: 1.72 Å, 2.700(2) Å, 171.9°). The *anti* NH is involved in

intramolecular N1–H1···N6 with tetrazinone ring N acceptor (N1–H1···N6: 2.27 Å, 3.036(2) Å, 131.1°). Water molecule donates its hydrogen atoms to amide carbonyl (O6–H6A···O1: 1.91 Å, 2.889(2) Å, 175.5°) and imidazole N acceptors of TMZ (O6–H6B···N2: 2.57 Å, 3.008(2) Å, 106.7°) and simultaneously accepts hydrogen bonding from hydroxyl group of p-hydroxybenzoic acid through O–H···O interaction (O3–H3A···O6: 1.68, 2.658(2) Å, 176.9°). Hydrogen bonding pattern of TMZ–PHBA monohydrate crystal structure is shown in Figure 9.

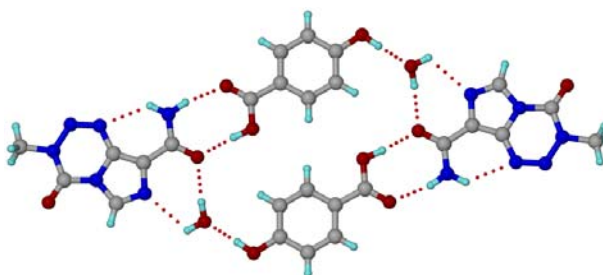


Figure 9 amide-acid hetsosynthon present in TMZ–PHBA monohydrate crystal structure.

Cocrystal of TMZ, formic acid monohydrate (TMZ–FOA.H₂O, 2:1:1)

The compound crystallized in the triclinic space group *P*-1 with two molecules of TMZ (conformers A, B), one molecule each of formic acid and water molecule in the asymmetric unit. There is a centrosymmetric amide dimer between the TMZ conformer *B* molecules using its *syn* NH (N1–H1A···O1: 1.85 Å, 2.859(2) Å, 176.9°). There is also another centrosymmetric dimer of two conformer *A* molecules, but interrupted by water and formic acid in a R₆⁴(20) network of hydrogen bonds (*syn* NH to formic acid (N7–H7A···O7: 1.96 Å, 2.951(2) Å, 165.4°), formic acid to water (O6–H8···O5: 1.66 Å, 2.641(2) Å, 175.4°) and water to carbonyl of TMZ (O5–H5A···O3: 1.83 Å, 2.694(2) Å, 144.5°). These two dimers are positioned adjacent to each other and are held by O5–H5B···N2 formed by water and imidazole N acceptor (O5–H5B···N2, 1.91 Å, 2.886 (2) Å, 173.6 °). A layered structure of TMZ–formic acid monohydrate is displayed in Figure 10.

Cocrystal of TMZ and acetic acid (TMZ-AA, 1:1)

The compound crystallized in the triclinic space group *P*-1 with one molecule of TMZ (conformer A) and one molecule of acetic acid in the asymmetric unit. The expected amide-acid heterosynthon is present (N1-H1A...O4: 2.05 Å, 2.923(4) Å, 163.9°; O3-H3...O1: 1.70 Å, 2.621(4) Å, 174.5°) using syn NH of the amide (figure 10). These hetero-dimer units are connected side-by-side via two hydrogen bonds: anti NH to oxygen of COOH (N1-H1B...O3: 2.29 Å, 3.074(5) Å, 157.1°) and imiadazole CH to tetrazine N (C4-H4...N6: 2.49 Å, 3.412(5) Å, 169.9°) and extend along the [100] direction. These molecules expand into sheet structure (Figure 11) via weak C-H...O interactions. The layers are separated by stacking and carbonyl...carbonyl dipolar attractions.

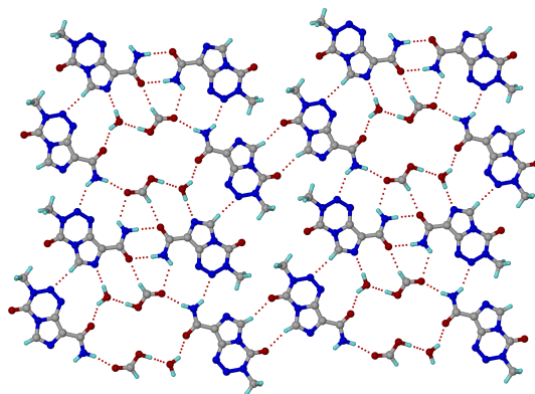


Figure 10 Hydrogen bonding in the layered structure of TMZ, formic acid monohydrate.

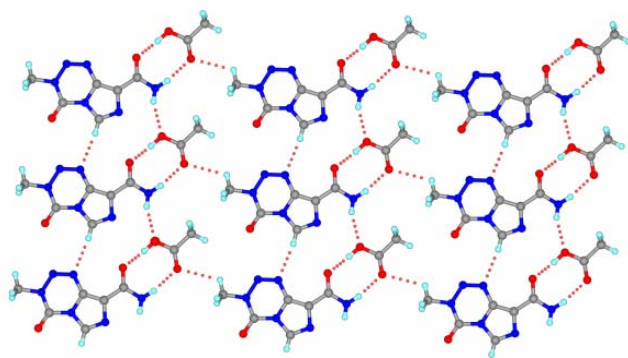


Figure 11 Amide-acid heterosynthon present in TMZ-acetic acid (1:1) cocrystal.

Cocrystal of TMZ and acetic acid monohydrate (TMZ-AA. H₂O, 1:1:1)

The compound crystallized in triclinic space group *P*-1 with one molecule each of TMZ (conformer A), acetic acid and water in the asymmetric unit. Two TMZ molecule form centrosymmetric dimer through N–H···N interaction (N1–H1···N2: 2.25, 3.053(2) Å, 150.8°). The acid–amide heterosynthon is interrupted by a water molecule to give R₃²(10) ring motif²³ (N1–H2···O3: 2.13 Å, 2.938(2) Å, 154.3°); O4–H4A···O5: 1.68 Å, 2.632(2) Å, 168.1°); O5–H6···O1: 1.84 Å, 2.759(2) Å, 176.3°). Again two TMZ molecule and two water molecule form tetramer through O–H···O hydrogen bond. The layered structure of TMZ–acetic acid monohydrate is displayed in Figure 12.

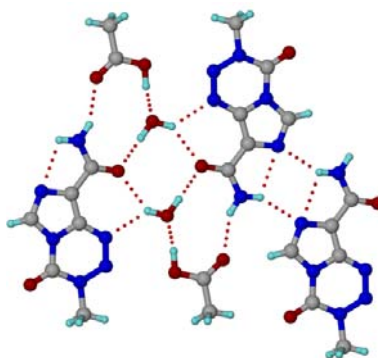


Figure 12 water molecule interrupted acid amide heterosynthon forming R₃²(10) ring formation in TMZ and acetic acid monohydrate.

Table 1 Crystallographic data of TMZ cocrystals/cocrystal hydrates

Crystal Data	TMZ–OA	TMZ–SA	TMZ–SAC
Emp. Formula	2(C ₆ H ₆ N ₆ O ₂). (C ₂ H ₂ O ₄)	2(C ₆ H ₆ N ₆ O ₂). (C ₄ H ₆ O ₄)	(C ₆ H ₆ N ₆ O ₂). (C ₇ H ₆ O ₃)
Formula wt.	478.37	506.42	332.29
Crystal system	Monoclinic	Monoclinic	Triclinic
Space group	<i>C</i> 2/ <i>c</i>	<i>P</i> 2 ₁ / <i>n</i>	<i>P</i> $\bar{1}$
<i>T</i> [K]	293(2)	100(2)	298(2)
<i>a</i> [Å]	14.882(2)	12.7511(13)	6.9915(14)
<i>b</i> [Å]	6.6222(9)	7.0092(7)	8.5449(17)
<i>c</i> [Å]	19.655(3)	12.9685(14)	12.682(3)
α [deg]	90	90	74.003(3)
β [deg]	101.156(2)	118.3580(10)	87.822(4)
γ [deg]	90	90	82.328(4)
<i>Z</i>	4	2	2

Volume [\AA^3]	1900.4(5)	1019.97(18)	721.8(3)
D_{calc} [g/cm^3]	1.672	1.649	1.529
R_1 [$I > 2\sigma(I)$]	0.0532	0.0512	0.0592
wR_2	0.1453	0.1161	0.1480
GOF	1.07	1.09	0.98

TMZ-MA	TMZ-ANA	TMZ-TA	TMZ- PHBA·H ₂ O
2(C ₆ H ₆ N ₆ O ₂). (C ₄ H ₅ O ₅)	2(C ₆ H ₆ N ₆ O ₂). (C ₇ H ₇ NO ₂)	(C ₆ H ₆ N ₆ O ₂). (C ₄ H ₆ O ₆)	(C ₆ H ₆ N ₆ O ₂). (C ₇ H ₆ O ₃). (H ₂ O)
521.42	525.47	344.26	350.30
Monoclinic	Triclinic	Triclinic	Monoclinic
$C2/c$	$P\bar{1}$	$P\bar{1}$	$P2_1/c$
298(2)	298(2)	298(2)	100(2)
22.597(16)	6.904(5)	7.725(2)	7.0761(7)
7.275(6)	10.624(7)	8.961(2)	8.4766(8)
13.144(10)	15.957(15)	10.791(2)	25.2205(19)
90	87.731(9)	80.51(2)	90
91.819(13)	81.223(15)	79.19(2)	104.727(3)
90	78.017(11)	75.11(2)	90
4	2	2	4
2160(3)	1131.5(15)	703.7(3)	1463.1(2)
1.603	1.542	1.625	1.590
0.0907	0.0555	0.0618	0.0406
0.1677	0.1439	0.2170	0.0974
1.14	0.988	1.097	1.12

TMZ-FOA·H ₂ O	TMZ-AA	TMZ-AA·H ₂ O
2(C ₆ H ₆ N ₆ O ₂). (CH ₂ O ₂). (H ₂ O)	(C ₆ H ₆ N ₆ O ₂). (C ₂ H ₄ O ₂)	(C ₆ H ₆ N ₆ O ₂). (C ₂ H ₄ O ₂). (H ₂ O)
452.38	254.22	272.24
Triclinic	Triclinic	Triclinic
$P\bar{1}$	$P\bar{1}$	$P\bar{1}$
100(2)	293(2)	100(2)
8.1307(6)	6.648(3)	6.8494(5)
11.4808(9)	8.960(4)	8.1872(6)
11.5455(9)	9.499(4)	11.3709(9)
66.040(1)	88.420(7)	105.917(1)
71.600(1)	78.748(7)	102.838(1)
88.823(1)	80.931(7)	90.757(1)
2	2	2
927.29(12)	548.0(4)	596.0(8)
1.620	1.541	1.517
0.0341	0.0665	0.0364

0.0947	0.1623	0.0901
0.994	1.01	1.048

Table 2 Hydrogen bond of crystal structures discussed. O–H, N–H and C–H bond distances are neutron normalized.

Compound	Interaction	H...A/ Å	D...A/ Å	∠D–H...A/ °
TMZ–OA	N1–H1A...O4	1.93	2.916(3)	164.4
	N1–H1B...N2	2.28	2.735(3)	105.6
	N1–H1B...O3	2.13	3.103(2)	160.3
	O3–H3...O1	1.59	2.557(2)	166.1
	C4–H4...N6	2.26	3.335(3)	172.5
	C6–H6A...O3	2.43	3.492(4)	167.7
TMZ–SA	N1–H1A...O3	1.93	2.903(3)	161.2
	N1–H1B...N2	2.36	2.771(3)	103.6
	N1–H1B...O2	2.21	3.022(3)	136.6
	O4–H4A...O1	1.63	2.609(2)	171.0
	C4–H4...N6	2.43	3.498(3)	167.6
TMZ–SAC	N1–H1A...O4	2.04	3.053(4)	162.5
	N1–H1B...N6	2.31	3.031(4)	127.6
	N1–H1B...N5	2.55	3.269(4)	127.8
	O3–H3...O4	1.67	2.603(3)	156.3
	O5–H5...O1	1.50	2.544(3)	169.3
	C4–H4...O3	2.32	3.315(3)	152.0
	C6–H6A...N2	2.53	3.462(4)	143.9
	C6–H6B...O4	2.48	3.433(4)	145.8
	C6–H6C...O2	2.35	3.435(4)	177.8
	C10–H10...O1	2.40	3.384(4)	150.8
TMZ–MA	N1–H1A...O3	1.91	2.913(5)	167.4
	N1–H1B...N2	2.32	2.759(6)	104.9
	N1–H1B...O2	2.17	3.018(5)	140.3
	O4–H4A...O1	1.62	2.589(5)	167.8
	C4–H4...N6	2.44	3.515(6)	170.9
	C6–H6B...O6	2.42	3.471(1)	162.4
	C6–H6C...O6	2.36	3.172(9)	130.4
	C10–H10...O1	2.40	3.384(4)	150.8
TMZ–ANA	N1–H1A...N2	2.38	2.789(4)	102.7
	N1–H1A...N2	2.28	3.114(4)	138.7
	N1–H1B...O4	2.02	3.021(4)	169.4
	O8–H8A...O7	1.76	2.694(4)	167.6
	N7–H7A...N8	2.11	3.017(4)	148.3
	N7–H7B...O2	2.02	3.005(4)	165.6
	N13–H13A...O3	2.02	3.002(4)	162.7
	N13–H13B...O7	1.95	2.684(4)	126.6
	N13–H13B...N12	2.36	2.980(4)	118.4
	C4–H4...O4	2.25	3.288(4)	159.0

TMZ-TA	C10-H10...O2	2.42	3.470(4)	162.8
	C12-H12...O8	2.30	3.229(4)	142.6
	N1-H1A...O3	2.33	3.144(4)	139.4
	N1-H1A...N2	2.39	2.825(4)	104.4
	N1-H1B...O7	2.29	3.180(4)	146.1
	N1-H1B...O3	2.32	3.047(4)	127.5
	O4-H4A...N6	1.92	2.897(3)	172.5
	O5-H5...O3	2.14	2.680(3)	113.1
	O5-H5...O7	1.91	2.760(3)	142.8
	O6-H6...O5	1.89	2.860(3)	165.7
	O8-H8...O1	1.59	2.567(3)	169.2
	C4-H4...O6	2.47	3.209(4)	123.9
	C4-H4...O2	2.28	3.267(4)	150.4
	C9-H9...O2	2.48	3.553(4)	170.9
TMZ-PHBA · H ₂ O	N1-H1...N6	2.27	3.036(2)	131.1
	N1-H2...O5	1.84	2.829(2)	165.9
	O4-H3...O1	1.72	2.700(2)	171.9
	O3-H3A...O6	1.68	2.658(2)	176.9
	O6-H6A...O1	1.91	2.889(2)	175.5
	O6-H6A...N2	2.55	3.008(2)	107.9
	O6-H6B...N2	2.57	3.008(2)	106.7
	O6-H6B...O3	2.11	3.066(2)	164.4
	C5-H5...O2	2.42	3.120(2)	121.3
	C14-H4B...O5	2.34	3.192(2)	134.6
TMZ-FOA · H ₂ O	N1-H1A...O1	1.85	2.859(2)	176.9
	N1-H1B...O7	2.48	3.116(2)	120.3
	N1-H1B...N6	2.21	2.991(2)	132.9
	O5-H5A...O3	1.83	2.694(2)	144.5
	O5-H5B...N2	1.91	2.886(2)	173.6
	N7-H7A...O7	1.96	2.951(2)	165.4
	N7-H7B...N8	2.35	2.783(2)	104.7
	N7-H7B...N5	2.22	3.141(2)	150.2
	O6-H8...O5	1.66	2.641(2)	175.4
	C4-H4...N11	2.16	3.216(2)	163.8
	C6-H6A...N8	2.33	3.407(2)	172.9
	C6-H6C...O6	2.52	3.404(2)	137.8
	C13-H7...O1	2.21	3.204(2)	151.7
	C10-H10...O4	2.23	3.283(2)	162.4
TMZ-AA	C12-H12A...O2	2.38	3.429(2)	160.7
	N1-H1A...O4	2.05	2.923(4)	163.9
	N1-H1B...O3	2.29	3.074(5)	157.1
	N1-H1B...N2	2.28	2.740(4)	114.7
	O3-H3...O1	1.70	2.621(4)	174.5
	C4-H4...N6	2.49	3.412(5)	169.9
	N1-H1...N2	2.43	2.816(2)	107.0
	N1-H1...N2	2.25	3.053(2)	150.8
TMZ-AA · H ₂ O	N1-H2...O3	2.13	2.938(2)	154.3

O4–H4A···O5	1.68	2.632(2)	168.1
O5–H5···O1	2.23	2.973(1)	141.0
O5–H6···O1	1.84	2.759(2)	176.3
C4–H4···O3	2.23	3.175(2)	170.2

5.4 FT-IR spectroscopy

The formation of a cocrystal via amide–acid synthon sustained by N–H···O and O–H···O hydrogen bonds is expected to change the frequencies of both OH and NH resonances relative to the pure components. Generally, hydrogen bonding is stronger in the cocrystal relative to the pure components, and so a red shift is expected upon cocrystal formation. IR stretching frequencies (Table 3) provide spectroscopic confirmation for cocrystal formation in each case.

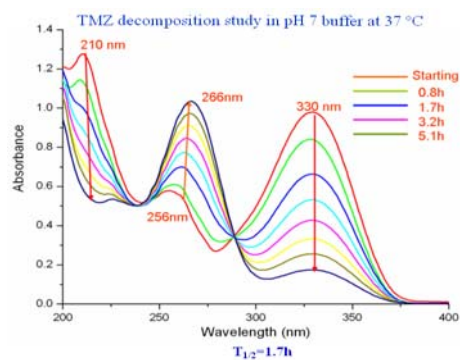
Table 3 FT-IR frequencies (cm^{−1}) of temozolomide cocrystals/cocrystal hydrates.

Solid forms	N–H stretching	C=O stretching	N–H bend	C–O stretch	C–N stretch
TMZ	3421.8, 3388.6, 3287.0	1758.3, 1733.8, 1679.2	1601.5	1218.6	1354.5
TM–OA	3403.0, 3256.1 (Broad)	1749.7, 1710.7	1592.6	1219.5	1359.1
TMZ–SA	3434.9, 3295.5, 3246.3	1731.7, 1686.2	1590.5	1200.8	1366.2
TMZ–SAC	3432.8, 3322.2	1754.4, 1677.4	1578.0	1227.8	1366.7
TMZ–MA	3412.0, 3302.7, 3230.1	1735.9, 1692.2	1587.8	1224.7	1363.8
TMZ–ANA	3439.2, 3329.3, 3183.3, 3126.4	1751.2, 1668.5	1585.8	1239.9	1362.3
TMZ–TA	3452.3, 3341.6, 3132.9	1750.4, 1701.2, 1650.1	1591.3	1222.2	1360.6
TMZ–PHBA·H ₂ O	3421.5, 3314.7, 3184.7, 3159.3	1754.2, 1701.5, 1662.9	1592.3	1219.0	1362.4
TMZ–FOA·H ₂ O	3422.2, 3401.8, 3344.6, 3304.0	1747.5, 1673.3	1602.4	1220.7	1359.5
TMZ–AA	3439.0, 3380.7	1743.4, 1703.2, 1679.8	1588.0	1215.9	1359.8

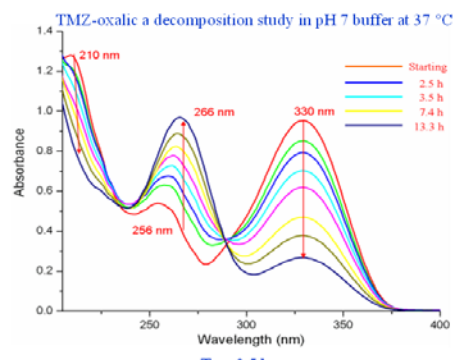
5.5 Hydrolytic Stability and Dissolution Rate

The rationale for making TMZ cocrystals with organic acids was that the COOH coformer will make the environment around the temozolomide molecule acidic enough that hydrolytic degradation of TMZ would be inhibited. A preliminary observation was

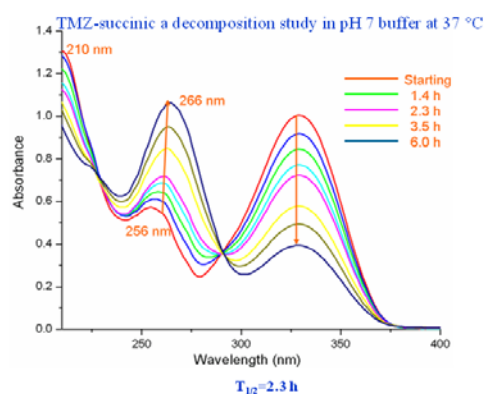
that polar solvents such as water and methanol used in co-crystallization experiments did not cause noticeable hydrolysis of TMZ even after one week crystallization experiments and stable cocrystal structure and/ or their hydrates/ solvates were crystallized. In contrast, pure TMZ dissolved in water (in the absence of carboxylic acid coformer) underwent decomposition within one day. The half-life ($T_{1/2}$) of TMZ is 1.8 h (1.7–1.9 h)^{20a,24} in blood plasma under physiological conditions at 10 μ M concentration. Hydrolysis of TMZ to AIC can be monitored by the intensity of UV-Vis maxima for the two species at 330 and 266 nm respectively.^{20b,25} The decomposition of TMZ cocrystals was compared with that of the reference drug at 10 μ M concentration in pH 7.0 buffer at 37 °C. A gradual increase in the half-life of temozolomide in its cocrystals was observed by UV-Vis waterfall plots: TMZ (1.7 h) < TMZ–ANT (2.2 h) < TMZ–SA (2.3 h) < TMZ–TA (2.5 h) < TMZ–MA (2.8 h) < TMZ–OA (3.5 h) < TMZ–SAC (3.6 h). The reference drug and TMZ–OA UV-Vis plots are shown in Figure 11. The time at which the intensity of the UV-Vis maxima at 330 and 266 nm for TMZ drug and AIC by-product are near equal was taken as the half-life of the compound. The three strong maxima in these UV-Vis plots are due to $n-\sigma^*$ (210 nm), $n-\pi^*$ (266 nm) and $\pi-\pi^*$ (310 nm) electronic transitions in the aromatic and amide/ urea carbonyl chromophores. There is moderate correlation in increase of drug half-life in the cocrystal with the acidity of the carboxylic acid. Remarkably, the half-life of all cocrystals is longer than that of the reference drug, thereby validating the cocrystal strategy for improving temozolomide stability. Again in pH 9.2 buffer, half-life of temozolomide is only 5 min, whereas $T_{1/2}$ of TMZ–SA and TMZ–SAC cocrystals are longer at 6 and 8 min (accelerated hydrolysis in basic conditions).



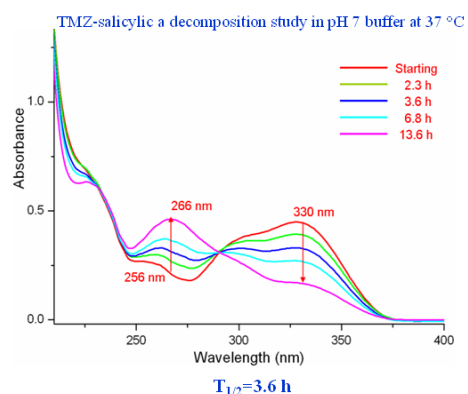
(a)



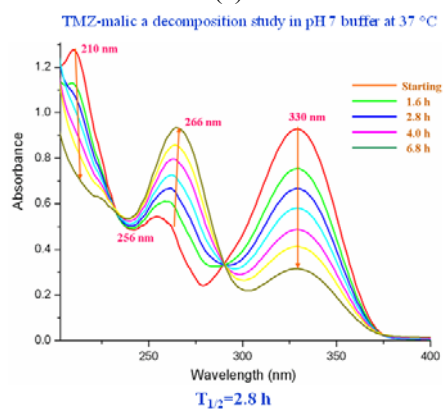
(b)



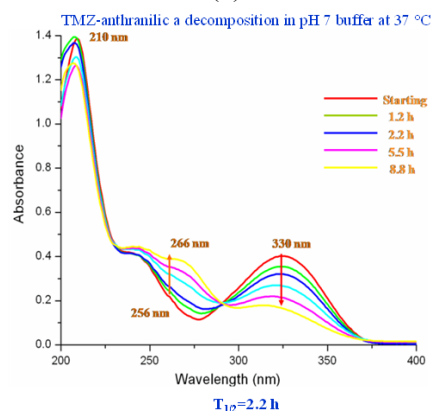
(c)



(d)



(e)



(f)

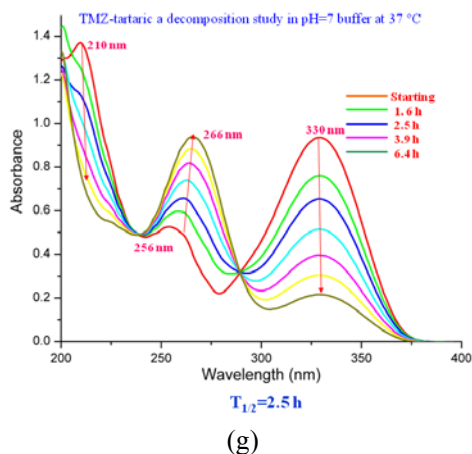


Figure 11 UV-Vis plots as a function of time to measure the half-life of TMZ and its cocrystals. (a) TMZ, (b) TMZ–OX, (c) TMZ–SA, (d) TMZ–SAC, (e) TMZ–MA, (f) TMZ–ANA, (g) TMZ–TA. Note that $T_{1/2}$ of TMZ–OA and TMZ–SAC are almost twice that of pure TMZ.

The improvement in stability of temozolomide as a cocrystal drug is useful only if the dissolution rate of stable cocrystal(s) is comparable (or better) than the reference drug. Intrinsic dissolution experiments were carried out for TMZ solid forms in pH 7 buffer medium up to 150 min and the amount of TMZ dissolved vs time was plotted in Figure 12 and IDR values were summarized in Table 4. The dissolution curves of TMZ–OA (red) and TMZ–SA (green) cocrystals nearly overlay on the profile of TMZ (black) up to 150 min, which is a good indicator of cocrystal solubility matching with that of the reference drug. The experiment could not be run for longer time because the tablet disk compressed in a laboratory IR press started to disintegrate after 3 h (4 ton pressure). Moreover, temozolomide has limited stability in aqueous medium. The dissolution profile was measured for a time long enough to assess drug dissolution in relation to the half-life of TMZ and its cocrystals. Pure TMZ was used as a reference in stability and dissolution experiments. Temozolomide is marketed as Temodar/ Temodal worldwide^{26a,b} and as Temonat/ Temorel^{26c,d} in India. Comparison of the commercial drug with a suitable formulation of the drug cocrystal containing excipients, stabilizers, polymers, etc. is currently under experimentation. The present data give a good idea of hydrolytic stability improvement in TMZ cocrystals.

Stability studies at accelerated ICH (International Conference on Harmonization) conditions²⁷ of 40 °C and 75% relative humidity (RH) were carried out on temozolomide and its six cocrystals. Powder XRD patterns were recorded at regular intervals of one week up to 28 weeks (6 months). TMZ was stable for one week in accelerated humidity conditions of 40 °C and 75% RH but started transforming to its hydrate (2 θ 11.6°) after 2 weeks, and a strong peak appeared at 2 θ 12.9° after 4-5 weeks indicative of decomposition to AIC hydrate (Table 5, Figure 13). Four cocrystals, those with oxalic acid, succinic acid, salicylic acid and malic acid, were stable for over 6 months. TMZ–SA, TMZ–OX and TMZ–SAC cocrystals did not show any discoloration or decomposition up to 28 weeks when kept at 40 °C and 75% RH in a stability chamber (see PXRD stack in Figure 13 and color visuals in Figure 14). Cocrystals with anthranilic acid and tartaric acid showed marginal improvement in stability. Even though cocrystals of hydroxy acids, e.g. MA and TA, did not show any degradation by PXRD lines, they showed a darkening of color (turned black) after a few weeks (see Figure 15). Considering both stability and solubility criteria, TMZ–succinic acid and TMZ–oxalic acid cocrystals appear to be the best candidates for further studies in developing an improved, stable and bioavailable temozolomide cocrystal formulation. The pure acids did not show any noticeable decomposition in the same period. In closing we note some of the technique limitations in assessing the stability of temozolomide and its cocrystals. Whereas powder XRD plots are good indicators of the solid composition at different time intervals of the stability experiments, more reliable techniques such as NMR and HPLC could not be used here because they would give a measure of cocrystal stability in aqueous medium. The main focus in this study was to evaluate improvement in solid form stability and minimum discoloration of temozolomide.

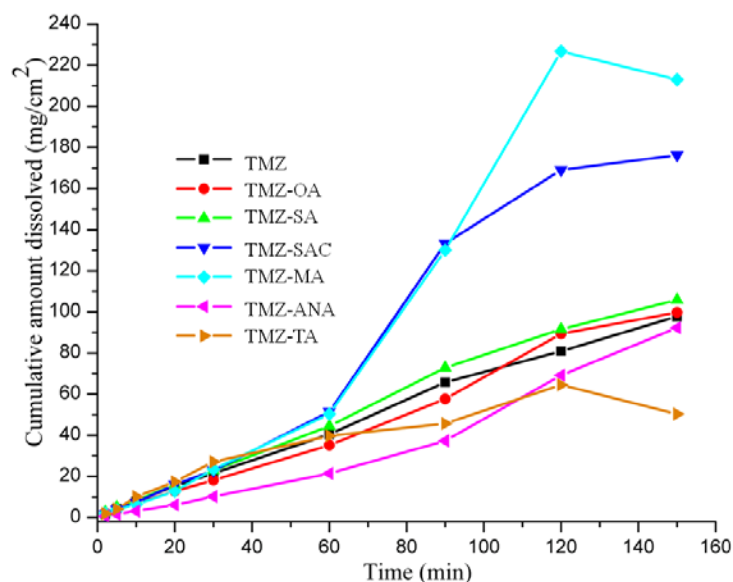


Figure 12 Intrinsic dissolution rates of TMZ and its cocrystals in pH 7 buffer medium. TMZ (black), TMZ-ANA (magenta), TMZ-SA (green), TMZ-TA (orange), TMZ-MA (light blue), TMZ-OA (red), TMZ-SAC (dark blue). Note that the dissolution profile of TMZ-OA (red) and TMZ-SA (green) cocrystals are comparable to that of TMZ up to 150 min.

Table 4 Dissolution rates (IDR) of TMZ cocrystals.

Drug	TMZ	TMZ-OA	TMZ-SA	TMZ-SAC	TMZ-MA	TMZ-ANA	TMZ-TA
ϵ , mM cm^{-1}	8.98	9.62	10.73	27.47	10.25	79.12	13.41
IDR, $(\text{mgcm}^{-2}) \text{min}^{-1}$	0.756	0.742	0.835	1.069	1.124	0.378	0.784

Table 5 Stability of TMZ cocrystals at 40 °C and 75% RH.

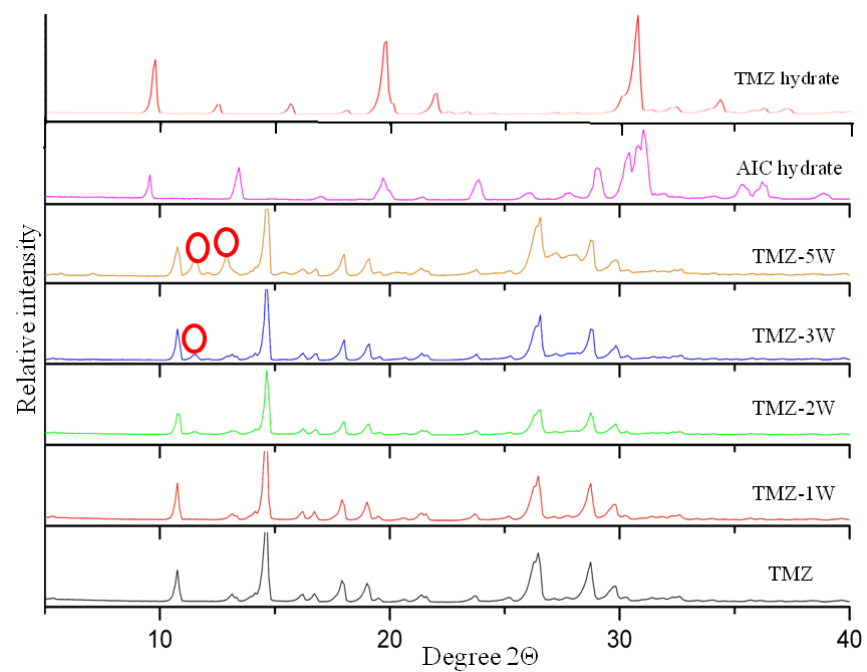
	1W	2W	3W	4W	8W	16W	18W	23W	26W	28W
TMZ	√	X	X	X	X	---	---	---	---	---
TMZ-OA	√	√	√	√	√	√	√	√	√	√
TMZ-SA	√	√	√	√	√	√	√	√	√	√
TMZ-SAC	√	√	√	√	√	√	√	√	√	√
TMZ-MA	√	√	√	√	√	√	√	√	√	√
TMZ-ANA	√	√	×	×	×	---	---	---	---	---
TMZ-TA	√	√	√	√	×	---	---	---	---	---

√ Compound matched with starting material by PXRD and FT-IR

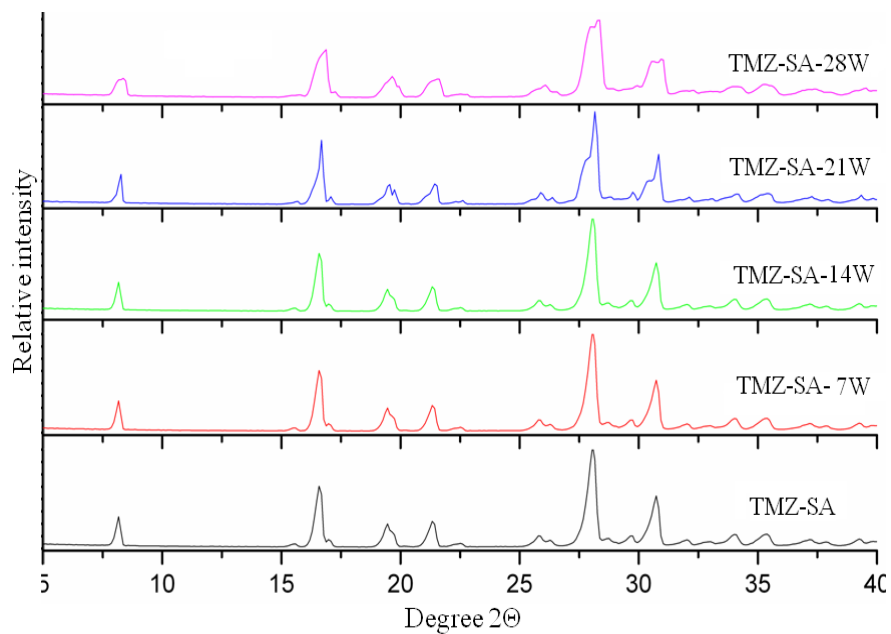
× Indicates hydrolysis products confirmed by PXRD and FT-IR

--- Experiment discontinued, material fully decomposed

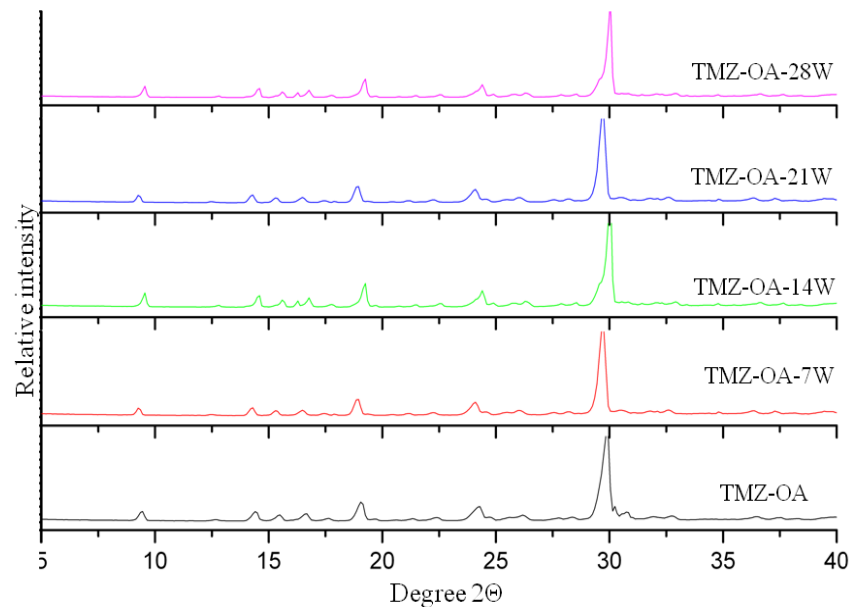
Note: Pure TMZ transformed to TMZ hydrate after 2 weeks and started to hydrolyze to AIC hydrate after 4 weeks.



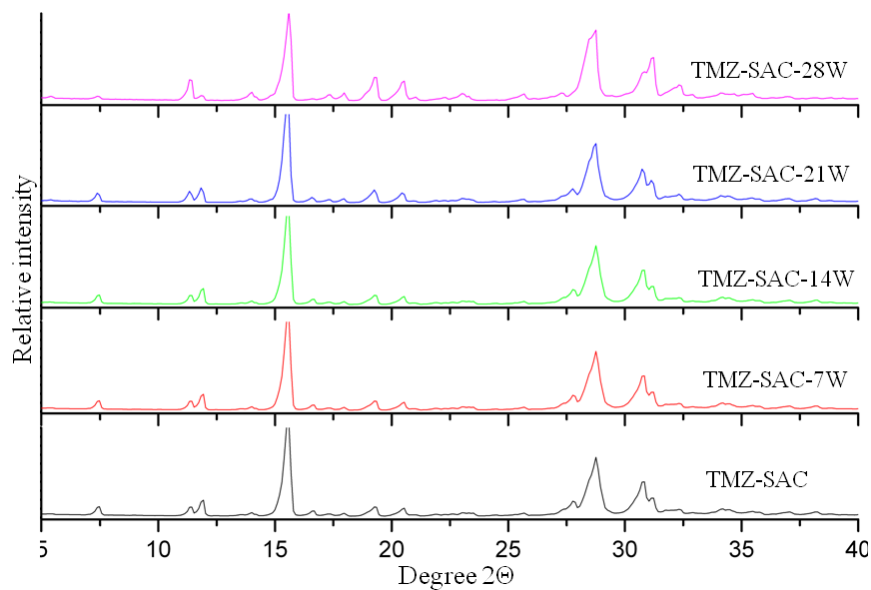
(a)



(b)



(c)



(d)

Figure 13 (a) PXRD of (a) TMZ at 40 °C and 75% RH at different time intervals. Peaks at 2θ 11.5°, 11.8° correspond to TMZ hydrate. Transformation of TMZ to TMZ hydrate was observed after 2 weeks in humidity conditions. The peak at 2θ 12.9° after 4-5 weeks is of AIC hydrate (2θ 13.0° in reference sample) suggesting that TMZ decomposition starts after 5 weeks (b) TMZ-SA, (c) TMZ-OA and TMZ-SAC cocrystals kept in

accelerated humidity conditions for over 6 months did not exhibit any sign of decomposition or dissociation by PXRD fingerprint lines match. There was no change in PXRD even after 1 year in laboratory conditions.

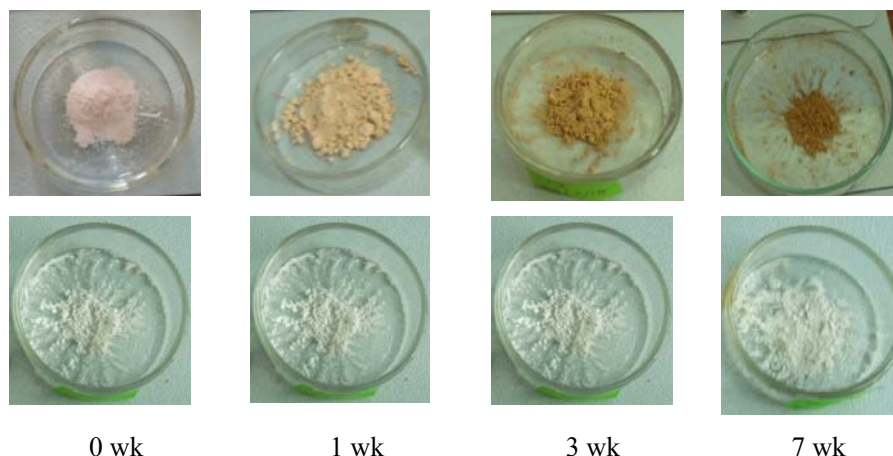


Figure 14 Physical stability and color comparison of pure TMZ (top panel) and TMZ–SA cocrystal (bottom panel) under accelerated ICH conditions of 40 °C and 75% RH. Pure TMZ showed darkening of color from pink/ light tan to dark brown starting in the first week and up to 7 weeks. The cocrystal was white in color for the entire duration. There was no color change or decomposition (by PXRD) of TMZ–SA cocrystal up to 28 weeks in the same conditions.

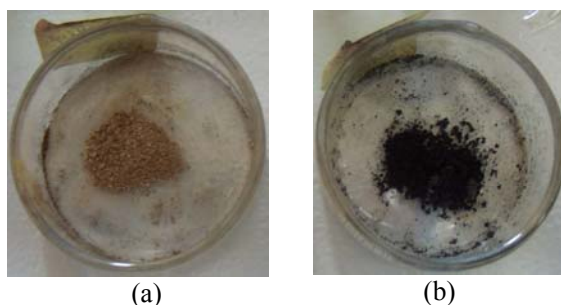


Figure 15 (a) TMZ–TA and (b) TMZ–MA kept at 40 °C and 75% RH showed dark coloration of white starting material after 26 weeks. However, their PXRDs were not indicative of serious degradation.

5.6 Conclusion

Chemical stability is of special concern for an otherwise very effective and potent antitumor drug temozolomide for the treatment of glioblastoma multiforme. This prodrug undergoes spontaneous degradation on storage in normal conditions. With the knowledge that TMZ is stable in acidic pH <5 but labile at basic pH >7, the drug was co-

crystallized with a few GRAS organic acids (pK_a 2-5) as pH adjusters to improve drug stability in the cocrystal. The carboxamide group of TMZ readily participated in hydrogen bonding with the carboxylic acid of cofomers via strong and robust amide–acid heterosynthon. All crystal structures were unambiguously characterized by single crystal X-ray diffraction to be cocrystals of a specific composition and fixed stoichiometry. Interestingly, cocrystals with COOH partners did not exhibit hydrolysis during crystallization in polar solvents (e.g. water, methanol, ethanol, CH₃CN etc.) even after one week whereas crystallization of pure temozolomide in the same solvents gave decomposition products in less than one day. Temozolomide cocrystals with oxalic acid and succinic acid are stable for up to one year in in-house laboratory conditions with no sign of degradation. The succinic acid cocrystal is not only stable for one year as confirmed by PXRD and IR, but it did not show any discoloration in the long term stability experiment. In contrast, temozolomide degraded within a few weeks in open conditions. Along with stability, bioavailability or dissolution is equally important for a solid oral drug to be therapeutically effective. When the multiple criteria of physical form stability and dissolution rate and white color on storage are applied, TMZ–succinic acid and TMZ–oxalic acid appear to be the most promising pharmaceutical cocrystals for formulation development.

5.7 Experimental Section

Temozolomide was purchased from Giovel Healthcare (New Delhi, India) and used directly for experiments. All other chemicals were of analytical or chromatographic grade. Melting points were measured on a Fisher-Johns melting point apparatus. Water filtered through a double deionized purification system (AquaDM, Bhanu, Hyderabad, India) was used in all experiments. All the cocrystals of TMZ were prepared by solvent assisted grinding (summarized in Table 6).

Table 6 Carboxylic acid cofomers used to crystallize cocrystals of Temozolomide.

Cocrystal	TMZ	Cocrystal former	Solvent/ Conditions	Time (days)
TMZ–OA (1:0.5) m.p. 170 °C (dec.)	40 mg (0.21 mmol)	9.5 mg (0.105 mmol) OA	9 mL of CH ₃ CN or 5 mL water	2-3

TMZ- SA (1:0.5) m.p. 165 °C (dec.)	50 mg (0.26 mmol)	15.5 mg (0.13 mmol) SA	8 mL of MeOH or 5 mL water	4-5
TMZ-SAC (1:1) m.p. 173 °C (dec.)	50 mg (0.26 mmol)	36 mg (0.26 mmol) SAC	5 mL of water or CH ₃ CN	2-3
TMZ-MA (1:0.5) m.p. 169 °C (dec.)	50 mg (0.26 mmol)	17 mg (0.13 mmol) MA	5 mL water	2-3
TMZ-ANA (2:1) m.p. 171 °C (dec.)	50 mg (0.26 mmol)	17.4 mg (0.13 mmol) ANA	5 ml CH ₃ CN	3-4
TMZ-TA (1:1) m.p. 170 °C (dec.)	50 mg (0.26 mmol)	39 mg (0.26 mmol) TA	10 mL of CH ₃ CN	4-5
TMZ-PHBA.H ₂ O (1:1:1)	50 mg (0.26 mmol)	35.9 mg (0.26 mmol) PHBA	5 mL CH ₃ CN	4-5
TMZ-FOA. H ₂ O (2:1:1)	50 mg (0.26 mmol)	FOA	2-4 mL Formic acid	4-5
TMZ-AA (1:1)	50 mg (0.26 mmol)	AA	2-4 mL of Acetic acid	4-5
TMZ-AA.H ₂ O (1:1:1)	50 mg (0.26 mmol)	AA	2-4 mL of Acetic acid	2-3

Note: Decomposition of cocrystals upon heating was observed similar to pure TMZ.

5.7.1 Cocrystal Stability

Pure temozolomide and the appropriate cocrystal containing 10 mg of the active drug were dissolved in 10 mL of pH 7 buffer solution. 1 ml of the resulting solution was then diluted to 100 times to get final stock solution. The absorbance of the final solution was measured at 37 °C using UV-Vis spectroscopy. The absorbance intensity of 210 nm, 256 nm and 330 nm peaks corresponding to amide carbonyl of AIC, and amide/tetrazinone group of TMZ were measured regular intervals of 15 min. The intensity of 330 and 210 nm bands decreased whereas 256 nm band increased with time progression, indicating hydrolysis of TMZ to AIC. The peaks at 330 nm and 256 nm were of about equal intensity after 1.7 h indicating that 50% of TMZ was hydrolyzed to AIC ($T_{1/2}$ value). The 256 nm peak shifted towards slightly higher wavelength (260-265 nm) as hydrolysis progressed. UV measurement of TMZ was recorded for 5 h.

Stability studies on TMZ and its cocrystals (about 200 mg) in solid state were carried out in a Newtronic Relative Humidity chamber (Mumbai, India) at accelerated ICH (International Conference on Harmonization) conditions of 40 °C and 75% relative

humidity (RH). The decomposition of solid phases was confirmed by comparing PXRD with the calculated X-ray patterns.

5.7.2 Intrinsic Dissolution Rate

Intrinsic dissolution rate (IDR) and solubility measurements were carried out on a USP-certified Electrolab TDT-08L Dissolution Tester (Electrolab, Mumbai, MH, India). Using the calibration curves of TMZ cocrystals discussed in this chapter molar extinction coefficients (ϵ) were calculated in pH 7 buffer. For intrinsic dissolution study, 200 mg of each TMZ cocrystal were compressed as a pellet in a hydraulic press at 4 ton pressure for 2-3 min. The pellet was compressed to provide a flat surface at one end and the other end was sealed. Then the pellet was dipped in 500 mL of pH 7 buffer solutions as the dissolution medium at 37 °C using a paddle rotation speed of 150 rpm. At 5-10 min time interval, 5 mL of the dissolution medium was withdrawn and replaced by an equal volume of fresh medium to maintain a constant volume. Samples were filtered through 0.2 μ m nylon filter and assayed for drug content spectrophotometrically at 210 nm. The amount of drug dissolved in each time interval was calculated using the calibration curve equation.

5.8 References

1. (a) Crystal Engineering: New concepts in Crystallography. R. Pepinsky, *Phys. Rev.* **1955**, *100*, 971. (b) Crystal Engineering. The design of Organic Solids, Elsevier, Amsterdam, 1989; G. R. Desiraju.
2. G. M. Whitesides, E. E. Simanek, J. P. Mathias, C. T. Seto, D. N. Chin, M. Mammen, D. M. Gordon, *Acc. Chem. Res.* **1995**, *28*, 3744. (b) M. C. T. Fyfe, J. F. Stoddart, *Acc. Chem. Res.* **1997**, *30*, 393.
3. S. Datta and D. J. W. Grant, *Nat. Rev. Drug Discovery*, **2004**, *3*, 42.
4. C. B. Aakeroy, M. E. Fasulo and J. Desper, *Mol. Pharmaceutics*, **2007**, *4*, 317.
5. P. V. Arnum, *Pharm. Technol.*, **2010**, *2*, 50.
6. (a) C. Leuner and J. Dressman, *Eur. J. Pharm. Biopharm.*, **2000**, *50*, 47. (b) J. C. Chaumeil, *Exp. Clin. Psychopharmacol.*, **1998**, *20*, 211. (c) K. Kawakami, N. Oda, K. Miyoshi, T. Funaki and Y. Ida, *Eur. J. Pharm. Sci.*, **2006**, *28*, 7. (d) D. Singhal and W. Curatolo, *Adv. Drug Delivery Rev.*, **2004**, *56*, 335. (e) A.

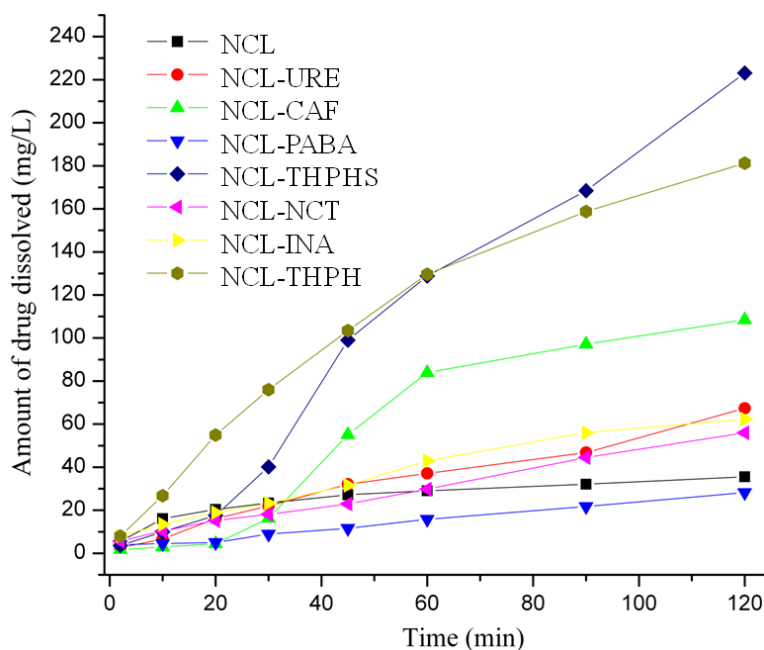
- Abdalla and K. Mäder, *Eur. J. Pharm. Biopharm.*, **2007**, *66*, 220. (f) K. Uekama, F. Hirayama and T. Irie, *Chem. Rev.*, **1998**, *98*, 2045. (g) J. Hecq, M. Deleers, D. Fanara, H. Vranckx and K. Amighi, *Int. J. Pharm.*, **2005**, *299*, 167.
7. (a) A. T. M. Serajuddin, *Adv. Drug Delivery Rev.*, **2007**, *59*, 603. (b) S. M. Berge, L. D. Bighley and D. C. Monkhouse, *J. Pharm. Sci.*, **1977**, *66*, 1. (c) A. T. M. Serajuddin and M. Pudipeddi, Salt Selection Strategies, in Handbook of Pharmaceutical Salts: Properties, Selection and Use, **2002**, pp. 135-160. (d) R. Banerjee, P. M. Bhatt, N. V. Ravindra and G. R. Desiraju, *Cryst. Growth Des.*, **2005**, *5*, 2299. (e) L. D. Bighley, S. M. Berge and D. C. Monkhouse, Salt Forms of Drugs and Absorption, in Encyclopedia of Pharmaceutical Technology, **1996**, *13*, pp. 453-499. (f) W. Q. Tong and G. Whitesell, *Pharm. Dev. Technol.*, **1998**, *3*, 215.
 8. (a) N. Rodríguez-Hornedo, *Mol. Pharmaceutics* **2007**, *4*, 299. (b) Ö. Almarsson, M. J. Zaworotko, *Chem. Commun.* **2004**, 1889. (c) P. Vishweshwar, J. A. McMahon; J. A. Bis, M. J. Zaworotko, *J. Pharm. Sci.* **2006**, *95*, 499. (d) W. Jones, W. D. S. Motherwell, A. V. Trask, *Mat. Res. Soc.* **2006**, *31*, 875. (e) S. L. Childs, Chyall, L. J.; J. T. Valeriya, N. Smolenskaya, B. C. Stahly, and G. P. Stahly, *J. Am. Chem. Soc.* **2004**, *126*, 13335. (f) P. Sanphui, N. R. Goud, U. V. R. Khandavilli, *Cryst. Growth & Des.*, **2011**, *11*, 4135.
 9. (a) S. Cherekuvada, N. J. Babu, A. Nangia, *J. Pharm. Sci.* **2011**, *100*, 3233. (b) S. Karki, M. Friščić, L. Fábán; P. R. Laity, G. M. Day, W. Jones, *Adv. Mater.* **2009**, *21*, 3905. (c) M. Khan, V. Enkelmann, G. Brunkaus, *J. Am. Chem. Soc.* **2010**, *132*, 5254.
 10. A. V. Trask, *Mol. Pharmaceutics*, **2007**, *4*, 301.
 11. (a) G. R. Desiraju, *Angew. Chem. Int. Ed. Engl.* **1995**, *34*, 2311. (b) A. Nangia, G. R. Desiraju, *Top. Curr. Chem.* **1998**, *198*, 57. (c) J. A. McMahon, J. A. Bis, P. Vishweshwar, T. R. Shattock, O. L. McLaughlin, and M. J. Zaworotko, *Z. Kristallogr.* **2005**, *220*, 340.
 12. (a) M. C. Etter, *Acc. Chem. Res.* **1990**, *23*, 120. (b) M. C. Etter, *J. Phys. Chem.* **1991**, *95*, 4601.
 13. (a) L. S. Reddy, P. M. Bhatt, R. Banerjee, A. Nangia, G. J. Kruger, *Chem. Asian J.* **2007**, *2*, 505. (b) A. V. Trask, W. Jones, *Top. Curr. Chem.* **2005**, *254*, 41. (c)

- A. Jayasankar, A. Somwangthanaroj, Z. J. Shao, N. Rodríguez-Hornedo, *Pharma. Res.* **2006**, *23*, 2381. (d) S. L. Childs, N. Rodríguez-Hornedo, L. S. Reddy, A. Jayasankar, C. Maheshwari, L. McCausland, R. Shipplett, B. C. Stahly, *CrystEngComm* **2008**, *10*, 856. (e) N. Rodríguez-Hornedo, S. J. Nehm, K. F. Seefeldt, Y. Pagán-Torres, C. J. Falkiewicz, *Mol. Pharmaceutics* **2006**, *3*, 362. (f) H. Abourahma, D. S. Cocuzza, J. Melendez and J. M. Urban, *CrystEngComm*, **2011**, *13*, 6442. (g) R. Thakuria and A. Nangia, *CrystEngComm*, **2011**, *13*, 1759.
14. (a) E. S. Newlands, M. F. Stevens, S. R. Wedge, R.T. Wheelhouse, C. Brock, *Cancer Treat. Rev.* **1997**, *23*, 35. (b) M. J. M. Darkes, G. L. Plosker, B. Jarvis, *Am. J. Cancer* **2002**, *1*, 55 (review).
15. (a) P. R. Lowe, C. E. Sansom, C. H. Schwalbe, M. F. G. Stevens, A. S. Clark, *J. Med. Chem.* **1992**, *35*, 3377. (b) L. J. Fairbairn, N. Chinnasamy, L. S. Lashford, D. Chinnasamy, J. A. Rafferty, *Cancer Gene Ther.* **2000**, *7*, 233.
16. (a) J. Arrowsmith, S. A. Jennings, A. S. Clark, M. F. G. Stevens, *J. Med. Chem.* **2002**, *45*, 5458. (b) <http://www.spfiles.com/pitemodar.pdf>.
17. (a) I. Adin, C. Lustain, US 0187206 A1, Aug. 25, **2005**. (b) N. J. Babu, L. S. Reddy, S. Aitipamula, A. Nangia, *Chem. – An Asian J.* **2008**, *3*, 1122. (c) B. Panda, G. C. Maikap, S. K. Agarwal, M. K. Singh, M. Jaggi, A. Nangia, N. J. Babu, L. S. Reddy, S. Aitipamula, WO 111092 A1, Sep. 18, **2008**.
18. (a) Physician's Desk Reference, 60th Edition, **2006**, <http://www.pdr.net>.
19. (a) O. Braverman, R. Feishtein, A. Weisman, J. Kaspi, US 2006/0222792 A1, Oct. 5, **2006**. (b) L. S. Pathi, R. D. Rao, K. R. Narayanrao, WO 2008/038031 A1. **2008**. (c) O. Etlin, M. Alnabari, Y. Sery, E. Danon, O. Arad, J. Kaspi, US 2006/0183898 A1. Aug 17, **2006**.
20. (a) B. J. Denny, R. T. Wheelhouse, M. F. G. Stevens, L. L. H. Tsang, J. A. Slack, *Biochemistry* **1994**, *33*, 9045. (b) J. Arrowsmith, S. A. Jennings, D. A. F. Langnel, R. T. Wheelhouse, M. F. G. Stevens, *J. Chem. Soc. Perkin Trans. I* **2000**, 4432. (c) G. Saravanan, M. Ravikumar, M. J. Jadhav, M. V. Suryanarayana, N. Someswararao, P. V. R. Acharyulu, *Chromatographica* **2007**, *66*, 291. (d) H. Kim, P. Likhari, D. Parker, P. Statkevich, A. Marco, C. Lin, A. A. Nomeir, *J. Pharma. Biomed. Anal.* **2001**, *24*, 461. (e) E. Fenyvesi, M.

- Vikmon, J. Szeman, E. Redenti, M. Delcanale, P. Ventura, J. Szejtli, *J. Inclusion Phenomena and Macrocyclic Chemistry* **1999**, 33, 339.
21. (a) Generally Regarded as Safe: <http://www.cfsan.fda.gov/~rdb/opa-gras.html> and <http://www.cfsan.fda.gov/~dms/grasguid.html>. (b) Everything Added to Food Stuff in the United States: <http://vm.cfsan.fda.gov/~dms/eafus.html>.
 22. (a) A. Nangia, G. R. Desiraju, *Top. Curr. Chem.* **1998**, 198, 57. (b) L. S. Reddy, P. M. Bhatt, R. Banerjee, A. Nangia, G. J. Kruger, *Chem. Asian J.* **2007**, 2, 505. (c) P. Vishweshwar, A. Nangia, V. M. Lynch, *Cryst. Growth Des.* **2003**, 3, 783. (d) A. Nangia, *J. Chem. Sci.* **2010**, 122, 295.
 23. M. C. Etter, J. C. Macdonald, *Acta Cryst.* **1990**, B46, 256. (b) J. Bernstein, R. E. Davis, L. Shimon, N.-L. Chang, *Angew. Chem., Int. Ed. Engl.* **1995**, 34, 1555.
 24. (a) E. S. Newlands, G. R. P. Blackledge, J. A. Slack, G. J. S. Rustin, D. B. Smith, N. S. A. Stuart, C. P. Quarterman, R. Hoffman, M. F. G. Stevens, M. H. Brampton, A. C. Gibson, *Br. J. Cancer* **1992**, 65, 287. (b) P. Beale, I. Judson, S. Moore, P. Statkevich, A. Marco, D. L. Cutler, P. Reidenberg, M. Brada, *Cancer Chemother. Pharmacol.* **1999**, 44, 389.
 25. S. D. Baker, M. Wirth, P. Statkevich, P. Reidenberg, K. Alton, S. E. Sartorius, M. Dugan, D. Cutler, V. Batra, L. B. Grochow, R. C. Donehower, E. K. Rowinsky, *Clin. Cancer Res.* **1999**, 5, 309.
 26. (a) <http://www.rxlist.com/temodar-drug.htm>. (b) <http://www.leiomyosarcoma.info/chemo64temo.htm>. (c) <http://www.indiamart.com/radhakishanpharmaceuticals/temonat.html>. (d) <http://www.rellife.com/pdf/temorelpack.pdf>
 27. (a) http://www.ema.europa.eu/docs/en_GB/document_library/Scientific_guideline/2_009/09/WC500002651.pdf. (b) ICH Harmonized Guideline, Q1A (R2) Stability Testing of New Drug Substances and Products, **2003**.

Chapter Six

Pharmaceutical Cocrystals of Niclosamide



Powder dissolution of Niclosamide (NCL) and its pharmaceutical cocrystals in 40% isopropanol-water medium showed that theophylline cocrystal (NCL-THPH) and NCL-THPHS cocrystal solvate dissolved 5-6 times faster than the pure API. All cocrystals transformed to niclosamide monohydrate during 24 h of slurry.

6.1 Introduction

Cocrystals of active pharmaceutical ingredients (APIs) with small organic molecules to design new crystalline forms is an important subject with pharmaceutical application.¹ Apart from patent life cycle management,^{1c,2} introducing a drug molecule in a crystal structure with another component makes it possible to modify the properties as compared to the individual solid phases (e.g. polymorphs, amorphous etc.). The novel solid forms are important because they allow biopharmaceutical properties to be controlled such as solubility, stability, bioavailability, hygroscopicity, tableting, etc. Selection of the most suitable forms in terms of superior physicochemical properties is desirable in drug formulation. This exercise requires inputs about crystallization, pharmacology and formulation. Cocrystals are suitable for direct compression.³ They are less hygroscopic,^{1c,4} and exhibit higher dissolution^{1b,4b,c} of the API. The first step in this exercise is to find a relation between crystal structure and properties in order to know which structures are required for achieving a desired physical property (better compressibility, a higher dissolution rate, higher thermal stability etc.). Second, it is necessary to learn how to produce desirable structures when one of the molecular components (API) is fixed, but the other can be varied, e.g. different pharmacologically acceptable safe coformers can be selected.

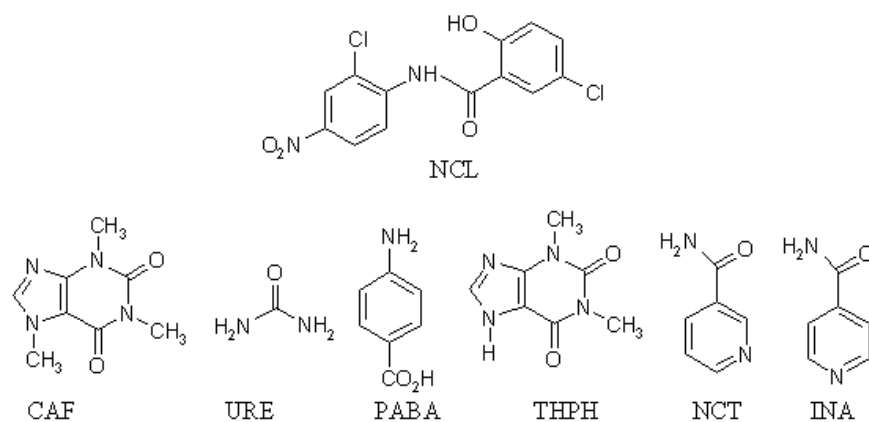
Poor aqueous solubility is an industry-wide problem in drug discovery and the predominant problem associated with developing orally active drugs.^{1b,5f,6} 80% of drugs are sold as tablets because of easy uptake for patients. 40% of drugs in the market have a solubility problem and 70-80% of drug candidates in the pipeline never realize their potential to be marketed because of poor solubility issue. In general, a favorable dissolution profile results from a complex interplay of i) interactions between molecules in the crystal, ii) solvent molecules and the crystal-forming molecules at the crystal faces, and iii) molecules of the dissolved crystal and their solvation shell in solution. It can therefore be assumed that modifying intermolecular interactions in the crystal and making the interactions between the solute and the solvent molecules competitive with those between the molecules in the crystal may have a positive effect on solubility. Generally salts are better to solve solubility problems and hence more than 50% APIs are marketed as salt forms.^{6b} Cocrystals are particularly relevant for APIs lacking ionizable

functional groups to improve the solubility and dissolution rate. Cocrystals are preferable over salts because ionic species (salts) are more prone to be hygroscopic. Cocrystal formation is one of the possible ways to modify the intermolecular interactions in the crystal and hence tune the physicochemical properties. In cocrystals formed by two components A and B, some (or all) of the homomolecular A–A and B–B interactions are substituted for heteromolecular A–B interactions, and this accounts for the change in interactions with solvent molecules on dissolution. Again pharmaceutical cocrystals are multicomponent solids of an API with another GRAS (Generally Regarded As Safe) molecule.⁷ One can suppose that, other parameters being similar, a cocrystal will dissolve faster as compared with the individual APIs if the coformer has high solubility and hence dissociation of cocrystals will be faster. An analysis of a series of cocrystals and of the individual compounds with their dissolution kinetics may help to understand the role of different intermolecular interactions and coformer on solubility.

6.2 Niclosamide

Niclosamide⁸ (chemical name 2, 5-dichloro-4-nitrosalicylanilide, Scheme 1), is an anthelmintic drug used for the treatment of worm infestations in humans and animals. It can inhibit the replication of several acute respiratory syndrome coronavirus.^{8c} It is available mainly as two types of dosage forms, tablets and suspensions. Niclosamide is a BCS (biopharmaceutical classification system) Class II drug, marketed as Niclocide tablet (500 mg dose and dose number, D₀ 200) brand name. Niclosamide is among the essential orally administered drugs with inclusive data.⁹ It is practically insoluble in water, sparingly soluble in various other solvents (e.g. ether, THF, ethyl acetate, dioxane etc.) and is usually formulated as a suspension, which allows for the development of a liquid dosage form containing an appropriate quantity of drug in a reasonably small volume. Both niclosamide anhydrate and monohydrate are available for formulation. However, niclosamide anhydrate has a high affinity for water and various suspension formulations form cement-like sediments during storage.¹⁰ Niclosamide is very much prone to make solvates similar to drug like axitinib and tenoxicam.¹¹ Two monohydrates, an anhydrate, various solvates of niclosamide have been reported in the literature.^{8c} The aqueous solubility of niclosamide is 13±3 mg/L. Solubility order of niclosamide crystalline forms is anhydrous>>solvates> hydrates.^{8d} There are niclosamide

phosphate, niclosamide ethanolamine salts and their better solubility reported in recent patents.¹² As salts have some limitation over hydration problems and the drug must possess ionizable functional groups, cocrystals are generally preferred because of their ability to improve solubility and stability. There are no cocrystals reported in the literature so far to improve the solubility of niclosamide. Crystal engineering approach was attempted to modify the solubility of solid dosage forms of niclosamide as well as to prevent formation of its hydrate which exhibited least solubility (0.45 mg/L). Anhydrous niclosamide (white material) transforms to monohydrate (greenish) within a month in storage at ambient conditions. As hydrates are the least soluble among all solid dosage forms, it is not the desired form, so solubility and stability of API are of concern for NCL. Pharmaceutical cocrystals of niclosamide with GRAS molecules (caffeine, urea, p-aminobenzoic acid, theophylline, nicotinamide and isonicotinamide) were prepared by solvent (dry) drop grinding and characterized by FT-IR, thermal analysis (DSC and TGA) and X-ray diffraction (both single crystal and powder X-ray diffraction) and solid state NMR spectroscopy. Coformers used with NCL are displayed in Scheme 1.



Scheme 1 Chemical structure of niclosamide (NCL) and coformers: caffeine (CAF), urea (URE), p-aminobenzoic acid (PABA), theophylline (THPH), nicotinamide (NCT) and isonicotinamide (INA). All niclosamide cocrystals are of 1:1 stoichiometry.

6.3 Results and discussions

Niclosamide has high tendency to form hydrate/solvates when it is crystallized from solvents. In literature, anhydrous form of niclosamide, monohydrate H_A and H_B , THF, triethylene glycol, DMF, DMSO, MeOH solvates were reported and characterized by PXRD, DSC, FT-IR etc.^{8a-c} No guest free crystal structure for the API was reported so far. Crystallization from solvents generally produces solvates. To obtain guest free niclosamide, solvent less method, melt and sublimation crystallizations¹³ were applied. Both sublimation and melt form afforded the same guest free structure of niclosamide. All the coformers used here are GRAS molecules. Niclosamide cocrystals (1:1) were obtained from dry EtOAc, CH_3CN solvents after grinding in mortar pestle. Dry solvents are necessary; otherwise there is a possibility of hydrate formation from moisture content present in solvents. The formation of new solid forms was preliminary confirmed by FT-IR, melting point and powder X-ray diffraction. Crystallographic parameters for niclosamide and its new cocrystals are summarized in Table 1.

6.3.1 Crystal structure description

Niclosamide (NCL)

Guest free niclosamide was crystallized in $P2_1/c$ space group in monoclinic crystal lattice with one molecule in the asymmetric unit. Niclosamide molecules are locked in nearly planar conformation which is stabilized by $N-H\cdots O$ ($N\cdots O$: 2.630 (2) Å, 142°) intramolecular hydrogen bond between amine ($-NH$) and hydroxyl group ($-OH$). Niclosamide molecules form intermolecular $O-H\cdots O$ ($O\cdots O$: 2.693 (2) Å, 173°) hydrogen bond from hydroxy to carbonyl forming chain along c -axis (Figure 1a). Normalized hydrogen bonds using Platon are summarized in Table 2. Two parallel niclosamide molecules are interconnected through $Cl\cdots NO_2$ dimer interaction ($Cl\cdots O$: 3.227 Å) with graph set notation¹⁴ of $R_2^2(12)$ ring. Molecules form ladder motif parallel to b -axis (Figure 1b). Packing diagram of guest free form of niclosamide is totally changed from its monohydrate crystal structure reported by Caira et al^{8d} where water molecules present in the cavity formed by niclosamide molecules and played an important role in stabilizing the crystal structure, using two hydrogens as donor to niclosamide molecules.

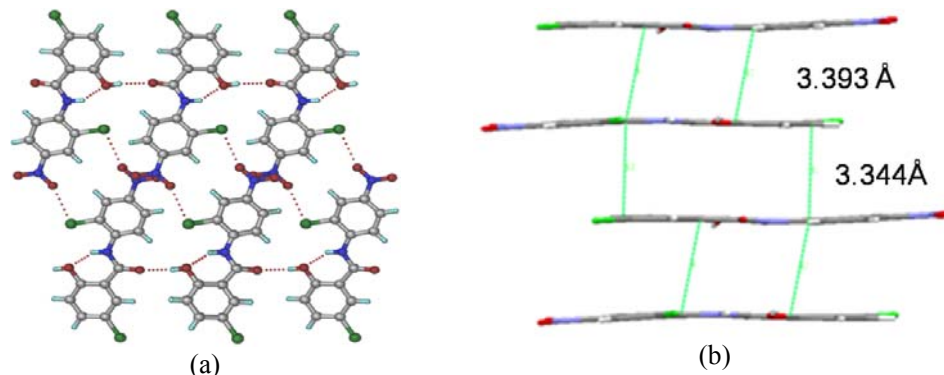


Figure 1(a) O–H···O interaction between niclosamide molecules through N–H···O (OH) hydrogen bond results layered structure along *c*-axis. (b) Niclosamide molecules form ladder motif between the layers parallel to *b*-axis.

Niclosamide–Caffeine cocrystal (NCL–CAF, 1:1)

The crystal structure of NCL–CAF (1:1) cocrystal was solved in the monoclinic $P2_1/c$ space group and the asymmetric unit contains one molecule each of niclosamide and caffeine. There is intramolecular N–H···O hydrogen bond (N···O: 2.630 (2) Å, 143°) between amine and hydroxyl group in niclosamide. Intermolecular hydrogen bond between niclosamide molecules were interrupted in the presence of caffeine, forming O–H···O (O···O: 2.640 (3) Å, 173°) hydrogen bond from O–H of niclosamide to the carbonyl acceptor of caffeine. Two niclosamide molecules form dimer through weak C–H···O (C···O: 3.182 (3), 141°) hydrogen bond in $R_2^2(12)$ ring motif. Caffeine and niclosamide molecules arranged in ABBA fashion along *a*-axis (Figure 2a). Layers are interconnected through π – π stacking interaction (π – π dist 3.32 Å) between niclosamide and caffeine molecules (Figure 2b).

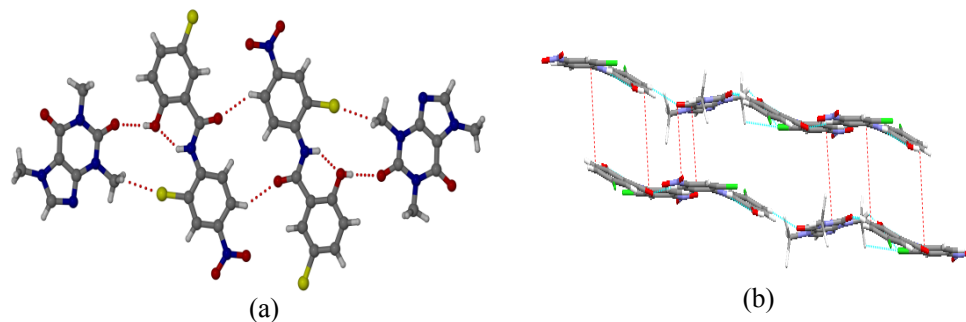


Figure 2(a) Niclosamide and caffeine form O–H···O and C–H···O hydrogen bonds in a 1D chain. (b) π – π stacking interaction (3.32 Å) between aromatic rings of niclosamide and also with caffeine in two layers along *a*-axis

Niclosamide–Urea cocrystal (NCL–URE, 1:1)

The asymmetric unit in space group $P2_1/c$ contains one molecule each of niclosamide and urea. Intramolecular hydrogen bond is formed through $N-H\cdots O$ ($N\cdots O$: 2.644 (2) Å, 139°) interaction in niclosamide. There is an intermolecular $O-H\cdots O$ ($O\cdots O$: 2.600 (1) Å, 176°) hydrogen bond between niclosamide and urea in a perpendicular fashion. The urea motif¹⁵ interacts in the cocrystal through $N-H\cdots O$ hydrogen bond ($N\cdots O$: 2.974(2) Å, 149°; $N\cdots O$: 2.918 (2) Å, 152°) along c -axis. Two niclosamide and two urea molecules form cyclic $R_6^4(20)$ ring motif between carbonyl oxygen of niclosamide molecule and urea $N-H$ which is not engaged in urea motif (Figure 3a). Unlike NCL–CAF cocrystal, here urea and niclosamide molecules are arranged in an alternative ABAB fashion. Niclosamide molecules are interconnected through π stacking interactions (π - π dist. 3.34 Å), present between the two antiparallel urea tape motifs (Figure 3b).

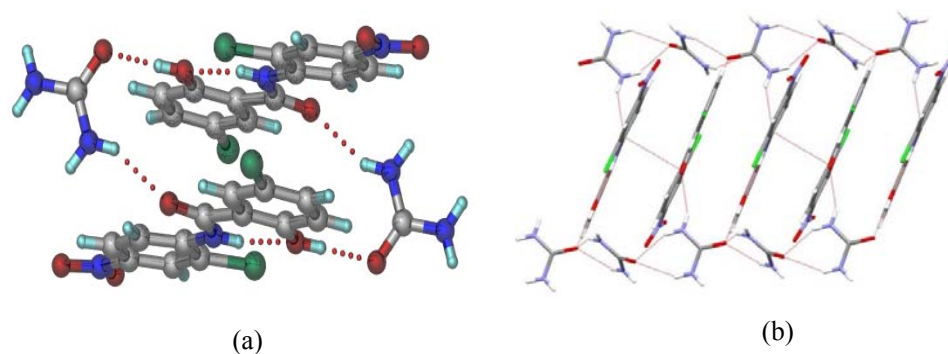


Figure 3 (a) Niclosamide and urea molecules form cyclic $R_6^4(20)$ ring motif between carbonyl oxygen of niclosamide molecule and urea $N-H$. (b) Two antiparallel urea tape form column in which niclosamide molecules are stacked through π - π interaction (stacking separation 3.34 Å).

Niclosamide–PABA cocrystal (NCL–PABA, 1:1)

NCL–PABA (1:1) cocrystal was solved and refined in the triclinic space group $P-1$ and the asymmetric unit contains one molecule each of niclosamide and PABA. Intramolecular hydrogen bond is formed through $N-H\cdots O$ ($N\cdots O$: 2.647 (2) Å, 140°) interaction in niclosamide. An intermolecular hydrogen bond between $O-H$ group of API and NH_2 of PABA through a weaker $O-H\cdots N$ ($O\cdots N$: 2.802 (3) Å, 173°) hydrogen bond than in NCL–CAF and NCL–URE cocrystals. PABA form centrosymmetric carboxylic acid dimer ($O\cdots O$: 2.617(2) Å, 179°) and hydrogen bonding to niclosamide

extends through $\text{NH}_2 \cdots \text{NO}_2$ hydrogen bond ($\text{N} \cdots \text{O}$: 3.134(2) Å, 154°) along the c axis (Figure 4a). Two niclosamide and two PABA molecules form tetramer of $\text{R}_6^4(16)$ ring motif through both $\text{N}-\text{H} \cdots \text{O}$ and $\text{O}-\text{H} \cdots \text{N}$ hydrogen bond ($\text{N} \cdots \text{O}$: 2.981(3) Å, 157°) parallel to (200) plane (Figure 4b). Niclosamide molecules connect to the next layer with another API through π stacking interactions (3.38 Å).

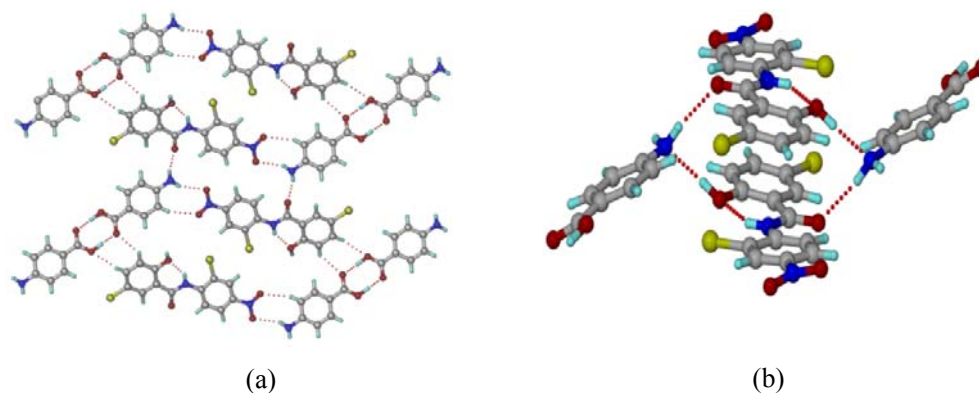


Figure 4 (a) Niclosamide and PABA molecules interact through $\text{NH}_2 \cdots \text{NO}_2$ hydrogen bond along c -axis. (b) Two niclosamide and two PABA molecules form tetramer of $\text{R}_6^4(16)$ Ring through $\text{N}-\text{H} \cdots \text{O}$ and $\text{O}-\text{H} \cdots \text{N}$ hydrogen bond.

Niclosamide–Theophylline cocrystal (NCL–THPH, 1:1)

NCL–THPH (1:1) cocrystal was synthesized from isopropyl acetate solvent and the crystal structure was solved in monoclinic $P2_1/c$ space group. There is one molecule each of niclosamide and theophylline in the asymmetric unit. Apart from the intramolecular $\text{N}-\text{H} \cdots \text{O}$ hydrogen bond ($\text{N} \cdots \text{O}$: 2.755(2) Å) in niclosamide, the API and theophylline form intermolecular hydrogen bond ($\text{O} \cdots \text{O}$: 2.676(3) Å, 179°) from hydroxyl group of API to carbonyl of theophylline. Theophylline molecules form centrosymmetric carboxamide dimer of $\text{R}_2^2(10)$ ring through $\text{N}-\text{H} \cdots \text{O}$ interaction ($\text{N} \cdots \text{O}$: 2.834(3) Å). There is weak $\text{C}-\text{H} \cdots \text{O}$ interaction ($\text{C} \cdots \text{O}$: 3.165(3) Å, 168°) between inversely related niclosamide molecules. Two niclosamide and two theophylline molecules are arranged as ABBA fashion along a -axis (Figure 5a). These tetramer units are connected to next layer by an auxiliary $\text{C}-\text{H} \cdots \text{O}$ ($\text{C} \cdots \text{O}$: 3.436(3) Å, 144°) hydrogen bond from theophylline aromatic ring $\text{C}-\text{H}$ to $-\text{NO}_2$ acceptor of niclosamide along c -axis in a sheet structure (Figure 5b).

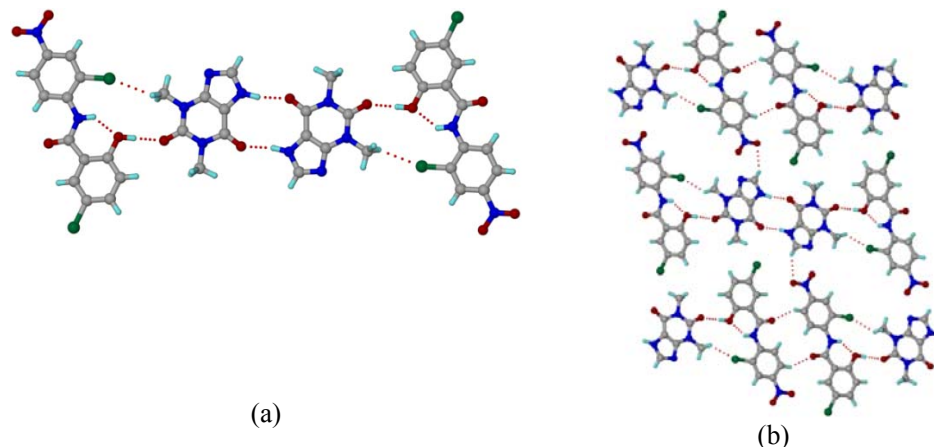


Figure 5 (a) Niclosamide and theophylline molecules arranged as ABBA fashion interacting through O–H \cdots O and N–H \cdots O hydrogen bonds. (b) Tetramer motif consisting of two niclosamide and two theophylline molecules further interacted through C–H \cdots O interaction between niclosamide and theophylline along *c*-axis to form overall packing.

Niclosamide–Theophylline-CH₃CN cocrystal solvate (NCL–THPHS, 1:1:1)

Niclosamide–theophylline-CH₃CN (1:1:1) cocrystal solvate was crystallized from EtOAc-CH₃CN solvent mixture. The structure was solved in the triclinic space group *P*-1 and the asymmetric unit contains one molecule of niclosamide, theophylline and acetonitrile solvent. The intermolecular hydrogen bond O–H \cdots O (O \cdots O: 2.638 (2) Å, 174°) is present between API (donor) and theophylline molecule (acceptor). Two theophylline molecules form centrosymmetric dimer through N–H \cdots O bond (N \cdots O: 2.755(2) Å, 175°) of R₂²(10) ring motif (Figure 6a). Similar to niclosamide-THF solvate,^{8a} acetonitrile solvent is present in the channel created by niclosamide and theophylline along *c*-axis (Figure 6b). The π stacking interactions (3.34 Å) aggregate between niclosamide molecules parallel to the *b*-axis. A characteristic feature of the crystal is desolvation of acetonitrile from the crystal lattice within 1 h and loss of crystallinity at ~80°C (discussed later).

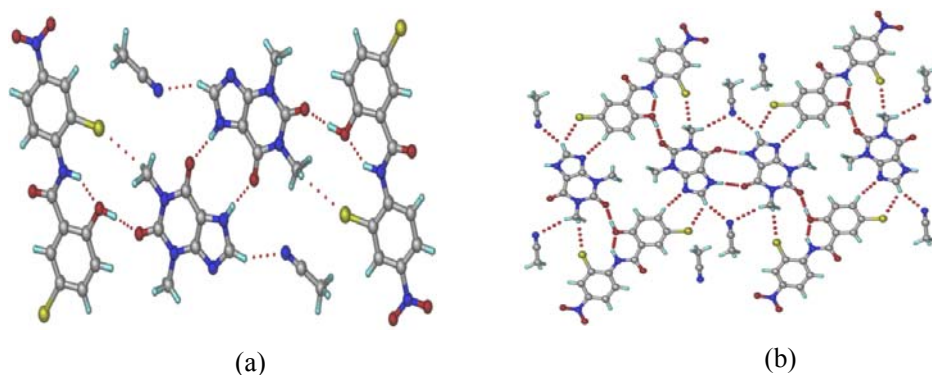


Figure 6 (a) Similar hydrogen bonded motif consisting of theophylline homodimer followed by intermolecular hydrogen bond between niclosamide and theophylline as NCL-THPH cocrystals. (b) Acetonitrile solvent resides in the channel along *a*-axis created by niclosamide and theophylline molecules.

Table 1 Crystallographic data of niclosamide and its cocrystals

Crystal Data	NCL	NCL-CAF	NCL-URE
Emp. Formula	C ₁₃ H ₁₂ N ₂ O ₄ Cl ₂	C ₁₃ H ₁₂ N ₂ O ₄ Cl ₂ . C ₈ H ₁₀ N ₄ O ₂	C ₁₃ H ₁₂ N ₂ O ₄ Cl ₂ . CH ₄ N ₂ O
Formula wt.	327.11	521.31	387.18
Crystal system	Monoclinic	Monoclinic	Monoclinic
Space group	<i>P</i> 2 ₁ / <i>c</i>	<i>P</i> 2 ₁ / <i>c</i>	<i>P</i> 2 ₁ / <i>c</i>
<i>T</i> [K]	100	100	100
<i>a</i> [Å]	13.485(2)	7.8756(4)	11.1272(10)
<i>b</i> [Å]	7.0669(11)	10.7632(6)	16.9312(14)
<i>c</i> [Å]	13.510(2)	25.8869(13)	8.5708(7)
α [deg]	90	90	90
β [deg]	98.345(2)	96.286(1)	93.312(1)
γ [deg]	90	90	90
<i>Z</i>	4	4	4
Volume [Å ³]	1273.9(3)	2181.2(2)	1612.0(2)
<i>D</i> _{calc} [g/cm ³]	1.706	1.588	1.595
<i>R</i> ₁ [<i>I</i> > 2σ(<i>I</i>)]	0.0349	0.0548	0.0313,
<i>wR</i> ₂	0.0931	0.1570	0.0782
GOF	1.093	1.039	1.069

NCL-PABA	NCL-THEOP	NCL-THEOPS
C ₁₃ H ₁₂ N ₂ O ₄ Cl ₂ . C ₇ H ₇ NO ₂	C ₁₃ H ₁₂ N ₂ O ₄ Cl ₂ . C ₇ H ₈ N ₄	C ₁₃ H ₁₂ N ₂ O ₄ Cl ₂ . C ₇ H ₈ N ₄ .C ₂ H ₃ N
464.25	507.29	548.34
Triclinic	Monoclinic	Triclinic

<i>P</i> -1	<i>P</i> 21/ <i>c</i>	<i>P</i> -1
298	298	100
7.2810(14)	9.1371(7)	8.598(2)
12.763(2)	10.8809(9)	10.762(3)
12.789(2)	22.4497(17)	13.246(3)
62.543(17)	90	105.635(3)
76.384(16)	99.924(8)	94.069(4)
74.384(15)	90	96.018(4)
2	4	2
1007.0(3)	2198.6(3)	1167.6(5)
1.531	1.533	1.560
0.0385,	0.0614,	0.1355
0.0856	0.1358	0.0468
0.856	0.998	1.03

Table 2 Neutron normalized hydrogen bonds in crystal structures.

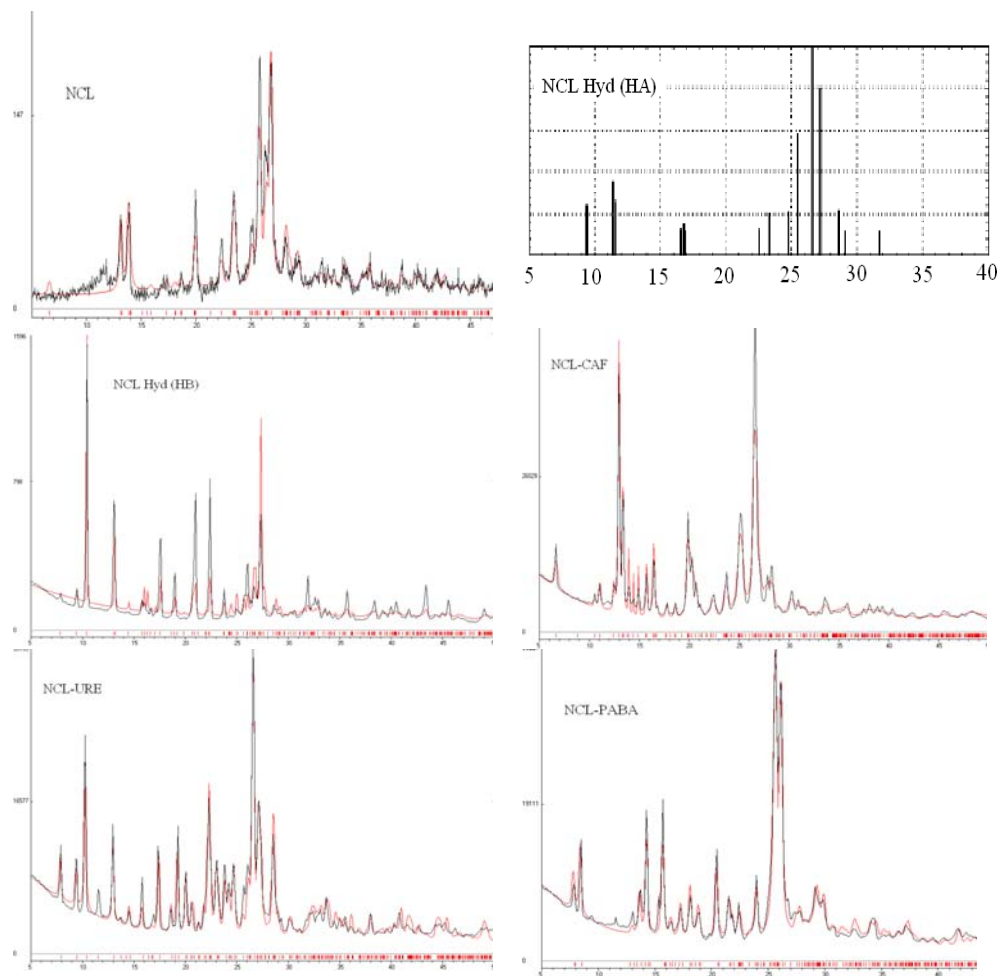
	Interaction	<i>d</i> (H⋯A) (Å)	<i>d</i> (D⋯A) (Å)	∠D–H⋯A (°)
NCL	N1–H1⋯Cl1	2.36	2.902 (15)	113
	N1–H1⋯O4	1.76	2.630 (2)	142
	O4–H2⋯O3	1.72	2.693 (2)	173
	C3–H3⋯O2	2.49	3.363 (2)	136
	C5–H5⋯Cl2	2.69	3.777 (2)	176
	C6–H6⋯O3	2.23	2.897 (2)	117
NCL – CAF (1:1)	N1–H1⋯Cl1	2.43	2.918 (2)	109
	N1–H1⋯O4	1.76	2.630 (3)	143
	O4–H2⋯O5	1.66	2.640 (3)	176
	C5–H5⋯O3	2.26	3.182 (3)	141
	C6–H6⋯O3	2.21	2.876 (3)	117
	C11–H11⋯O6	2.26	3.304 (3)	160
	C14–H14B⋯O6	2.24	2.731 (4)	105
	C16–H16A⋯O5	2.32	2.779 (4)	103
	C16–H16A⋯Cl1	2.79	3.275 (2)	107
	C20–H20B⋯O2	2.39	3.387 (4)	152
NCL– URE (1:1)	N1–H1⋯Cl2	2.45	2.959 (1)	111
	N1–H1⋯O4	1.79	2.644 (2)	139
	O4–H2⋯O5	1.62	2.60 (1)	176
	N3–H3A⋯Cl1	3.07	3.631(1)	116
	N3–H3A⋯O5	2.09	2.974 (2)	145
	N3–H3B⋯Cl1	2.57	3.530 (1)	157
	N3–H3B⋯O2	2.56	3.279 (2)	128
	N4–H4A⋯O3	1.99	2.921 (2)	152
	N4–H4B⋯O5	1.98	2.918 (2)	152
	C3–H3⋯Cl1	2.68	3.751 (2)	168
	C6–H6⋯O3	2.12	2.814 (2)	119
	C11–H11⋯O1	2.23	3.238(2)	153

NCL-PABA (1:1)	C12-H12...O5	2.63	3.365(2)	124
	N1-H1...O4	1.82	2.667(2)	140
	O4-H2...N3	1.82	2.802(3)	173
	N3-H3A...O3	2.02	2.981(3)	157
	N3-H3B...O1	2.19	3.134(3)	154
	O6-H6A...O5	1.63	2.617(2)	179
NCL-THPH (1:1)	C6-H6...O3	2.13	2.827(3)	119
	C11-H11...O6	2.38	3.401(3)	155
	N2-H1...Cl1	2.35	2.927 (2)	115
	N2-H1...O4	1.85	2.654 (2)	135
	O4-H2...O6	1.69	2.676(3)	179
	N5-H5A...O5	1.84	2.834(3)	168
NCL-THPHS (1:1:1)	C5-H5...O3	2.24	3.165(3)	142
	C16-H16...O2	2.56	3.436(3)	144
	C6-H6...O3	2.19	2.807(3)	119
	C19-H19A...O1	2.51	3.246(3)	124
	C19-H19B...O5	2.27	2.739(3)	104
	C20-H20B...N6	2.46	2.942(3)	105
	O3-H3A...O2	1.66	2.638(2)	174
	N4-H4A...O1	1.75	2.755(2)	175
	N6-H6A...Cl1	2.44	2.936(2)	109
	N6-H6A...O3	1.79	2.650(2)	141
	C2-H2...O4	2.24	3.149(3)	140
	C10-H10...O2	2.35	3.150(3)	129
	C11-H11...O4	2.14	2.811(3)	117
	C12-H12...N3	2.37	3.429(3)	163
	C21-H21A...Cl2	2.71	3.628(3)	142
	C21-H21B...O6	2.47	3.542(3)	170

6.3.2 Powder X-ray diffraction

Niclosamide was purchased from Sigma-Aldrich and used without further purification. But within one month at ambient condition of 30-40 °C and 50-75% relative humidity, white colored anhydrous niclosamide turned to greenish niclosamide monohydrate. However niclosamide hydrate transformed to anhydrous form without decomposition after keeping for 5-6 h at ~100 °C. PXRD is a diagnostic tool to differentiate between cocrystals from coformers based on line profile by taking a safe threshold of $\Delta 2\theta > \pm 0.2^\circ$. The PXRD traces of the guest free forms of niclosamide (reported earlier) matched the calculated lines from the X-ray crystal structures, confirming the purity of the bulk phases. Two type of niclosamide monohydrate (H_A and H_B) were reported in the literature.^{8a} PXRD of niclosamide monohydrate (H_A) exhibit characteristic reflections at about 2θ 9.47, 11.40, 16.83, 22.43 and $25.54 \pm 0.2^\circ$. Again

monohydrate (H_B, CSD refcode OBEQER)^{8a} exhibits characteristic reflections at about 2θ 10.37, 13.07, 17.63, 19.02 and 21.0 ±0.2°. There are noticeable differences in the peak positions of niclosamide and its cocrystals from the API and coformer. PXRD comparison of bulk amount of API and its cocrystals were compared with the calculated X-ray lines to confirm the purity of new phases (Figure 7).



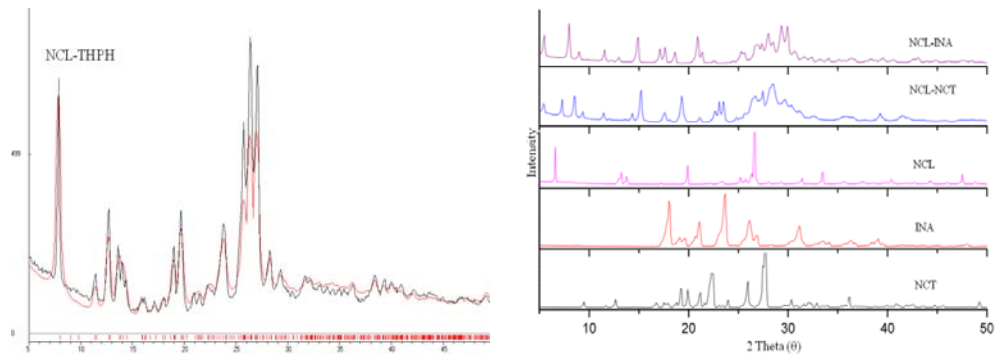


Figure 7 PXRD comparison of niclosamide and its cocrystals with their calculated X-ray lines obtained from single crystal X-ray structures. PXRD comparison of NCL–NCT and NCL–INA cocrystals with that of coformers indicates new solid phases formed.

6.3.3 Thermal stability of niclosamide and its cocrystals

The relative stability and inter conversion of crystalline solids are important to study during drug formulation, because an incorrect choice of formulation may cause an adverse effect on the issue of physical stability and pharmacokinetic profile. Differential scanning calorimetry (DSC) measurements indicate the thermal characteristics of the new solid forms. Among niclosamide cocrystals, NCL–THPH and NCL–NCT showed a second endotherm before melting which suggested phase transition or decomposition. Again NCL–THPHS cocrystal solvate releases CH_3CN solvent at 82 °C and second endotherm is the melting point of desolvated niclosamide theophylline cocrystals. DSC endotherm of niclosamide and its cocrystals exhibited single endotherm confirming uniformity of the new solid phases (Figure 8). Thermogravimetric analysis (TGA) suggests the exact equimolar stoichiometry of niclosamide–theophylline– CH_3CN (1:1:1) as theoretical and experimental weight loss are in good agreement (Figure 9). However NCL–CAF, NCL–URE and NCL–INA cocrystals showed single endotherm suggesting no decomposition before melting. All the cocrystals showed melting point in between that of API and coformer. There is no correlation between melting point and solubility (will be discussed later). Generally lower the melting point, better the solubility of API cocrystals.

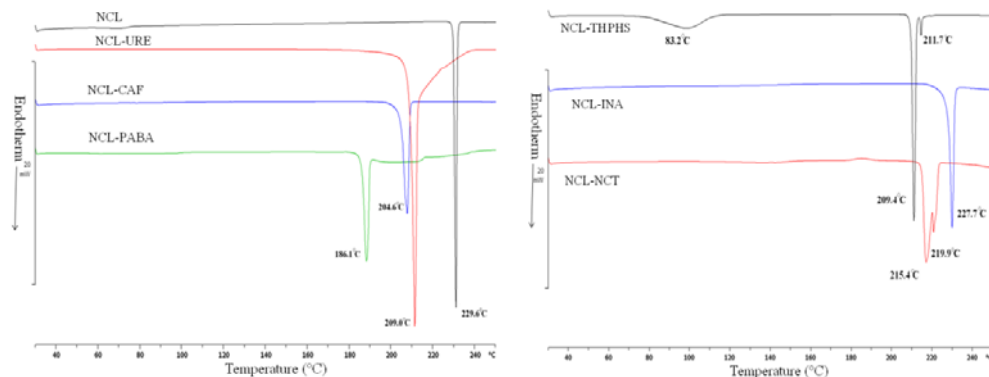


Figure 8 DSC endotherms of niclosamide and its cocrystals indicate new solid phases. The single endotherm at a temperature different from the melting points of the pure components is indicative of a homogeneous cocrystal phase. Caffeine (m.p. 227-228 °C), Urea (m.p. 132-135 °C), PABA (m.p. 187-189 °C), Theophylline (m.p. 270-274 °C), Nicotinamide (m.p. 128-131 °C), Isonicotinamide m.p. 157-158 °C).

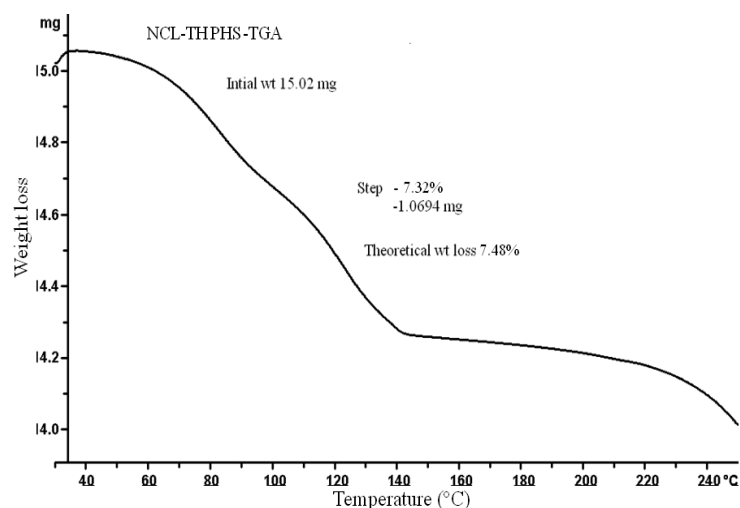


Figure 9 Thermogravimetric analysis (TGA) of Niclosamide–theophylline-CH₃CN cocrystal solvate (NCL–THPHS) indicates the exact stoichiometric ratio 1:1:1 of the cocrystals solvate.

6.3.4 FT-IR spectroscopy

Infrared spectroscopy^{8a,16} provides useful information about the vibrational modes of a compound, and these changes are due to the physical state of the sample and because of hydrogen bonding and molecular conformations. Generally phenolic–OH group absorbs strongly in the stretching frequencies of 3700-3584 cm⁻¹ regions. Intermolecular hydrogen bonding increases as the concentration of the solution increases,

and additional bands start to appear at lower frequencies, 3550-3200 cm^{-1} . According to Moffat et al,^{16c} principal peaks of niclosamide analyzed in a KBr disc appear at wave numbers 1572 (N-H bend), 1515 (NO_2 asymmetric), 1613 (C=C), 1650 (C=O), and 1218 (C-O) cm^{-1} . Niclosamide hydrate exhibits characteristic O-H peaks at 3490.4 and 3577.3 cm^{-1} . In the IR spectra (KBr disc) of the anhydrate and cocrystals, some of the bands were shifted relative to the pure API and coformers. The wave numbers of major bands are summarized in Table 3. A change in both carbonyl and amide stretching frequencies in the IR spectra of niclosamide cocrystals compared to individual components shows the formation of new solid phase (cocrystal). FT-IR Vibrational frequencies comparisons for NCL-NCT and NCL-INA cocrystals were displayed in Figure 10. Though single crystals could not be grown for NCL-NCT and NCL-INA cocrystals, IR spectra comparison suggest that new solid phases were obtained from liquid assisted grinding.

Table 3 FT-IR frequencies (vbar , cm^{-1}) of niclosamide and its cocrystals.

	O-H stretch	N-H stretch	N-H bend	C=C stretch	C=O stretch	C-O stretch	NO_2 sym Stretch
NCL	----	3242.7, 3199.5	1570.4	1613.5, 1588.9	1652.7	1217.9	1348.4, 1329.7
NCL Hyd	3577.3, 3490.4	3241.5, 3197.9	1569.7	1613.2, 1604.8	1680.1, 1652.9	1218.1	1348.2, 1328.3
NCL-CAF	--	3256.2	1556.5	1605.1, 1581.5	1705.3, 1674.9	1216.4	1340.0, 1323.3
NCL-URE	3491.6, 3438.5	3352.9, 3249.5	1545.0	1605.3	1673.9	1225.3	1342.9, 1321.1
NCL-PABA	3461.9	3364.1, 3253.9	1547.8	1606.6	1672.0	1217.7	1344.1, 1320.5
NCL-THPH	--	3260.4, 3160.6	1555.9	1601.4	1697.5, 1674.7	1218.7	1343.8, 1323.5
NCL-THPHS	--	3262.3,	1552.3	1604.0	1698.0,	1219.0	1340.3,

		3126.1		1673.0,		1321.4
				1639.5		
NCL-NCT	3409.0	3305.4,	1557.5	1607.4,	1737.2,	1225.0
		3235.8,		1582.6	1712.7,	1322.7
		3168.8		1665.0		
NCL-INA	3445.2	3237.3,	1560.7	1609.2,	1707.4,	1220.1
		3159.6		1583.2	1665.0	1323.8

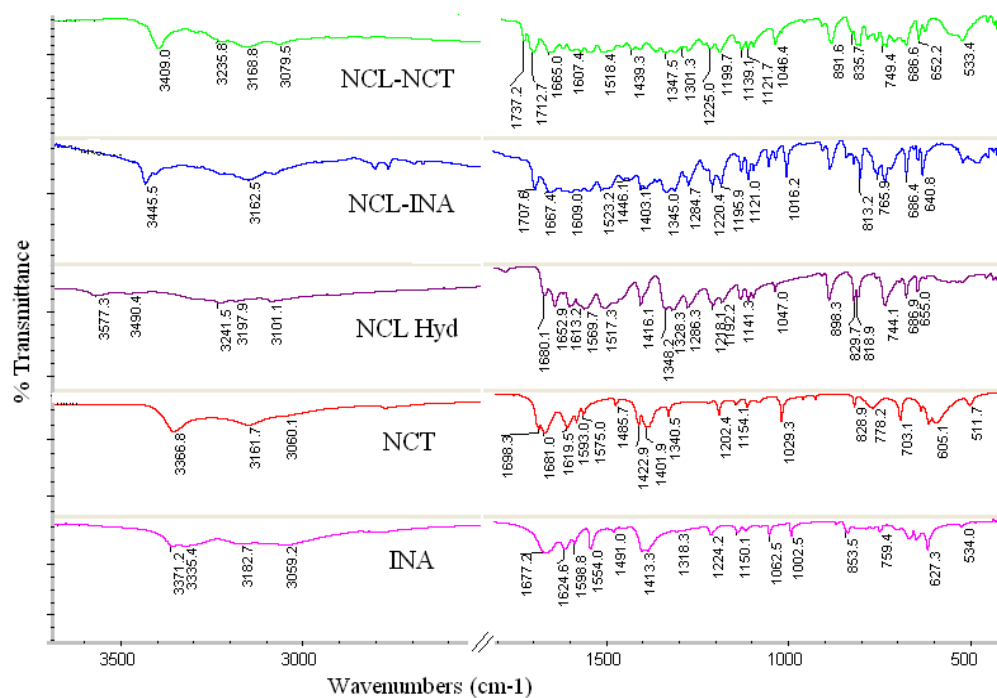


Figure 10 FT-IR spectra comparison between NCL-NCT, NCL-INA with coformers, indicated new solid phases prepared from wet granulation. There is no hydrate peak (1680 cm^{-1}) in the new solid phases.

6.3.5 Solid state NMR spectroscopy

Solid-state ^{13}C NMR spectroscopy¹⁷ provides structural information on differences in hydrogen bonding, molecular conformations, and molecular mobility. To confirm the purity as well as stoichiometry of the cocrystals, solution NMR were recorded in d^6 -DMSO solvent for NCL-NCT and NCL-INA cocrystals and further characterized by solid state ^{13}C NMR spectroscopy. Solid state NMR of API, coformers

as well as NCL–NCT and NCL–INA cocrystals were taken to compare and confirm the new solid phase (Figure 11). In NCL–NCT cocrystals, carbonyl carbon in niclosamide is deshielded from 161.7 ppm to 163.1 ppm and that for nicotinamide it is upfield from 168.9 ppm to 167.7. In NCL–INA cocrystal, carbonyl carbon in niclosamide is deshielded from 161.7 ppm to 164.9 ppm and that for isonicotinamide it is shielded from 171.8 ppm to 168.3. The change in chemical shift is certainly due to formation of new solid phase (cocrystal) and the change in the local molecular environment. Both solution and solid state NMR spectra suggest a 1:1 stoichiometry of NCL–NCT and NCL–INA cocrystals.

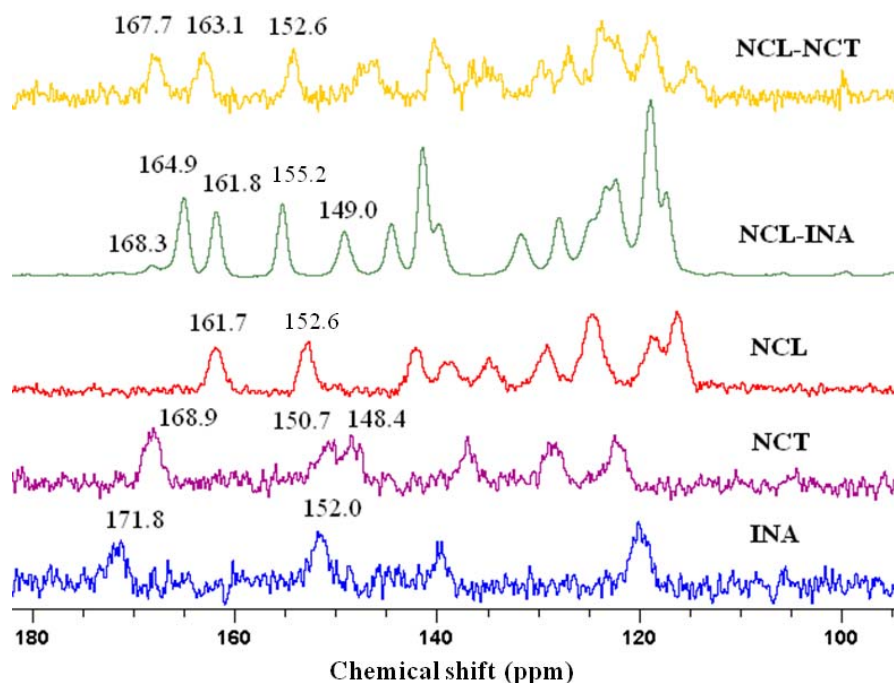


Figure 11 Solid state ^{13}C -NMR comparisons of NCL–NCT and NCL–INA cocrystals with API and coformers. Main differences are observed in the carbonyl region.

6.3.6 Solubility of niclosamide and its cocrystals

Most notably, cocrystallization is often used to modulate the solubility of an API. Whenever solubility is a limiting factor in the bioavailability of a compound, a change of solubility can produce drastic effects. Thus, we reasoned that niclosamide would be a good candidate through cocrystallization as its salt are difficult to prepare because of

absence of ionizable functional group in niclosamide. Since different crystal forms have different lattice energies and enthalpies, it follows that their solubility's must differ as well. Niclosamide is sparingly soluble (13 ± 3 mg/L) in water. Vantonder et al.^{8c} performed dissolution experiments of niclosamide and its monohydrates (H_A and H_B) in 40% isopropanol-water medium. Solubility of niclosamide increased to 43 mg/L in the alcohol-water mixture. Powder dissolution experiments of niclosamide and its cocrystals were carried out on *U.S. Pharmacopeia* (USP) approved dissolution tester in same medium by the rotating paddle method (rotation 100 rpm) after screening the material sieved to ~ 200 μm particle size. Powder dissolution curve for niclosamide and its cocrystals are shown in Figure 12. It should be noted that an increase in solubility may increase the tendency for phase transformation to occur. Here almost all the crystalline forms of niclosamide transform to monohydrate within 1 h of dissolution experiment. Absorbance peak at 221 nm was observed in UV-Vis spectrum indicative of niclosamide monohydrate formation. Among all the crystalline forms niclosamide–theophylline acetonitrile complex (NCL–THPHS) exhibited highest dissolution rate and solubility (223.1 mg/L at 2 h). Again NCL–THPH cocrystals showed comparable dissolution rate upto 90 min as the NCL–THPHS complex, and showed second highest solubility (181.2 mg/L) at 2 h of powder dissolution experiment. Rather NCL–CAF cocrystals showed intermediate solubility (108.4 mg/L) between NCL and NCL–THPHS complex. Other cocrystals NCL–URE, NCL–NCT and NCL–INA showed comparatively less solubility of 67.3 mg/L, 55.9 mg/L and 62.3 mg/L respectively. But NCL–PABA cocrystals had the least solubility (28.2 mg/L) lower than the API in dissolution experiment. In NCL–PABA cocrystals, intermolecular hydrogen bond distance between API and PABA is 1.82 Å which is weakest among all cocrystals and as a result cocrystals may dissociate faster and hydration lead to API resulting in low solubility of the drug. Among the cocrystals of niclosamide, NCL–THPHS complex and NCL–THPH cocrystals are 6.3 and 5.1 time more soluble than niclosamide at 2 h of dissolution. Recently Zaworotko et al.¹⁸ reported quercetin–caffeine (1:1) and quercetin–caffeine MeOH (1:1:1) cocrystal solvate increased the solubility of quercetin by 14 and 8-fold and bioavailability by 10 folds when compared to quercetin dihydrate. Generally solvates are not preferred in formulation for an API because of their instability and likelihood of phase transformation during storage. Here acetonitrile solvates are not stable enough at ambient condition and

also class II solvent¹⁹ (permissible concentration limit 410 ppm). Comparatively NCL-THPH cocrystals will be the best choice and also moderately stable at ambient condition (discussed next), which can be selected for further studies. Most drugs exert their therapeutic effect within 4-6-8 h of oral administration. It is suggested that more soluble cofomers improve solubility of the cocrystals.²⁰ In this case urea (solubility 1.1 g/ml) has highest solubility, but NCL-URE cocrystal showed only two times higher solubility than niclosamide. Again theophylline (solubility 8 mg/ml) is least soluble cofomer here, but NCL-THPH cocrystals showed highest solubility. All the new cocrystals showed less melting point than niclosamide. Similarly there is no correlation between melting point of the cocrystals and solubility for niclosamide cocrystals. E.g. NCL-PABA cocrystals have lowest melting point (186.1°C) and also least soluble cocrystals. Again NCL-INA cocrystals have highest melting point (227.7 °C), but are nearly two times more soluble.

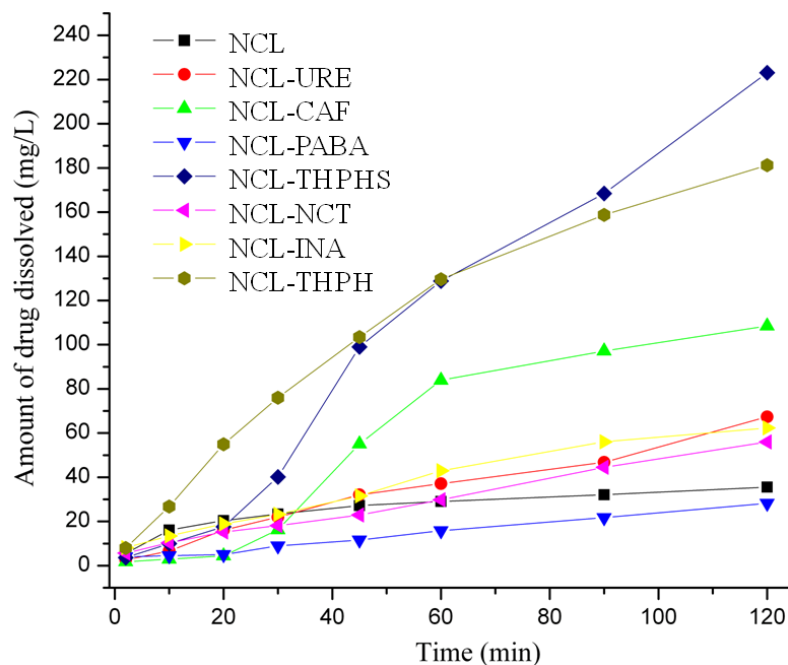


Figure 12 Powder dissolution of niclosamide and its cocrystals indicated that NCL-THPHS (1:1:1) complex exhibited highest dissolution rate in 40% isopropanol-water mixture, but NCL-THPH (1:1) cocrystals dissolved comparatively upto 90 min.

Solubility is a thermodynamic quantity and usually taken as the concentration of the solute at 24 or 48 h after mixing in a solvent. The solubility measurement is unsuited for those drug forms that are metastable and undergo phase transformation during the slurry conditions of dissolution. To obtain the equilibrium solubility, all crystalline forms (100 mg) were dissolved in a minimum amount (5 ml) of 40% isopropanol-water solvent and continued stirring for 24 h at 37 °C. Niclosamide showed higher solubility (43 mg/L) in alcohol-water mixture, which is nothing but solubility of niclosamide monohydrate after 24 h slurry experiment. The solubility from dissolution experiment at 2 h and solubility at 24 h for all forms are summarized in Table 4. It was observed that after 24 h, all crystalline forms converted to niclosamide monohydrate (H_A) (confirmed from IR spectroscopy) and for this reason solubility of all crystalline materials are very close.

Table 4 Solubility profile of niclosamide and its cocrystals

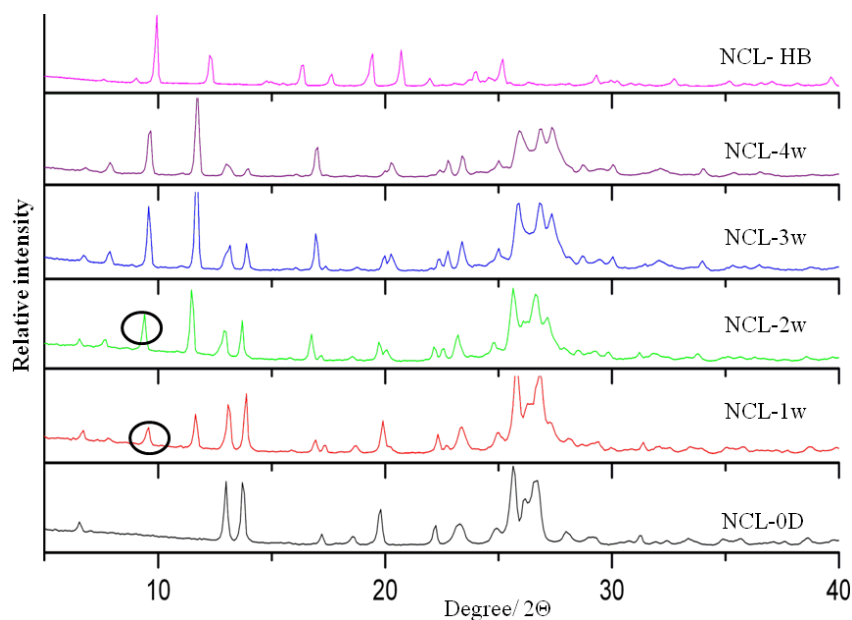
	Absorption coefficient ($\text{mM}^{-1} \text{cm}^{-1}$)	Solubility (mg/L) at 37°C (24h) in 40% Isopropanol-water	Solubility at 37 °C in 40% Isopropanol-water (mg/L) at 2h of dissolution ^a
NCL	16.95	42.8	35.53
NCL-CAF	19.18	56.7	108.45 (x 3.0)
NCL-URE	13.35	84.3	67.34 (x1.9)
NCL-PABA	19.89	32.8	28.22 (x 0.8)
NCL-THPH	13.01	60.4	181.19 (x5.1)
NCL-THPHS	16.02	56.2	223.09 (x6.3)
NCL-NCT	14.72	53.1	55.97 (x1.6)
NCL-INA	15.87	71.9	62.33 (x1.7)

^aNote 'n' fold increase of solubility compared to niclosamide kept in parenthesis

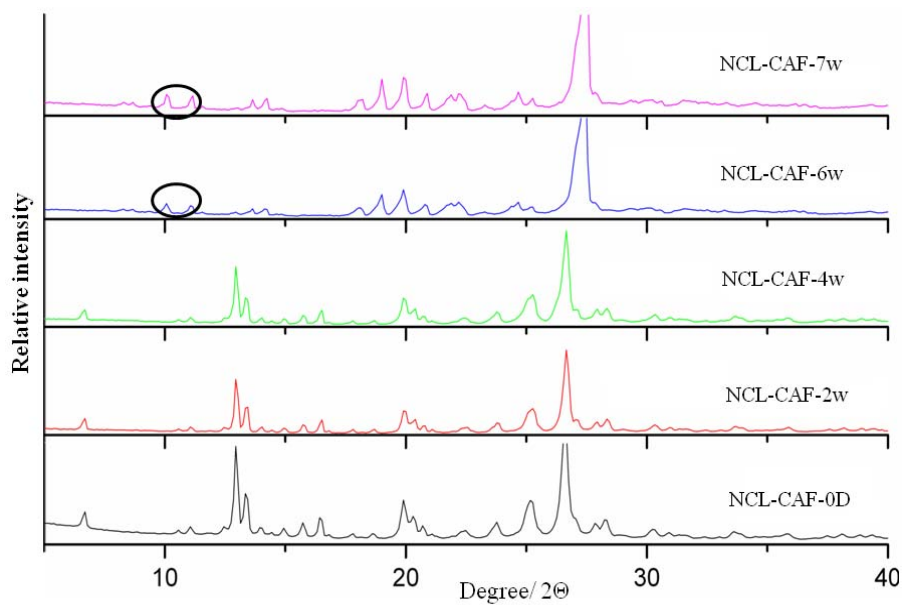
6.3.7 Physical form stability

Niclosamide has high tendency to convert to monohydrates even in solid state if kept at ambient condition (30-40 °C and 60-75% relative humidity) after 1 month. To prevent monohydrate formation, which has the lowest solubility (0.45 mg/L),^{8c} cocrystals were prepared because of their better solubility and stability. It is reported^{8a} that anhydrous niclosamide kept at 37 °C and 75% RH condition for 2 weeks converted to

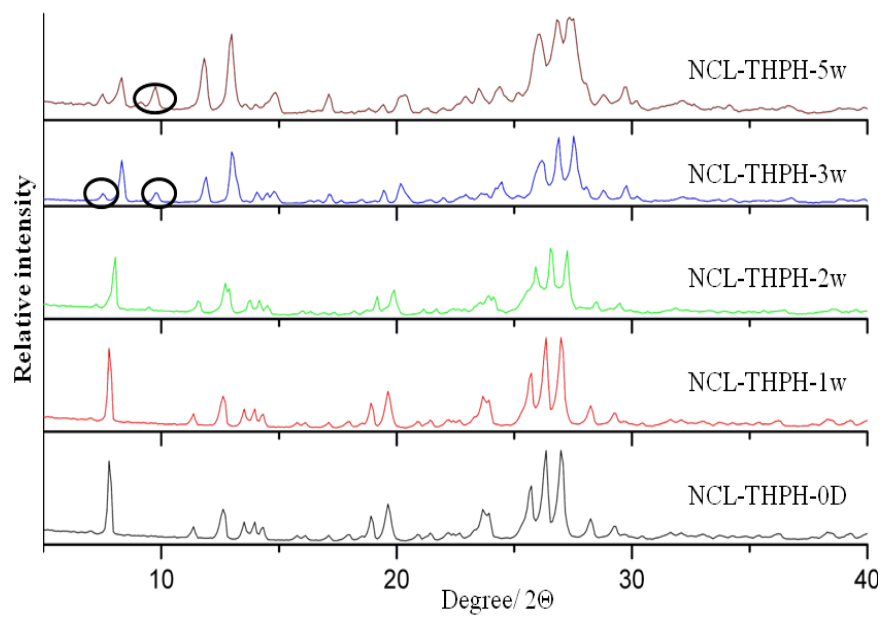
monohydrate as indicated by color change from colorless to green. At accelerated ICH conditions²¹ of 40 °C and 75% relative humidity both niclosamide and niclosamide-theophylline-CH₃CN complex converted to niclosamide monohydrate (H_B) within 1 week, as confirmed by PXRD. However PABA, urea and caffeine cocrystals were stable upto 2, 4 and 6 weeks respectively. NCL-THPH cocrystals are stable upto 2 weeks, and then hydrate formation started (from PXRD and DSC). There is a possibility of NCL-THPH-H₂O crystalline forms after 2-3 weeks kept in humidity chamber. But there is no hydrate formation for NCL-NCT and NCL-INA cocrystals upto 7 weeks in the same condition suggesting good stability against hydration. Humidity profile of niclosamide and its cocrystals are summarized in Table 5 and PXRD comparison of NCL, NCL-CAF, NCL-THPH and NCL-NCT cocrystals upto 7 weeks are displayed in Figure 13.



(a) NCL



(b)NCL-CAF



(c)NCL-THPH

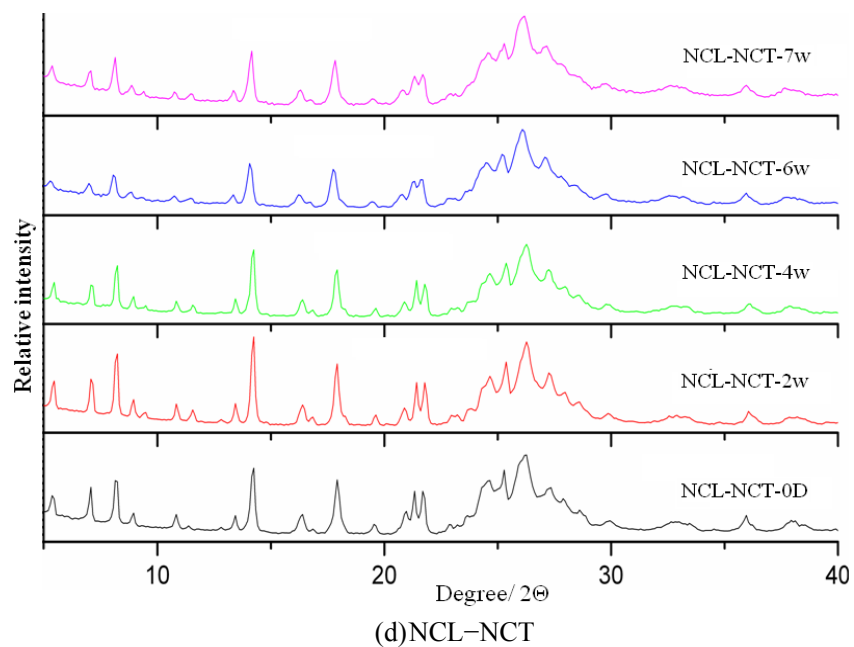


Figure 13 PXRD stacks of (a) NCL, (b) NCL–CAF and (c) NCL–THPH (d) NCL–NCT kept in accelerated Relative Humidity condition in different time interval. Peak at 7.86, 9.47, 10.37, 11.40, 16.83, 19.02 2θ value suggest the formation of niclosamide hydrate after 1 week. NCL–NCT cocrystals are stable upto 7 weeks.

Table 5 Relative humidity (40°C and 75%) study of Niclosamide and its cocrystals

	After 1W	After 2W	After 3W	After 4W	After 5W	After 6W	After 7W
NCL	X	X	X	X	X	X	X
NCL–CAF	√	√	√	√	√	X	X
NCL–URE	√	√	√	X	X	X	X
NCL–PABA	√	X	X	X	X	X	X
NCL–THPH	√	√	X	X	X	X	X
NCL–THPHS	X	X	X	X	X	X	X
NCL–NCT	√	√	√	√	√	√	√
NCL–INA	√	√	√	√	√	√	√

X=hydrate formation starts (not stable), √=No hydrate formation (stable)

6.4 Conclusion

The ability to tune the physical properties of a crystalline solid containing an API by introducing a pharmaceutically acceptable molecular species into a unique crystal lattice presents an opportunity to modify the properties of a solid-state dosage form at the molecular level. Niclosamide is almost insoluble in water. To modify its solubility and also stability, pharmaceutical cocrystals were prepared with GRAS molecules for the first time to our knowledge. Niclosamide is highly prone to solvate formation and one should be careful to make cocrystals by wet-granulation in presence of dry solvents. All the crystalline forms were characterized by spectroscopy, thermal analysis and X-ray diffraction. Intermolecular hydrogen bond between niclosamide molecules were interrupted in presence of coformers in the cocrystals results heterosynthon. Among the cocrystals, NCL–THPHS cocrystal acetonitrile solvates showed best dissolution rate (6 times), but highly prone to hydrate formation within 2-3 days under ICH conditions. NCL–THPHS cocrystal acetonitrile solvate suffers from the problem that acetonitrile is class II solvent and has limited toxicity. However NCL–THPH cocrystals showed second best dissolution rate (5 times) and also moderate stability (upto 2 weeks) towards hydration and may be the best choice for niclosamide formulation purpose. Except NCL–PABA, all cocrystals showed better dissolution rate as well as stability towards hydration. Search for new GRAS coformers with better improvement in solubility and stability will be studied. Particle size reduction for niclosamide is another approach to improve the solubility by increasing the surface area, free energy and solute-solvent interactions.

6.5 Experimental section

Niclosamide and other GRAS coformers were purchased from Sigma-Aldrich (Hyderabad, Andhra Pradesh, India) and used directly for experiments.

Niclosamide, NCL

Niclosamide crystals were obtained from sublimation at 190-200 °C. Good quality rectangular plate crystals appeared after 4-5 h. Single crystal can be obtained from AcOH solvent also. m.p. 229-230 °C.

Niclosamide–Caffeine cocrystal (NCL–CAF, 1:1)

100 mg (0.31 mmol) niclosamide and 59.4 mg (0.31 mmol) caffeine were ground in mortar-pestle for 15 min after adding 5 drops of dry EtOAc, and then kept for crystallization in 10 mL EtOAc. Suitable square block crystals appeared at ambient condition after 3-4 days. m.p. 204-206 °C

Niclosamide–Urea, cocrystal (NCL–UREA, 1:1)

100 mg (0.31 mmol) niclosamide and 18.4 mg (0.31 mmol) urea were ground in mortar-pestle for 15 min after adding 5 drops of dry EtOAc, and then kept for crystallization in 10 mL EtOAc. Suitable thick plate crystals were harvested at ambient condition after 3-4 days. m.p. 209-210 °C

Niclosamide–PABA cocrystal (NCL–PABA, 1:1)

100 mg (0.31 mmol) niclosamide and 41.9 mg (0.31 mmol) PABA were ground in mortar-pestle for 15 min after adding 5 drops of dry EtOAc, and then kept for crystallization in 10 mL EtOAc. Suitable block crystals were obtained at ambient condition after 3-4 days. m.p. 186-188 °C.

Niclosamide–Theophylline cocrystal (NCL–THPH, 1:1)

100 mg (0.31 mmol) niclosamide and 55.1 mg (0.31 mmol) theophylline were ground in mortar-pestle for 15 min after adding 5 drops of dry isopropyl acetate, and then kept for crystallization in 10 mL isopropyl acetate. Suitable block crystals were harvested at ambient condition after 3-4 days. m.p. 209-210 °C.

Niclosamide–Theophylline acetonitrile complex (NCL–THPHS, 1:1:1)

100 mg (0.31 mmol) niclosamide and 55.1 mg (0.31 mmol) theophylline were ground in mortar-pestle for 15 min after adding 5 drops of dry acetonitrile, and then kept for crystallization in 10 mL EtOAc acetate-acetonitrile (1:1) solvent mixture. Suitable block crystals appeared at ambient condition after 3-4 days. m.p. 209.4 °C. Desolvation temperature for acetonitrile solvate was 83.2 °C

Niclosamide–Nicotinamide (NCL–NCT, 1:1) and Niclosamide–Isonicotinamide (NCL–INA, 1:1) cocrystal

100 mg (0.31 mmol) niclosamide and 37.4 mg (0.31 mmol) nicotinamide/isonicotinamide were ground in mortar-pestle for 15 min after adding 5 drops of dry EtOAc. However no single crystal was obtained irrespective of solvents tried. ¹³C

Solution and ss-NMR suggest that both cocrystals consist of 1:1 of niclosamide and coformers. m.p. of NCL–NCT (1:1) and NCL–INA (1:1) are 215-216 and 227-229 °C respectively.

6.6 References

1. (a) S. L. Morissette, O. Almarsson, M. L. Peterson, J. F. Remenar, M. J. Read, A. V. Lemmo, S. Ellis, M. J. Cima and C. R. Gardner, *Adv. Drug Delivery Rev.*, **2004**, *56*, 275. (b) N. Blagden, M. de Matas, P. T. Gavan and P. York, *Adv. Drug Delivery Rev.*, **2007**, *59*, 617. (c) N. Schultheiss and A. Newman, *Cryst. Growth Des.*, **2009**, *9*, 2950 (d) W. Jones, W. D. S. Motherwell and A. V. Trask, *MRS Bull.*, **2006**, *31*, 875 (e) P. Vishweshwar, J. A. McMahon, J. A. Bis and M. J. Zaworotko, *J. Pharm. Sci.*, **2006**, *95*, 499. (f) B. S. Sekhon, *Ars Pharmaceutica*, **2009**, *50*, 99. (g) T. Friščić and W. Jones, *J. Pharm. Pharmacol.*, **2010**, *62*, 1547.
2. A. V. Trask, *Mol. Pharmaceutics*, **2007**, *4*, 301.
3. (a) S. Karki, T. Friscic, L. Fabian, P. R. Laity, G. M. Day and W. Jones, *Adv. Mater.*, **2009**, *21*, 3905. (b) C. C. Sun and H. Hou, *Cryst. Growth Des.*, **2008**, *8*, 1575.
4. (a) A. V. Trask, W. D. S. Motherwell and W. Jones, *Cryst. Growth Des.*, **2005**, *5*, 1013 (b) S. Basavoju, D. Boström and S. P. Velaga, *Pharm. Res.*, **2008**, *25*, 530. (c) S. Cherukuvada, N. J. Babu and A. Nangia, *J. Pharm. Sci.*, **2011**, *100*, 3233.
5. (a) D. J. Good and N. Rodriguez-Hornedo, *Cryst. Growth Des.*, **2010**, *10*, 1028. (b) D. J. Good and R.-H. Naír, *Cryst. Growth Des.*, **2009**, *9*, 2252. (c) D. P. McNamara, S. L. Childs, J. Giordano, A. Iarriccio, J. Cassidy, M. S. Shet, R. Mannion, E. O'Donnell and A. Park, *Pharm. Res.*, **2006**, *23*, 1888. (d) Z. J. Li, Yu. Abramov, J. Bordner, J. Leonard, A. Medek and A. V. Trask, *J. Am. Chem. Soc.*, **2006**, *128*, 8199. (e) K. Shiraki, N. Takata, R. Takano, Y. Hayashi and K. Terada, *Pharm. Res.*, **2008**, *25*, 2581. (f) N. J. Babu and A. Nangia, *Cryst. Growth Des.*, **2011**, *11*, 2662.
6. (a) C. Lipinski, *Amer. Pharm. Rev.*, **2002**, *5*, 82. (b) D. L. Prohotsky, F. Zhao, *J. Pharm. Sci.* **2012**, *101*, 1.
7. (a) Generally Regarded as Safe: <http://www.cfsan.fda.gov/~rdb/opa-gras.html> and <http://www.cfsan.fda.gov/~dms/grasguid.html> (b) Everything Added to Food Stuff in the United States: [Http://vm.cfsan.fda.gov/~dms/eafus.html](http://vm.cfsan.fda.gov/~dms/eafus.html).

8. (a) E. C. Vantonder, M. D. Mahlatji, S. F. Malan, W. Liebenberg, M. R. Cairn, M. Song, M. M. D. Villers, *J crystal growth* **2004**, 5, 1. (b) M. R. Cairn, E. C. Vantonder, M. M. D. Villers, A. P. Lötter, *J inclusion phenom & mol recogn Chem.* **1998**, 31, 1. (c) E. C. Vantonder, T. S. P. Maleka, W. Liebenberg, M. Song, D. E. Wurster, M. M. D. Villers, *Int. J. pharm.* **2004**, 269, 417. (d) M. M. D. Villers, M. D. Mahlatji, E. C. Vantonder, S. F. Malan, A. P. Lötter, W. Liebenberg, *Drug dev & Indust. pharm.* **2004**, 30, 581. (e) C. -J. Wu, J.-T. Jan, C. -M. Chen, H. -P. Hsieh, D. -R. Hwang, H.-W. Liu, C. -Y. Liu, H. -W. Huang, S. -C. Chen, C. -H. Hong, R. -K. Lin, Y.-S. Chao, J. T. A. Hsu, *Eur. J. Pharm. & Biopharm.*, **2004**, 58, 265.
9. M. Lindenberg, S. Kopp, J. B. Dressman, *Eur. J. Pharm. & Biopharm.*, **2004**, 58, 265.
10. British Pharmacopeia, **1993**. Her Majesty's Stationary Office, London, p. 445. (b) E. C. Van Tonder, **1996**. Preparation and characterization of niclosamide crystal modifications. Ph.D. Thesis, Potchefstroom University for CHE, South Africa. (c) T.S.P. Maleka, **2000**. Aqueous adsorption and desorption behaviour of niclosamide anhydrate and monohydrates. M.Sc.
11. (a) A. M. Campeta, B. P. Chekal, Y. A. Abramov, P. A. Meenan, M. J. Henson, B. Shi, R. A. Singer, K. R. Horspool, *J Pharm. Sci.* **2010**, 99, 3874. (b) R. G. Cantera, M. G. Leza, C. M. Bachiller, *J Pharm. Sci.* **2002**, 91, 2240.
12. (a) K. Ding, D. Pei, J. Zhou, Euro Patent No. CN101775032 (A), **2010**. (b) D. J. A. Zhang, Euro Patent No. CN101006778 (A), **2007**.
13. B. Sarma, S. Roy, A. Nangia, *ChemCommun*, **2006**, 4918. (b) B. Sarma, P. Sanphui, A. Nangia, *Cryst. Growth Des.* **2010**, 10, 2388. (c) G. S. McGrady, M. Odlyha, P. D. Prince, J. W. Steed, *CrystEngComm* **2002**, 4, 271. (d) J. L. Atwood, L. J. Barbour, A. Jerga, B. L. Schottel, *Science* **2002**, 298, 1000.
14. (a) J. Grell, J. Bernstein, G. Tinhofer, *Acta Cryst* **1999**, B55, 1030. (b) J. Bernstein, R. E. Davis, L. Shimon, N. -L. Chang, *Angew. Chem.Int. Ed.* **2003**, 34, 1555.
15. (a) D. Mullen, V. Hellner. *Acta Cryst* **1978**, B34, 1624. (b) M. D. Hollingsworth, M. E. Brown, B. S. Santeriero, J. C. Huffman, C. R. Goss, *Chem Mater.* **1994**, 6, 1227.
16. (a) B. H. Stuart, *Infrared Spectroscopy: Fundamentals and Applications*, **2004**, John-Wiley, UK. (b) M. A. Moffat, J. V. Jackson, M. S. Moss, B. Widdop, eds. Clarke's

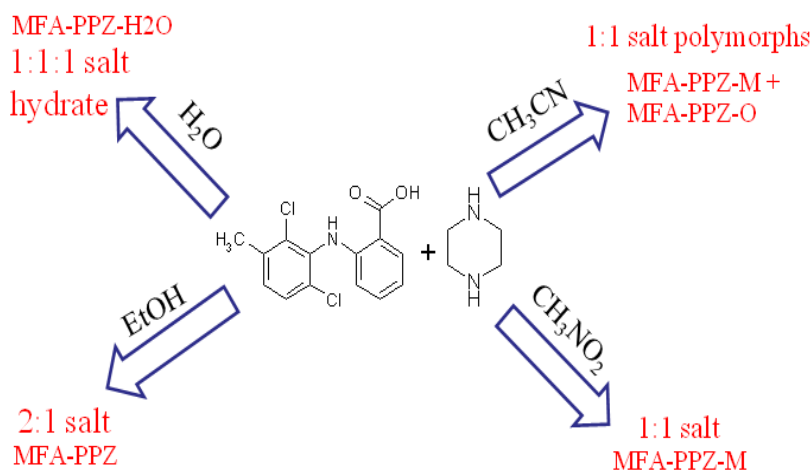
Isolation and Identification of Drugs in Pharmaceuticals, Body Fluids, and Post Mortem Materials. 2nd ed. London, UK: pharmaceutical Press; **1986**.

17. (a) F. G. Vogt, J. S. Clawson, M. Strohmeier, A. J. Edwards, T. N. Pham, S. A. Watson, *Cryst. Growth Des.* **2009**, 9, 921. (b) P. A. Tishmack, D. E. Bugay, S. R. Byrn, *J. Pharm. Sci.* **2002**, 92, 441. (c) N. R. Goud, S. Gangavaram, K. Suresh, S. Pal, S. G. Manjunatha, S. Nambiar, A. Nangia, *J. Pharm. Sci.* **2012**, 101, 664.
18. A. J. Smith, P. Kavuru, L. Wojtas, M. J. Zaworotko, and R. D. Shytle, *Mol. Pharaceutics*, **2011**, 8, 1816.
19. http://www.ema.europa.eu/docs/en_GB/document_library/Scientific_guideline/2009/09/WC500002674.pdf
20. (a) S. L. Childs, K. I. Hardcastle, *Cryst. Growth Des.* **2007**, 7, 1291. (b) R. Banerjee, P. M. Bhatt, N. T. Ravindra, G. R. Desiraju, *Cryst. Growth Des.* **2005**, 5, 2299. (c) Z. J. Li, Y. Abramov, J. Bordner, J. Leonard, A. Medek, A. V. Trask, *J. Am. Chem. Soc.* **2006**, 128, 8199. (d) P. Sanphui, N. R. Goud, U. V. R. Khandavilli, A. Nangia, *Cryst. Growth Des.*, **2011**, 11, 4135.
21. (a) http://www.ema.europa.eu/docs/en_GB/document_library/Scientific_guideline/2009/09/WC500002651.pdf. (b) ICH harmonized guideline, Q1A (R2) stability testing of new drug substances and products, 2003.

Chapter Seven

High Solubility Piperazine Salts of NSAID

Meclofenamic Acid



Piperazinium meclofenamate salts of variable stoichiometry obtained by liquid-assisted grinding. The monoclinic 1:1 salt exhibited the highest dissolution rate, comparable to meclofenamate sodium.

7.1 Introduction

Solid dosage forms of a drug are desirable because of ease of handling and lower production and storage costs. An understanding of the solid state properties of crystalline and amorphous forms of an active pharmaceutical ingredient (API) are therefore extremely important in the development of a new drug.¹ Accordingly, there has been a tremendous impetus to identify novel polymorphs, solvates (pseudopolymorphs), salts, and cocrystals of APIs.² The scientific importance arises from the fact that new API solid forms are designed to have better solubility, stability, and/or bioavailability. The legal significance arises from the fact that novel polymorphs, solvates, cocrystals, and salts can be used by industry to introduce generic versions of a drug in the regulated market. These matters are of great concern to innovator and generic pharmaceutical companies worldwide. Solubility and bioavailability of an API are important, even though they are not directly correlated. Solubility is a thermodynamic parameter whereas bioavailability is kinetic dissolution in aqueous medium APIs have been formulated as salts to change the solubility (increase or decrease) and/or obtain better bioavailability.

About 40% of new molecular entities coming out of the drug discovery pipeline will never advance in the development chain because of biopharmaceutical issues, such as poor aqueous solubility, low dissolution rate, low permeability, and first-pass metabolism in the liver. An enhancement of drug solubility for therapeutic agents can improve their bioavailability. Identifying the optimum solid form of an active pharmaceutical ingredient (API) is always desirable for clinical use. Over 80% of all drugs are marketed as tablets and oral administration is the most preferred drug delivery route. An estimated half of all drug molecules used in medicine are administered as salts so that the formation and the selection of a suitable salt for a drug candidate are recognized as essential steps in the preclinical phase of modern drug development.³ Crystal engineering is particularly well suited to co-crystallization of drugs with safe cofomers.⁴ The advantage of cocrystals and salts for improving physical properties is that the structure of the drug molecule is unchanged but the modification is at the supramolecular level (intermolecular interactions, hydrogen bonding, molecular packing).⁵ A practical advantage is that the extent of solubility enhancement for

cocrystals (4-20 times) is an order of magnitude higher than that for polymorphs (2-3 times). Pharmaceutical salts of course are the most preferred formulation for solubility enhancement (100-1000 times).⁶ On the down side, salts are more likely to form hydrates (often a drawback in terms of stability) compared to cocrystals. The ΔpK_a rule, wherein $\Delta pK_a = pK_a(\text{conjugate acid of base}) - pK_a(\text{acid})$, is a useful guide to know beforehand if an acid–base complex will give a neutral cocrystal ($\Delta pK_a < 3$) or an ionic salt ($\Delta pK_a > 3$). A more practical cut-off for organic salts is $\Delta pK_a < 0$ for cocrystal, $\Delta pK_a > 3$ for salts, and the range $0 < \Delta pK_a < 3$ being an unpredictable zone wherein different proton states could be observed depending on the external conditions.⁷

7.2 Meclofenamic acid

Meclofenamic acid⁸ (Figure 1) is a nonsteroidal anti-inflammatory, antipyretic, analgesic drug used in the treatment of postoperative and traumatic inflammation and swelling by the inhibition of prostaglandin biosynthesis pathway. Twisted conformation in meclofenamic acid (discussed later) was believed to have a proper fit to the receptor site of the enzyme arachidonic acid cyclooxygenase.^{8a} It is a selective cyclo-oxygenase-2 (COX-2) inhibitor.^{8b} Similar to diclofenac, meclofenamic acid is also used as a KCNQ2/Q3 potassium channel opener, depression of cortical neuron activity, and exhibits anticonvulsant activity.^{8c} Meclofenamic acid has a transient effect on platelet aggregation, but unlike aspirin, it does not cause bleeding.^{8h} It is a BCS class II drug of low solubility (30 mg/L) and high permeability ($\log P_{ow} = 5$).⁹ Novel gel and cream formulation of meclofenamic acid provide maximal topical activity to the drug.^{8c} Exposure of dilute solutions of meclofenamic acid to visible or UV light resulted in fairly rapid decomposition.^{8f} Due to its low aqueous solubility⁹ and thus bioavailability, the sodium salt of meclofenamic acid (solubility >250 g/L)^{9b} is marketed as 100 mg capsules under brand names Meclomen, Melvon, Movens, and Arquel. Fábán et al.^{10a} recently published cocrystals of flufenamic acid, niflumic acid, tolfenamic acid and mefenamic acid with nicotinamide, but they mentioned some difficulty with meclofenamic acid. Aakeröy^{10b} reported cocrystals of diclofenac with 2-aminopyrimidines, 2-amino-4,6-dimethylpyrimidine and 2-amino-4-chloro-6-methylpyrimidine characterized by X-ray diffraction, DSC and IR spectroscopy. During the late stages of our results on meclofenamic acid, Fini et al.^{10c} reported salts of

diclofenac with cyclic aliphatic amines and their thermal behavior. Our results on cocrystals and salts of meclofenamic acid demonstrate that organic salts of API's can exhibit comparable dissolution rate to traditional metal ion salts. The novel cocrystals and salts of meclofenamic acid with isonicotinamide, 4,4'-bipyridine, piperazine, aminopyridine, etc. were prepared by solvent-assisted grinding and their solubility was measured in a USP dissolution tester. Crystal structures, phase transformations, and solubility of meclofenamic acid cocrystals and salts are discussed in this chapter.¹¹

7.3 Results and Discussion

The sodium salt of meclofenamic acid (MFA) was obtained from Sigma-Aldrich, India and converted to the free acid with aq. HCl. The Na salt of MFA is readily soluble in water. Vijayan et al^{12a} (1981) published the first crystal structure of meclofenamic acid but it had a high R-factor of 0.135. The same authors reported crystal structure of the 1:1 complex of MFA with choline hydrate and ethanolamine.^{12b} The disorder in the methyl group orientation of meclofenamic acid (Figure 1) persisted at low temperature. We have now obtained good quality single crystals of MFA by sublimation and collected data at 298 K and 100 K. There are no reports on crystal structures of meclofenamic acid and its salt/ cocrystal in the interim period. Crystallographic parameters for all crystal structures are listed in Table 1.

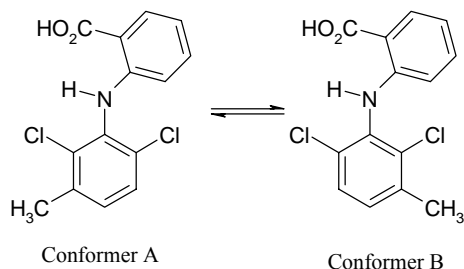


Figure 1 Two conformers (A and B) of meclofenamic acid (MFA) present in crystals structures.

7.3.1 Crystal structure description

Meclofenamic acid (MFA)

Meclofenamic acid consists of two aryl moieties, the N-2,6-dichloro-3-methylphenyl group and the N-2-benzoic acid group. The aryl rings are twisted almost in a perpendicular orientation of 82° dihedral angle between the two ring planes. This twist relieves steric congestion of ortho-substituted phenyls at the secondary amine. Meclofenamic acid was crystallized by slow sublimation at $190\text{--}200^\circ\text{C}$ over 4–5 h to afford diffraction quality single crystals which solved in the triclinic space group $P\bar{1}$ with one molecule in the asymmetric unit. Similar to other fenamic acids, e.g. mefenamic acid and tolfenamic acid,¹³ two meclofenamic acid molecules form a centrosymmetric carboxylic acid dimer of $\text{O}\cdots\text{O}$ hydrogen bond ($\text{O}\cdots\text{O}$, $2.632(4)$ Å) in $R_2^2(8)$ ring motif.¹⁴ An intramolecular $\text{N}\cdots\text{O}$ hydrogen bond ($\text{N}\cdots\text{O}$, $2.679(4)$ Å) of $R_1^1(6)$ ring motif (Figure 2a) rigidifies the molecule. Hydrogen bond parameters in crystal structures are listed in Table 2. The 3-methyl group is disordered over two positions with unequal site occupancy factor (s.o.f. conformer B = $0.58(1)$ and A = $0.42(1)$, see Figure 1) at 298 K (RT structure). X-ray reflections for meclofenamic acid crystal were collected at 100 K (LT structure) in an attempt to resolve the disorder issue (R-factor 0.110). The disorder of Me group persisted, now with s.o.f. of conformer B = $0.577(15)$ and A = $0.423(15)$. The elongated thermal ellipsoid of Cl2 (chlorine atom 2) perpendicular to the aromatic plane in the RT structure could be modeled as Cl2A and Cl2B (chlorine 2A and 2B) with s.o.f. of $0.55(3)$ and $0.45(3)$ in the LT structure (Figure 2b). The RT structure of MFA is described in this paper because it has better refinement parameters and lower R-factor (0.083).

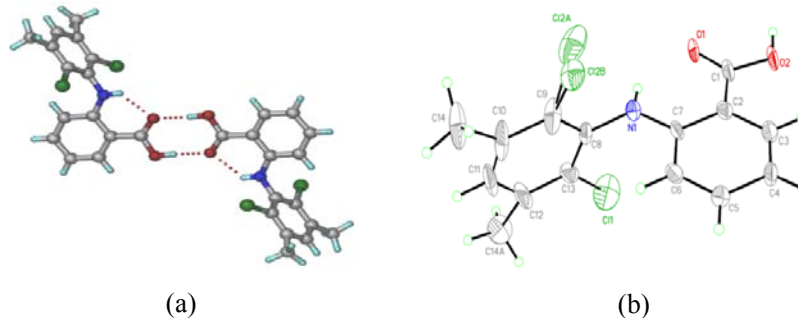


Figure 2 (a) Centrosymmetric carboxylic acid dimer is present in MFA. The methyl group is disordered in the crystal structure of meclofenamic acid with s.o.f. $0.58(1)$ and $0.42(1)$. (b) ORTEP diagram of MFA at 100K suggests that Me and one of the $-\text{Cl}$ atom are disordered.

Meclofenamic acid–Isonicotinamide cocrystal (1:1, MFA–INA)

Meclofenamic acid–isonicotinamide (1:1) cocrystal was prepared by solid-state grinding and the resulting solid was crystallized from acetonitrile to afford the single crystal X-ray structure in monoclinic space group $P2_1/c$, which contained conformer A of MFA. The carboxylic acid dimer in the reference drug crystal structure is replaced by carboxylic acid–pyridine heterosynthon ($O\cdots N$, 2.657(4) Å, $\angle O-H\cdots N$, 174°) as the main bimolecular $R_2^2(7)$ ring motif (Figure 3a). Isonicotinamide molecules aggregate via the carboxamide dimer ($N\cdots O$, 2.926(4) Å, $\angle N-H\cdots O$, 169°) at the secondary level. Such 4-molecule supramolecular units are connected via $C-Cl\cdots O$ interaction (3.254 Å) in a ladder motif along the b -axis (Figure 3b).

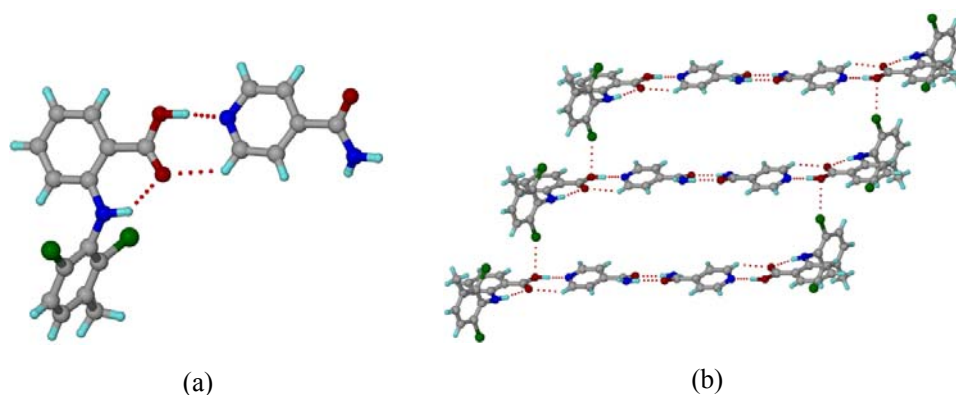


Figure 3 (a) Acid–pyridine heterosynthon in MFA–INA (1:1) cocrystal. (b) Acid–pyridine heterosynthon, amide dimer homosynthon and $C-Cl\cdots O$ interaction along the b -axis in crystal structure.

Meclofenamic acid–4,4'-Bipyridine cocrystal (1:0.5, MFA–BPY)

Meclofenamic acid–4,4'-bipyridine (1:0.5) cocrystal (crystallized from acetonitrile) was solved in monoclinic space group $P2_1/c$ and contains meclofenamic acid conformer A. The acid–pyridine heterosynthon ($O\cdots N$, 2.668(4) Å, $\angle O-H\cdots N$, 178°; $R_2^2(7)$ ring motif) is supported by an auxiliary $C-H\cdots O$ hydrogen bond ($C\cdots O$, 3.194(6) Å) between the pyridine ortho $C-H$ to the carbonyl of carboxylic acid (Figure 4a). The trimolecular units in the cocrystal make a step ladder motif along the c -axis

(Figure 4b). Meclofenamic acid–4,4'-bipyridine (1:1) is a cocrystal based on C–O bond distances of 1.215(8) Å and 1.316(7) Å in the carboxylic acid group and $\angle\text{C–N–C}$ bond angle of 115.7(6)° in the pyridine ring.

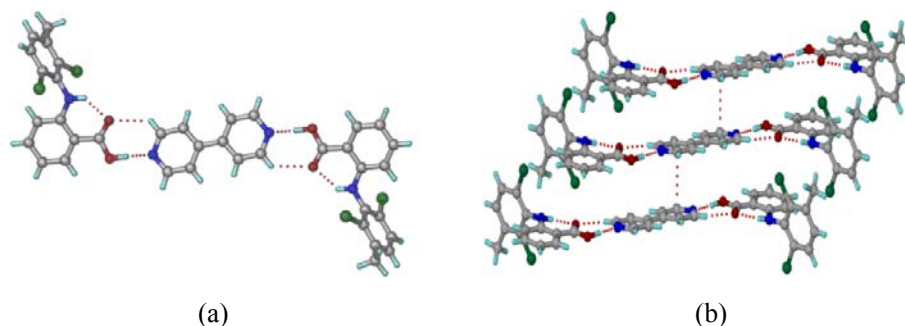


Figure 4 (a) Acid–pyridine heterosynthon form termolecular unit in MFA–BPY (1:0.5) cocrystal structure. (b) Ladder structure along the *c*-axis.

Piperazinium meclofenamate salt polymorphs (1:1, MFA–PPZ-M and MFA–PPZ-O)

Piperazinium meclofenamate salt (1:1) crystallized as monoclinic ($P2_1/c$) and orthorhombic ($P2_12_12_1$) polymorphs concomitantly obtained from acetonitrile solvent. There is one molecule each of meclofenamate anion (conformer B) and piperazinium cation in the asymmetric unit of monoclinic polymorph. Compared to the cocrystal, proton transfer occurred in the salt structure from carboxylic acid to the N–H base of piperazine. In the monoclinic structure (MFA–PPZ-M), each piperazinium cation forms four hydrogen bonds with two meclofenamates and two piperazinium cations through ionic $\text{N}^+ \cdots \text{H} \cdots \text{O}^-$ ($\text{N} \cdots \text{O}$, 2.677(4) Å) and neutral $\text{N–H} \cdots \text{N}$ ($\text{N} \cdots \text{N}$, 2.851(4) Å) and $\text{N–H} \cdots \text{O}$ ($\text{N} \cdots \text{O}$, 2.949(4) Å) hydrogen bonds (Figure 5a). The carboxylate C–O bond distances are 1.236(4) Å and 1.271(4) Å and piperazinium $\angle\text{C–N–C}$ is 112.0(4)° suggesting an ionized species. The C–O bond distances difference (ΔCO) is less than 0.1 Å compared to the neutral species.

The packing of meclofenamate anions (conformer A) and piperazinium cations is similar in the orthorhombic polymorph (MFA–PPZ–O). Each piperazinium cation forms four hydrogen bonds with two meclofenamate anions and two piperazinium cations through $\text{N}^+ \cdots \text{H} \cdots \text{O}^-$ (2.698(3) Å), $\text{N–H} \cdots \text{N}$ (2.858 (3) Å), and $\text{N–H} \cdots \text{O}$ (2.960 (3) Å) hydrogen bonds (Figure 5b). C–O bond distances (1.226(6) Å,

1.263(5) Å) and $\angle\text{C-N-C}$ angle ($111.8(3)^\circ$) are consistent with a salt species.⁷ In both polymorphs, six piperazine cations are sandwiched between three meclofenamate anions along the *c*-axis. A minor difference between the two polymorphs is the orientation of the methyl group in meclofenamic acid, i.e. conformer A or B. Piperazine is a small cyclic secondary diamine that is pharmaceutically acceptable and has anthelmintic activity.¹⁵ Piperazine ($\text{p}K_a = 9.72$) can act both as a neutral and a cationic coformer to give a cocrystal or salt product with an acidic API. The Cambridge Structural Database (CSD ver. 5.32, 2010, November 2011 update)¹⁶ contains about 20 organic cocrystals and 25 salts or salt hydrates of piperazine. Surprisingly there is only one piperazinium monocation (Refcode CUKVOU) listed with a carboxylate counterion up to the recent update of the CSD; there are 73 refcodes for piperazinium dication. We report three piperazinium monocations with meclofenamate anion in MFA-PPZ-M, MFA-PPZ-O and MFA-PPZ-H₂O (will be discussed next) crystal structures. Furthermore, there are no examples of piperazine salts which are polymorphic. MFA-PPZ (1:1) is the first example of piperazine salt polymorphs with 3D coordinates determined. Crystal density ($1.312, 1.381 \text{ g cm}^{-3}$), packing fraction (64.2, 68.0%, calculated in Platon), and lattice energy ($-176.93, -186.39 \text{ kcal mol}^{-1}$, calculated using Compass force field in Cerius²)¹⁷ of monoclinic and orthorhombic polymorphs suggest that the orthorhombic form should be more stable. However, DSC measurements (discussed later) indicate that melting point of the monoclinic form is higher and we show that MFA-PPZ-M is the stable polymorph.

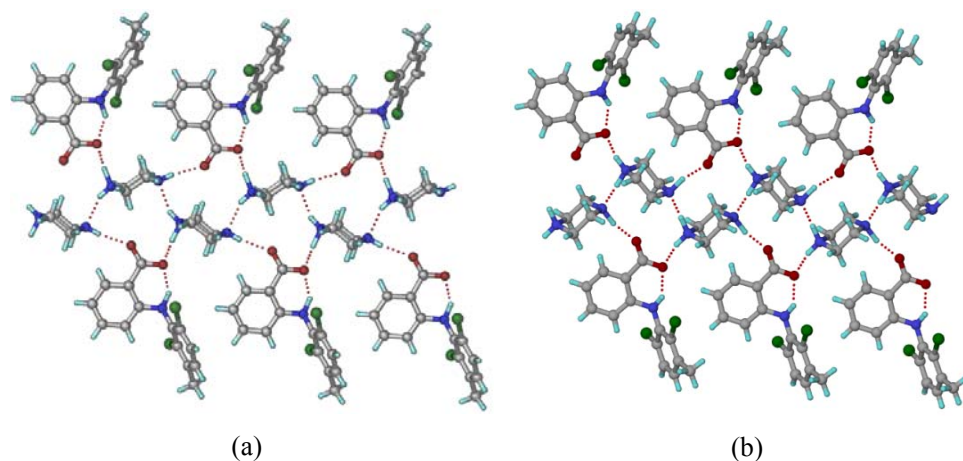


Figure 5 Crystal packing in (a) monoclinic form of MFA-PPZ-M (1:1) viewed along

the *b*-axis, and (b) orthorhombic polymorph MFA–PPZ–O (1:1) along the *a*-axis. The main difference is in the orientation of Me group in MFA, i.e. conformer B (in M) and A (in O).

Piperazinium meclofenamate salt (2:1, MFA–PPZ)

Piperazinium meclofenamate salt (2:1) was obtained when the components were ground with a few drops of EtOH added. The crystal structure of MFA–PPZ (2:1) was solved in *P*-1 space group with two crystallographic meclofenamate anions (conformer A and B) and two half nonequivalent piperazinium cations in the asymmetric unit. The two conformers of MFA are arranged in an alternate fashion ABAB parallel to the *b*-axis and piperazinium cations are sandwiched between the anions. Each piperazinium dication forms four $N^+-H\cdots O^-$ ionic hydrogen bonds ($N3^+-H3A\cdots O1^-$, 2.690(3) Å; $N3^+-H3B\cdots O4^-$, 2.731(3) Å; $N4^+-H4A\cdots O2^-$, 2.750(3) Å and $N4^+-H4B\cdots O3^-$, 2.695(3) Å with meclofenamate anions A and B (shown in thick bond and ball and stick models, Figure 6). This is the only crystal structure of MFA salts with both conformers A and B in the same lattice.

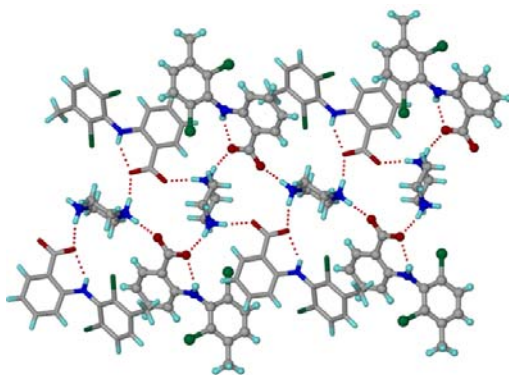


Figure 6 Two crystallographic molecules of meclofenamate (A = thick bond, B = ball-stick) and two half molecules of piperazine cations form $N^+-H\cdots O^-$ hydrogen bonds in the 2:1 salt of MFA–PPZ.

Piperazinium meclofenamate salt hydrate (1:1:1, MFA–PPZ–H₂O)

Piperazinium meclofenamate salt hydrate (1:1:1) was obtained during grinding of meclofenamic acid with piperazine hydrate or meclofenamic acid and piperazine in the presence of water. It crystallized in the monoclinic space group *P*2₁/c with conformer B. Two meclofenamate anions and two water molecules form ring motif of

graph set notation $R_4^4(12)$. Water molecules are present as spacers between two meclofenamates. Two piperazinium cations form $N^+-H\cdots O$ hydrogen bond ($N2^+-H2\cdots O3$, 3.029(4) Å) with water (Figure 7a). The $N-H\cdots N/O$ hydrogen bond network ($N3^+-H1B\cdots O1^-$, 2.842(4) Å, $N3^+-H1A\cdots N2$, 2.939(4) Å) is shown in Figure 7b. Water molecules reside in channels along the c -axis (Figure 7c). Thermogravimetric analysis (TGA) confirmed the stoichiometry as a monohydrate (calc. 4.68%, obsd. 4.71%). A mefenamic acid piperazine salt hydrate (2:1:4) was recently reported,¹⁸ but its crystal structure is completely different from our results because of hydrogen bonding to four water molecules.

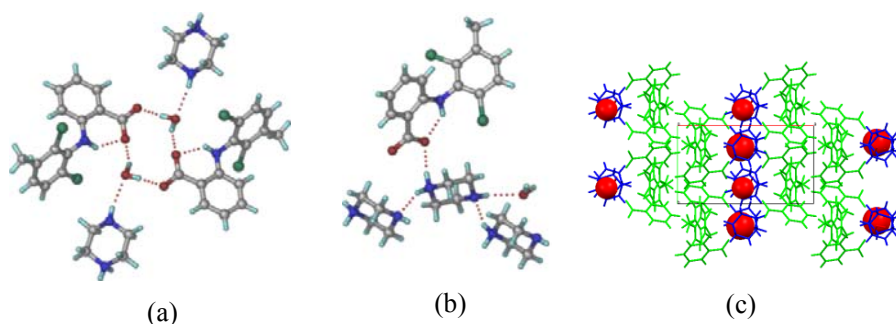


Figure 7 (a) Tetramer $R_4^4(12)$ ring motif between two meclofenamate anions and two water molecules in MFA-PPZ- H_2O (b) A piperazinium cation is surrounded by two similar cations, one water molecule, and one meclofenamate anion. (c) Water molecules are present in channels along the c -axis.

2-Aminopyridinium meclofenamate salt (1:1, MFA-2-APY)

The organic cation and anion form $R_2^2(8)$ ring motif between aminopyridinium and carboxylate via $N-H\cdots O$ bonds ($N\cdots O$, 2.642(3) Å, 2.841(3) Å). Such dimer units are connected via amino $N-H\cdots O$ ($N\cdots O$ 2.897(3) Å) hydrogen bond (Figure 8a). The molecular packing extends via $Cl\cdots Cl$ type I interaction (3.472(2) Å, $\theta_1 = \theta_2 = 135.8^\circ$) and $C-H\cdots Cl$ interaction ($H\cdots Cl$, 2.92(3) Å) in a zigzag chain along the b -axis (Figure 8b). Carboxylate $C-O$ bond distances (1.252(3), 1.263(3) Å) and pyridinium $\angle C-N-C$ bond angle ($121.7(2)^\circ$) are consistent with a salt structure.

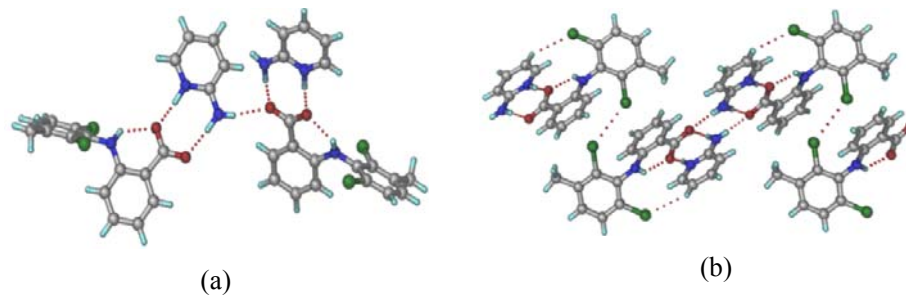


Figure 8 (a) Pyridine (NH^+) \cdots OOC^- synthon in MFA-2-APY (conformer B of drug). (b) $\text{Cl}\cdots\text{Cl}$ and $\text{C-H}\cdots\text{Cl}$ interactions connect the molecules in a 1D wavelike chain.

4-Aminopyridinium meclofenamate salt hydrate (1:1:1, MFA-4-APY- H_2O)

Proton transfer occurred from MFA to pyridine base in this salt hydrate. The expected carboxylate-pyridinium $\text{R}_2^2(7)$ ring motif is absent presumably due to stronger H bonds of carboxylate with water molecules. Two water molecules now makes a dimeric $\text{R}_4^4(12)$ ring motif¹⁴ capped with two carboxylates through $\text{O-H}\cdots\text{O}^-$ ($\text{O}\cdots\text{O}$, 2.761(4) Å, 2.713(4) Å) hydrogen bonds. The 4-aminopyridinium cation interacts with two water molecules through both ionic $\text{N}^+-\text{H}\cdots\text{O}$ ($\text{N}\cdots\text{O}$, 2.837(4) Å) (Figure 9a) and neutral $\text{N-H}\cdots\text{O}$ ($\text{N}\cdots\text{O}$, 2.993 (4) Å) and one meclofenamate ion through $\text{N-H}\cdots\text{O}^-$ ($\text{N}\cdots\text{O}$, 3.018 (4) Å) hydrogen bonds (Figure 9b). Water molecules are strongly hydrogen bonded in channels formed by MFA and 4-APY ions along the c -axis (Figure 9c). Carboxylate nature (C-O 1.261, 1.266 Å and $\angle\text{C-N-C}$ 121.1°) and water stoichiometry were confirmed by TGA (calc 4.40%, obsd. 4.40%) in the monohydrate salt. Hydrogen bonding and unit cell parameters (see appendix) similarity of MFA-PPZ- H_2O and MFA-4-APY- H_2O (1:1:1) suggest 2D isostructurality and isomorphism, but there are differences in the 3D packing (Figure 7c vs. 9c).

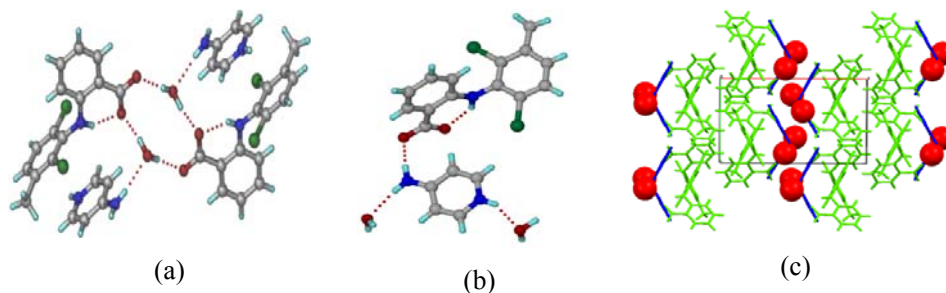


Figure 9 (a) Two meclofenamate anions (conformer A) and two water molecules form $\text{R}_4^4(12)$ ring through $\text{O-H}\cdots\text{O}^-$ hydrogen bond in MFA-4-APY- H_2O . (b) 4-

Aminopyridinium cation interacts with one meclofenamate anion and two water molecules through $\text{N}-\text{H}\cdots\text{O}^-$ and $\text{N}^+-\text{H}\cdots\text{O}$ hydrogen bonds. (c) Water molecules reside in channels formed along the c -axis.

The conformation of meclofenamic acid is different in crystal structures (Table 3). Both conformers A and B are well distributed in cocrystals/salts. A small contribution from an alternate conformation could be detected in a few cases (e.g. MFA-INA cocrystal) by the unassigned difference electron density (Q peaks of about 0.5-0.7 electron) but it was difficult to refine it as partial Me group occupancy. The small amount of Me group disorder in these structures is difficult to model accurately. The intramolecular $\text{N}-\text{H}\cdots\text{O}$ hydrogen bond locks the anthranilic acid fragment in a planar conformation while the phenyl ring bearing the Cl and Me groups can rotate around the $\text{N}-\text{C}$ bond. The formation of cocrystal or salt followed the ΔpK_a rule,⁷ i.e. $\Delta\text{pK}_a > 3$ gives salt, $\Delta\text{pK}_a < 0$ is for cocrystal, and the region $0 < \Delta\text{pK}_a < 3$ is a difficult to predict zone. The pK_a 's (calculated using SPARC calculator in water medium) are listed in Table 4. The acid-acid dimer (synthon energy 15 KJ/mol) of MFA crystal structure is replaced by acid-pyridine heterosynthon (synthon energy 10 KJ/mol) in MFA-INA and MFA-BPY cocrystals. Charge assisted $\text{N}^+-\text{H}\cdots\text{O}^-$ hydrogen bonds reproducibly give salts of meclofenamic acid and piperazine / aminopyridine base. The N base inserts between the carboxylic acid groups to replace the carboxylic acid $\text{O}-\text{H}\cdots\text{O}$ homosynthon with the pyridinium/piperazinum-carboxylate charge assisted $\text{N}^+-\text{H}\cdots\text{O}^-$ heterosynthon. This strong heterosynthon in meclofenamic acid salts/cocrystals is a reliable tool for crystal engineering.

Table 1 Crystallographic data for meclofenamic acid and its new solid phases

Crystal Data	MFA-100K	MFA-RT	MFA-INA
Emp. Formula	$\text{C}_{14}\text{H}_{10}\text{Cl}_2\text{NO}_2$	$\text{C}_{14}\text{H}_{10}\text{Cl}_2\text{NO}_2$	$\text{C}_{14}\text{H}_{11}\text{Cl}_2\text{NO}_2 \cdot \text{C}_6\text{H}_6\text{N}_2\text{O}$
Formula wt.	295.13	295.13	418.27
Crystal system	Triclinic	Triclinic	Monoclinic
Space group	$P-1$	$P-1$	$P2_1/c$
T [K]	100	298	298
a [Å]	8.5209(11)	8.566(3)	7.5327(13)
b [Å]	8.8775(11)	8.968(3)	31.313(5)
c [Å]	9.1986(12)	9.378(3)	9.601(3)
α [deg]	104.265(2)	103.090(6)	90

β [deg]	103.337(2)	103.194(6)	121.439(16)
γ [deg]	91.569(2)	92.538(6)	90
<i>Z</i>	2	2	4
Volume [Å ³]	653.56(14)	679.7(4)	1932.2(7)
<i>D</i> _{calc} [g/cm ³]	1.500	1.442	1.438
N-total	5863	6239	9616
N-independent	2153	2227	3944
N-observed	1954	1698	1932
<i>R</i> ₁ [<i>I</i> >2σ(<i>I</i>)]	0.1106	0.0833	0.0567
<i>wR</i> ₂	0.2193	0.1910	0.1547
GOF	1.209	1.122	0.915

MFA-BPY	MFA-PPZ-M	MFA-PPZ-O	MFA-PPZ
C ₁₄ H ₁₁ Cl ₂	C ₁₄ H ₁₀ Cl ₂ NO ₂	C ₁₄ H ₁₀ Cl ₂ NO ₂	2(C ₁₄ H ₁₀ Cl ₂ NO ₂).
0.5(C ₁₀ H ₈ N ₂)	C ₄ H ₁₁ N ₂	C ₄ H ₁₁ N ₂	C ₄ H ₁₂ N ₂
374.23	382.28	382.28	678.42
Monoclinic	Monoclinic	Orthorhombic	Triclinic
<i>P</i> ₂ /c	<i>P</i> ₂ /c	<i>P</i> ₂ ₁ 2 ₁ 2 ₁	<i>P</i> -1
298	298	298	298
7.4180(6)	16.3805(13)	7.929(3)	7.9109(3)
8.2144(6)	8.3717(5)	8.168(3)	11.1289(4)
28.770(2)	14.4609(11)	28.381(15)	18.1180(7)
90	90	90	81.943(3)
97.099(7)	102.347(8)	90	80.424(4)
90	90	90	88.809(3)
4	4	4	2
1739.6(2)	1934.8(3)	1838.1(13)	1557.36(11)
1.429	1.312	1.381	1.447
8621	8452	5203	12514
2487	3956	3366	6346
1726	1574	1540	3882
0.0892	0.0641	0.0597	0.0687
0.2088	0.1850	0.0663	0.1770
1.127	1.209	0.865	1.030

MFA-PPZ-H ₂ O	MFA-2-APY	MFA-4-APY-H ₂ O
C ₁₄ H ₁₀ Cl ₂ NO ₂	C ₁₄ H ₁₀ Cl ₂ NO ₂	C ₁₄ H ₁₀ Cl ₂
C ₄ H ₁₁ N ₂ · H ₂ O	C ₅ H ₇ N ₂	NO ₂ ·C ₅ H ₇ N ₂ · H ₂ O
400.29	390.26	408.27
Monoclinic	Monoclinic	Monoclinic
<i>P</i> ₂ /c	<i>P</i> ₂ /n	<i>P</i> ₂ /c
298	298	298
16.137(4)	14.675(4)	16.227(4)
8.4889(15)	7.1318(15)	8.4770(15)
15.596(3)	18.605(6)	15.686(4)

90	90	90
114.94(3)	110.73(3)	116.18(3)
90	90	90
4	4	4
1937.1(7)	1821.2(8)	1936.2(7)
1.373	1.423	1.401
6934	8452	5203
3283	3956	3366
1942	1574	1540
0.0868	7324	8218
0.2540	3721	3958
1.046	2081	2641

Table 2 Hydrogen bonds in crystal structures (neutron-normalized distances).

Crystal forms	Interaction	H...A / Å	D...A / Å	∠D-H...A / °
MFA	N1-H1...O1	1.95	2.679 (4)	126
	O2-H2...O1	1.66	2.632 (4)	171
MFA-INA	N1-H1...O1	1.83	2.653(4)	137
	O2-H2...N3	1.68	2.657(4)	174
	N2-H2A...O3	1.93	2.926(4)	169
MFA-BPY	N1-H1...O1	1.84	2.640(4)	133
	O2-H2...N2	1.69	2.668(4)	178
	C15-H15...O1	2.41	3.194(4)	129
MFA-PPZ-M	N1-H1...O1	1.75	2.604(4)	140
	N2-H2...O1	1.68	2.677(4)	171
	N2-H2...O2	2.53	3.231(4)	126
	N2-H2A...N3	1.89	2.851(4)	159
	N3-H3A...O2	1.99	2.949(4)	157
MFA-PPZ-O	N1-H1...O1	1.79	2.619(3)	137
	N2-H2...O1	1.71	2.698(3)	164
	N2-H2...O2	2.48	3.246(3)	133
	N2-H2A...N3	1.85	2.858(3)	178
	N3-H3A...O2	1.97	2.960(3)	165
MFA-PPZ (2:1)	C6-H6...Cl1	2.71	3.201(4)	107
	N1-H1...O1	2.05	2.682 (3)	119
	N2-H2...O3	1.99	2.642 (3)	120
	N3-H3A...O1	1.70	2.690(3)	164
	N3-H3B...O4	1.74	2.731(3)	167
	N4-H4A...O2	1.77	2.750(3)	162
	N4-H4B...O3	1.72	2.695(3)	162
	C29-H29B...O3	2.49	3.318(3)	132

	C32–H32B···C13	2.67	3.446(3)	128
MFA–PPZ–	N1–H1···O1	1.91	2.699(3)	133
H ₂ O	N3–H1A···N2	1.99	2.939(4)	155
	N3–H1B···O1	1.90	2.842(4)	154
	N2–H2···O3	2.10	3.029(4)	152
	O3–H3A···O1	1.87	2.796(4)	155
	O3–H3B···O2	1.72	2.692(4)	170
	C16–H16B···O2	2.43	3.488(4)	167
	C17–H17B···O3	2.35	3.356(4)	155
	C3–H3···C11	2.67	3.607(4)	145
MFA–	N1–H1···O1	1.88	2.631(3)	128
2-APY	N2–H2···O1	1.64	2.642(3)	175
	N3–H3A···O2	1.84	2.841(3)	173
	N3–H3B···O2	1.92	2.897(3)	164
MFA–	N1–H1···O2	1.79	2.603(4)	135
4-APY–H ₂ O	N2–H2···O3	1.92	2.837(4)	149
	N3–H3A···O1	2.07	3.017(4)	156
	N3–H3B···O3	2.00	2.993(4)	169
	O3–H3C···O1	1.78	2.761(4)	173
	O3–H3D···O2	1.75	2.713(4)	166
	C17–H17···O1	2.48	3.301(4)	131

Table 3 Torsion angles (°) in meclofenamic acid crystal structures.

	∠C2–C7– N1–C8(°)	∠C7–N1– C8–C9(°)	∠C7–N1– C8–C13(°)	∠C7–C2– C1–O2(°)	Conformer of MFA
MFA	173.46(2)	92.72(3)	86.44(3)	177.71(2)	Disorder
MFA–INA	163.21(2)	99.01(2)	81.84(2)	174.63(2)	A
MFA–BPY	172.84(1)	86.50(1)	93.76(1)	175.45(1)	A
MFA– PPZ–M	165.93(1)	98.87(1)	83.43(2)	176.64(1)	B
MFA– PPZ–O	167.98(3)	66.12(4)	115.44(3)	179.45(2)	A
MFA–PPZ	157.82(1), 161.44(1)	98.31(1), 84.42(1)	84.52(1), 95.47(1)	171.35(1), 165.67(1)	A + B
MFA–PPZ– H ₂ O	167.43(2)	108.04(3)	74.59(3)	173.55(2)	B
MFA–2- APY	177.91(7)	71.22(11)	111.85(9)	174.43(7)	B

MFA-4- APY-H ₂ O	171.60(4)	84.65(5)	98.50(5)	176.02(4)	A
--------------------------------	-----------	----------	----------	-----------	---

Table 4 Coformers attempted to make cocrystal/salts with meclofenamic acid and ΔpK_a values. pK_a 's were calculated in water using SPARC pK_a calculator, <http://archemcalc.com/sparc/test/login.cfm?CFID=11677&CFTOKEN=94786654>

	pK_a/pK_b (water)	ΔpK_a	Cocrystal/salt
Meclofenamic acid	4.56	-	
Isonicotinamide	4.17	0.39	1:1 cocrystal
4,4'-Bipyridine	4.61	0.05	1: 0.5 cocrystal
Piperazine	9.72	5.16	1:1 salt polymorphs
Piperazine	9.72	5.16	1:1:1 salt hydrate
Piperazine	9.72	5.16	2:1 salt
2-Amino pyridine	6.68	2.12	1:1 Salt
4-Amino pyridine	8.59	4.03	1:1:1 Salt hydrate

7.3.2 Powder X-ray diffraction

Powder X-ray diffraction¹⁹ is a reliable characterization technique to establish the formation of new solid materials. Rapid 'fingerprinting' of the product phase (cocrystal/ salt) compared to characteristic peaks in the starting materials (drug, coformer) is possible by eye-balling of the line patterns. PXRD comparison of piperazine salts prepared in this work with their calculated X-ray patterns (Figure 10) confirmed the purity and homogeneity of each crystalline phase by an excellent overlay of the experimental PXRD with the calculated lines from the crystal structure.

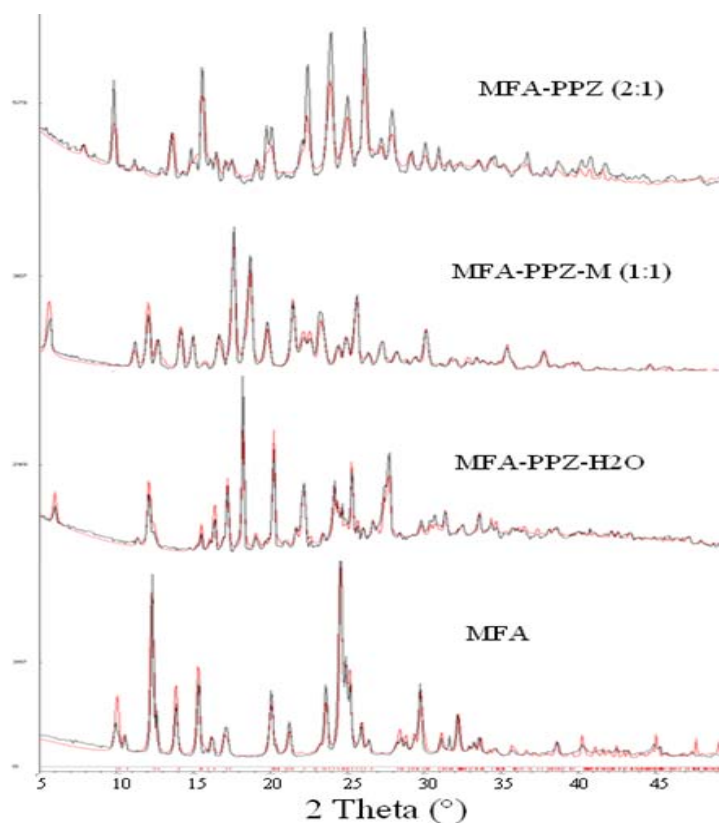


Figure 10 PXRD comparisons of experimental patterns (black) with calculated lines of piperazinium salts of meclofenamic acid from the X-ray crystal structure (red) indicate bulk phase purity.

7.3.3 Thermal Analysis

A change in the melting point of cocrystal/ salt in DSC thermogram is usually indicative of a new phase. Any dissociation/ decomposition and/ or phase changes upon heating are indicated by endo/ exotherm in DSC trace. The monoclinic and orthorhombic polymorphs of MFA–PPZ (1:1) melt at 162.6 °C and 145.8 °C suggesting that the high melting monoclinic form is more stable (Figure 11). The metastable orthorhombic form could not be reproduced in bulk scale purity. The DSC of polymorphic mixture (O+M) and pure monoclinic form are shown to compare their thermal behavior. Melting points are listed in Table 5. Dehydration of MFA–PPZ–H₂O resulted in an anhydrate that matched with the stable monoclinic form (MFA–PPZ-M). The dissociation of the

cocrystal/ salt to meclofenamic acid above 240 °C is indicated by the broad endotherm after melting, similar to the results of diclofenac salts.^{10c}

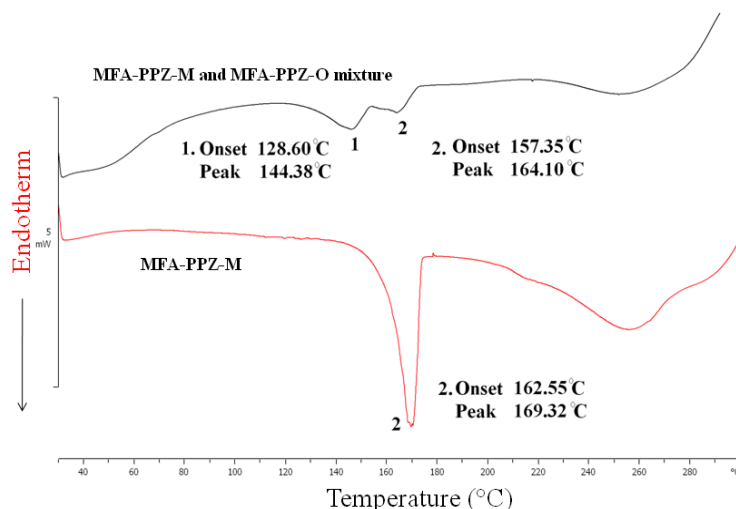


Figure 11 DSC endotherm comparisons for MFA–PPZ (1:1) salt polymorphs monoclinic (M) and orthorhombic (O).

Table 5 Melting point (°C) of cocrystal/salt compared with MFA and coformers.

	m.p. of MFA / coformer (°C)	m. p. of cocrystal/ salt (°C), (DSC, T _{onset})
MFA	257-260	---
MFA–INA	155-158	176.8
MFA–BPY	110-114	207.1
MFA–PPZ-M	106-108	169.3
MFA–PPZ-O	106-108	144.4
MFA–PPZ–H ₂ O	106-108	97.3, 163.3
MFA–PPZ	106-108	171.9
MFA–2-APY	57-60	145.6
MFA–4-APY–H ₂ O	157-161	93.6, 111.7

7.3.4 FT-IR Spectroscopy

FT-IR Spectroscopic analysis²⁰ showed clear differences in hydrogen bonding of salt/ cocrystal compared to the pure components. Such peak shifts are useful to know specific functional groups which are involved in intermolecular interactions. Generally

speaking, for fenamic acids,^{20b} NH stretch appears at 3300-3350 cm⁻¹. The band at about 3335 cm⁻¹ arises from the amino group internally hydrogen bonded to the C=O of meclofenamic acid. Carboxylic acid C=O stretch is normally at 1700-1720 cm⁻¹, but due to intramolecular hydrogen bond in MFA the C=O stretch is red shifted at 1655 cm⁻¹. Bands due to C–O stretch and O–H bend appear at 1256 cm⁻¹ and 1400 cm⁻¹. The carboxylate anion in salts showed two bands, a strong asymmetric stretch at 1650-1550 cm⁻¹ and a weaker symmetric stretch near 1450 cm⁻¹. FT-IR frequencies are summarized in Table 6.

Table 6 FT-IR stretching modes (ν_s , cm⁻¹) of meclofenamic acid and its cocrystals/salts.^a

	N–H stretch	C=O stretch	N–H bend	C–O stretch (asym)	C–O stretch (sym)
MFA	3335.1	1655.4	1575.3	1437.4	1256.6
MFA–INA	3447.0, 3227.2	1694.8	1559.5	1449.5	1261.5
MFA–BPY	3245.9	1675.4	1600.4, 1581.4	1451.0	1259.7
MFA–PPZ–M	3216.9	---	1582.4,	1452.9	1289.1
MFA–PPZ–H ₂ O	3208.4, 3172.6	---	1576.4	1452.1	1282.5
MFA–PPZ	3497.3, 3267.0	---	1577.8	1452.5	1287.6
MFA–2-APY	3268.5, 3199.8	---	1577.7	1449.1, 1458.1	1288.1, 1255.0
MFA–4-APY	3436.7,	---	1574.7	1455.2	1288.0
–H ₂ O	3346.2, 3301.2				

^a IR spectrum of MFA–PPZ–O salt could not be recorded due to insufficient sample and contamination from the stable monoclinic polymorph in the bulk phase.

7.3.5 Solid State NMR Spectroscopy

ss-NMR spectroscopy²¹ of MFA–PPZ (1:1), MFA–PPZ monohydrate (1:1:1) and MFA–PPZ (2:1) was informative about local short-range order in these solid-state structures (Figure 12). Two peaks at δ 18.34 and 20.06 ppm represent the methyl group of meclofenamic acid which is disordered over two positions. The chemical shifts in NMR spectra of MFA–PPZ–M (1:1) and MFA–PPZ–H₂O (1:1:1) salts are similar because the same conformer B of meclofenamic acid is present in both structures. There

is an extra ^{13}C peak in MFA-PPZ (2:1) for piperazinium cation at δ 37.33 ppm, methyl carbon at 21.23 ppm, and carboxylate peak at δ 175.07 ppm, consistent with the crystal structure which showed two MFA conformers A and B and two non-equivalent piperazinium cations. The downfield region peaks in the ss-NMR spectrum of salts (COO^-) are shifted relative to the free acid (COOH).

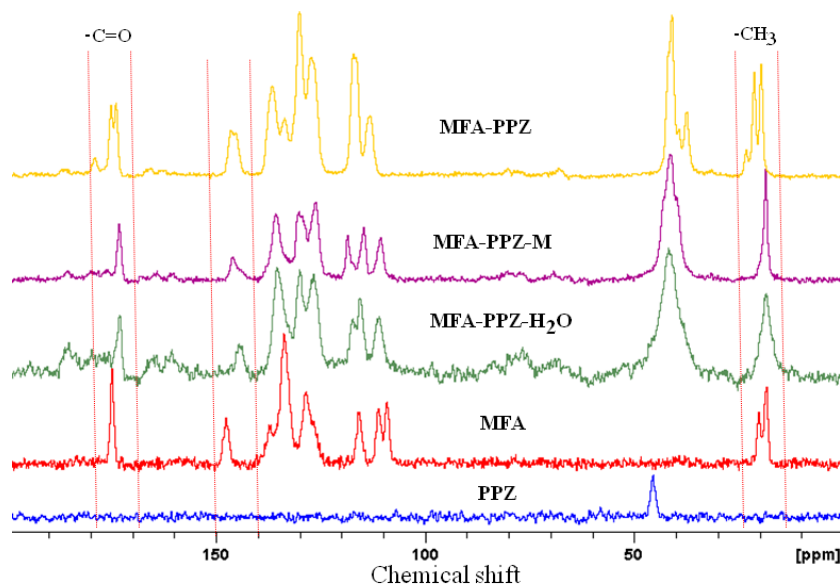


Figure 12 Solid state ^{13}C NMR spectra of MFA-PPZ-M (1:1, pink) and MFA-PPZ- H_2O (1:1:1, green) and MFA-PPZ (2:1, brown) salts along with the pure components. The peaks in the salt are shifted relative to the pure components because of carboxylic acid to carboxylate in MFA. The regions of main chemical shift differences are indicated in red line border.

7.3.6 Solution Mediated Phase Transformations

Solution mediated phase transformations²² are common in pharmaceuticals, i.e. the transformation of one phase to another in a suspension or slurry medium. Such phase changes can also occur upon wet granulation and thus need to be monitored in dosage formulation. 50% EtOH-water solvent was used because the drug and cocrystals/ salts are soluble in this medium. The same solvent system was used for solubility and dissolution experiments (discussed next). Piperazinium meclofenamate (1:1) and (1:1:1) salt hydrate converted to piperazinium meclofenamate (2:1) after 24 h slurry in 50%

EtOH–water at 37 °C (Figure 13, 14). The product 2:1 salt converted to meclofenamic acid after another 24 h in the same slurry medium (Figure 15). Fini et al.^{10c} reported 1:1 and 2:1 salts of diclofenac-piperazine while our work was in review. Their 1:1 salt transforms to the less soluble 2:1 salt after one week in distilled water during slurry experiments, similar to our results. We surmise that the more soluble coformer piperazine dissociates from the salt in the aqueous medium and the less soluble drug MFA precipitates after 48 h. The dissociation of piperazine from the salt occurs in stages: half equivalent in 24 h (1:1 to 2:1 salt), and then another half equivalent in next 24 h (to give MFA) as confirmed by PXRD of the solid residue. The stability of variable stoichiometry salts in slurry medium may be related to their hydrogen bonding in the crystal structures: the 1:1 salt contains one $N^+-H\cdots O^-$ and one $N-H\cdots O$ hydrogen bond between meclofenamate and piperazinium, whereas one meclofenamate interacts with a di-piperazinium through two $N^+-H\cdots O^-$ hydrogen bonds in the 2:1 salt. The stronger ionic hydrogen bonds result in greater stability of the 2:1 salt over the 1:1 salt. MFA–PPZ monohydrate (1:1:1) showed similar results. The cocrystals, on the other hand, were more stable to slurry conditions: meclofenamic acid–isonicotinamide transformed to 86% meclofenamic acid and 14% cocrystal remained after 24 h, as confirmed by PXRD. A calibration sample of 85% MFA and 15% cocrystal suggested that the standard deviation of PXRD is $\pm 3\%$. Meclofenamic acid–4,4'-bipyridine cocrystal was unusually stable for up to 72 h in 50% EtOH–water medium (Figure 16). These stability trends may be ascribed to congruent and incongruent systems.²³ When the solubility of the drug and the coformer are similar in the same medium (both are insoluble/ less soluble), such systems are congruent and tend to be stable. For incongruent systems, the high solubility coformer leaches into the solvent medium in which it readily dissolves, and in this way the salt/ cocrystal dissociates faster. The soluble cocrystals will usually have a highly soluble coformer partner and this in turn makes the salt/ cocrystal of limited stability. This in effect puts a limit to the stability of more soluble pharmaceutical cocrystals in slurry medium. The stability order in aqueous slurry medium is (less to more stable): MFA–PPZ (1:1) < MFA–PPZ monohydrate (1:1:1) < MFA–PPZ (2:1) < MFA–INA (1:1) < MFA–BPY (1:0.5). Solution-mediated phase transformations can occur during dissolution and solubility measurements (discussed next), and the above stability order will help to explain any unusual trends.

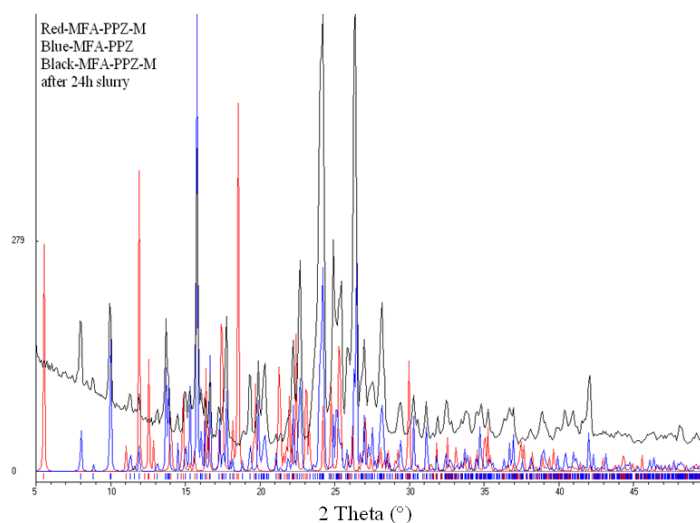


Figure 13 PXRD comparison of MFA-PPZ-M (black) after 24 h slurry experiments with calculated X-ray lines of MFA-PPZ-M (red) and MFA-PPZ (blue) in 50% EtOH-water medium. PXRD lines were matched with calculated X-ray lines of MFA-PPZ salt indicates solvent mediated phase transformation from MFA-PPZ-M to MFA-PPZ salt after 24 h.

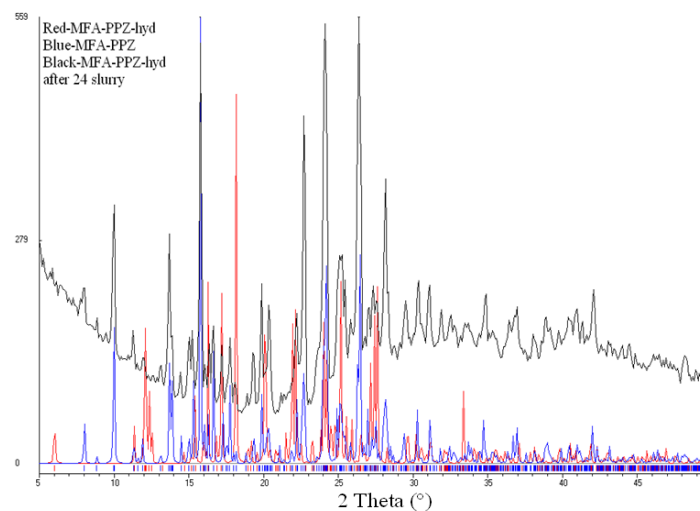


Figure 14 PXRD comparison of MFA-PPZ-H₂O (black) after 24 h slurry experiment with calculated X-ray lines of MFA-PPZ-H₂O (red) and MFA-PPZ (blue) in 50% EtOH-water medium. PXRD lines were matched with calculated X-ray lines of MFA-PPZ salt indicates solvent mediated phase transformation from MFA-PPZ-H₂O to MFA-PPZ salt after 24 h .

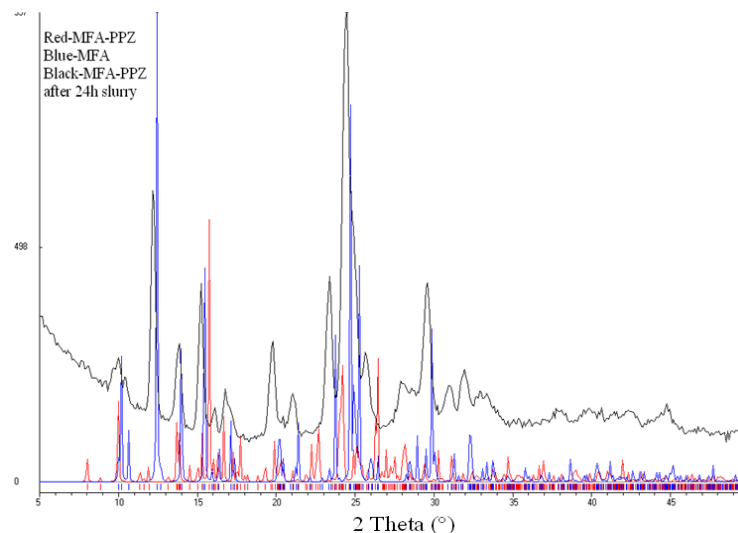


Figure 15 PXRD comparison of MFA-PPZ (black) after 24 h slurry experiment with calculated X-ray lines of MFA-PPZ (red) and MFA (blue) in 50% EtOH-water medium. PXRD lines were matched with calculated X-ray lines of MFA indicates solvent mediated phase transformation from MFA-PPZ to MFA after 24 h.

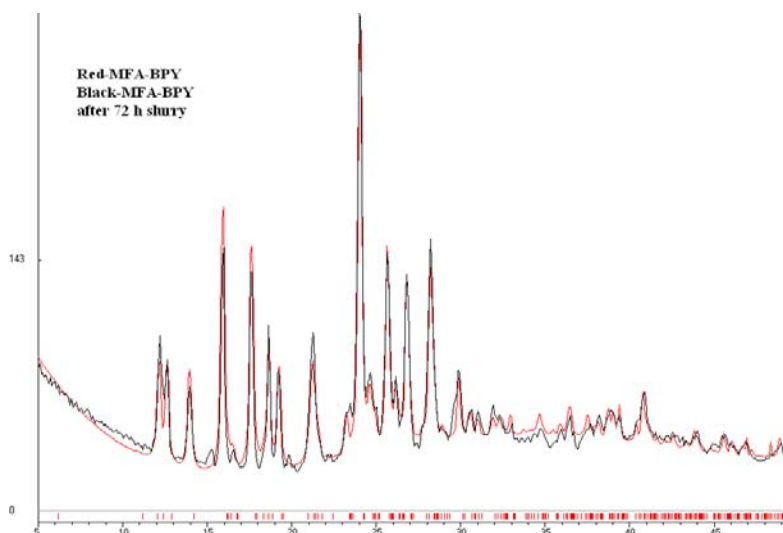


Figure 16 PXRD of MFA-BPY cocrystals after 72 h slurry in 50% EtOH-water medium. The match of experimental pattern (black trace) with that of the pure crystalline phase (red trace) indicates the stability of this cocrystal in solution.

7.3.7 Solubility and Dissolution Experiments

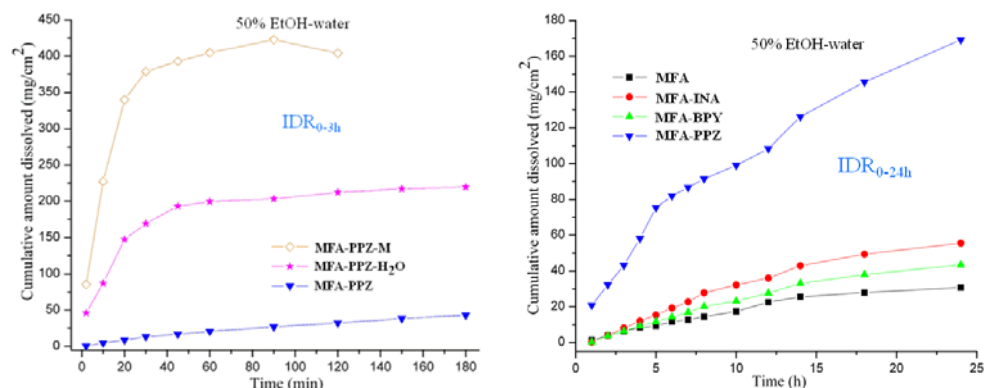
The rate of dissolution and solubility of the solid drug in water or aqueous solvent mixtures is necessary for good oral bioavailability. The aqueous solubility of the drug must be at least 100 mg/L for fast dissolution of tablet.^{1a} The aqueous solubility of meclofenamic acid is 30 mg/L and other fenamic acids (e.g. mefenamic acid, tolfenamic acid and diclofenac acid) are also low solubility BCS class II drugs. The sodium salt of meclofenamic acid (MFA-SS) is marketed as capsules (solubility >250 g/L). The aqueous solubility for cocrystals and salts of MFA were measured in 50% EtOH–water medium at 37 °C (Table 7). Although solubility is a good indicator of drug bioavailability, the method is applicable only for those solid-state drug forms which are stable in the test medium/ slurry. The intrinsic dissolution rate (IDR) is a kinetic parameter and is a useful indicator for those solid forms which undergo phase transformation or dissociation during the experiment. Most drugs exert their therapeutic effect within 4-6-8 h of oral administration, and IDR is a good indicator of drug dissolution in such cases. IDR measurements show that piperazine salts reached peak concentration within 30-45 mins of drug dissolution (Figure 17). The most stable 2:1 MFA-PPZ salt exhibited a gradual increase in dissolution rate up to 24 h. The cumulative amount of meclofenamic acid dissolved (mg cm^{-2}) vs. time (min) were plotted to compare the IDR of piperazine meclofenamates (Figure 17a). The highest solubility of MFA-PPZ-M (1:1) is driven by the high solubility of piperazine > MFA-PPZ-H₂O (1:1:1) because hydrates are generally less soluble than anhydrate drugs > (MFA-PPZ (2:1) due to lower piperazine content. In contrast to salts, MFA-INA (1:1) and MFA-BPY (1:0.5) cocrystals exhibited poor dissolution rates (Figure 17b), but they were quite stable for over 24 h. Further the highest solubility salt MFA-PPZ (1:1) was compared with MFA-SS in aqueous medium (IDR of sodium salt is 28.76 and piperazinium salt is 13.72 (mg cm^{-2}) min^{-1} ; Figure 17c). The marketed sodium salt of meclofenamic acid has 2.1 times higher IDR than the equimolar piperazine salt. PXRD of the residue from MFA-PPZ dissolution experiment after 11 min matched with the 2:1 salt (70%) and monohydrate (30%), the 1:1 salt showed transformation to piperazine salt hydrate and 2:1 salt, whereas MFA sodium salt transformed to its hydrate after 8 min in the dissolution medium and showed plateau region. These results suggest that 1:1 MFA-

PPZ is more stable than the marketed sodium salt to hydration in aqueous medium. PXRD of melofenamic acid sodium salt after 24 h of slurry stirring in water is different from the starting material (MFA-SS). Thermogravimetric analysis indicated water content of 13.92% (2.8-2.9 equivalent) in MFA-SS hydrate formed in the aqueous medium, further confirmed by DSC (Figure 18). Again MFA-PPZ-M transformed to MFA-PPZ (2:1) salt after 24 h slurry experiments in water, confirmed by PXRD. The aqueous solubility of sodium salt of meclofenamic acid ($>250 \text{ g/L}$)^{9b} is 46 times the value for MFA-PPZ 1:1 salt in water (5.4 g/L), but its dissolution rate is two times faster in the first 10 min of measurement.

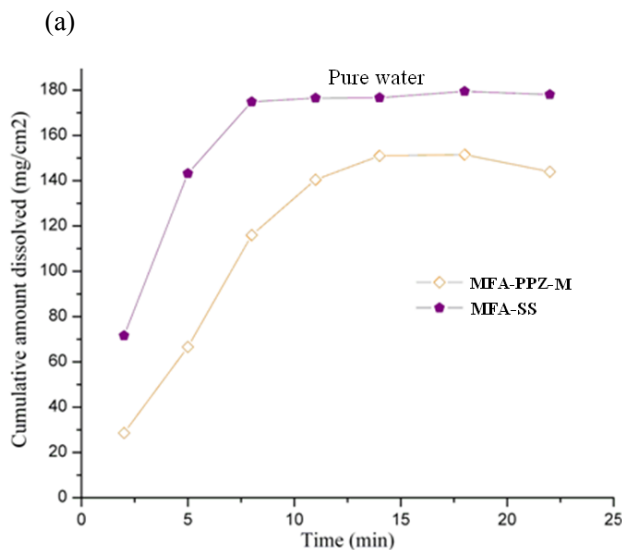
Table 7 Solubility and dissolution rate of meclofenamic acid and its cocrystals and salts.^a

Solid form	Absorption coefficient (ϵ , $\text{mM}^{-1} \text{ cm}^{-1}$)	Equilibrium solubility after 24 h slurry in 50% EtOH-water (mg L^{-1})	IDR ($(\text{mg cm}^{-2}) \text{ min}^{-1}$) ^a
MFA	6.94	203.11	0.03074
MFA-INA	4.10	581.43 (x 2.9)	0.04858 (x 1.6)
MFA-BPY	5.74	1638.07 (x7.6)	0.03822 (x 1.2)
MFA-PPZ-M	3.38	553223.061 (x 2724)	27.4976 (x 894.5)
MFA-PPZ	7.95	10211.954 (x 50)	0.31477 (x 10.2)
MFA-PPZ-H ₂ O	4.82	270966.397 (x1334)	9.8044 (x 318.9)

^a Number in parenthesis indicates how many times higher solubility/IDR compared to reference drug.



(b)



(c)

Figure 17 Intrinsic dissolution rate (IDR) measurements of (a) MFA-PPZ-M (1:1), MFA-PPZ-H₂O (1:1:1) and MFA-PPZ (2:1) performed upto 3 h, (b) MFA-PPZ (2:1), MFA-INA (1:1), MFA-BPY (1:0.5) and MFA over 24 h in 50% EtOH-water medium and (c) MFA-PPZ (1:1) and MFA-SS (sodium salt of meclofenamic acid) over 22 minutes in distilled water. The amount of meclofenamic acid dissolved in the test medium was monitored by UV-Vis spectroscopy.

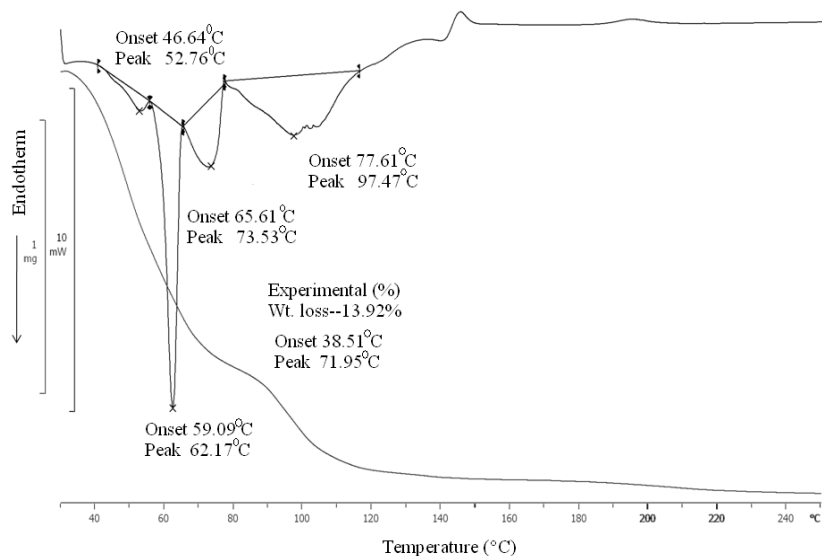


Figure 18 DSC and TGA thermograms of MFA–SS after slurry for 24 h in water indicate 2.8-2.9 equivalents of water content.

7.4 Conclusion

Meclofenamic acid is the most potent non-steroidal anti-inflammatory drug because of its proper fit to the receptor side of the enzyme arachidonic acid cyclooxygenase. A few cocrystals and salts of meclofenamic acids were crystallized using crystal engineering principles. All new crystalline phases were characterized by X-ray diffraction, IR and ss-NMR spectroscopy, and DSC/ TGA. Meclofenamic acid exists in two different conformers A and B due to tolyl group rotation about the N–C bond. Whereas the crystal structure of meclofenamic acid has disordered methyl group, the drug molecule is in an ordered orientation in its cocrystals and salts, perhaps rigidified due to stronger hydrogen bonding. The dissolution rate and solubility of MFA–PPZ-M 1:1 salt is the highest among the novel solid-state forms studied and slightly lower than the marketed sodium salt of meclofenamic acid. Their stability to hydration is comparable in aqueous medium. Thus piperazinium meclofenamate salt has equivalent dissolution and stability profile to the marketed sodium salt. Four different piperazinium salts were crystallized: monoclinic and orthorhombic polymorphs of MFA–PPZ (1:1), its monohydrate, and MFA–PPZ (2:1) salts. This is the first example of polymorphic and variable stoichiometry piperazinium salts with X-ray crystal structures solved to good accuracy.

7.5 Experimental Section

Meclofenamic acid and isonicotinamide were purchased from Sigma-Aldrich (Hyderabad, Andhra Pradesh, India) and used directly for experiments. All other chemicals were of analytical or chromatographic grade. Melting points were measured on a Fisher-Johns melting point apparatus. Water filtered through a double deionized purification system (AquaDM, Bhanu, Hyderabad, India) was used in all experiments. Single crystals were obtained via slow evaporation of stoichiometric amounts of starting materials in an appropriate solvent. Cocrystals and salts were characterized by infrared spectroscopy (IR), powder X-ray diffraction (PXRD), differential scanning calorimetry

(DSC), thermogravimetric analysis (TGA), and single crystal X-ray diffraction (SC-XRD).

Meclofenamic acid, MFA

Normally cracked crystals of meclofenamic acid appeared after crystallization from organic solvents. Sublimation of meclofenamic acid at 190-200 °C produced good quality block shaped crystal after 2-3 hours. Melting point 257-260 °C (literature value).^{9a,23}

Meclofenamic acid–Isonicotinamide, MFA–INA (1:1) cocrystal

Meclofenamic acid (100 mg, 0.34 mmol) and isonicotinamide (41.5 mg, 0.34 mmol) were ground in a mortar pestle for 15 min using acetonitrile as solvent-assisted grinding. After confirming a new solid phase by IR and PXRD, the bulk material was dissolved in acetonitrile. Good quality single crystals appeared at ambient conditions after 2-3 days. m.p. 175-177 °C

Meclofenamic acid–4,4'-bipyridine, MFA–BPY (1:0.5) cocrystal

Meclofenamic acid (100 mg, 0.34 mmol) and 4,4'-bipyridine (26.5 mg, 0.17 mmol) were ground in a mortar pestle for 15 min using acetonitrile as solvent-assisted grinding. After confirming a new solid phase by IR and PXRD, the bulk material was dissolved in acetonitrile. Thick plate crystals were harvested at ambient conditions after 2-3 days. m.p. 204-207 °C.

Piperazinium meclofenamate, MFA–PPZ (1:1) salt polymorphs

Meclofenamic acid (100 mg, 0.34 mmol) and piperazine (29.3 mg, 0.34 mmol) were ground in a mortar pestle for 15 min using acetonitrile as solvent-assisted grinding. After confirming a new solid phase by IR and PXRD, the bulk material was dissolved in acetonitrile. Block (monoclinic, form M) and thick long needle (orthorhombic, form O) crystals were harvested concomitantly at ambient condition after 2-3 days. Monoclinic form (plate) was obtained exclusively from CH₃NO₂ solvent. m.p. of monoclinic and orthorhombic forms are 162-166 °C and 144-147 °C respectively.

Piperazinium meclofenamate, MFA–PPZ (2:1) salt

Meclofenamic acid (100 mg, 0.34 mmol) and piperazine (29.3 mg, 0.34 mmol) were ground in a mortar pestle for 15 min using acetonitrile as solvent-assisted grinding. After

confirming a new solid phase by IR and PXRD, bulk material was dissolved in EtOH. Suitable thick plate (triclinic) crystals were harvested at room temperature after 3-4 days. m.p. 166-169 °C.

Piperazinium meclofenamate monohydrate, MFA–PPZ–H₂O (1:1:1) salt

Meclofenamic acid (100 mg, 0.34 mmol) and piperazine hydrate (35.4 mg, 0.34 mmol) were ground in a mortar pestle for 15 min. After confirming a new solid phase by IR and PXRD, the bulk material was dissolved in nitromethane. m.p. of salt 154-158 °C and dehydration temperature 92-95 °C.

2-Aminopyridinium meclofenamate, MFA–2-APY (1:1) salt

Meclofenamic acid (100 mg, 0.34 mmol) and 2-aminopyridine (32 mg, 0.34 mmol) were ground in a mortar pestle for 15 min using acetonitrile as solvent-assisted grinding. After confirming new solid phase by IR and PXRD, the bulk material was dissolved in acetonitrile. Plate crystals were harvested after 2-3 days at ambient condition. m.p. 143-146 °C.

4-Aminopyridinium meclofenamate monohydrate, MFA–4-APY–H₂O (1:1:1) salt

Meclofenamic acid (100 mg, 0.34 mmol) and 4-aminopyridine (32 mg, 0.34 mmol) were ground in a mortar pestle for 15 min using acetonitrile as solvent-assisted grinding. After confirming new solid phase by IR and PXRD, bulk material was dissolved in acetonitrile. Suitable thick plate crystals were harvested after 2-3 days at ambient condition. m.p. 104-108 °C and dehydration temperature 80-84 °C.

7.5.1 Dissolution and solubility measurements

Intrinsic dissolution rate (IDR) and solubility measurements were carried out on a USP-certified Electrolab TDT-08L Dissolution Tester (Electrolab, Mumbai, MH, India). A calibration curve was obtained for all the new solid phases including meclofenamic acid by plotting absorbance vs. concentration UV-Vis spectra curves on a Thermo Scientific Evolution EV300 UV-Vis spectrometer (Waltham, MA, USA) for known concentration solutions in 50% EtOH–water medium. The mixed solvent system (EtOH–water) was selected for its higher solubility of meclofenamic acid in this medium. The slope of the plot from the standard curve gave the molar extinction coefficient (ϵ) by applying the Beer-Lambert's law. Equilibrium solubility was

determined in 50% EtOH–water medium using the shake-flask method.²⁴ To obtain the equilibrium solubility, 100 mg of each solid material was stirred for 24 h in 5 mL 50% EtOH–water at 37 °C, and the absorbance was measured at 318 nm. The concentration of the saturated solution was calculated at 24 h, which is referred to as the equilibrium solubility of the stable solid form.

100 mg of the solid (drug, cocrystal, salt) was taken in the intrinsic attachment and compressed to a 0.5 cm² pellet using a hydraulic press at a pressure of 2.5 ton/inch² for 2 min. The pellet was compressed to provide a flat surface on one side and the other side was sealed. Then the pellet was dipped into 900 mL of 50% EtOH–water medium at 37 °C with the paddle rotating at 150 rpm. At regular interval of 5-10 min, 5 mL of the dissolution medium was withdrawn and replaced by an equal volume of fresh medium to maintain a constant volume. Samples were filtered through 0.2 µm nylon filter and assayed for drug content spectrophotometrically at 318 nm on a Thermo-Nicolet EV300 UV-Vis spectrometer. There was no interference to meclofenamic acid UV-Vis maxima at 318 nm by coformers isonicotinamide and bipyridine which absorb strongly at 250-270 nm. Piperazine is UV-Vis inactive. The amount of drug dissolved in each time interval was calculated using the calibration curve. The linear region of the dissolution profile was used to determine the intrinsic dissolution rate (IDR) of the compound (= slope of the curve, i.e. amount of drug dissolved divided by the surface area of the disc (0.5 cm²) per minute). The dissolution rates for meclofenamic acid, its cocrystals and salts were computed from their IDR values. Similarly IDR experiments of MFA–PPZ-M and MFA–SS salts were carried out in distilled water and absorbance were measured at 318 nm in a UV-Vis spectrophotometer.

7.6 References

1. (a) S. R. Byrn, R. R. Pfeiffer, J. G. Stowell, *Solid-State Chemistry of Drugs*; SSCI: West Lafayette, IN, 1999. (b) S. L. Morissette, Ö. Almarsson, M. L. Peterson, J. F. Remenar, M. J. Read, A. V. Lemmo, S. Ellis, M. J. Cima, C. R. Gardner, *Adv. Drug Delivery Rev.* **2004**, 56, 275.
2. (a) J. Bernstein, *Polymorphism in Molecular Crystals*; Clarendon Press: Oxford, 2002. (b) C. P. Price, A. L. Grzesiak, A. J. Matzger, *J. Am. Chem. Soc.* **2005**,

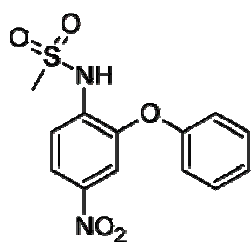
- 127, 5512. (c) A. T. Hulme, S. L. Price, D. A. Tocher, *J. Am. Chem. Soc.* **2005**, 127, 1116. (d) A. V. Trask, N. Shan, W. D. Motherwell, W. Jones, S. Feng, R. B. Tan, K. J. Carpenter, *Chem Commun.* **2005**, 880. (e) D. J. W. Grant, S. R. Byrn *Adv. Drug Delivery Rev.* **2004**, 56, 237. (f) A. D. Bond, R. Boese, and G. R. Desiraju, *Angew. Chem. Int. Ed.* **2007**, 46, 618. (g) J. C. Burley, M. J. Duera, R. S. Steina, R. M. Vrcelj, *Eur. J. Pharm. Sci.* **2007**, 31, 271.
3. (a) C. H. Gu, D. J. W. Grant, In *Handbook of Experimental Pharmacology: Stereochemical Aspects of Drug Action and Disposition*; M. Eichelbaum, B. Testa, A. Somogyi, Eds.; Springer, Berlin, 2003. (b) M. Puddipeddi, A. T. M. Serajuddin, D. J. W. Grant, P. H. Stahl, In *Handbook of Pharmaceutical Salts: Properties, Selection, and Use*; P. H. Stahl, C. G. Wermuth, Eds.; Wiley, Weinheim, 2002; pp 19-38. (c) D. L. Prohotsky, F. Zhao, *J. Pharm. Sci.* **2012**, 101, 1.
4. (a) G. R. Desiraju, *Crystal Engineering: The Design of Organic Solids*. Elsevier, Amsterdam, 1989. (b) G. R. Desiraju, *Angew. Chem., Int. Ed.*, **2007**, 46, 8342. (c) N. Blagden, M. D. Matas, P. T. Gavan, and P. York, *Adv. Drug Del. Rev.*, **2007**, 59, 617.
5. (a) S. Karki, T. Friščić, L. Fábián, P. R. Laity, G. M. Day, and W. Jones, *Adv. Mater.* **2009**, 21, 3905. (b) S. L. Childs, L. J. Chyall, J. T. Dunlap, V. N. Smolenskaya, B. C. Stahly, G. P. Stahly, *J. Am. Chem. Soc.* **2004**, 126, 13335. (c) J. F. Remenar, S. L. Morissette, M. L. Peterson, B. Moulton, J. M. MacPhee, H. R. Guzmán, Ö. Almarsson, *J. Am. Chem. Soc.* **2003**, 125, 8456. (d) M. L. Cheney, N. Shan, E. R. Healey, M. Hanna, L. Wojtas, M. J. Zaworotko, V. Sava, S. Song, J. R. Sanchez-Ramos, *Cryst. Growth Des.* **2010**, 10, 395. (d) P. Sanphui, N. R. Goud, U. B. R. Khandavilli, A. Nangia, *Cryst. Growth Des.* **2011**, 11, 4135.
6. (a) A. Portell, R. Barbas, M. Font-Bardia, P. Dalmases, R. Prohens, and C. Puigjaner, *CrystEngComm*, **2009**, 11, 791. (b) R. Thakuria, and A. Nangia, *CrystEngComm* **2011**, 13, 1759. (c) R. Banerjee, P. M. Bhatt, N. V. Ravindra, and G. R. Desiraju, *Cryst. Growth Des.* **2005**, 5, 2299.
7. (a) C. B. Aakeröy, M. E. Fasulo, and J. Desper, *Mol. Pharmaceutics* **2007**, 4, 317. (b) B. Sarma, N. K. Nath, B. R. Bhogala, and A. Nangia, *Cryst. Growth*

- Des.* **2009**, *9*, 1546. (c) S. L. Childs, G. P. Stahly, and A. Park, *Mol. Pharmaceutics* **2007**, *4*, 323.
8. (a) R. J. Flower, *Pharm. Res.* **1974**, *26*, 33. (b) P. Moser, A. Salimann, and I. wissenberg, *J. Med. Chem* **1990**, *33*, 2358. (c) E. J. Bowen, and J. H. D. Eland, *Proc. Chem. Soc.* **1963**, 202. (d) T. Narsinghania, S. C. Chaturvedi, *Biorg. Med. Chem. Lett.* **2006**, *16*, 461. (e) A. Peretz, N. Degani, R. Nachman, Y. Uziyel, G. Gibor, D. Shabat, and B. Attali, *Mol Pharmacol* **2005**, *67*, 1053. (f) S. C. Belsole, N. J. Chester, US patent **1986**, 4602040. (g) J. Philip, and D. H. Szulczewski, *J. Pharm. Sci.* **1973**, *62*, 1479. (h) <http://www.elephantcare.org/Drugs/meclofen.htm>.
 9. (a) <http://www.drugbank.ca/drugs/DB00939>.
(b) <http://www.orgyn.com/resources/genrx/D001710.asp>.
 10. (a) L. Fábíán, N. Hamill, K. S. Eccles, H. A. Moynihan, A. R. Maguire, L. McCausland, and S. E. Lawrence, *Cryst. Growth Des.* **2011**, *11*, 3522. (b) C. B. Aakeröy, A. B. Grommet and J. Desper, *Pharmaceutics* **2011**, *3*, 601. (c) A. Fini, C. Cavallari, G. Bassini, F. Ospitali, R. Morigi, *J. Pharm. Sci.* **2012**, DOI: 10.1002/jps.23052.
 11. P. Sanphui, G. Bolla, A. Nangia, *Cryst. Growth Des.* **2012**, *12*, 2023.
 12. (a) H. M. K. Murthy, M. Vijayan, *Acta Cryst.* **1981**, *B37*, 1102. (b) V. Dhanraj, M. Vijayan, *Biochim. Biophys. Acta* **1987**, *924*, 135.
 13. (a) M. Takasuka, H. Nakai, and M. Shiro, *J. Chem. Soc., Perkin Trans. II* **1982**, 1061. (b) J. F. McConnell, F. Z. Company, *Cryst. Struct. Commun.* **1976**, *5*, 861. (c) V. López-Mejías, J. W. Kapyf, and A. J. Matzger, *J. Am. Chem. Soc.* **2009**, *131*, 4554.
 14. (a) M. C. Etter, J. C. Macdonald, *Acta Cryst.* **1990**, *B46*, 256. (b) J. Bernstein, R. E. Davis, L. Shimoni, N. -L. Chang, *Angew. Chem., Int. Ed. Engl.* **1995**, *34*, 1555.
 15. (a) P. H. Stahl, C. G. Wermuth, Eds.; *Handbook of Pharmaceutical Salts: Properties, Selection and Use*. Verlag Helvetica Chimica Acta: Zürich, 2002. (b) Generally Regarded as Safe: <http://www.cfsan.fda.gov/~rdb/opa-gras.html> and <http://www.cfsan.fda.gov/~dms/grasguid.html>.

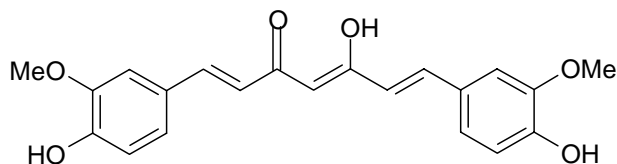
16. Cambridge Structural Database, Ver. 5.32, 2010, November 2011 update, Cambridge Crystallographic Data Center, UK, www.ccdc.cam.ac.uk.
17. Cerius² Materials Studio, <http://accelrys.com/products/cerius2>, Lattice energy calculation of crystal structures.
18. M. S. Fonari, E. V. Ganin, A. V. Vologzhanina, M. Y. Antipin, V. C. Kravtsov, *Cryst. Growth Des.* **2010**, *10*, 3647
19. (a) S. Karki, T. Frišćić, L. Fábrián, W. Jones, *CrystEngComm.* **2010**, *12*, 4038. (b) J. F. Remenar, M. L. Peterson, P. W. Stephens, Z. Zhang, Y. Zimenkov, M. B. Hickey, *Mol. Pharmaceutics* **2007**, *4*, 386. (c) V. André, A. Fernandes, P. P. Santos, M. T. Duarte, *Cryst. Growth Des.* **2011**, *11*, 2325.
20. (a) R. M. Silverstein, *Spectrometric Identification of Organic Compounds*. 6th Ed. John Wiley & Sons, Inc. **2002**, pp. 71-143. (b) R. K. Gilpin, W. Zhou, *Vibrational Spectroscopy* **2005**, *37*, 53. (b) S. Romero, B. Escalera, P. Bustamante, *Int. J. Pharm.* **1999**, *178*, 193.
21. (a) K. Greco, D. P. Mcnamara, R. Bogner, *J. Pharm. Sci.* **2011**, *100*, 2755. (b) D. Murphy, F. Rodríguez-Cintrón, B. Langevin, R. C. Kelly, N. Rodríguez-Hornedo, *Int. J. Pharm.* **2002**, *246*, 121. (c) E. S. Ferrari and R. J. Davey, *Cryst. Growth Des.* **2004**, *4*, 1061. (d) S. Cherukuvada, N. J. Babu, A. Nangia, *J. Pharm. Sci.* **2011**, *100*, 3233.
22. (a) T. Frišćić, S. L. Childs, S. A. A. Rizvi, W. Jones, *CrystEngComm*, **2009**, *11*, 418. (b) A. Alhalaweh, S. P. Velega, *Cryst. Growth Des.* **2010**, *10*, 3302. (c) N. Rodríguez-Hornedo, S. J. Nehm, K. F. Seefeldt, Y. Pagán-Torres, C. J. Falkiewicz, *Mol. Pharmaceutics* **2006**, *3*, 362. (d) N. R. Goud, S. Gangavaram, K. Suresh, S. Pal, N. G. Manjunatha, S. Nambiar, *J. Pharm. Sci.* **2012**, *101*, 664.
23. M. Fawzi, M. Mahjour, US Patent, **1994**, 5,373,022.
24. A. Glomme, J. Marz, J. B. Dressman, *J. Pharm. Sci.* **2005**, *94*, 1.

Chapter Eight

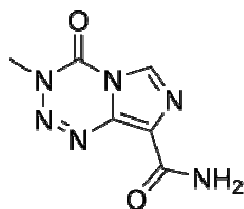
Conclusion and Future Prospects



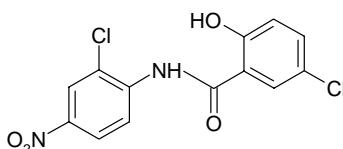
Nimesulide
(Chapter 2)



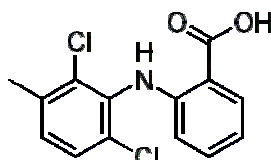
Curcumin
(Chapter 3 & 4)



Temozolomide
(Chapter 5)



Niclosamide
(Chapter 6)



Meclofenamic acid
(Chapter 7)

The physicochemical properties of four important APIs and one bioactive molecule were improved by discovery and selection of solid-state forms such as polymorphs, amorphous form, cocrystals, salts etc.

This thesis covers the identification and characterization of new polymorphs of APIs (Chapter 2 and 3), and pharmaceutical cocrystals (Chapter 4, 5 & 6) and salts (Chapter 7) and the controlled modification of physicochemical properties such as solubility, dissolution rate and stability.

Summary of Results

Nimesulide is a nonsteroidal anti-inflammatory drug (NSAID) and a COX-2 inhibitor. The native crystal structure of Nimesulide (or form I) has been characterized by X-ray powder diffraction lines whereas full 3D coordinates are known for a second polymorph (form II). A detailed structural characterization and phase stability of nimesulide polymorphs was carried out. Rod like crystals of Form I (space group $Pca2_1$, number of symmetry-independent molecules, $Z' = 2$, A and B) were crystallized from EtOH concomitantly with Form II ($C2/c$, $Z' = 1$). These conformational polymorphs have different torsion angles at the phenoxy and sulfonamide groups. The crystal structures are stabilized by N–H \cdots O hydrogen bonds and C–H \cdots O, C–H $\cdots\pi$ interactions. The packing diagram for the two polymorphs shows a tape sequence of N–H \cdots O $_2$ N hydrogen bond as XYYX in form I and XYXY in form II, viewed along the b-axis (Figure 1). Phase transition from the metastable form (II) to the stable modification (I) was studied using DSC, HSM, solid-state grinding, solvent-drop grinding, and slurry crystallization. The phase transition was monitored by IR, Raman and ss-NMR spectroscopy, and XRPD and single crystal X-ray diffraction. The stable polymorph I was obtained in excess during solution crystallization, grinding and slurry methods. Intrinsic dissolution and equilibrium solubility experiments showed that the metastable form II dissolved much faster than the stable form I in pH 7 buffer (Figure 2). However stability of metastable form II is of concern since solid state grinding for 30 min in CH₃CN solvent assisted grinding gave the stable form I. The search for additives, cofomers, excipients, and polymers to stabilize the metastable polymorph will be a practical way forward.

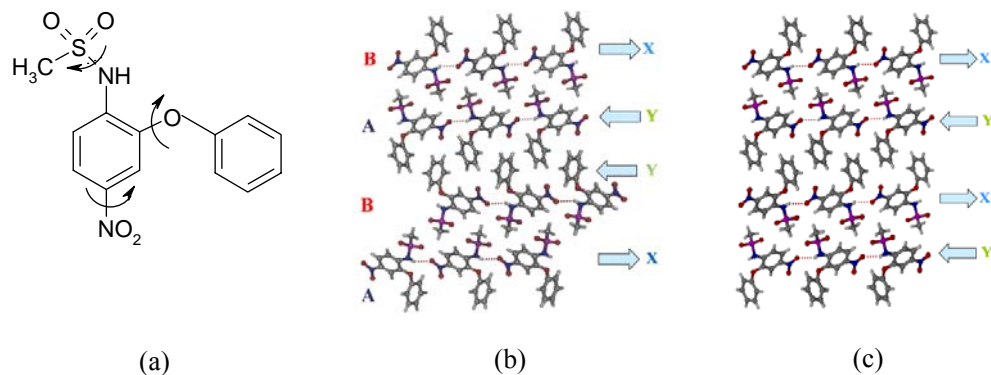


Figure 1 Flexible torsions in (a) Nimesulide and packing differences between (b) form I and (c) form II.

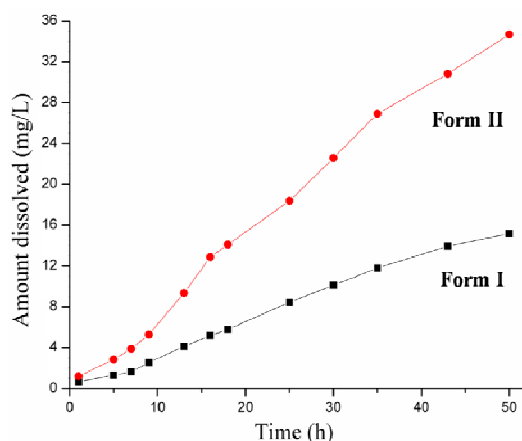


Figure 2 Intrinsic dissolution profile of nimesulide Form I and Form II in pH 7 buffer

Curcumin, a hydrophobic phenol, is the principal curcuminoid in the popular Indian dietary spice turmeric. It is derived from the rhizome of the herb *Curcuma longa*. Curcumin is known for its diverse pharmacological activity such as an antioxidant, antimalarial, anti-carcinogenic, anti-HIV agent, etc. Curcumin is safe even at high dose of 12 g/day in animal and human experiments. Despite its efficacy and safety, curcumin is not approved as a therapeutic agent because of poor absorption and bioavailability, and rapid metabolism and systematic elimination. The crystal structure of stable form 1 ($P2_1/n$, $Z'=1$) of curcumin is reported. During attempted cocrystallization experiments of curcumin, two new polymorphs, form 2 ($Pca2_1$, $Z'=2$) and form 3 ($Pbca$, $Z'=1$) were

obtained in the presence of 4-hydroxypyridine and pyrimidine respectively. A new amorphous phase was obtained from melt crystallization. Three crystalline polymorphs and one amorphous phase of curcumin are displayed in the Figure 3a. Form 2 amorphous dissolved 3.1 and 1.8 times faster than commercial form 1 in 40% EtOH-water medium (Figure 3b). The stabilization of form 2 and amorphous phase through additives, excipients, polymers, etc. could lead to the development of curcumin as a more bioavailable active ingredient.

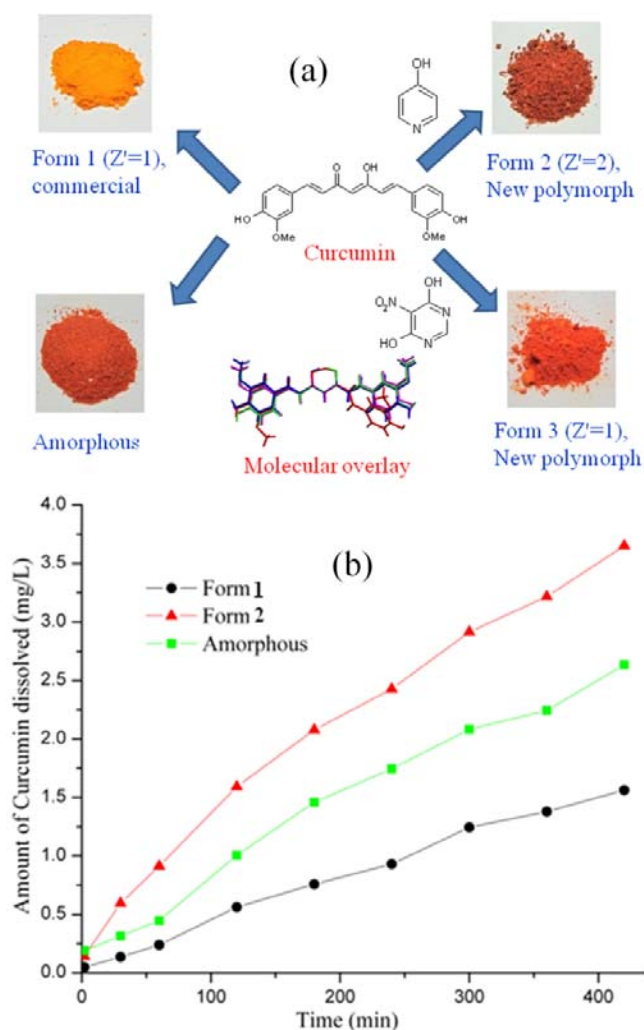


Figure 3 (a) Three crystalline polymorphs and one amorphous phase of Curcumin, (b) Dissolution rates of Curcumin polymorphs.

We report novel cocrystals of curcumin (**1**) with resorcinol and pyrogallol obtained by liquid-assisted grinding (Figure 4a). Curcumin–resorcinol (**1a**) (1:1) and curcumin–pyrogallol (**1b**) (1:1) cocrystals were characterized by X-ray diffraction, thermal analysis, FT-IR, FT-Raman, and ss-NMR spectroscopy. The 1:1 cocrystal stoichiometry is sustained by O–H···O hydrogen bonds between the phenolic OH groups of the coformers to the carbonyl group of curcumin. The melting point of the cocrystals is in between that of curcumin and the coformer and the lower melting cocrystal **1b** is more soluble than higher melting **1a**. The dissolution rates of curcumin–resorcinol (**1a**) and curcumin–pyrogallol (**1b**) in 40% EtOH–water are ~5 and ~12 times faster than that for curcumin (Figure 4b). The presence of water soluble phenolic coformers could be a reason for the improved aqueous solubility of curcumin. The present results on more soluble cocrystals of curcumin could provide faster dissolving solid forms of curcumin that are relatively stable for drug development. Pending in vivo clinical data, we believe that the faster dissolving curcumin cocrystals hint at improved bioavailability than pure curcumin.

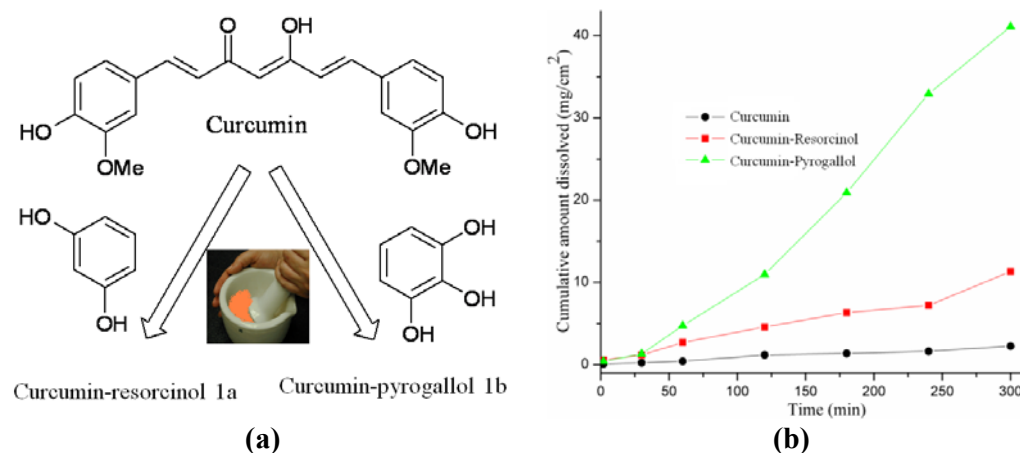
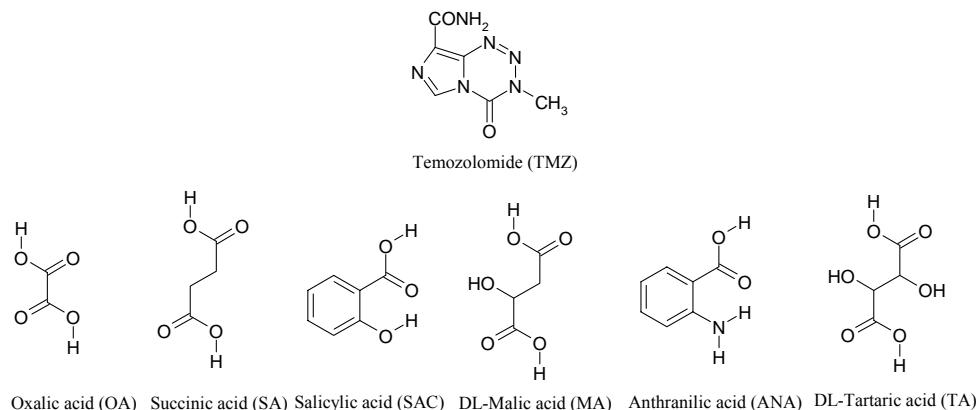


Figure 4 (a) Two novel cocrystals of curcumin with resorcinol and pyrogallol. (b) IDR experiments of cocrystals **1a** and **1b** compared to stable Form 1 indicates higher solubility compared to native Curcumin.

The antitumor prodrug Temozolomide (TMZ) decomposes in pH ≥ 7 aqueous medium but is relatively stable in acidic conditions. Pure TMZ obtained as a white powder turns pink and then of brown color which is indicative of chemical degradation. Pharmaceutical cocrystals of TMZ were engineered with safe coformers (generally

recognized as safe, GRAS chemicals) such as oxalic acid, succinic acid, salicylic acid, anthranilic acid, D,L-malic acid, D,L-tartaric acid, etc. to stabilize the drug as a cocrystal (Scheme 1). All cocrystals were characterized by FT-IR, FT-Raman, powder X-ray diffraction (PXRD), and single crystal X-ray diffraction. Temozolomide cocrystals with organic acids in the pK_a range 2–6 were found to be more stable than the reference drug in physiological conditions. The half-life ($T_{1/2}$) of TMZ–oxalic and TMZ–salicylic acid is two times longer than TMZ (3.5 and 3.6 h vs. 1.7 h), and TMZ–succinic acid, TMZ–tartaric acid and TMZ–malic also exhibited longer half life (2.3, 2.5, 2.8 h) in pH 7 buffer medium, indicating that cocrystals are more stable compared to the reference drug. The intrinsic dissolution rate (IDR) profile of TMZ–oxalic acid and TMZ–succinic acid cocrystals is comparable to that of TMZ whereas cocrystals with malic acid and salicylic acid dissolved faster than TMZ. Among the Temozolomide cocrystals examined, those with succinic acid, oxalic acid and salicylic acid exhibited improved stability and comparable or faster dissolution rate than the reference drug. Even TMZ–succinic acid cocrystals are stable in accelerated humidity conditions (40 °C and 75% RH) upto 28 weeks, whereas TMZ transformed to hydrate after 2 weeks and then converted to decomposed AIC hydrate after 5 weeks, confirmed from PXRD (Figure 5). Under accelerated ICH conditions of 40 °C and 75% RH, pure temozolomide turned pink to tan to dark brown in color due to degradation, TMZ–succinic acid and TMZ–oxalic acid cocrystal remained white (stable) for the entire duration. Along with stability, bioavailability or dissolution is equally important for a solid oral drug to be therapeutically effective. When the multiple criteria of physical form stability and dissolution rate and white color on storage are applied, TMZ–succinic acid and TMZ–oxalic acid appear to be the most promising pharmaceutical cocrystals for formulation development.



Scheme 1 Chemical structures of antitumor prodrug TMZ and GRAS cofomers organic acid used as pH adjuster.

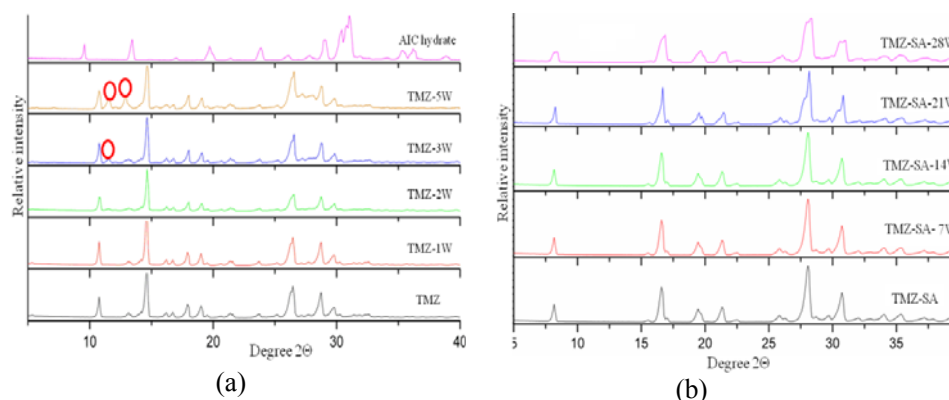
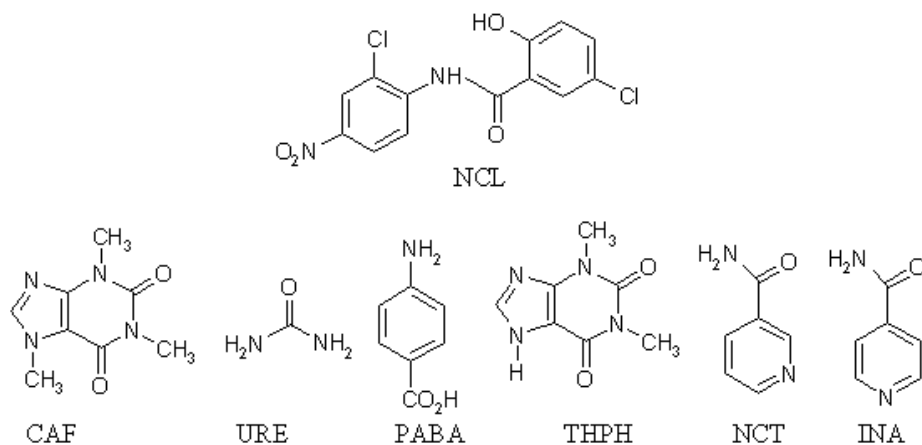


Figure 5 XRPD stack of TMZ and (b) TMZ-SA cocrystals kept at 40 °C and 75% RH, indicates that cocrystals is stable without degradation to TMZ or decomposed AIC even after 28 weeks, but TMZ transformed to monohydrate within 2 weeks and started to decompose within 5 weeks.

Niclosamide (NCL, Scheme 2) is an anthelmintic BCS class II drug having low solubility ($D_o=200$) and high permeability ($\log P_{ow}=3.91$). To improve the solubility of niclosamide, pharmaceutical cocrystals were prepared with GRAS molecules e.g. caffeine (CAF), urea (URE), p-aminobenzoic acid (PABA), theophylline (THPH), nicotinamide (NCT) and isonicotinamide (INA) etc. Neat grinding, wet-granulation and slow evaporation methods were employed to synthesize niclosamide cocrystals. All the crystalline forms were characterized by m.p., FT-IR, X-ray diffraction to confirm purity of the bulk phases. Crystal structures of niclosamide and its cocrystals were

characterized by single crystal X-ray diffraction to know the structural aspects and hydrogen bonding in the molecular structure. The presence of intermolecular O—H...O hydrogen bond from hydroxyl to carbonyl group in niclosamide was replaced by acceptor atom of coformer in the cocrystalline phases. Cocrystals with nicotinamide and isonicotinamide were further characterized by ^{13}C ss-NMR spectroscopy. All the cocrystals, except NCL–PABA, showed better powder dissolution rate than the reference API. Niclosamide–theophylline acetonitrile (NCL–THPHS) complex showed highest dissolution rate among all crystalline forms (Figure 6). But acetonitrile is a class II solvent, and has limits of toxicity. Comparatively NCL–THPH cocrystals showed moderate solubility and stability against hydration. Equilibrium solubility measurement showed that all the niclosamide cocrystals along with API converted to monohydrate within 24 h slurry experiment in 40% isopropanol–water medium. Search for new GRAS coformers with better improvement in solubility and stability of niclosamide is the next goal.



Scheme 2 Chemical structure of niclosamide (NCL) and coformers: caffeine (CAF), urea (URE), p-aminobenzoic acid (PABA), theophylline (THPH), nicotinamide (NCT) and isonicotinamide (INA). All niclosamide cocrystals maintain 1:1 stoichiometry.

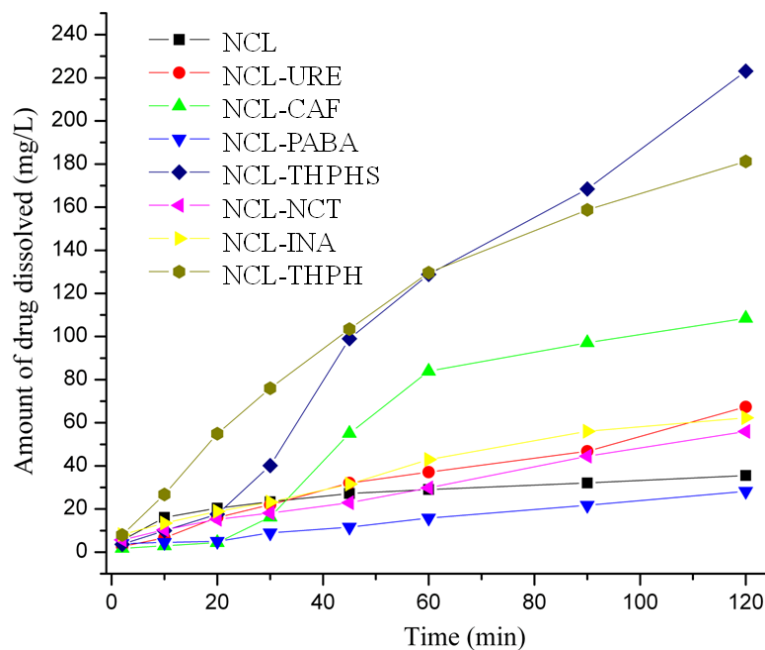
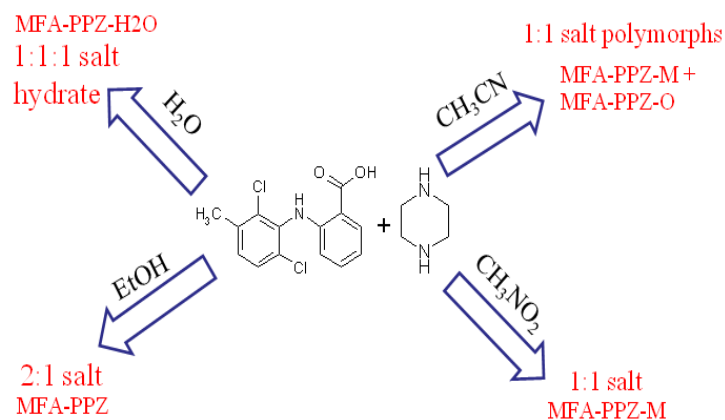


Figure 6 Dissolution curves of niclosamide and its cocrystals in 40% isopropanol-water.

Meclofenamic acid (MFA, Scheme 3) is the most potent anti-inflammatory drug among the fenamic acids. In this chapter are presented (1) two cocrystals of MFA with isonicotinamide (INA) and 4,4'-bipyridine (BPY); (2) polymorphs of MFA and piperazine (PPZ) 1:1 salt (orthorhombic $P2_12_12_1$ and monoclinic $P2_1/c$), MFA-PPZ 1:1:1 salt hydrate, MFA-PPZ 2:1 salt; and (3) MFA and 2-aminopyridine (2-APY) 1:1 salt, MFA and 4-aminopyridine (4-APY) 1:1:1 salt hydrate. Sublimation of meclofenamic acid gave single crystals for X-ray diffraction which provided good quality data for refinement and all atomic coordinates. The cocrystal and salt structures are assembled via neutral $O-H\cdots O$, $O-H\cdots N$, $N-H\cdots O$, $N-H\cdots N$ and ionic $O-H\cdots O^-$, $N^+-H\cdots O^-$ hydrogen bonds. The disorder of methyl group in meclofenamic acid crystal structure is absent in the cocrystal and salt structures, which contain different conformers (A or B) of methyl group orientation. The solubility of meclofenamic acid-isonicotinamide (1:1) and meclofenamic acid-4,4'-bipyridine (1:0.5) cocrystals is 2.9 and 7.6 times higher than that of MFA at 37 °C in 50% EtOH-water. Interestingly, MFA-PPZ 1:1 salt and its 1:1:1 hydrate are 2724 and 1334 fold more soluble than meclofenamic acid. Both these salts transformed in 50% EtOH-water slurry at 37 °C to 2:1 MFA-PPZ salt after 24 h, which

in turn transformed to meclofenamic acid after another 24 h of slurry stirring. Remarkably, the dissolution rate of MFA–PPZ (1:1) salt in water is just slightly lower than that of marketed sodium meclofenamate (Figure 7). This is the first example of polymorphic and variable stoichiometry piperazinium salts with X-ray crystal structures solved to good accuracy.



Scheme 3 Piperazinium meclofenamate salts of variable stoichiometry obtained by liquid-assisted grinding.

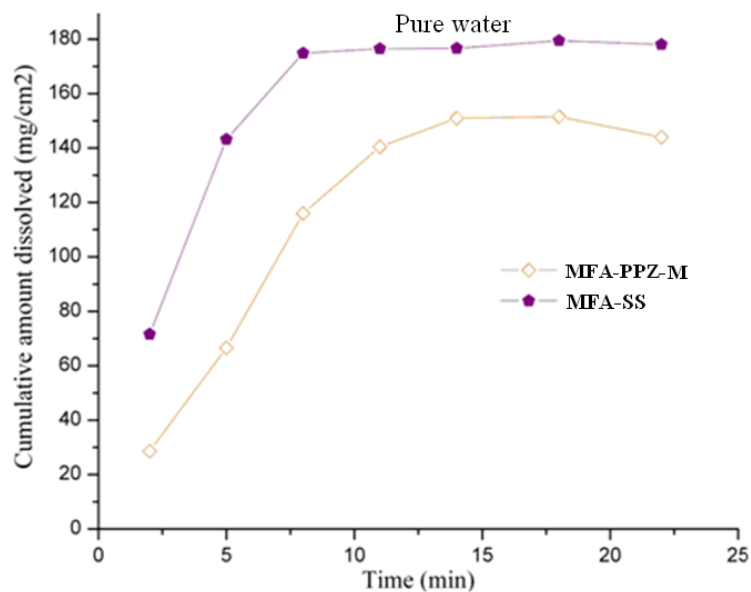


Figure 7 Comparation of dissolution rates of MFA–PPZ-M and MFA-SS in water

● Future Prospects

Stabilizing the metastable form and amorphous phase of API by addition of polymer, excipients etc. are an alternative to solubility manipulation. Salts are useful in terms of solubility improvement of APIs having ionizable functional groups. Pharmaceutical cocrystals are applicable for all APIs (both neutral/ionic) and provide dual advantage of solubility and stability improvement in same solid dosage form. Nutraceutical is a food or food product that reportedly provides health and medical benefits, including the prevention and treatment of chronic disease in addition to the basic nutritional value found in foods. Resveratrol (grapes), flavanoids e.g. catechin (green tea), quercetin (fruits), ellagic acid (strawberries), caffeine (coffee), theobromine (dark chocolates), anthocyanins (berries), citric acid (lemon), curcumin (turmeric), pyrogallol (amla) are well known Nutraceuticals (Figure 8). Nutraceuticals foods exhibit generally low solubility, and hence poor bioavailability and difficult to formulate as tablets or capsules. For e.g. curcumin (8.7 mg/L), resveratrol (30 mg/L), quercetin (2 mg/L) are poorly water soluble. Aqueous solubility of these Nutraceuticals could be enhanced by particle size reduction, hydrotropic agents, lyophilization, micelles, additives, and also new crystalline forms such as polymorphs, salts, or cocrystals.

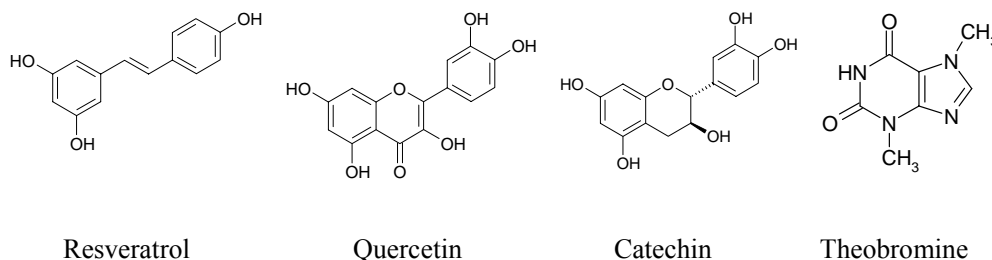


Figure 8 Chemical structures of few nutraceuticals having poor aqueous solubility.

ABOUT THE AUTHOR

Palash Sanphui, son of Late Mr. Indranath Sanphui and Mrs. Basanti Sanphui, was born in Bagaria, South 24 Paraganas district of West Bengal, India, in 1985. He completed his secondary school education at Srichanda M. N. M. Institution, Srichanda. He then completed his Intermediate education (2002) and B. Sc. (2005) from New Alipore College, Kolkata, affiliated to University of Calcutta. After the completion of his M.Sc. (Chemistry) from IIT Kharagpur (2005), West Bengal, he joined School of Chemistry, University of Hyderabad, to pursue PhD in 2007 under the supervision of Prof Ashwini Nangia. He qualified CSIR-UGC-National Eligibility Test for Junior Research Fellowship (JRF) held in December 2006 and June 2007 and was awarded research fellowship by the University Grant Commission (UGC) for 2007-2012 tenure (JRF and SRF). He has obtained 1st runner prize of K. V. Rao society memorial and Oration awards in the category of Young Research Scientist award in July 2011 for oral presentation on research work basis. He has attended and presented poster in XXII IUCR General Congress Assembly, held in Madrid, Spain on 22-30 august, 2011. He has presented lecture on research work basis in “ Indo-US Bilateral meeting on Solid State Chemistry of drugs” held in Gurgaon, India on 2-4th february, 2012.

LIST OF PUBLICATIONS

1. Stable cocrystals of Temozolomide
Ashwini Nangia, N. Jagadeesh Babu and **Palash Sanphui**,
Indian Patent Application No. 2303/CHE/2009.
2. Polymorphism in Isomeric Dihydroxybenzoic Acids
Bipul Sarma, **Palash Sanphui** and Ashwini Nangia*, *Cryst. Growth Des.*, **2010**, *10*, 2388.
3. Polymorphism in Secondary Benzene Sulfonamides
Palash Sanphui, Bipul Sarma and Ashwini Nangia*, *Cryst. Growth Des.*, **2010**, *10*, 4550.
4. Novel polymorphs and cocrystals of Curcumin
Ashwini Nangia, **Palash Sanphui**, N. Rajesh Goud, U. B. Rao Khandavilli
Indian Patent Application 3190/CHE/2010.
5. Conformational polymorphs and phase transition in nimesulide
Palash Sanphui, Bipul Sarma and Ashwini Nangia*, *J. Pharm. Sci.* **2011**, *100*, 2287.
6. New polymorphs of Curcumin
Palash Sanphui, N. Rajesh Goud, U. B. Rao Khandavilli, Sreenu Bhanoth and
Ashwini Nangia*, *Chem. Commun.* **2011**, *47*, 5013.
7. Fast dissolving Curcumin cocrystals
Palash Sanphui, N. Rajesh Goud, U. B. Rao Khandavilli and Ashwini Nangia* .
Cryst. Growth Des. **2011**, *11*, 4135.
8. Crystal Engineering of Stable Temozolomide Cocrystals
N. Jagadeesh Babu, **Palash Sanphui** and Ashwini Nangia*, *Chem. Asian J.*
2012, DOI: 10.1002/asia.201200205.
9. High Solubility Piperazine Salts of NSAID Meclofenamic Acid
Palash Sanphui, Geetha Bolla and Ashwini Nangia*, *Cryst. Growth Des.* **2012**, *12*, 2023.
10. Pharmaceutical cocrystals of Niclosamide
Palash Sanphui, S. Sudalai Kumar and Ashwini Nangia*

(Manuscript under preparation).

11. New solid forms of anti-inflammatory drug acetaminophen and their solubility improvement.

Palash Sanphui, Geetha Bolla and Ashwini Nangia*

(Manuscript under preparation).

Symposium attended

1. Indo-U.S. Workshop on Pharmaceutical Cocrystals and Polymorphs, Mysore, Feb 8-10, **2009**.
2. MEDCHEM-2009, Conference Cum workshop on Current trends in Medicinal Chemistry, April 2-4, **2009**, IIT Madras.
3. 4th International Symposium on "Current Trends in Drug Discovery Research" (CTDDR-2010), 17-21st Feb, **2010**, CDRI, Lucknow.
4. International symposium on Facets of Weak Interactions in Chemistry, 13-15 February **2011**, Univ. of Calcutta.
5. "International conference of Chemistry of the Organic solid" ICCOSSXX, 26-30th June, **2011**, IISC Bangalore, India.
6. XXII Congress and General Assembly of the International Union of Crystallography, 22-30 August, **2011**, Madrid, Spain.
7. Indo-US symposium on "Evolution of Solid state science in the Pharmaceutical industry", 2-4th Feb, **2012**, Gurgaon, Delhi.